Involvement of CTGF in eye development and the pathology of glaucoma

Dissertation

ZUR ERLANGUNG DES DOKTORGRADES DER NATURWISSENSCHAFTEN
(DR. RER. NAT.)
DER FAKULTÄT FÜR BIOLOGIE UND VORKLINISCHE MEDIZIN
DER UNIVERSITÄT REGENSBURG

Durchgeführt am Lehrstuhl für Humananatomie und Embryologie
der Universität Regensburg

vorgelegt von

Andrea E. Dillinger

aus Landau a. d. Isar

im Jahr 2018

Promotionsgesuch wurde eingereicht am:

28.03.2018

Die Arbeit wurde angeleitet von:

Prof. Dr. Rudolf Fuchshofer

Unterschrift

Meinen Eltern

Table of content

Abstract

Primary open angle glaucoma, a neurodegenerative disease of the optic nerve (ON), is one of the leading cause of blindness worldwide (Quigley 1996). In progression of the disease the optic nerve head (ONH) undergoes marked structural extracellular matrix changes (ECM), which lead to its permanent deformation and can contribute to the degeneration of ON axons. The changes in ECM in the ONH correlate with an increased reactivity of astrocytes. An intraocular pressure (IOP), which is too high for the health of the ON axons, was identified as the major risk factor for the development for the POAG (Collaborative-Normal-Tension-Glaucoma-Study-Group, 1998; The AGIS Investigators2000; Gordon et al. 2002; Lichter et al., 2001; Johnson et al., 2002; Kass et al. 2002; Leske et al., 2003). In POAG the homeostatic balance of different growth factors, affecting the resistance of the outflow pathway is altered (Inatani et al. 2001, Min et al. 2006, Ochiai & Ochiai 2002, Ozcan et al. 2004, Picht et al. 2001, Tripathi et al. 1994, Trivedi et al. 2011). In the last years, the Connective Tissue Growth Factor (CTGF) came into focus as a lens-specific overexpression of CTGF in the mice results in an elevated IOP and a significant progressive loss of retinal ganglion cell (RGC) axons over time (Junglas et al., 2012). CTGF is a member of matricellular regulatory proteins and downstream mediator of Transforming Growth Factor β2, and is involved in many different functions, like migration, adhesion, differentiation and ECM production. By its modular organization CTGF can arrange various interactions with different growth factors, integrins and ECM proteins. In this study we investigated the involvement of CTGF during eye development and the pathology of POAG. The effect of alterations in substratum stiffness on an increased astrocyte reactivity and the implication of possible mechanosensors was analyzed. The final aspect of the study was to develop siRNA coated NP for specific delivery to the AH outflow pathway tissue and cells.

During eye development CTGF is expressed in various eye structures. In early embryonic development an expression in the outer and inner layer of the optic cup as well as the lens vesicle was observed. In the following embryonic and postnatal developmental stages, CTGF expression was detected in tissues of the anterior eye segment like corneal endothelium, epithelium and stroma, in the TM and ciliary body. In the posterior eye segment an expression could be found in the retina, choroidea, sclera, ONH and dura mater. During the development of the eye CTGF expression showed tissue specific changes in the cornea, the ciliary body, the retina, the ONH and the dura mater, whereas the expression the TM remained constantly high. The characterization of the CTGF expressing cells types revealed that the trabecular meshwork cells, Müller cells, amacrine cells, ON astrocytes and endothelial cells of the SC and of the retinal and choroidal vasculature, were the source of the CTGF signal. An important role for CTGF

in the correct formation of astrocytic morphology in the retina and the ONH could be shown in CTGF conditional knockdown mice.

Beside the involvement of CTGF in developmental processes a correlation between CTGF expression and pathological changes in the murine glaucoma model was observed. An increased astrocyte reactivity was associated with an enhanced CTGF synthesis in the ONH related to the chronic elevated IOP, whereas none of those changes were observed in the adjacent parts of the ON. Interestingly, cultured murine ON astrocytes could sense changes in stiffness of the surrounding ECM causing the same changes like in the *in vivo* glaucoma model. The analysis of mechanosensitive ion channels showed a broad spectrum of expression changes dependent on the substratum stiffness, but the most promising changes were seen in Caveolin expression. An enhanced Caveolin synthesis in ON astrocytes was detected on increasing substratum stiffness and after treatment with CTGF and TGF-β2 *in vitro* and in the ONH of the murine glaucoma model.

Layer-by-layer coated NPs were designed and successfully delivered by anterior chamber perfusion to the outflow pathway tissues of porcine and human eyes. CD44 was identified as an ideal target for HA coated NPs, as CD44 is permanently present in cultured HTM cells, in the anterior chamber angle of murine and human donor eyes. The implication of CD44 in POAG could be shown by the enhanced expression in glaucomatous SC cells and the anterior chamber angle of human glaucomatous donor eyes. Finally, siRNA coated NP’s could successfully reduce CTGF synthesis in HTM cells *in vitro*.

We observed that CTGF is highly expressed in various ocular structures and we conclude that CTGF plays an essential role in the formation of astrocyte structures during development. Further we state that astrocyte reactivity induced by increasing stiffness of their surrounding matrix lead to increased levels of CTGF, which in turn contribute to the changes in ECM observed in POAG. Furthermore, the results of this study indicate that siRNA delivery to the AH outflow pathway tissue and cells based on HA-coated NPs could have a great potential in treatment of POAG.

1. Introduction

Glaucoma, a neurodegenerative disease of the optic nerve (ON), is one of the leading causes of blindness worldwide (Quigley 1996). Within the heterogenous group of disease the Primary Open Angle Glaucoma (POAG) is the most common form (Tham et al. 2014). An intraocular pressure (IOP), which is too high for the health of the ON axons, was identified as the major risk factor for the development of POAG (1998, 2000, Gordon et al. 2002, Johnson et al. 2002, Kass et al. 2002, Leske et al. 2003, Lichter et al. 2001) In recent years, the Connective Tissue Growth Factor (CTGF) came into focus as a lens-specific overexpression of CTGF in mice results in an elevated IOP and a significant progressive loss of Retinal Ganglion Cell (RGC) axons over time (Junglas et al. 2012)). These investigations point out that CTGF is a crucial player in the pathogenesis of POAG and can function as point of action to develop therapeutic approaches for treatment to reduce IOP in POAG. CTGF (also known as CCN2) is a member of matricellular regulatory proteins, which also includes Cyr61, NOV, WISP1, WISP2 and WISP3 (Bork 1993, Dockrell et al. 2009, Moussad & Brigstock 2000, Perbal 2004) The several proteins of this family have a 40-60% sequence homology and are characterized by four highly conserved domains. Module 1 is an insulin-like growth factor (IGF) – binding domain, module 2 is a von Willebrand type C domain (Bork, 1993), module 3 is a thrombospondin – 1 domain and module 4 is a C-terminal domain containing a putative cysteine knot (Grotendorst et al. 1996) . The CCN proteins are associated with the ECM and are involved in many biological processes, like adhesion, proliferation, differentiation, apoptosis, production of the ECM, migration and angiogenesis (Brigstock 2003) . CTGF acts primarily on the expression of ECM proteins and the organization of the actin cytoskeleton (Heusinger-Ribeiro et al. 2001) and can arrange various interactions with growth factors, integrins and ECM components (Abreu et al. 2002, Bork 1993, Bornstein 2001, Lau & Lam 1999) . By its modular organization CTGF can arrange various interactions with different growth factors, integrins and ECM proteins (Abreu et al. 2002, Dudley et al. 1995, Furuta & Hogan 1998, Jena et al. 1997, Luo et al. 1995, Sanford et al. 1997, Wawersik et al. 1999). Since CTGF has a broad range of functions within the cellular arrangement, it is of huge interest to identify it defined role in development and maintenance of ocular structures in order, to exclude side effects of potential CTGF reducing POAG treatments.

1.1. Mouse eye development

1.1.1. Embryonic mouse eye development

For an ideal function of the eye, particularly of the retina, which transduces the light into electrical signals, the individual tissues in the eye follow a defined morphogenesis and development to ensure an optimal function. The development of the mouse eye starts

shortly after gastrulation, identifiable by first visible signs of the eye field (Adelmann HB 1929, Li et al. 1997, Wilson & Houart 2004).The eye primordium is defined in the medial anterior neural plate, comprising all progenitors of neural-derived eye structures (Li et al. 1997, Wilson & Houart 2004, Zaghloul et al. 2005).As a first step of eye morphogenesis, the walls of the diencephalon evert at E 8.5-9.0, to form the optic vesicles resulting in a close contact with the surface ectoderm, to generate the lens placode (Spemann H.H. 1901) (Figure 1-1 A, B). The optic vesicle forms the lens vesicle and the bilayered optic cup (Pei & Rhodin 1970) (Figure 1-1 C). The presumptive corneal epithelium, remaining a 1-2 cell layer until birth, is formed by the overlying surface ectoderm (Figure 1-2 A). The distal optic vesicle becomes the inner layer of the optic cup, the future neural retina and the proximal optic vesicle becomes the retinal pigmented epithelium (RPE). The layers of the optic cup are connected to the diencephalon by the optic stalk (Figure 1-1 C).

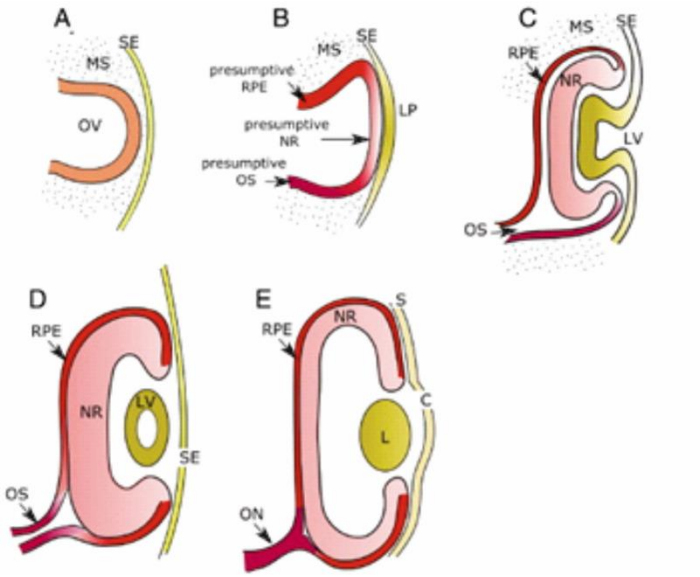

Figure 1-1: Schematic representation of vertebrate eye development. (A) Forming of the optic vesicle. (B) Generation of presumptive RPE, neural retina, optic stalk and lens placode. (C) Forming of the optic cup and lens vesicle. (D-E) Maturation of the optic cup. Lens vesicle becomes a robust structure. Optic stalk gives rise to the optic nerve and surface ectoderm gives rise to the cornea epithelium.: C: cornea; L: lens; LP: lens placode; LV: lens vesicle; MS: mesenchyme; NR: neural retina; ON: optic nerve; OS: optic stalk; OV: optic vesicle; RPE: retinal pigment epithelium; S: sclera; SE: surface ectoderm. (Adapted and modified from Adler and Canto-Soler, Molecular mechanisms of optic nerve vesicle development: Complexities, ambiguities and controversies)

Forming the presumptive corneal stroma and endothelium, the neural crest-derived mesenchymal cells start to migrate between the surface ectoderm and the lens vesicle (Figure 1-2 B). Mesenchymal cells differentiate into corneal stroma keratocytes, which synthesize specialized extracellular matrix (ECM), like collagen and a variety of proteoglycans resulting in the transparence of the cornea (Figure 1-2 C). The formation

of the iris and the ciliary body starts with growing of the edge of the optic cup into the cavity between corneal endothelium and lens along the anterior lens surface.

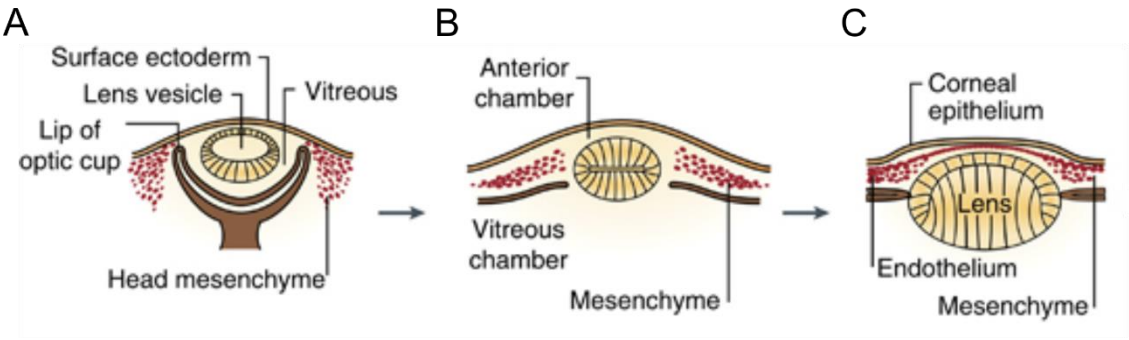

Figure 1-2: Initial steps of corneal development. (A) Forming of presumptive epithelium by the overlying surface ectoderm. (B) Mesenchymal cells migrate between the surface ectoderm and lens vesicle. (C) Mesenchymal cells differentiate to form the corneal endothelium and stroma. (Adapted from Zavala et al., 2013).

The origins of iris and ciliary body are mesenchymal cells migrating into the anterior eye. The anterior and posterior chamber are constituted by the initial formation of the iris, which separates the cavity between lens and cornea. At the final stages of embryonic development, a distinct demarcation between developing iris and cornea and the formation of the ciliary body gives rise to the first appearance of the iridocorneal angle, between the iris root and the cornea (Figure 1-3 A, small angle recess depicted with a). Within the iridocorneal angle, the trabecular meshwork (TM) and the Schlemm's canal (SC) develop in the postnatal period of eye development. The future location of the TM is already present at the later stages of embryonic development (Figure 1-3 A, arrow).

1.1.2. Postnatal mouse eye development

1.1.2.1. Postnatal development of the anterior eye structures

In contrast to the human eye, the mouse eye is not completely developed at birth. The different eye structures are already existing, but lids are still closed, while iris, ciliary body, cornea, retina and TM are still immature (GYLLENSTEN & HELLSTROM 1954, Smith et al. 2001).Therefore, the maturation of the individual tissues take place during postnatal development.(Baulmann et al. 2002, 2002, Smith et al. 2001). The cornea is the outermost tissue of the eye. At birth, the three layers of the cornea are well defined. The corneal epithelium, providing the barrier to the external environment and protecting the eye from infectious agents, is 1-2 cell layers thick and proliferates rapidly within the first two weeks to form a 5-6 cell layered epithelium. The corneal stroma, composing 90% of corneal thickness, exhibits the key component for corneal transparency with its collagenous lamellae orientated parallel to the corneal surface. It decreases in cell density during postnatal development. The corneal endothelium, a monolayer of

endothelial cells, forms the surface to the anterior chamber and is essential for hydration and nutrient supply from the aqueous humor (AH) for the corneal stroma. The specialized basement membrane of the corneal endothelium, the Descement's membrane is first evident within the first days after birth.

In comparison to the cornea, the other structures of the anterior eye segments undergo their main morphogenesis during the postnatal development. At birth the first appearance of the iridocorneal angle with densely packed mesenchyme and elongated and less rounded cells is determined. Some of the cells start to form the iris stroma and synthesizes pigment, which makes them distinguishable from the future TM (Figure 1-3 B; depicted with arrow). By formation of the ciliary body, the iris and the ciliary body are separated and can be well defined within the first four days after birth (Figure 1-3 B, ciliary processes depicted with arrow; Figure 1-3 C; Smith et al., 2001). From postnatal day 2 (P2) to P4, the mesenchyme of the future TM is densely packed (Figure 1-3 C) (Smith et al. 2001). Within the dense mass of mesenchymal cells, the cells elongate in the region of the developing TM and small spaces are filled with extracellular fibers, which are orientated into lamellae and beams.

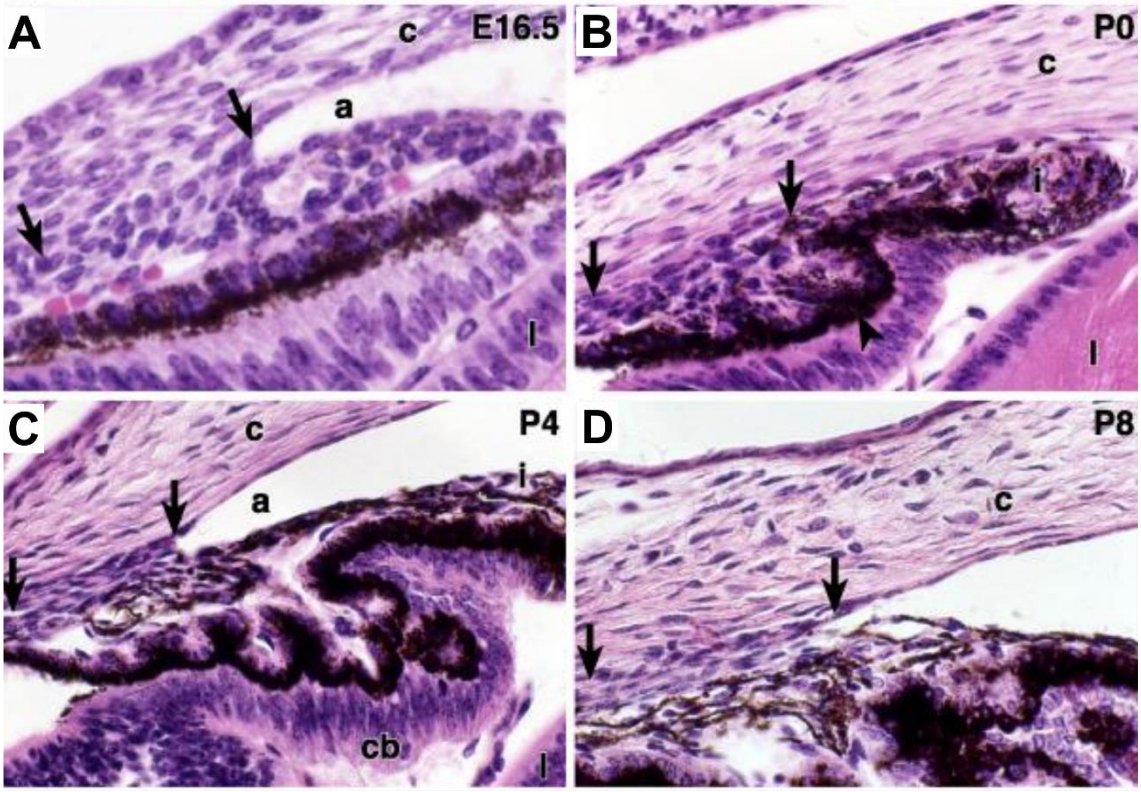

Figure 1-3: Development of iridocorneal angel in mice. (A) At E16.5, a small angle recess is present (a) and the location of the future TM is visible (arrow). (B) At P0, the mesenchyme of iris and TM is distinguishable (arrow) and the ciliary body starts to form (arrowhead). (C) At P4, a long angle recess can be recognized, and iris and ciliary body are well formed. TM is depicted with arrows. (D) At P8, in the region of the TM the cells are more elongated and small spaces are filled with extracellular fibers (TM depicted with arrow). (Adapted from (Smith et al. 2001)).

For proper maturation of the TM the intertrabecular spaces must be opened up, involving morphogenesis of the mesenchyme mass, without cell death and atrophy (Figure 1-4 A; TM depicted with arrow; (Smith et al. 2001)). For generation of the SC the scleral blood vessels next to the iridocorneal angle combine to form the SC, which is in close contact to the TM. By P14, the SC (Figure 1-4 A; SC depicted with arrow) appears as a small lumen lined with endothelial cells (Figure 1-4 A; vascular structures depicted with arrowhead), followed by the presence of abundant giant vacuoles at P18. Finally, by P21 the iridocorneal angle is fully developed. To increase the intertrabecular spaces the remodeling of ECM in the TM continues in the following weeks and is completed around seven weeks after birth. (Figure 1-4) (Smith et al. 2001).

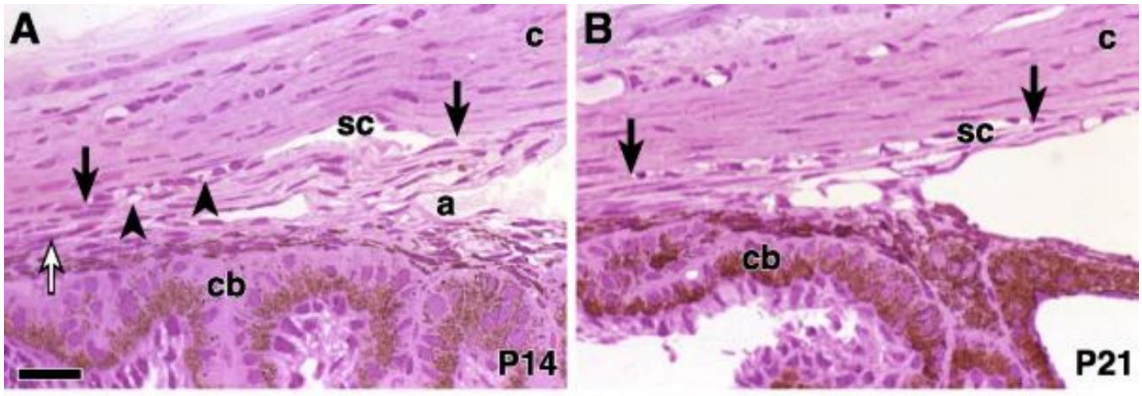

Figure 1-4: Postnatal development and remodeling of iridocorneal angel in mice. (A) At P14, the SC (arrow) is evident and contains vascular structures (arrowhead). The developing ciliary muscle is present (open arrow) and a deep angle recess can be observed (a). (B) At P21, the development of structures of the iridocorneal angle is completed. The SC extends from the posterior ciliary body to the end of Descement's membrane (arrow). (Adapted from Smith et al., 2001).

1.1.2.2. Postnatal development of the retina

The mouse retina exhibits an immature retinal vasculature and a persistent hyaloid vessel at birth (GYLLENSTEN & HELLSTROM 1954). Angiogenesis in the mouse retina occurs within the first three weeks after birth, starting with the radial outgrowth of vessels of the ON at P1 to form the superficial plexus. In this initial outgrowth, the retinal vessels follow the astrocyte network, which also spread from the ON (Jiang et al. 1995, Ling et al. 1989, Stone & Dreher 1987). The vertical sprouting of superficial capillaries generates the deep plexus from P7 to P12, located in the outer plexiform layer (OPL) and the intermediate plexus from P12 to P15, resident in the inner plexiform layer (IPL). The mature retina is a neuronal network with a stratified organization, composed of specialized sensory and projective neurons (Figure 1-5 A). In the process of retinal neurogenesis retinal progenitor cells run through symmetric and asymmetric cell division. RGC, horizontal interneurons, cone photoreceptors and amacrine cells are generated

during the early neuronal differentiation, followed by a second differentiation wave, producing rod photoreceptors, bipolar interneurons and Müller glia cells. The stratified composition of the retina is well organized, as the sensory neurons, like cone and rod photoreceptors are arranged in the outer nuclear layer (ONL) and the horizontal, bipolar and amacrine interneurons in the inner nuclear layer (INL) (Figure 1-5 B). RGC, functioning as projective neurons, are located in the ganglion cell layer (GCL) (Figure 1-5 B). In the OPL and IPL the synaptic connections are formed (Figure 1-5 B). Additionally, the specialized radial glia, the Müller glia cells structure and control the retinal environment (Figure 1-5 B). They span the entire neural retina, and together with astrocytes form the inner limiting membrane (ILM), the innermost boundary of the retina, and the outer limiting membrane (OLM), by creating junctional complexes with photoreceptors. The Müller cells provide support for the retinal neurons, by removing metabolites, and maintaining the inner retinal-blood barrier and regulating the blood flow (Choi & Kim 2008, Metea & Newman 2006, Tout et al. 1993, Tsacopoulos & Magistretti 1996).

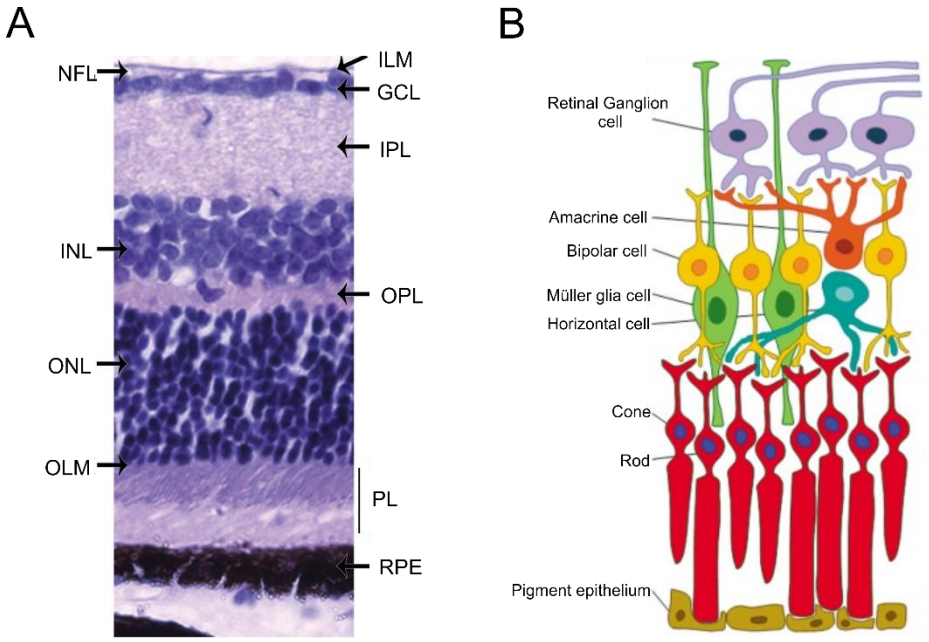

Figure 1-5: Stratified organization of the Retina. (A) The retina can be divided into different layers. ILM: inner limiting membrane; NFL: nerve fiber layer; GCL: ganglion cell layer; IPL: inner plexiform layer; INL: inner nuclear layer; OPL: outer plexiform layer; ONL: outer nuclear layer; OLM: outer limiting membrane; PL: photoreceptor layer; RPE: retinal pigmented layer (Adapted and modified from (Willermain et al. 2014)). (B) Schema of retinal cell types. (Adapted and modified from (Gramage et al. 2014)).

1.1.3. Signaling pathways in eye development

The accurate morphogenesis of the eye is based on many different, intricately engaging processes. For this precise progression, a predefined interaction of transcription factors

and signaling pathways is obvious. A breakdown of this interaction results in false development of different eye tissues, which could lead to various developmental disorders and reduced visual function or even to blindness. A multitude of studies could identify several transcription factors expressed during eye development and essential for its morphogenesis. The signaling pathways of retinoic acid (RA), fibroblast growth factors (FGFs), sonic hedgehog (Shh), WNTs and the, transforming growth factor β (TGF-β) superfamily are known to be involved in the interaction between the neuroepithelium, the surface ectoderm and the extraocular mesenchyme (Ashery-Padan & Gruss 2001, Chow & Lang 2001, Dudley et al. 1995, Furuta & Hogan 1998, Gehring & Ikeo 1999, Jena et al. 1997, Luo et al. 1995, Lupo et al. 2005, Martinez-Morales et al. 2005, Sasagawa et al. 2002, van Raay & Vetter 2004, Wawersik et al. 1999). One of the key regulators of the eye development is Pax6, a member of the paired box family of transcription factors, which is necessary for eye formation (Ashery-Padan & Gruss 2001, Chow & Lang 2001, Gehring & Ikeo 1999). Pax6 is essential for the establishment of lens progenitor cells and the multipotency of retinal progenitor cells during the early stages of development (Cvekl & Duncan 2007, Marquardt et al. 2001). In later stages, Pax6 regulates the development of the anterior chamber, the lacrimal gland and the neuroretina (Cvekl & Tamm 2004, Makarenkova et al. 2000, Marquardt & Gruss 2002). Different matricellular proteins and growth factors are co-expressed with Pax6, the co-localization and interaction with TGF-β leads to the hypothesis that the activity of Pax6 is controlled by TGF-β signaling (Shubham & Mishra 2012). TGF-β itself is directly involved in the morphogenesis of the eye, since homozygous TGF-β knockout mice show a reduced corneal stromal layer and a hypercellularity of the posterior chamber (Saika et al. 2001, Sanford et al. 1997). Similarity in the developmental defects of both homozygous TGF-β and heterozygous Pax6 knockout mice confirms the hypothesis that Pax6 activity during eye formation can be controlled by TGF-β signaling (Baulmann et al. 2002, Collinson et al. 2001, Saika et al. 2001, Sanford et al. 1997). Another group of proteins involved in the morphogenesis of the eye are the bone morphogenic proteins (BMPs), belonging to the TGF-β superfamily. Mice with a BMP-4 or BMP-7 deficiency show impaired lens induction and formation (Dudley et al. 1995, Furuta & Hogan 1998, Jena et al. 1997, Luo et al. 1995, Wawersik et al. 1999).

The important role of CTGF during skeletal development was demonstrated in CTGF deficient mice, which show multiple skeletal defects, like expanded hypertrophic zones of long bones (Ivkovic et al. 2003). CTGF can arrange interactions with different growth factors, which are essential for the development of the eye (Abreu et al. 2002, Dudley et

al. 1995, Furuta & Hogan 1998, Jena et al. 1997, Luo et al. 1995, Sanford et al. 1997, Wawersik et al. 1999).

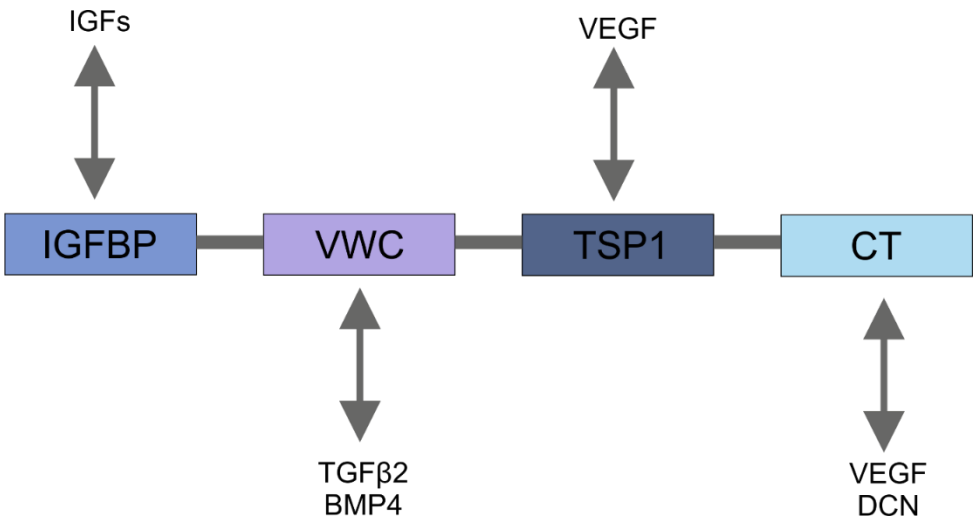

Figure 1-6: Protein structure of CTGF and interaction partners. The CTGF protein is characterized by four highly conserved domains and can arrange various interactions with different proteins. IGBP: insulin-like growth factor binding domain; VWC: von Willebrand factor-C repeat domain; TSP1: thrombospondin type 1 repeat module; CT: C-terminal cystine knot; VEGF: vascular endothelial growth factor; TGFβ: transforming growth factor β; BMP4: bone morphogenic protein 4; DCN: decorin.

The binding of CTGF to BMPs or TGFβ, causes the inhibition of BMP and enhancement of TGF-β signaling (Abreu et al. 2002). Additional to the interaction with growth factors implicated in differentiation and morphogenesis, CTGF can coalesce interactions with vascular endothelial growth factor (VEGF), which is essential for angiogenesis during development (Ferrara et al. 1996). CTGF forms VEGF-CTGF complexes, leading to an inhibition of VEGF induced angiogenesis and in contrast VEGF can induce CTGF (He et al. 2003, Inoki et al. 2002, Jang et al. 2004, Kuiper et al. 2007, Suzuma et al. 2000). The interaction of CTGF with different factors essential for eye formation leads to the hypothesis that CTGF may play a role during the development of the mouse eye. Little is known about the expression pattern of CTGF during the development of the eye and its role in the early and later stages of the morphogenesis. The expression of CTGF was already shown in pericytes, endothelial cells and tip cells of the superficial plexus in CTGFp-GFP mice, which express GFP under the CTGF promotor (Pi et al. 2011) during development. The role of CTGF during the development of the superficial plexus, was shown by blocking CTGF with a specific antibody, which results in a reduced development (Pi et al. 2011). The exact distribution pattern and function of CTGF during embryonic and postnatal mouse eye development is still unclear, therefore it was of huge interest to analyze the CTGF promotor activity during embryonic and postnatal

development and in the adult eye. CTGF$^{LacZ+/-}$mice, which express β-galactosidase under the control of the CTGF promotor were used for histological and immunohistochemical studies. Since the embryonic lethality of a CTGF knockout, CTGF$^{Coin/Coin}$;CAGGCre-ER mice, which allow a conditional deletion of CTGF via the Cre-loxP system were used to study the effect of CTGF deficiency on eye development.

1.2. The pathology of POAG

1.2.1. The trabecular meshwork and aqueous humor outflow

1.2.1.1. Structure and function of the trabecular meshwork

Under normal conditions the IOP is in a steady state, as the outflow rate across the TM is equal to the production of aqueous humor (AH) by the ciliary body epithelium, lining the ciliary processes (Tamm 2009). The AH is a clear fluid, which fills the anterior and posterior chamber and provides nutrition for avascular structures, such as cornea and lens. Additionally, the AH is necessary for removing excretory products from metabolism, transporting neurotransmitter, stabilizing the ocular structure and contributes to the regulation of the homeostasis. The main drainage system is the conventional or trabecular outflow pathway, including the TM (corneo-scleral meshwork and the juxtacanalicular connective tissue (JCT)), the endothelial lining of SC, the collector channels and the aqueous veins (Figure 1-7 B).

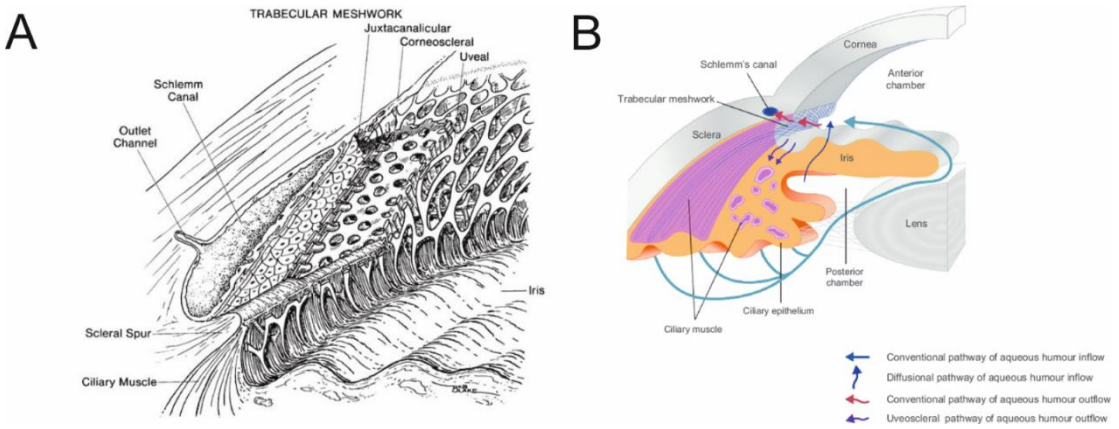

Figure 1-7: Schematic representation of TM components and AH drainage. (A) Three layers of TM (shown in cutaway views): uveal, corneoscleral, and juxtacanalicular layer. (B) Schematic representation of different AH outflow pathways. (Adapted from: (A) Shield and Kriegelstein, 1993 (B (Crawley et al. 2012))

The TM is enclosed in the internal scleral sulcus, a slight groove in the region of the corneo-scleral limbus (Figure 1-7 A). The TM is assembled from connective tissue

beams and lamellae, of densely packed collagen and elastic fibers, covered with TM cells (Marshall et al. 1991a, 1991b). The inner layer of the TM, the uveal meshwork consists of three layers of connective tissue beams and TM cells, with irregular intertrabecular fenestrations (Lütjen-Drecoll et al. 1981, Lütjen-Drecoll 1999, Lutjen-Drecoll E 1994, 2001, Tamm 2009) The corneo-scleral TM is similarly constructed, composed of 8-15 layers of perforated sheets of fibers, also covered by TM cells, with intertrabecular spaces becoming smaller closer to the SC. The lamellae and beams in the uveal and corneo-scleral TM are built up by densely packed collagen, mostly collagen type I and III and elastic fibers (Marshall et al. 1991a). The cells in the inner portions of the TM function mostly as phagocytic pre-filters, removing cellular debris. The outermost portion, the JCT represents almost all resistance to aqueous humor outflow, therefore the intertrabecular spaces become smaller (Figure 1-7 A) (Lütjen-Drecoll et al. 1981, Lütjen-Drecoll 1999, Lutjen-Drecoll E 1994, 2001, Tamm 2009)). In the JCT the discontinuous distribution of several layers of JCT cells are embedded in loose connective tissue. The ECM in the outflow pathway is constituted of several different components like laminin, type IV collagen, perlecan and fibronectin (Fuchshofer et al. 2006, Tamm 2009, Tawara et al. 1989, Ueda et al. 2002). The arrangement of the JCT cells and the ECM fibrils presents an irregular network. The ground substance in this network is constituted of proteoglycans and hyaluron (Gong et al. 1992, Lütjen-Drecoll et al. 1990, Tawara et al. 1989). As the SC is the proximate structure in the AH drainage system, the JCT cells are in contact to the endothelial cells lining the inner wall of SC (Grierson et al. 1979, Grierson & Lee 1974, 1978, Lütjen-Drecoll et al. 1981, Lütjen-Drecoll 1999). The AH is transported though the inner wall of SC by giant vacuoles and transendothelial pores (Braakman et al. 2015, Johnson 2006). Finally, the AH is drained to several collector channels, which are connected to the lumen of the SC. While the structure of the human TM and SC is similar to that in mice, the porcine outflow pathway differs by formation of an angular aqueous plexus (McMenamin & Steptoe 1991).

1.2.1.2. Pathological changes in the trabecular outflow pathway

In the pathogenesis of POAG no macroscopic changes are observed in the TM and SC confine it from other forms of glaucoma. Indeed, in POAG structural changes are observed in the TM, especially in the JCT, affecting the normal outflow pathway of AH, and creating an increased resistance and finally an elevation in IOP (Acott & Kelley 2008, Gordon et al. 2002, Johnson 2006, Leske et al. 2003). A characteristic sign of POAG is the increased fibrillar ECM in the JCT (Tektas & Lütjen-Drecoll 2009). The nature of this so called sheath-derived (SD) material has not been identified, but there is evidence that collagen type VI and FN are included (Hann et al. 2001, Lütjen-Drecoll et al. 1989, Lütjen-Drecoll 1999). It is thought that this accumulation of ECM contributes to the increased

outflow resistance in glaucoma. In addition to the alterations in ECM organization and structure, the outflow resistance is influenced by the actomyosin contractility of TM cells (Tian et al. 2000, Wiederholt et al. 2000).

TGF-β2, the predominant isoform of transforming growth factor β in the eye seems to be involved in the pathogenesis of POAG. TGF-β2, present in the normal AH, was shown by many studies to be elevated in the AH of POAG patients (Inatani et al. 2001, Min et al. 2006, Ochiai & Ochiai 2002, Ozcan et al. 2004, Picht et al. 2001, Tripathi et al. 1994, Trivedi et al. 2011). TGF-β2 causes ECM remodeling and organization, by an increased synthesis and a reduced degradation of ECM components. For instance, the synthesis of plasminogen activator inhibitor-1 (PAI-1) is induced by TGF-β2, leading to a reduced activity of the matrix metalloproteinase 2 (MMP2) (Fuchshofer et al. 2003). In recent years, the downstream mediator of TGF-β2, CTGF was implicated in the pathological changes occurring in the TM and SC in POAG. Analysis of CTGF levels in the AH of glaucoma patients, revealed a slight increase in POAG (Browne et al. 2011). Interestingly, another study detected highly increased levels of CTGF in the AH of POAG patients (Fahmy IA). Furthermore, enhanced levels were detected in SC cells of glaucomatous donors (Overby et al. 2014). The implication of CTGF in the ECM reorganization and actin cytoskeleton arrangement supports the assumption that it is involved in the processes observed in the TM and SC in POAG. This assumption can be confirmed as TM cells cultured on stiffer substratum manifest higher levels of CTGF, furthermore CTGF modulate the actin cytoskeleton of TM cells and the effect of TGFβ2 on the ECM is mediate by CTGF (Junglas et al. 2009, Junglas et al. 2012, Raghunathan et al. 2013). Intriguingly, the lens specific overexpression of CTGF in mice results in an elevated IOP and a significant progressive loss of RGC axons over time (Junglas et al. 2012).

Therefore, CTGF can function as the ideal point of action for therapeutic treatment strategies, as a reduction would cause a distinct effect on the dysregulation in the tissue of the outflow pathway tissue and thus may regulate the IOP.

1.2.2. The optic nerve head and the *Lamina cribrosa*

1.2.2.1. Structure of the optic nerve head and the *Lamina cribrosa*

The optic nerve head (ONH) is a light site in the sclera in the posterior eye (Figure 1-8 A) (Bellezza et al. 2000), where the axons of the RGCs leave the eye. Besides the axons of the RGCs, the ON contains astrocytes, mircoglia, oligodendrocytes, blood vessels and depending on the species Lamina cribrosa (LC) cells. In humans, a prominent structure within the ONH is the Lamina cribrosa (LC; *Lamina cribrosa sclerae*), a sieve-like plate of connective tissue and elastic fibers, which are lined by astrocytes (Figure 1-8 B)

(Hernandez et al. 2008). In addition to astrocytes, the LC cells, a GFAP negative unique cell type within the ONH, are also located in the LC (Hernandez et al. 1988).

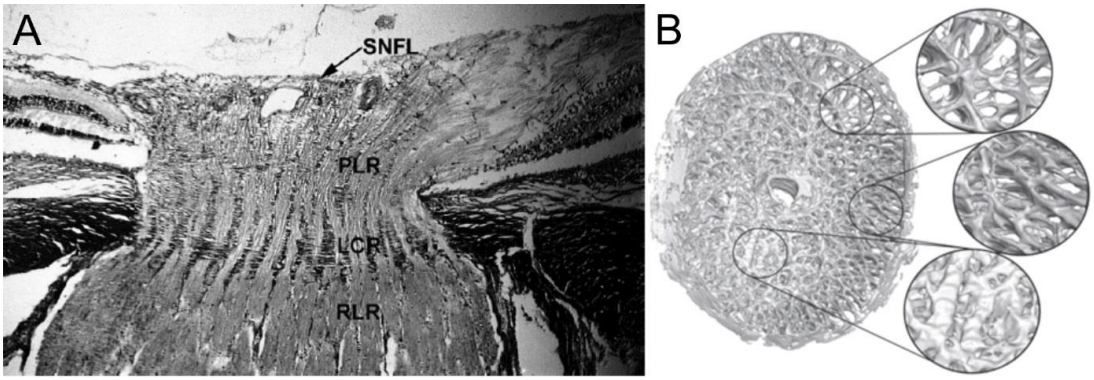

Figure 1-8: Vertical section of human ONH and 3D-representation of LC. (A) Vertical section of the ONH divided into its different parts. (B) 3-D representation of LC, depicting different constituents of connective tissue in different regions. SNFL: surface nerve fiber Layer; PLR: prelaminar region; LCR: lamina cribrosa region; RLR: retrolaminar region. (Adapted from: (A (Hayreh 2011); Ischemic Optic Neuropathies) (B (Sigal IA et al. 2009))

Astrocytes, lining the connective tissue plates in the LC in primates and forming the glial tubes in mice are the important common element of both structures. Type 1B astrocytes are the major cell type in the ONH and are accountable for ECM macromolecule synthesis in the LC (Hernandez et al. 1991, Pena et al. 1996, Ye et al. 1994). In general, astrocytes have a widely spread field of function. They are responsible for maintaining the structural rigidity, regulating blood flow, releasing neurotransmitter, modulating synaptic function and plasticity, keeping the extracellular environment and are involved in scarring and repair processes (Haydon 2001, Iadecola & Nedergaard 2007, Magistretti 2006, Nedergaard et al. 2003, Newman 2003, Rossi et al. 2007, Takano et al. 2006, Ullian et al. 2001)). Within the LC they provide a supporting function to the surrounding axons, by their connections to the connective tissue and the surrounding blood vessels (Hernandez et al. 2008).

1.2.2.2. The structure of the optic nerve head in mice

In comparison to the human optic nerve head, in mice, a dense meshwork built up by astrocytes missing the connective tissue plates and with only low expression of ECM components, like collagen can be found. Because of the formation of glial tubes, illustrating a honeycomb structure where the axons of the RGCs pass through, this structure is called the glial lamina (Figure 1-9) (Fujita et al. 2000, Howell et al. 2007, May & Lütjen-Drecoll 2002, Morcos & Chan-Ling 2000, Sun et al. 2009). In addition to the mostly absence of ECM, the transition zone between unmyelinated and myelinated

region is directly behind the LC in primates, but more posteriorly in mice (Oyama et al. 2006, Sun et al. 2009).

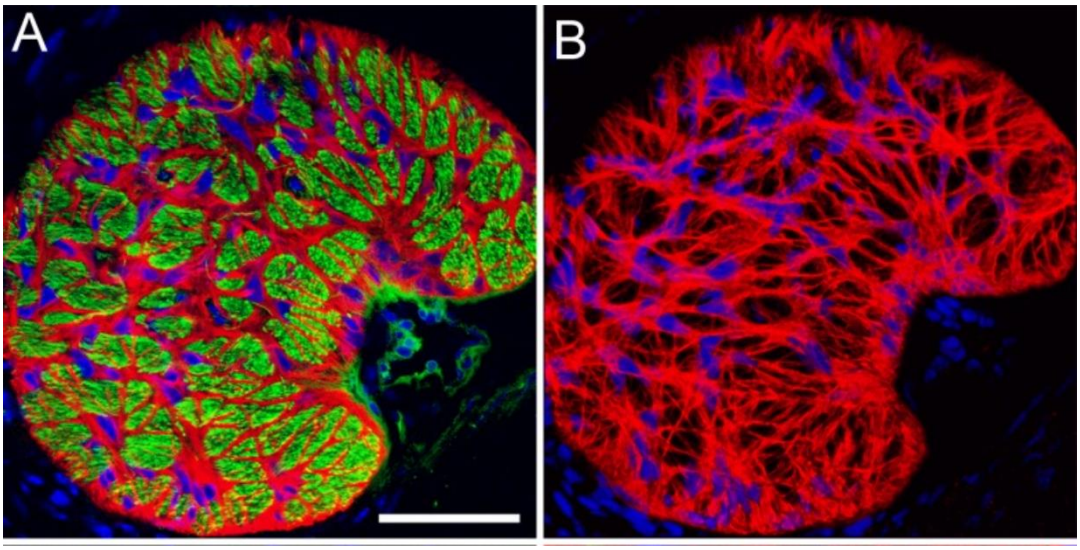

Figure 1-9: Section through a glial lamina of mouse ONH. (A) Honeycomb structure of the glial lamina constituted of astrocytes (red). Axons are counterstained with green (neurofilament). (B) Astrocytes (red) network forming glial tubes. (Adapted from Lye-Barthel et al., 2013).

1.2.2.3. Pathological changes in the optic nerve head and the *Lamina cribrosa*

The characteristic sign of POAG is the irreversible and progressive loss of axons of the RGCs. This significant damage is suggested to occur mostly at the level of the LC in the ONH (Hayreh 1978, Quigley et al. 1992). The distinct structural changes occurring in the LC lead to the permanent deformation, called excavation or cupping, differentiating it from other optic neuropathies (Figure 1-10) (Quigley 1983).

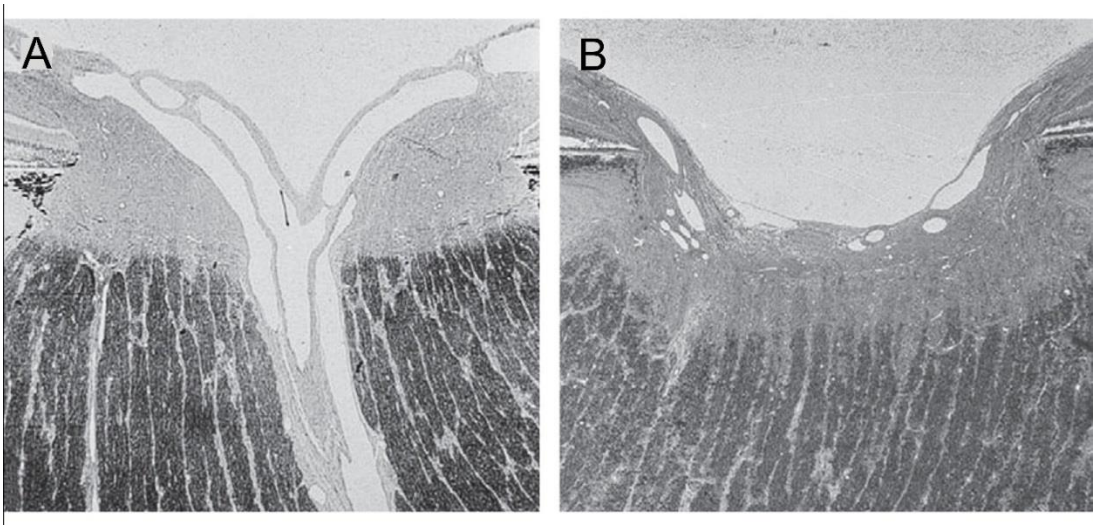

Figure 1-10: The ONH of healthy and glaucomatous patients. (A) The healthy, normal appearance of the ONH. (B) Typical changes in the ONH of glaucomatous patients, with tissue loss and cupping of the ONH. (Adapted from: (Quigley 2011)).

Thereby, it is hypothesized that a disruption of the retrograde and anterograde transport of neurotrophins is generated by axonal compression, which results in the death of RGC cells (Pease et al. 2000, Quigley et al. 2000). In the glaucomatous ONH a wide variety of structural changes in the ECM and in the major cell type, the astrocytes arise in response to elevated IOP (Fukuchi et al. 1992, Fukuchi et al. 1994, Gong et al. 1997, Hernandez et al. 1990, Hernandez 1992, Hernandez et al. 1994, Morrison et al. 1989, Morrison et al. 1990, Pena et al. 1996, Pena et al. 1998, Pena et al. 1999, Quigley 1983, Quigley et al. 1991). The ECM of the LC is dramatically reorganized, such as abnormal deposition of elastin, increased levels of collagen type IV and the connective tissue sheath around the capillaries in the prelaminar region are thickened (Hernandez 1992, Hernandez et al. 1994, Pena et al. 1998, Pena et al. 2001, Tektas et al. 2010). In summary, these changes include variations in both quality and quantity of ECM components (Hernandez 2000, Hernandez et al. 2002, Pena et al. 2001). Molecular signaling mechanisms contributing to or involved in these processes are not known yet, but increased amounts of TGF-β2 were detected in the ONH of glaucomatous patients (Pena et al. 1999, Zode et al. 2011). As astrocytes and LC cells assemble the LC it is likely that one or both cell types are contributing to structural changes developing in the LC (Hernandez 2000). There is evidence that reactive astrocytes are the major source of growth factors and ECM component upregulation, as it was shown that TGF-β2 is extensively localized to reactive astrocytes in the glaucomatous ONH (Pena et al. 2001). Furthermore, previous studies of our group and others could show that TGF-β2 leads to an increase in ECM protein level in ONH astrocytes, and that this effect is dependent on its downstream mediator CTGF (Fuchshofer et al. 2005, Neumann et al. 2008, Zode et al. 2011). In the glaucomatous ONH, a change in astrocyte morphology occurs, indicated by cellular hypertrophy, increased GFAP immunoreactivity, rounded cell bodies with retracted cell processes and a migration from the core of the cribriform plates into the nerve bundles (Varela & Hernandez 1997). These changes are associated with alterations in gene expression (Liu & Neufeld 2000, Neufeld et al. 1997, Yan et al. 2000) These reactive changes, including migration, hypertrophy, upregulation of GFAP and gliosis are observed in human glaucoma and animal models of glaucoma (Hernandez 2000, Lye-Barthel et al. 2013, Morrison et al. 1990, Quigley et al. 1991, Sun et al. 2010, Sun & Jakobs 2012). Similar results could be shown for LC cells which react to the TGF-β2 treatment with increased ECM expression and synthesis (Kirwan et al. 2005, Kirwan et al. 2009, Zode et al. 2011)

1.2.2.4. Pathological changes in the peripapillary sclera

In addition, to the alteration occurring in the ONH, implications of the peripapillary sclera, the part of the sclera around the ONH, in the pathogenesis of the POAG are existing. In

general, the sclera, built up by different collagen types, elastic fibrils and proteoglycans, constitutes three quarters of human ocular circumference (Rada et al. 2006). The structure of the peripapillary sclera differs in the arrangement of collagen and elastic fibrils, as they are oriented circumferentially around the ONH. By this formation, a mechanical reinforcement against the stress in this region can be provided (Gelman et al. 2010, Girard et al. 2009b, Girard et al. 2009a, Hernandez et al. 1987, Pijanka et al. 2012, Quigley et al. 1991, Yan et al. 2000). As corneal hysteresis and myopia, both linked to the thinning of sclera are glaucoma risk factors, there is strong evidence that the composition of the sclera is a crucial component of glaucoma development (Boland & Quigley 2007, Congdon et al. 2006). Increased scleral stiffness was shown in human glaucoma and experimental glaucoma models, in monkey and mice (Coudrillier et al. 2012, Downs et al. 2008, Hommer et al. 2008, Nguyen et al. 2013). Furthermore, scleral cross-linking is associated with greater RGC and axon loss (Kimball et al. 2014). As the astrocytes in the ONH stay in close contact with their processes to the peripapillary sclera and are sensitive to mechanical stress, it can be suggested that the mechanical behavior of the sclera influences the stress and deformation of the LC and that this mechanical stress is sensed by astrocytes, causing changes occurring in the ONH and its astrocytes (Coudrillier et al. 2012, Coudrillier et al. 2013, Girard et al. 2009b, Girard et al. 2009a, Hernandez 2000, Norman et al. 2011, Rogers et al. 2012, Sigal et al. 2005, Sigal et al. 2011).

2. Aim of the study

The aim of the study is to investigate the involvement of CTGF in eye development and the pathology of POAG. The expression of CTGF during eye development and in the adult eye will be investigated in different ocular tissues. Furthermore, the CTGF expressing cell types will be identified. It is also of interest to clarify the involvement of CTGF in the ONH pathology of POAG. Therefore, the correlation between CTGF expression changes and astrocyte reactivity in the ON and ONH will be examined related to mechanical stress *in vivo* and by increasing substratum stiffness *in vitro*. Additionally, possible mechanosensing proteins will be investigated. Furthermore, an aim of this study is to develop siRNA coated layer-by-layer nanoparticles as a new tool to reduce CTGF in the AH outflow pathway tissue and cells.

The following experiments were carried out to achieve these aims:

- Analysis of CTGF promotor activity in $CTGF^{LacZ+/-}$ mice during development and in the adult eye
- Identification of CTGF expressing ocular cell types in $CTGF^{LacZ+/-}$ mice during development and in the adult eye
- Analysis of CTGF and GFAP levels in the ON and ONH of 1-month and 2-month-old βB1-CTGF1 mice
- Analysis of the effect of increasing substratum stiffness on CTGF levels and reactivity in murine ON astrocytes *in vitro*
- Analysis of the effect of increasing substratum stiffness on Trp-channel and Caveolin1 expression in murine ON astrocytes
- Analysis of Caveolin1 expression in murine ON astrocytes after CTGF and TGF-β2 treatment, and in the ON and ONH of βB1-CTGF mice
- Evaluation of CD44 prevalence in HTM cells after CTGF and TGF-β2 treatment, in the outflow pathway structures of βB1-CTGF mice and glaucomatous and healthy human donor eyes
- Analysis of nanoparticle distribution after perfusion of porcine and human eyes with different nanoparticles
- Evaluation of CTGF knockdown after transfection with siRNA coated nanoparticles in HTM cells

- Generation and confirmation of a conditional, inducible CTGF knockout
- Analysis of the influence of conditional CTGF knockout on eye morphology

3. Material and methods

3.1. Materials

3.1.1. Reagents

Reagents	Source of supply
2,4,6-Tri(dimethylaminomethyl) phenol (DPM-30)	Roth, Karlsruhe, Germany
0.05 % Trypsin/EDTA	PAA The Cell Culture Company, Pasching, Austria
2-Mercaptoethanol	Roth, Karlsruhe, Germany
Acetic acid, glacial	Merck, Darmstadt, Germany
Acetone	Merck, Darmstadt, Germany
Albumin Fraction V (BSA)	Roth, Karlsruhe, Germany
Agarose	Biozym Scientific, Oldendorf, Germany
AK10 plasticizer silicone oil	Wacker Chemie, Munich, Germany
Ammonium persulfate (APS), 10% (w/v)	Roth, Karlsruhe, Germany
Aminopropyl-triethoxysilane (APTES)	Sigma-Aldrich, Taufkirchen, Germany
Astrocyte growth supplement (AGS)	Sciencell, Carlsbad, USA
BC Assay Reagent A+B	Interchim, Wörgl, Österreich
BC Assay Reagent 1+2	Roth, Karlsruhe, Germany
CDP-Star	Roche, Penzberg, Germany
Chloroform	Roth, Karlsruhe, Germany
Coomassie®Brillant Blue R-250	Sigma-Aldrich, Taufkirchen, Germany
Connective tissue growth factor	Self purification
Connective tissue growth factor	Prospec, Rehovot, Israel
Connective tissue growth factor	EMP, Ingolstadt, Germany
cross linker 210	Evonik Hanse GmbH, Gesthach, Germany
Desoxynukleosid-Triphosphate (dNTPs)	Qiagen, Hilden, Germany
Dimethylsulfoxid (DMSO)	Roth, Karlsruhe, Germany
Divinyl tetramethyl disiloxane	Evonik Hanse GmbH, Gesthach, Germany

DL-Dithiothreitol (DTT)	Sigma-Aldrich, Taufkirchen, Germany
Dulbecco's Modified Eagle Medium (DMEM) F12	PAA The Cell Culture Company, Pasching, Austria
Dulbecco's Modified Eagle Medium (DMEM)	PAA The Cell Culture Company, Pasching, Austria
EDTA	Roth, Karlsruhe, Germany
Ethanol 100%	Roth, Karlsruhe, Germany
Ethidiumbromide	Serva, Heidelberg, Germany
Fetal calve serum (FCS)	Biochrom AG, Berlin, Germany
Fluorescent Mounting Medium	DakoCytomation, Hamburg, Germany
Formaldehyde	Roth, Karlsruhe, Germany
Epon	Serva, Heidelberg, Germany
Gelatine	Sigma-Aldrich, Taufkirchen, Germany
Glutaraldehyde, 25% in water	Serva, Heidelberg, Germany
Glycerine	Roth, Karlsruhe, Germany
Glycin	Merck, Darmstadt, Germany
Guanidin HCl	Roth, Karlsruhe, Germany
Hydrochloric acid (37%)	Merck, Darmstadt, Germany
Isoflurane	Baxter, Heidelberg, Germany
Isopropanol	Roth, Karlsruhe, Germany
Ketamine	Wirtschaftsgenossenschaft Deutscher Tierärzte (WDT), Garbsen, Germany
Luminata Forte, Western HRP	Millipore Cooperation, Billerica, USA
Magnesium chloride (50 mM)	Bioline, Luckenwalde, Germany
Methanol	Merck, Darmstadt, Germany
methylhydrosiloxane-dimethylsiloxane AB116655 cross linker	ABCR GmbH, Karlsruhe, Germany
Milk powder (MM)	Roth, Karlsruhe, Germany
N,N,N`,N`,-Tetramethylethylendiamine, (TEMED)	Roth, Karlsruhe, Germany
Paraformaldehyde (PFA)	Sigma-Aldrich, Taufkirchen, Germany

PBS	PAA The Cell Culture Company, Pasching, Austria
Penicilllin-Streptomycin	PAA The Cell Culture Company, Pasching, Austria
peqGold TriFast™ (Trizol)	PeqLab, Erlangen, Germany
Phalloidin	Sigma-Aldrich, Taufkirchen, Germany
Phosphatase-Inhibitor-Mix	Sigma-Aldrich, Taufkirchen, Germany
Potassium chloride	Roth, Karlsruhe, Germany
Potassium dihydrogen phosphate	Roth, Karlsruhe, Germany
Protease-Inhibitor-Mix M	Serva Electrophoresis GmbH, Heidelberg, Germany
Proteinase K	Sigma-Aldrich, Taufkirchen, Germany
Pt-catalyst 510	Evonik Hanse GmbH, Gesthach, Germany
Rotiphorese® Gel 30 (30 % Acrylamid, 0.8 % Bisacrylamid; 37.5:1)	Sigma-Aldrich, Taufkirchen, Germany
Saccharose	Roth, Karlsruhe, Germany
SDS (Sodium dodecylsulfat)	Roth, Karlsruhe, Germany
SIH-terminated polydimethyl siloxane	Evonik Hanse GmbH, Gesthach, Germany
Sodium chloride	Roth, Karlsruhe, Germany
Sodium dihydrogen phosphate	Merck, Darmstadt, Germany
Sodium hydroxide	Roth, Karlsruhe, Germany
Sodium phosphate	Roth, Karlsruhe, Germany
SYBR-Green I	Qiagen, Hilden
Tissue-Tek®	Sakura, Zoeterwoude, Netherlands
Transforming Growth Factor 2 (TGF- β2)	R&D Systems, Minneapolis, USA
Tris HCl	Roth, Karlsruhe, Germany
Triton X 100	Roth, Karlsruhe, Germany
Tween 20	Roth, Karlsruhe, Germany
Vectashield Mounting Medium for Fluorescence with DAPI	Vector Laboratories, Burlingame, USA

vinyl-functional polydimethylsiloxane	Evonik Hanse GmbH, Gesthach, Germany
Water Rotisolv (Rnase-free)	Roth, Karlsruhe, Germany
Xylazine	Serumwerk Bernburg, Bernburg, Germany

Table 3-1: Reagents

3.1.2. Enzymes and Reagent-Kits

Enzymes and Reagent-Kits	Source of supply
qScript™cDNA Synthesis Kit	Quanta Biosciencies, Gaithersburg, USA
Mango Taq	Bioline, Luckenwalde, Germany
Proteinase K	Roth, Karlsruhe, Germany
Taq DNA Polymerase	Self purification
Universal SYBR Green Master (ROX)	Roche, Mannheim, Germany
TaqMan®Fast Advanced Master Mix (2x)	ThermoFisher, Darmstadt, Germany

Table 3-2: Enzymes and Reagent Kits

3.1.3. Oligonucleotide primers and Taqman probes

Primer	Species	Orientation	Sequence
βB1	*mus musculus*	forward	GGAAGTGCCAGCTCATCAGT
βB1	*mus musculus*	reverse	GTGCGGGACAGAAACCTG
SV40	*mus musculus*	forward	GTGAAGGAACCTTACTTCTGTGGTG
SV40	*mus musculus*	reverse	GTCCTTGGGGTCTTCTACCTTTCTC
LacZ	*mus musculus*	forward	GCCGTCTGAATTTGACCTGA
LacZ	*mus musculus*	reverse	TCTGCTTCAATCAGCGTGCC
CAG-Cre	*mus musculus*	forward	ATGCTTCTGTCCGTTTGCCG
CAG-Cre	*mus musculus*	reverse	CCTGTTTTGCACGTTCACCG
Coin/Coin	*mus musculus*	forward	CACTTTCTACTCTGTTGAC
Coin/Coin	*mus musculus*	reverse	CCTTACATGTTTTACTAG

Exons2	*mus musculus*	forward	CCTGCTATGGGCCAGGACTG
Exons2	*mus musculus*	reverse	CCAAAAGGTGAGGCCTCTGC

Table 3-3: Oligonucleotide primers for genotyping

Primer	Species	Orientation	Position	Sequence
CTGF	*mus musculus*	forward	948-970	TGACCTGGAGGAAAACATTAAGA
CTGF	*mus musculus*	reverse	1038-1059	AGCCCTGTATGTCTTCACACTG
GFAP	*mus musculus*	forward	1156-1174	TCGAGATCGCCACCTACAG
GFAP	*mus musculus*	reverse	1201-1222	GTCTGTACAGGAATGGTGATGC
CD44	*mus musculus*	forward	2270 - 2289	ACTCAAGTGCGAACCAGGAC
CD44	*mus musculus*	reverse	2338 - 2357	GCCAAGATGATGAGCCATTC
RPL32	*mus musculus*	forward	29-47	GCTGCCATCTGTTTTACGG
PRL32	*mus musculus*	reverse	107-126	TGACTGGTGCCTGATGAACT
Trpc1	*mus musculus*	forward	1233-1258	TGAACTTAGTGCTGACTTAAAGGAAC
Trpc1	*mus musculus*	reverse	1307-1287	CGGGCTAGCTCTTCATAATCA
Trpv2	*mus musculus*	forward	1578-1598	CACCATAGTTGCCTACCACCA
Trpv2	*mus musculus*	reverse	1621-1640	GTCGCTTTTGATGAGGGAAT
Trpm7	*mus musculus*	forward	205-224	AGACGCTTTCCGATAGATGG
Trpm7	*mus musculus*	reverse	294-317	AAAGTGCTCTCTATCCAGGATTTC
Piezo1	*mus musculus*	forward	1064-1083	ATGAGGAGCATGAGCTGGAA
Piezo1	*mus musculus*	reverse	1130-1148	GTGGTCATGGGCATCTCAC
Piezo2	*mus musculus*	forward	5211-5229	GGACACAATCGACGAGCAC
Piezo2	*mus musculus*	reverse	5305-5323	GCAGGGTCGCTTCAGTGTA
Caveolin 1	*mus musculus*	forward	389-407	AACGACGACGTGGTCAAGA
Caveolin 1	*mus musculus*	reverse	474-493	CACAGTGAAGGTGGTGAAGC
Caveolin 2	*mus musculus*	forward	144-163	CCTCACCAGCTCAACTCTCA

Caveolin 2	*mus musculus*	reverse	245-269	CACATATTTGCTGATTTCAAAGAGA
CD44	*human*	forward	1942-1960	GACACATTCCACCCCAGTG
CD44	*human*	reverse	2048-2067	TGGAATTTGGGGTGTCCTTA
RPL32	*human*	forward	319 - 338	GAAGTTCCTGGTCCACAACG
RPL32	*human*	reverse	377 - 395	GCGATCTCGGCACAGTAAG

Table 3-4: Oligonucleotide primers for Real-time RT-PCR

All primers were purchased from Invitrogen, Karlsruhe, Germany.

Target	Probe	Amplicon Length	Source of Supply
RPL32	Mm02528467_g1	69	ThermoFisher Scientific, Darmstadt, Germany
GFAP	Mm01253033_m1	75	ThermoFisher Scientific, Darmstadt, Germany
CTGF	Mm01192933_g1	67	ThermoFisher Scientific, Darmstadt, Germany

Table 3-5: Taqman® probes

3.1.4. Antibodies and molecular weight standards

Protein	Primary antibody	Source of supply
CTGF	polyclonal goat anti-CTGF	Santa Cruz, Dallas, USA
GFAP	polyclonal chicken anti-GFAP	LifeSpan Biosciences, Seattle, USA
Vimentin	polyclonal goat anti-Vimentin	Sigma-Aldrich, Taufkirchen, Germany
CD44	polyclonal mouse anti-CD44	R&D systems, Minneapolis, USA

CD44	polyclonal rabbit anti-CD44	antibodies-online GmbH, Aachen, Germany
β-galactosidase	polyclonal rabbit anti- β-galactosidase	icllab, Portland, Germany
CD31	polyclonal goat anti-CD31	R&D systems, Minneapolis, USA
β-catenin	polyclonal rabbit anti- β-catenin	Cell Signaling Technology, Danvers, MA, USA
Glutamine synthetase	polyclonal goat anti-Glutamine synthetase	Santa Cruz, Dallas, USA
CTGF	polyclonal rabbit anti-CTGF	GeneTex, Irvine, USA
α-tubulin	polyclonal rabbit anti- α-tubulin	Rockland Immunochemicals, Limerick, USA
Caveolin1	polyclonal rabbit anti-Caveolin1	BD Life Sciences, Heidelberg, Germany
Caveolin1	polyclonal rabbit anti-Caveolin1	Cell Signaling Technology, Danvers, MA, USA
myelin basic protein (MBP)	polyclonal rabbit anti-MBP	Dako, Agilent Technologies Company, Santa Clara, USA
Calcium binding adaptor molecule 1 (IBA1)	polyclonal rabbit anti-IBA1	Wako, Neuss, Germany

Table 3-6: Primary Antibodies for Western blot, immunohistochemical and immunocytochemical staining

Secondary antibody	**Source of supply**
Alexa Fluor® 488 goat anti-chicken IgG (H+L)	Eurogene, Oregon, USA
Alexa Fluor® 488 goat anti-rabbit IgG (H+L)	Invitrogen, Carlsbad, USA
Alexa Fluor® 488 goat anti-mouse IgG (H+L)	Invitrogen, Carlsbad, USA
Alexa Fluor® 488 donkey anti-goat IgG (H+L)	Biotium, Inc., Fremont, CA, USA
Alexa Fluor® 647 donkey anti-mouse IgG (H+L)	Invitrogen, Carlsbad, USA
Alexa Fluor® 647 donkey anti-rabbit IgG (H+L)	Invitrogen, Carlsbad, USA
Cy™3-conjugated AffiniPure goat anti-rabbit IgG (H+L)	Jackson Research Laboratories, West Grove, PA, USA
Biotinylated anti-goat IgG (H+L)	Vector Laboratories, Burlingame, CA, USA
Biotinylated anti-rabbit IgG (H+L)	Vector Laboratories, Burlingame, CA, USA
rabbit anti-chicken IgG-h+l HRP	Bethyl Laboratories, Montgomery, USA

goat anti-rabbit IgG-h+l AP	Bethyl Laboratories, Montgomery, USA
goat anti-rabbit HRP	Cell Signaling Technology, Danvers, MA, USA
goat anti-rabbit AP	Cell Signaling Technology, Danvers, MA, USA
horse anti-mouse HRP	Cell Signaling Technology, Danvers, MA, USA
donkey anti-goat IgG-h+l HRP	Bethyl Laboratories, Montgomery, USA
Streptavidin Alexa Fluor® 488	Invitrogen, Carlsbad, USA

Table 3-7: Secondary Antibodies for Western blot, immunohistochemical and immunocytochemical staining

Description	Source of supply
Gene Ruler 100bp Plus DNA Ladder	Fermentas, Schwerte, Deutschland
EZ-Run Pre-Stained Rec Protein Ladder	Fisher Scientific, Schwerte, Deutschland

Table 3-8: molecular weight standards

3.1.5. Chemical composition of gels, solvents and buffers

Solvents and buffers	Compounds
0.1M Cacodylate Buffer	10.7g Cacodylate acid in 500 ml dH_2O
0.1 M Phosphate Buffer (Php), pH 7,4	100 ml 0.2 M Na_2HPO_4 x $2H_2O$ with 0.2 M NaH_2PO_4 x H_2O, pH 7.4 dilute with dH_2O to 0.1M
10 x Electrode Buffer	250mM Tris/HCl 400mM Glycine 1% (w/v) SDS solved in dH_2O; ad 1 l
Coomassie-Destaining Solution	500 ml Methanol 10 ml Acetic acid filled up with H_2O to 1 l
Coomassie-Staining Solution	40 ml Methanol 2 ml Acetic acid 0.2 g Coomassie-Brilliant Blue R-250 dilute in dH_2O, ad 100 ml
Detection Buffer, pH 9	15.76 g 0,1 M Tris/HCL (pH 6,8) 5.84 g 0,1 M NaCl dilute in dH_2O; ad 1 l
EM fixative	2.5% paraformaldehyde 2.5% glutaraldehyde in 0.1M cacodylatbuffer
Epon stem A	62ml Glycidether 100 with 100ml DDSA
Epon stem B	100ml Glycidether 100 with 89ml NMA
LacZ fixative	48,4 ml 0.1MPhp pH7.3 100µl 1M $MgCl_2$ 1ml 0.250M EGTA pH7.3 0.4ml Glutaraldehyde
LacZ-Staining Solution	72ml LacZ Washing Buffer

	3ml X-Gal (25mg/ml in DMSO) 0.159g $K_4Fe(CN)_6$ $3H_2O$ 0.123g $K_3Fe(CN)_6$
LacZ-Washing Solution	1ml 1M MgCl2 5ml 1% NaDC 5ml 2% Tergitol 489ml 0.1M Php pH 7.3
Lyse Buffer	1.87 g KCL 5ml 1M Tris-HCl pH 8.3 255mg $MgCl_2$-$6H_2O$ 50mg galantine 2.25 ml Tergitol 2.25 ml Tween 20
Mowiol with Dapi	2.4 g Mowiol 4-88 6.0 g Glycerin 6.0 ml H_2O dest. 12.0 ml 0.2 M Tris-HCl (pH 8.5) 25.0 ml DABCO per 1.0 ml DAPI (1:10)
PBS, 10x, pH 7,4	80 g NaCl 2 g KCl 4.4 g Na_2HPO_4 2.4 g KH_2PO_4 dH_2O ad 1 l, autoclave
SDS-Solution, 10 % (w/v)	10 g SDS in dH_2O; ad 100 ml
SDS-PAGE-Running Buffer, 10x	250mM Tris/HCl 400mM Glycin 1% (w/v) SDS in dH_2O; ad 1 l
SDS-Sample Buffer, 4x	0.25M Tris/HCl, pH 6.8 30% Glycerin 8% (w/v) SDS 0.02% (w/v) Bromphenolblau 0.3M DTT and 10% β-Mercaptoethanol
TBE, 10x	108g Tris-base 55g boric acid 40ml 0.5M EDTA pH 8.0 dilute in H_2O, ad 1 l pH 7.0
TBS, 10x, pH 7,4	30 g Tris 80 g NaCl 2 g KCl dH_2O ad 1 l, autoclave
TBST, 1x	100 ml 10x TBS 0.05% (v/v) Tween 20 dH_2O ad 1 l
Transfer Buffer, 10x	5.8 g Tris 2.9 g Glycine 200 ml Methanol 3.7 ml 10% (w/v) SDS dilute in dH_2O, ad 1 l
Tris/HCl, 1.0 M, pH 6.8	121.14 g Tris dH_2O; ad 1 l
Tris/HCl, 1.5 M, pH 8.8	181.71 g Tris

	dH_2O; ad 1 l
Washing Buffer for protein isolation	0.3 M Guanidin HCL in 95 % Ethanol

Table 3-9: Chemical composition of gels, solvents and buffers

3.1.6. Laboratory Equipment

Description	Source of supply
Axiovert 40 CFL	Zeiss, Göttingen, Germany
CFX Connect Real-Time System	BioRad, Munich, Germany
Embedder	EM TP Leica, Wetzlar, Germany
FastPrep 24TM	MP Biomedicals, Burlingame, USA
HeatSealer RS 232	4titude, Berlin, Germany
Hera Cell 150 incubator	Heraeus, Hanau, Germany
Hera Safe steril working bench	Heraeus, Hanau, Germany
Inolab pH-Meter	Inolab pH-Meter
Julabo SW20 Wasserbad	JulaboLabortechnik GmbH, Seelbach
Kern PJL 2100-2M Analysenwaage	Kern & Sohn GmbH, Balingen-Fommern
LAS 3000 Intelligent Dark Box	Fujifilm, Düsseldorf
Memmert water bath	Memmert GmbH, Schwabach
Mettler AE 163 special accurancy scales	Mettler Toledo, Giessen
Microm HM 500 OM Kryostat	Microm International, Walldorf
Mikroskop Axio Imager.Z1	Zeiss, Göttingen
MilliQ Plus PF water purification system	Millipore Corporation, Billerica, USA
Model 45-101-i ClassII Electrophoresis System	Peqlab Biotechnologie GmbH, Erlangen
NanoDrop-1000 Spectrophotometer	Peqlab Biotechnologie GmbH, Erlangen
Pipetman Pipets	Gilson, Middleton, USA
Research Pipets	Eppendorf, Hamburg, Germany
Roti®speed mixing tool	Carl Roth GmbH, Karlsruhe, Germany
Semi-Dry Electrophoretic Transfer Cell	Peqlab Biotechnologie GmbH, Erlangen
Sunrise-Basic ELISA Reader	Tecan Austria GmbH, Grodig, AUS

SuperCut 2050	Cambridge Instruments, Nußloch, Germany
Systec V75 Autoclave	Systec GmbH, Wettenburg
Thermomixer comfort	Eppendorf, Hamburg
TonoLab Tonometer	Icare Finnland, Helsinki, Finnland
universal oven Memmert UF30Plus	Memmert GmbH, Schwabach, Germany
UV-light screen	Bachhofer Laboratoriumsgeräte, Reutlingen, Germany
Ultracut E-Ultramicrotom	Reichert-Jung, Kirchseeon, Germany
Ultra Thurax	Biolabproducts, Bebensee, Germany
Vortex Genie 2	Scientific Industries Inc., New York, USA
Centrifuges 5415D, 5415R, 5804R, 5810R	Eppendorf, Hamburg, Germany

Table 3-10: Laboratory Equipment

3.1.7. Consumables

Description	Source of supply
µ-dish 35mm, high, uncoated	ibidi, Martinsried, Germany
3MM Blotting ("Whatman") –Paper	Neolab, Heidelberg, Germany
Biosphere Filter Tips	Sarstedt, Nürnbrecht, Germany
CellScraper	Sarstedt, Nürnbrecht, Germany
Culture Slides	BD Falcon, Bedford, USA
Cover slips, 24 x 60mm	Menzel-Gläser, Braunschweig, Germany
Dispomed Syringe, single use	Dispomed Witt oHG, Geinhausen, Germany
EasyFlasks Nunclon™ Δ T25, T75	Nunc, Roskilde, Denmark
Ecoflo Dissecting instruments	Dispomed Witt oHG, Geinhausen, Germany

Falcon“ Reaction Tubes 15 ml, 50 ml	Sarstedt, Nürnbrecht, Germany
Glasware	Schott, Roth, VWR, Germany
Green Nitrile gloves	Kimtech, Koblenz, Germany
Hard-Shell® PCR plates 96-well, thin-wall	BioRad, Munich, Germany
Liquid Blocker PAP-Pen	SCI Science Services, München, Germany
Lysing Matrix D	MP Biomedicals, Burlingame, USA
Multidishes Nunclon™ Δ 6-	Nunc, Roskilde, Denmark
Multi-Reaction Tubes 0,5 ml; 1,5 ml; 2,0 ml	Roth, Karlsruhe, Germany
Omnifix syringe, sterile	B. Braun, Wertheim, Germany
Optically Clear Heat Seal	BioRad, Munich, Germany
Parafilm	Pechiney Plastic Packaging, Chicago, USA
Pasteurpipets	Brand, Wertheim, Germany
PCRSoftTubes, 0.2ml	Biozym, Hessisch Oldendorf, Germany
Personna RRazor blades	American Safety Razor Company, Verona, USA
Pipet tips	Sarstedt, Nürnbrecht, Germany
Petri dishes 94x16 mm PS	Greiner bio-one, Kremsmünter, Austria
Petrisoft 35, Collagen Coat 8kPa	Cell Guidance Systems Ltd, Cambridge, UK
Petrisoft 35, Collagen Coat 25kPa	Cell Guidance Systems Ltd, Cambridge, UK
Petrisoft 35, Collagen Coat, 50kPa	Cell Guidance Systems Ltd, Cambridge, UK
Pro Free Blue gloves	Ulma, Neu-Ulm, Germany
PVDF membrane (Roti®-PVDF), 0.45µm	Roth, Karlsruhe, Germany
Serological pipets	Sarstedt, Nürnbrecht, Germany
Sterican injection cannula	B. Braun, Wertheim, Germany
SuperFrost®Plus object slides	Menzel-Gläser, Braunschweig, Germany

Table 3-11: Consumables

3.2. Cell linies

For *in vitro* studies murine optic nerve astrocytes and human trabecular meshwork (HTM) cells were used. Murine optic nerve astrocytes were isolated from the ON of CD1 wild type mice (see 3.7.3.) and HTM cells were available in the Institute of Human Anatomy and Embryology and the protocol was published previously (Stamer et al. 1995, Stamer et al. 2000, Tamm et al. 1996, 1996).

3.3. Animal models

3.3.1. Animals and animal husbandry

βB1-CTGF1, $CTGF^{LacZ+/-}$, $CTGF^{Coin/Coin}$;CAGGCre-ER mice and CD1 wild type mice were used in the *in vivo* experiments of this study. βB1-CTGF1 mice were generated in our own working group and provided by Prof. Dr. R. Fuchshofer (Junglas et al. 2012). $CTGF^{LacZ/+}$ were generated and kindly provided by M. Gannon (Department of Medicine, Division of Diabetes, Endocrinology, and Metabolism, Vanderbilt University Medical Center, Nashville, Tennessee; Crawford et al., 2009). $CTGF^{Coin/Coin}$ were generated and kindly provided by E. Canalis (Department of Research, Saint Francis Hospital and Medical Center, Hartford, Connecticut; (Canalis et al. 2010). CD1 wild type and CAGGCre-ER mice were bred in the animal facility of Prof. Dr. E. Tamm, Institute of Human Anatomy and Embryology, University of Regensburg, started with a first breeding pair purchased from Charles River, Sulzfeld, Germany. Mice were housed under standardized conditions of 62% air humidity and 21°C room temperature. Feeding was *ad libitum.* Animals were kept at a 12-hour light/ dark cycle (6:00 – 18:00), accordingly to the ARVO Statement for the use of animals in ophthalmic and vision research.

3.3.2. βB1- CTGF mice

The βB1-CTGF1 mice carry a plasmid, expressing murine CTGF cDNA under the control of the chicken βB1 promotor, resulting in a high and specific expression of the transgene in the lens fibers of the mouse eye. Additionally, the plasmid contains the simian virus 40 (SV-40) small T-intron and the SV-40 poly(A) sequence, to ensure a higher stability of the CTGF cDNA. For the *in vivo* experiments the βB1-CTGF1 mice were breed with CD1 wild type mice to receive the appropriate control group for each experiment. Genotyping of the mice was performed as described in 3.4.2.1.

Figure 3-1: βB1 construct of βB1-CTGF1 mice.

3.3.3. CTGF$^{LacZ/+}$ mice

CTGF$^{LacZ/+}$ mice were generated and kindly provided by M. Gannon (Department of Medicine, Division of Diabetes, Endocrinology, and Metabolism, Vanderbilt University Medical Center, Nashville, Tennessee; (Crawford et al. 2009). In this mouse line the CTGF gene is destroyed by replacing the coding sequence of CTGF within the exon 3 to the end of the coding sequence in exon 5 with a transmembrane domain-LacZ cassette (Crawford et al., 2009). As WT animals were used as controls in the following experiments, heterozygous CTGF$^{LacZ/+}$ mice were mated, resulting WT and CTGF$^{LacZ+/-}$ mice. Since the homozygous knockout of CTGF is embryonic lethal, no homozygous offspring were expected.

3.3.4. CD1 wildtype mice

The initial CD1 wild type mice was purchased form Charles River, Sulzfeld, Germany and afterwards bred in the animal facility of the Institute of Human Anatomy and Embryology (Prof. Dr. E. Tamm), University of Regensburg.

3.3.5. CTGF$^{Coin/Coin}$;CAGGCre-ER mice

CTGF$^{Coin/Coin}$ mice were generated and kindly provided by E. Canalis (Department of Research, Saint Francis Hospital and Medical Center, Hartford, Connecticut; Canalis et al., 2010). By the conditional-by-inversion (COIN) approach a conditional null allele of CTGF was generated. The COIN intron was inserted into exon2, resulting in splitting of exon2 in two exons. This modification allows a regular expression of CTGF. The COIN intron is flanked by two loxP sequences, after Cre recombination the two loxP sites recombine and thereby invert the COIN intron, resulting in the inactivation of CTGF (Canalis et al., 2010). CTGF$^{Coin/Coin}$ mice were bred with CAGGCre-ER mice (Jackson Laboratory, Bar Harbor, Maine, USA). Finally, Mice with two Coin-Introns (CTGF$^{Coin/Coin}$) were crossed with CTGF$^{Coin/Coin}$;CAGGCre-ER mice, which are heterozygous for the Cre-recombinase, to receive an cohort of experimental mice (CTGF$^{Coin/Coin}$;CAGGCre-ER) mice and control mice (CTGF$^{Coin/Coin}$).

3.4. Biomolecular Techniques

3.4.1. Isolation of mouse tail DNA

For genotype determination of different mouse strains, a 2 mm piece of the mouse tail was cut of under isoflurane anesthesia to obtain genomic DNA. The tissue was lysed under addition of 200 µl Lysebuffer and 5 µl proteinase K overnight at 55°C. The next day, proteinase K was inactivated at 95°C for 10 min and centrifugated for 10 min. DNA samples were stored at 4°C.

3.4.2. Genotyping

Polymerase chain reaction (PCR) was used to determine genotypes of in this study used animals. For each mouse strain specific primer (Table 3-) and reaction mix (Table 3-12, 13, 16, 18, 19, 20) were used. PCR products were analyzed by agarose gel electrophorese.

3.4.2.1. Genotyping of βB1-CTGF1 mice

For genotyping of βB1-CTGF1 mice two different PCRs (βB1 and SV40) were performed, which are both specific for transgenic animals. PCR reaction mix are shown in table 3-12 and 3-13. Appropriate cycler programs are shown in table 3-14 and 3-15.

βB1 PCR	
H_2O	11.25µl
Q buffer	1.5µl
βb1 forward primer (10 µM)	0.3µl
βb1 reverse primer (10 µM)	0.3µl
dNTP`s (10mM)	0.3µl
Taq DNA-polymerase	0.15µl
DNA	1.2µl

Table 3-12: Reaction mix for βB1 PCR

SV40 PCR	
H2O	7.15µl
Q buffer	1.5µl
SV40 forward primer (10 µM)	0.3µl
SV40 reverse primer (10 µM)	0.3µl
dNTP`s (10mM)	0.3µl
Taq DNA-polymerase	0.15µl
glycerol	3µl
$MgCl_2$ (25mM)	0.3µl
DNA	2µl

Table 3-13: Reaction mix for SV40 PCR

βB1 PCR Cycler Program			
	temperature (°C)	duration	
initiation	96	2min	
denaturation	94	30sec	
annealing	65	30sec	x32
elongation	72	20sec	
elongation	72	2min	
hold	4	∞	

Table 3-14: βB1 PCR Cycler Program

SV40 PCR Cycler Program			
	temperature (°C)	duration	
initiation	94	2min	
denaturation	94	30sec	
annealing	55	30sec	x 35
elongation	72	45sec	
elongation	72	5min	
hold	4	∞	

Table 3-15: SV40 PCR Cycler Program

3.4.2.1. Genotyping of CTGF$^{LacZ/+}$ mice

Genotyping of CTGF$^{LacZ/+}$ mice was performed with two primers specific for the LacZ cassette. Reaction mix is shown in table 3-16. Appropriate cycler program is shown in table 3-17.

CTGF$^{LacZ/+}$ PCR	
H_2O	16.55 µl
5x PCR buffer	5 µl
LacZ forward primer (10 µM)	0.5 µl
LacZ reverse primer (10 µM)	0.5 µl
dNTP's (10 mM)	0.5 µl
$MgCl_2$ (50 mM)	0.75 µl
Mango Taq DNA-polymerase	0.15 µl
DNA	1 µl

Table 3-16: Reaction mix for CTGF$^{LacZ/+}$ PCR

$CTGF^{LacZ/+}$ PCR Cycler Program			
	temperature (°C)	duration (min)	
initiation	95	6	x 30
denaturation	95	1	
annealing	50	1	
elongation	72	1	
elongation	72	6	
hold	4	∞	

Table 3-17: $CTGF^{LacZ/+}$ PCR Cycler Program

3.4.2.3. Genotyping of $CTGF^{Coin/Coin}$;CAGGCre-ER mice

For genotyping of $CTGF^{Coin/Coin}$;CAGGCre-ER mice three individual PCR, specific either of the Exon2 WT allele, the Coin-Intron or the Cre recombinase were performed. Reaction mix are shown in table 3-18, 3-19 and 3-20. Appropriate cycler programs are shown in table 3-21, 3-22 and 3-23.

CAGGCre PCR	
H_2O	9.45µl
5x PCR buffer	3µl
LacZ forward primer (100µM)	0.3µl
LacZ reverse primer (100µM)	0.3µl
dNTP's (10mM)	0.3µl
$MgCl_2$ (50mM)	0.5µl
Taq DNA-polymerase	0.15µl
DNA	1µl

Table 3-18: CAGGCre PCR Cycler Program

Coin/Coin PCR	
H_2O	16.55 µl
5x PCR buffer	5 µl
LacZ forward primer (100µM)	0.5 µl
LacZ reverse primer (100µM)	0.5 µl
dNTP_`s (10mM)	0.5 µl
$MgCl_2$ (50mM)	0.75 µl
Mango Taq DNA-polymerase	0.15 µl
DNA	1 µl

Table 3-19: Coin/Coin PCR Cycler Program

Exon2 PCR	
H_2O	16.55 µl
5x PCR buffer	5 µl
LacZ forward primer (100µM)	0.5 µl
LacZ reverse primer (100µM)	0.5 µl
dNTP's (10mM)	0.5 µl
$MgCl_2$ (50mM)	0.75 µl
Taq DNA-polymerase	0.15 µl
DNA	1 µl

Table 3-20: Exon2 PCR Cycler Program

CAGGCre PCR Cycler Program			
	temperature (°C)	duration	
initiation	95	3 min	x34
denaturation	95	30 sec	
annealing	61	30 sec	
elongation	72	35 sec	
elongation	72	5min	
hold	4	∞	

Table 3-21: CAGGCre PCR Cycler Program

Coin/Coin PCR Cycler Program			
	temperature (°C)	duration	
initiation	94	6 min	x 40
denaturation	94	30 sec	
annealing	50.4	30 sec	
elongation	72	30 sec	
elongation	72	6 min	
hold	4	∞	

Table 3-22: Coin/Coin PCR Cycler Program

Exon2 PCR Cycler Program			
	temperature (°C)	duration	
initiation	94	6 min	x 35
denaturation	94	30 sec	
annealing	60	30 sec	
elongation	72	30 sec	
elongation	72	6 min	
hold	4	∞	

Table 3-23: Exon2 PCR Cycler Program

3.4.3. Agarose gel-electrophorese

After amplification, PCR products were analyzed by agarose gel-electrophorese. Therefore, 1 g agarose was dissolved in 100ml TBE buffer and 3 µl Ethidium bromide (EtBr) was added to a final concentration of 50 ng/ml. The characteristic of EtBr to intercalate into DNA was utilized to make the DNA fragments visible under UV light. 12µl of each sample was loaded on the gel and separated for 30 min at 120 V. To determine the size of the PCR products an additional standard DNA ladder was loaded on the gel. DNA fragments were visualized and analyzed under the UV light (302nm).

3.5. Expression analysis

3.5.1. RNA isolation

RNA from mouse tissue as well as from human and murine cells was isolated after Chomczyski and Sacchi (Chomczynski & Sacchi 1987).For detachment of both cell types and digestion of mouse tissue and cells peqGold TriFast™ Trizol reagent was used.

PeqGold TriFast™ Trizol is a single-phase solution containing phenol and guanidinisothiocyanat. By addition of chloroform three different phases, the aqueous phase containing the RNA, the interphase including the DNA and the organic phase containing proteins, are generated. RNA isolation was performed as follows according to the manufactures instructions. 500 µl peqGold TriFast™ Trizol reagent was added to the mouse tissue and cell culture samples. Anterior eye segments and retinae were digestated via the Ultra Thurax (Biolabproducts, Bebensee, Germany), optic nerves, optic nerve heads and corneal scleral rims with Shredder Tubes (Lysing Matrix D, MP Biomedicals, Burlingame, USA) via the FastPrep-24™ instrument (MP Biomedicals, Burlingame, USA) and cells were removed by using a cell scraper. Phase separation was made by adding 200 µl chloroform, shaking and centrifugation at 12000 rpm for 20 min. Aqueous phase containing the RNA was transferred to a new tube and 250 µl isopropanol was added to precipitate RNA and incubated overnight at 4°C. After centrifugation (12000 rpm, 20 min) the supernatant was removed, and the pellet was washed twice with 75 % ethanol and centrifugation at 12000 rpm for 10 min. RNA pellet was finally dissolved in 10 µl RNase free water and stored at -80°C.

3.5.2. RNA quantification

With the NanoDrop photometer the RNA concentration and quality were measured. RNA concentration was determined with the absorption measurement at the wavelength 260 nm. To detect protein and solvent contamination an additional measurement at the absorptions spectrum 220 nm to 350 nm was made. For pure RNA the A260/A280 quotient should be between 1.9-2.1.

3.5.3. cDNA synthesis

At the procedure of the cDNA synthesis, the mRNA is transcribed via the enzyme Reverse Transcriptase. Therefore, the appropriate amount of RNA was mix with qScript Reaction Mix (5x) and qScript Reverse Transcriptase and the cycling program mentioned below (Table 3-23) was carried out (+RT). To test contamination of RNA negative controls, without Reverse Transcriptase) were performed for each sample (-RT).

Reagent	Amount
RNA	0.1 – 0.5µg
qScript Reaction Mix (5x)	2µl
qScript Reverse Transcriptase	0.5µl
RNase free H2O	to 7.5µl

Table 3-24: Reaction mix for cDNA synthesis

Temperature	Duration
22 °C	5 min
42°C	30 min
85 °C	5 min
4°C	hold

Table 3-25: Cycler Program for cDNA synthesis

3.5.4. Real-time RT-PCR

The relative mRNA expression for the *in vitro* and *in vivo* experiments was determined via Real-time RT-PCR. The analysis was performed on the CFX Connect Real-Time System (BioRad, Munich, Germany), with the temperature profile as follows: 50 cycles of 20 s melting at 94°C, 10 s of annealing at 60°C and 20 s of extension at 60°C. All primers were purchased from Invitrogen and extended over exon-intron boundaries. RNA that was not reverse transcribed served as negative control (-RT) for Real-time RT-PCR. For relative quantification of the experiments, *RPL32* was used as a housekeeping gene. Quantification was performed using Bio-Rad iQ5 Standard Edition software version 2.0.148.60623 (BioRad). The mean value obtained from untreated cells or wild type mice was set at 1. The reaction mix was performed was follows.

Reagent	Amount for 1x reaction	
Universal SYBR Green Master (ROX)	7.5µl	
Forward Primer	2.5µl	Final concentration 300mM
Reverse Primer	2.5µl	Final concentration 300mM
Nuclease-free water	2.2µl	
template (+RT, -RT, nuclease-free water)	0.3µl	

Table 3-26: Reaction mix for Real-Time RT-PCR.

3.5.5. TaqMan® Gene Expression Assay

As in the ON and ONH of 1-month-old βB1-CTGF1 mice CTGF and GFAP are expressed in very low levels. Therefore TaqMan® Gene Expression Assay were performed for an improved amplification in comparison to the conventional Real-time RT-PCR. The

sequence specific Taqman® probes were obtained from ThermoFisher Scientific (Darmstadt, Germany), containing an Applied Biosystems™ FAM dye label on the 5'end and a minor groove binder (MGB) and non-fluorescent quencher (NFQ) on the 3'end. A suitable TagMan™Fast Advanced Master Mix, containing AmpliTaq®Fast DNA Polymerase, uracil-N glycosylase (UNG), dNTPs with dUTP, ROX™ dye (as a passive reference) and optimized buffer components was used for TaqMan® Gene Expression Assay. During denaturation step the signal form the fluorescent dye on the 5'end is quenched by the NFQ on the 3'end. In the next step, the specific TaqMan probe anneal to its specific target sequence. Taq DNA polymerase starts to synthesize the new strand. At the position of the TaqMan probe the 5'nuclease activity cleaves the probe and thereby separating the dye from the quencher. The produced fluorescent signal can be detected comparable to the conventional Real-time RT-PCR.

Component	Amount (µl)
TaqMan®Fast Advanced Master Mix (2x)	10
TaqMan® probe	1
cDNA template	2
Nuclease-free water	7
Total volume per reaction	20

Table 3-27: Reaction mix for TaqMan® Gene Expression Assay

TaqMan® Gene Expression Assay Cycler Program			
	temperature (°C)	duration (sec)	
Polymerase activation	95	20	
denaturation	95	1	x50
anneal/extend	60	20	

Table 3-28: TaqMan® Gene Expression Assay Cycler Program

3.6. Biochemical techniques

3.6.1. Protein isolation via peqGold TriFast™ Trizol method

Besides RNA isolation, the peqGold TriFast™ Trizol method is utilized for protein isolation in the in vitro and in vivo experiments. Therefore, the total protein in the remaining organic phase contains the total protein, which was precipitated by addition of 750µl isopropanol. After three washing steps with Washing Buffer for protein isolation (0.3 M Guanidine HCL in 95 % Ethanol) for 20 min following a centrifugation step for 5 min at 700g and the final washing step with 95% ethanol (7600g, 5min), the protein

samples are dried. Finally, the protein pellet was dissolved in 1% SDS, containing protease- and phosphatase inhibitor and stored for further use at -80°C.

3.6.2. Bicinchoninic Assay (BCA assay)

The BCA assay is a photometric method for protein concentration measurement. The method relies on two reactions. The peptide bonds of the proteins reduce the Cu^{2+} to Cu^{+} and this Cu^{+} chelate to a purple-colored complex that absorbs light at a wavelength at 562 nm. This colored complex was measured on the Sunrise-Basic ELISA Reader (Tecan Austria GmbH, Groding, Austria). A standard row was additionally applied to the measurement, by this the concentration of the protein of human and murine cells as well as mouse tissue can be determined as the color change is proportional to the total protein amount.

3.6.3. SDS polyacrylamide gel-electrophorese

Proteins were separated for further Western Blot analysis by SDS polyacrylamide gel-electrophorese (Laemmli 1970). Therefore, the suitable SDS polyacrylamide gel for the molecular weight of each protein was prepared, according to the following protocol (Table 3-29).

Reagent	**Stacking gel**	**Running gel**			
		6%	10%	12%	15%
dH2O	0.68µl	2.6µl	1.9µl	1.6µl	1.1µl
Rotiphorese® mix	0.17µl	1.0µl	1.7µl	2.0µl	2.5µl
1.5 M Tris/HCl pH 8.8	-	1.3µl	1.3µl	1.3µl	1.3µl
1.0 M Tris/HCl pH 6.8	0.13µl	-	-	-	-
10% SDS	0.01µl	0.05µl	0.05µl	0.05µl	0.05µl
10% APS	0.01µl	0.05µl	0.05µl	0.05µl	0.05µl
TEMED	0.001µl	0.004µl	0.002µl	0.002µl	0.002µl

Table 3-29: Components of SDS-gels.

The protein samples were blended with 5x Laemmli buffer and heated at 100°C for 5 min, for protein denaturation. After the polymerization of the gels, 25 µl of each sample was loaded on the gel. For determination of molecular protein weight an additional molecular weight standard was added to one line. The electrophoresis was performed at 20 mA for one gel for 1 to 1.5 h.

3.6.4. Semidry-Blotting

The proteins separated after the electrophoresis were then transferred on a PVDF membrane (pore size 0.45 µm) by semidry blotting. Therefor the membrane was activated in methanol for 1 min and the blots were assembled as follows: Cathode, 3 Whatman paper, Running gel, PVDF membrane, 2 Whatman paper, Anode. Blotting was performed at 14 V, 190 mA per gel for 45 min.

3.6.5. Detection of specific proteins

Protein bands of the target protein in the Western blot analysis were detected by specific antibodies. The primary antibody is specific for the antigen of the desired protein. The originated antibody-antigen complex is then being targeted by the secondary antibody. By conjugate the secondary antibody with horseradish peroxidase (HRP) or alkaline phosphatase (AP) the binding complex can be visualized by adding a HRP- or AP-substrate respectively. The protein synthesis analysis in this study were performed as follows.

Protein	Blocking solution	Primary antibody	Secondary antibody
CTGF	5% BSA in TBST	goat anti-CTGF 1:500 in 0.5% BSA in TBST	donkey anti-goat IgG HRP, 1:2000 in 0.5% BSA in TBST
GFAP	5% MM in TBST	chicken anti-GFAP, 1:10000 in 0.5% MP in TBST	rabbit anti-chicken IgG HRP, 1:2000 in 0.5% MP in TBST
Vimentin	5% MM in TBST	goat anti-Vimentin, 1:500 in 0.5% MP in TBST	donkey anti-goat IgG HRP, 1:2000 in 0.5% MP in TBST
CD44	5% BSA in TBST	mouse anti-CD44, 1:500 in 0.5% BSA in TBST	horse anti-mouse IgG HRP, 1:2000 in 0.5% BSA in TBST

α-tubulin	5% BSA in TBST	rabbit anti- α-tubulin, 1:2500 in 0.5% BSA in TBST	goat anti-rabbit IgG AP, 1:2000 in 0.5% BSA in TBST
Caveolin1	5%BSA in TBST	rabbit anit-Caveolin1 1:4000 in 0.5% BSA in TBST	goat anti-rabbit IgG HRP, 1:5000 in 0.5% BSA in TBST

Table 3-30: Used blocking solutions, primary and secondary antibodies used for Western Blot analysis.

3.6.6. Coomassie staining

Via the Coomassie staining (Sambrook J. 1989) the whole amount on the membrane can be detected. Therefor the membrane was incubated in the Coomassie solution during shaking for 10 min. Afterwards the membrane was washed until the protein bands were visible. Finally, the dried membrane was recorded on the LAS 3000 Intelligent Dark Box.

3.7. Cell culture

3.7.1. Cell lines and culture conditions

Cell line	Medium	Culture condition
murine optic nerve astrocytes	DMEM F12 + 10% (v/v) FCS, 1% astrocyte growth supplement, 100 U/ml Penicillin, 100 µg/ml Streptomycin	37°C, 5% CO_2
human trabecular meshwork (HTM) cells	DMEM F12 + 5% (v/v) FCS, 100 U/ml Penicillin, 100 µg/ml Streptomycin	37°C, 7% CO_2

Table 3-31: Used cell lines, appropriate medium and culture conditions

3.7.2. General working conditions

Cells were cultured in an incubator (Hera Safe, Heraeus, Hanau, Germany) with stable temperature and CO_2 conditions. All treatments, passaging and other procedures of the

cells as well as production of buffers and solutions were performed under a sterile working bench (Hera Safe, Heraeus, Hanau, Germany). Glassware, buffers and solutions were autoclaved prior to use and plastic material was packed sterile.

3.7.2.1. Passaging of cells

Once cells reached 100% confluence, cells were removed from the bottom of the cell culture flask and transferred into a new flask. Therefore, the cell culture medium was removed, and cells were washed once with 1x PBS to get rid of remaining medium. By adding 1 ml 0.25% Trypsin cells were removed from the surface. After inactivation of the trypsin by adding FCS containing medium and centrifugation (5 min, 1000 rpm), the cell pellet was resuspended in cell culture medium and a defined number of cells were seeded in a new cell culture dish. For treatment cells were counted using Neubauer counting chamber and a defined number of cells was seeded in 6 wells.

3.7.3. Isolation of murine optic nerve astrocytes

CD1 mice were used for the isolation of ON astrocytes. After the mice were sacrificed, both eyes were enucleated, and the ON were cut off the globes. After removal of the dura, ON samples were digested in 200 µl 0.25% Trypsin (Gibco BRL, Karlsruhe, Germany) for 30 min at 37°C. The tissue was then sheared by repeated pipetting and plated on laminin-coated 6-well plates. Cells were grown in DMEM F12 (Gibco BRL, Karlsruhe, Germany) enriched with 10% fetal bovine serum (FBS, Gibco BRL, Karlsruhe, Germany), 1% penicillin/streptomycin (Gibco BRL, Karlsruhe, Germany) and 1% astrocyte growth supplement (Sciencell, Carlsbad, CA, USA). Medium was not changed in the following seven days to allow the cells to attach to the tissue culture plates. After seven days, the medium was changed three times a week. A pure astrocyte culture was obtained by shaking the wells for 12 h to remove less adhesive cells. Cells were maintained in an incubator at 37°C and 5% CO_2. After cells reached 100% confluence, they were seeded in 25 cm^2 cell culture flasks (Nunc, VWR, Darmstadt, Germany). Astrocytes were characterized via GFAP-staining. Only cells from passage 2 to 10 were used for experiments.

3.7.4. *In vitro* experiments

3.7.4.1. Treatment with CTGF and TGF-β2

HTM and murine optic nerve astrocytes were treated either with 1ng/ml TGF-β2, 50ng/ml CTGF or left untreated as control. Therefore, the cells were seeded in 6wells and cultured until they reached confluency. Next the medium was replaced with medium containing 1% FCS (murine optic nerve astrocytes) or serum free medium (HTM cells) for 24 h. Prior to treatment the medium was replaced with fresh medium and the

appropriate amount of each growth factor was added. The cells were cultured again for 24 h and harvest for RNA and protein analysis.

3.7.4.2. Transfection of siRNA coated nanoparticles (NP)

HTM cells in passage 5 to 7 were grown in 6-well cell culture dishes for several days. After reaching 80% confluency, cells were cultivated for 24 hours without serum and another 24 h with the addition of 1 ng/mL TGF-β2. NP (80 µg/mL) samples were prepared in Leibovitz media containing 0.35 % serum and 1 ng/mL TGF-β2 and left one hour at room temperature to form a protein corona. Cells were treated for four hours, washed with PBS once and left for 24 h in serum-supplemented medium. Thereafter, cells were cultured for additional 24 h without serum before RNA and protein extraction.

3.7.4.3. Cultivation of murine ON astrocytes on increasing substratum stiffness

To analyze the influence of increasing substratum stiffness murine optic nerve astrocytes were seeded on PDMS based cell culture (see 3.10.) dishes, for immunocytochemical staining (35 mm) or expression analysis (100 mm) and grown for week in serum containing medium. 24 h prior before harvesting the cells, the medium was exchanged with 1% FCS containing medium and cells were finally cropped for the corresponding analysis.

3.8. *In vivo* experiments

3.8.1. Preparation of anterior eye segments, retinae and corneal-scleral rims

Before enucleation of the eyes, mice were anesthetized with CO_2 and euthanized by atlanto-occipital dislocation. For the preparation of the anterior eye segments, the posterior part of the eye was separated along the *ora serrata* and the whole anterior eye segment, including the cornea, trabecular meshwork, iris and ciliary muscle was transfer in a tube containing peqGold TriFast™ Trizol. The remaining retina in the posterior part was additionally taken out and, also transferred to a tube. For the preparation of the corneal scleral rims, the anterior eye segment was separated from the posterior part of the eye along the *ora serrata* and the lens was taken out. The anterior eye segment was cut in half and most of the cornea was removed. The hereby received tissue was transferred in containing peqGold TriFast™ Trizol containing tube for further expression analysis.

3.8.2. Preparation of optic nerves and optic nerve heads

Before enucleation of the eyes, mice were anesthetized with CO_2 and euthanized by atlanto-occipital dislocation. First the anterior eye segment, the lens and retina were removed, and the optic nerve was cleaned from muscles and connective tissue. The sclera was cut away from the optic nerve head and potentially remaining parts of sclera and retina were removed. Second the optic nerve tissue was separated from the optic

nerve head. Both optic nerve and optic nerve head were stored in peqGold TriFast™ Trizol prior to RNA isolation.

3.8.3. Preparation of retinal flat mounts

Mice were anesthetized with CO_2 and euthanized by atlanto-occipital dislocation and eyes were enucleated and fixed in 4% (w/v) paraformaldehyde (PFA) for 2 h. First the anterior eye segment and lens were removed, and the whole retina was taken out. To spread the retina flat on an object slide, it was incised on four opposite positions. The retinal flat mount was circuited with a fat pen (PapPen) and moisturized with 0.1 M Php.

3.8.4. Transcardial perfusion

Mice were anesthetized by injecting intraperitioneally a solution of ketamine (75 mg/ml) and Xylazine (5 mg/ml). As soon as the mice were completely anesthetized, the thoracic cavity was opened, and the heart was exposed. The injection needle was set into the left ventricle and the right atrial auricle was cut with a little incision and the mice were perfused first with 0.89 % NaCl and finally for fixation with 4% PFA (w/v). For retinal flat mounts mice were perfused with FITC-Dextran. Eyes were enucleated and incubated additionally in 4 % PFA (w/v) overnight.

3.8.5. Perfusion of porcine and human eyes

After the extraocular tissue was removed, the porcine and human eyes were submerged to the limbus in 0.89 % NaCl at 35°C. The perfusion system contained a perfusion chamber and a collection chamber. The infusion needle was inserted intracamerally through the transparent cornea into each eye and connected to the perfusion chamber. The needle was then carefully pushed through the pupil and the tip of the needle was placed in the posterior chamber. Next a second needle was placed intracamerally into the anterior chamber and connected to the collection reservoir. It is closed during the perfusion excepted during the exchanges. First a volume of 3 ml NPs was exchanged which took about 10 to 15 min, to ensure that the perfusion system as well as the anterior eye segment was filled with the perfusate. The eyes were either perfused with NP-hyaluron (HA) or for control with NP-poly(ethylene imine) (PEI). In the next step, the collection chamber was closed, and the eyes were perfused at 10 mmHg constant pressure for 3 h. To rinse the perfused eyes, a second exchange with 3 ml 5 mM glucose was performed, which took again 10 to 15 min, followed by a second perfusion for 2 h with 5 mM glucose. For fixation, the eyes were additionally perfused with 4% (w/v) PFA for 30 min, again with a previous exchange step with 3 ml 4% (w/v) PFA. To get information about the distribution of NPs, the anterior chamber was dissected from the rest of the eyes and the iris was removed to free the outflow pathway. By fluorescent imaging the whole outflow ring was analyzed and regions with homogeneous distribution

of NPs were chosen for further investigations by marking them with needles. The probe was dissected and most of the sclera and cornea was removed. The small pieces were fixed with 4 % (w/v) PFA for 4 h and washed three times with 0.1 M Php.

3.9. Histological techniques

3.9.1. Cryo embedding and preparation of sections

Eyes were incubated in 4 % (w/v) PFA overnight at 4°C. After three washing steps with 0.1 M Php, the eyes were incubated in 10 %, 20 % and 30 % sucrose for 4 h respectively. Eyes were embbeded in Tissue-Tek® and stored at -20°C for further use. 12 µm tangential or sagittal sections were performed with the Microm HM500 OM Cryostat (Microm International, Walldorf, Germany).

3.9.2. Paraffin embedding and preparation of sections

Eyes were incubated in 4% (w/v) overnight and washed three times with 0.1 M phosphate buffer. Afterwards eyes were dehydrated in an ascending alcohol series and paraffin embedding was performed according to a standardized protocol (see table 3-32).

Reagent	Duration
50% isopropanol	1h
70% isopropanol	1h overnight 1h
80% isopropanol	1h
96% isopropanol	1h 1h
100% isopropanol	1h 1h 2h
100% Xylol	1h 1.5h
100% paraffin	4h 8h

Table 3-32: Protocol for ascending alcohol series and paraffin embedding

Afterwards eyes were embedded in liquid paraffin and by help with the cornea and the optic nerve the eyes were taken to a sagittal position. On the Supercut-Mikrotom 6 µm sections were carried out and the they were dried overnight at 37°C and stored at RT for further use.

3.9.3. Epon embedding and preparation of semi thin sections

Eyes were fixed in EM-Fixative for 24h, following by three washing steps for 20 min with 0.1 M cacodylate buffer. Afterwards eyes were additionally fixed with 1% osmimumtetraoxid and washed again with 0.1 M cacodylate buffer. Next eyes were dehydrated by an ascending alcohol series (70 %, 80 %, 90 %, 100 %). The Epon embedding was performed according to a standardized protocol: Ethanol/Acetone 1:1, Acetone 100 %, Epon/Acetone 1:2, Epon/Acetone 2:1, Epon 100 %. Eyes were hardened for 24 h at 60°C and 48 h at 90°C. For embedding with 2 % DMP-30 (Roth, Karlsruhe, Germany), Epon stem A and Epon stem B were mixed 1:1. Finally, 1 µm sections were performed and analyzed by light microscopy.

3.9.4. Immunohistochemical staining of cryo sections

Cryo sections were fixed to an objected slide and dried for 5 min. To remove remaining embedding medium slides were washed with 0.1 M phosphate buffer for 5 min. Sections were orbited with a fat pen (PapPen) and incubate for 1 h at RT with the appropriate blocking solution. Afterwards the sections were incubated with the primary antibody at 4°C overnight. Next the sections were washed three times with 0.1 M Php for 5 min and incubated with the secondary antibody for 1 h at RT. Appropriate staining protocol for each protein of this study is listed in the table below.

Protein	**Blocking solution**	**Primary antibody**	**Secondary antibody**
CTGF	2% BSA, 0.2% CWFG, 0.1% Triton, 0.1M Php	rabbit anti-CTGF 1:100 in 0.2% BSA, 0.02% CWFG, 0.01% Triton, 0.1M Php	goat anti-rabbit Cy™3 IgG 1:2000 in 0.2% BSA, 0.02% CWFG, 0.01% Triton, 0.1M Php
GFAP	2% BSA, 0.2% CWFG, 0.1% Triton, 0.1M Php	chicken anti-GFAP 1:2000 in 0.2% BSA, 0.02% CWFG,	goat anti-chicken Alexa Fluor® 488 IgG 1:1000 in 0.2% BSA,

		0.01% Triton, 0.1M Php	0.02% CWFG, 0.01% Triton, 0.1M Php
CD44	2% BSA, 0.2% CWFG, 0.1% Triton, 0.1M Php	mouse anti-CD44 1:100 in 0.2% BSA, 0.02% CWFG, 0.01% Triton, 0.1M Php	donkey anti-mouse Alexa Fluor® 488 IgG 1:1000 in 0.2% BSA, 0.02% CWFG, 0.01% Triton, 0.1M Php
CD44	2% BSA, 0.2% CWFG, 0.1% Triton, 0.1M Php	rabbit anti-CD44 1:100 in 0.2% BSA, 0.02% CWFG, 0.01% Triton, 0.1M Php	goat anti-rabbit Cy™3 IgG 1:2000 in 0.2% BSA, 0.02% CWFG, 0.01% Triton, 0.1M Php
β-catenin	2% BSA, 0.2% CWFG, 0.1% Triton, 0.1M Php	rabbit anti-β-catenin 1:100 in 0.2% BSA, 0.02% CWFG, 0.01% Triton, 0.1M Php	1. Biotinylated anti-rabbit IgG 1:500 in 0.2% BSA, 0.02% CWFG, 0.01% Triton, 0.1M Php 2. Streptavidin Alexa Fluor® 488 1:1000 in 0.2% BSA, 0.02% CWFG, 0.01% Triton, 0.1M Php
CD31	2% BSA, 0.1% Triton, 0.1M Php	goat anti-CD31 1:100 in 0.2% BSA, 0.01% Triton, 0.1M Php	1. Biotinylated anti-goat IgG 1:500 in 0.2% BSA, 0.02% CWFG, 0.01% Triton, 0.1M Php

			2. Streptavidin Alexa Fluor® 488 1:1000 in 0.2% BSA, 0.02% CWFG, 0.01% Triton, 0.1M Php
β-galactosidase	2% BSA, 0.2% CWFG, 0.1% Triton, 0.1M Php	rabbit anti-β-galactosidase 1:100 in 0.2% BSA, 0.02% CWFG, 0.01% Triton, 0.1M Php	donkey anti-rabbit Alexa Fluor® 647 IgG 1:200 in 0.2% BSA, 0.02% CWFG, 0.01% Triton, 0.1M Php
Glutamine synthetase	2% BSA, 0.2% CWFG, 0.1% Triton, 0.1M Php	goat anti-Glutamine synthetase 1:100 in 0.2% BSA, 0.02% CWFG, 0.01% Triton, 0.1M Php	donkey anti-goat Alexa Fluor® 488 IgG 1:1000 in 0.2% BSA, 0.02% CWFG, 0.01% Triton, 0.1M Php
Caveolin1	2% BSA, 0.2% CWFG, 0.1% Triton, 0.1M Php	rabbit anti-Caveolin1 1:100 in 0.2% BSA, 0.02% CWFG, 0.01% Triton, 0.1M Php	goat anti-rabbit Cy™3 IgG 1:2000 in 0.2% BSA, 0.02% CWFG, 0.01% Triton, 0.1M Php
Myelin basic protein (MBP)	2% BSA, 0.1% Triton, 0.1M Php	rabbit anti-MBP 1:200 in 0.2% BSA, 0.01% Triton, 0.1M Php	goat anti-rabbit Cy™3 IgG 1:2000 in 0.2% BSA, 0.01% Triton, 0.1M Php
Calcium binding adaptor molecule (IBA1)	2% BSA, 0.2% CWFG, 0.1% Triton, 0.1M Php	rabbit anti-IBA1 1:100 in 0.2% BSA, 0.01% Triton, 0.1M Php	goat anti-rabbit Cy™3 IgG 1:2000 in 0.2% BSA, 0.02% CWFG, 0.01% Triton, 0.1M Php

Table 3-33: Antibodies used for immunohistochemical staining

As a control for unspecific binding of the secondary antibody, negative controls were performed. Finally, 4,6-diamidino-2-phenylindole (DAPI) (Vector Laboratories, Burlingame, USA) was added to counterstain nuclear DNA.

3.9.5. Immunohistochemical staining of paraffin sections

Before immunohistochemical staining sections were deparaffinized (see table 3-34).

Reagent	Duration
100% Xylol	2x 10min
100% isopropanol	2x 10min
96% isopropanol	2x 5min
80% isopropanol	2x 5min
70% isopropanol	1x 5min
50% isopropanol	1x 5min
dH_2O	1x 5min

Table 3-34: Protocol for deparaffinizing of paraffin sections

In comparison to immunohistochemical staining on cryo sections, paraffin section must be pretreated before the actual staining. The pretreatment and the antibody staining were performed as follows.

Protein	Pretreatment	Blocking solution	Primary antibody	Secondary antibody
CD44	0.2M citric acid/ 0.2M sodium citrate, 30min, boiling	2% BSA, 0.2% CWFG, 0.1% Triton, 0.1M Php	mouse-anti CD44 1:100 in 0.2% BSA, 0.02% CWFG, 0.01% Triton, 0.1M Php	donkey anti-mouse Alexa Fluor® 647 IgG 1:200 in 0.2% BSA, 0.02% CWFG, 0.01% Triton, 0.1M Php
β-galactosidase	0.2M citric acid/ 0.2M sodium citrate, 30min, boiling	2% BSA, 0.2% CWFG, 0.1% Triton, 0.1M Php	rabbit-anti β-galactosidase 1:100 in 0.2% BSA, 0.02% CWFG, 0.01% Triton, 0.1M Php	donkey anti-rabbit Alexa Fluor® 647 IgG 1:200 in 0.2% BSA, 0.02% CWFG,

				0.01% Triton, 0.1M Php
GFAP	0.2M citric acid/ 0.2M sodium citrate, 30min, boiling	2% BSA, 0.2% CWFG, 0.1% Triton, 0.1M Php	chicken-anti GFAP 1:2000 in 0.2% BSA, 0.02% CWFG, 0.01% Triton, 0.1M Php	goat anti-chicken Alexa Fluor® 488 IgG 1:1000 in 0.2% BSA, 0.02% CWFG, 0.01% Triton, 0.1M Php
CD31	1. 0.05 M TRIS-HCL, 5 min 2. 3. 2 N HCL, 30 min	2% BSA, 0.2% CWFG, 0.1% Triton, 0.1M Php	goat anti-CD31 1:100 in 0.2% BSA, 0.01% Triton, 0.1M Php	1. Biotinylated anti-goat IgG 1:500 in 0.2% BSA, 0.02% CWFG, 0.01% Triton, 0.1M Php 2. Streptavidin Alexa Fluor® 488 1:1000 in 0.2% BSA, 0.02% CWFG, 0.01% Triton, 0.1M Php

Table 3-35: Pretreatment and antibodies used for immunohistochemical staining

As a control for unspecific binding of the secondary antibody, negative controls were performed. Finally, 4,6-diamidino-2-phenylindole (DAPI) (Vector Laboratories, Burlingame, USA) was added to counterstain nuclear DNA.

3.9.6. Immunohistochemical staining of retinal flat mounts

Protein	Pretreatment	Blocking solution	Primary antibody	Secondary antibody
β-galactosidase	50mM NH_4Cl, 1h, RT 0.5% Triton-X 100, 0.5h, RT	2% BSA, 0.2% CWFG, 0.1% Triton, 0.1M Php, 1h, RT	rabbit-anti β-galactosidase 1:100 in 0.2% BSA, 0.02% CWFG, 0.01% Triton, 0.1M Php, 2h, RT, following overnight at 4°C	goat anti-rabbit Cy™3 IgG 1:2000 in 0.2% BSA, 0.02% CWFG, 0.01% Triton, 0.1M Php, 1h, RT, following overnight at 4°C

Table 3-36: Pretreatment and antibody used for immunohistochemical staining of retinal flat mounts

As a control for unspecific binding of the secondary antibody, negative controls were performed.

3.9.7. Immunocytochemical staining

HTM cells, seeded on coverslips and treated with either 1 ng/ml TGFβ2, 50 ng/ml CTGF or left untreated as controls and murine optic nerve astrocytes, cultured on cell culture dishes with increasing substratum stiffness were used for immunocytochemical staining in this study. Cells were washed twice with PBS, fixed with 4 % (w/v) PFA for 5 min and washed again three times with PBS. Specific antibodies were used as follows:

Protein	Blocking solution	Primary antibody	Secondary antibody
CTGF	2% BSA, 0.2% CWFG, 0.1% Triton, 0.1M Php	rabbit-anti CTGF 1:100 in 0.2% BSA, 0.02% CWFG, 0.01% Triton, 0.1M Php	goat anti-rabbit Alexa Fluor® 488 IgG 1:1000 in 0.2% BSA, 0.02% CWFG, 0.01% Triton, 0.1M Php
GFAP	2% BSA, 0.2% CWFG, 0.1% Triton, 0.1M Php	chicken-anti GFAP 1:2000 in 0.2% BSA, 0.02%	goat anti-chicken Alexa Fluor® 488 IgG 1:1000 in

		CWFG, 0.01% Triton, 0.1M Php	0.2% BSA, 0.02% CWFG, 0.01% Triton, 0.1M Php
CD44	2% BSA, 0.2% CWFG, 0.1% Triton, 0.1M Php	mouse-anti CD44 1:100 in 0.2% BSA, 0.02% CWFG, 0.01% Triton, 0.1M Php	donkey anti-mouse Alexa Fluor® 488 IgG 1:1000 in 0.2% BSA, 0.02% CWFG, 0.01% Triton, 0.1M Php
Caveolin1	2% BSA, 0.2% CWFG, 0.1% Triton, 0.1M Php	rabbit-anti Caveolin1 1:100 in 0.2% BSA, 0.02% CWFG, 0.01% Triton, 0.1M Php	donkey anti-rabbit Alexa Fluor® 647 IgG 1:200 in 0.2% BSA, 0.02% CWFG, 0.01% Triton, 0.1M Php

Table 3-37: Antibodies used for immunocytochemical staining

As a control for unspecific binding of the secondary antibody, negative controls were performed. Finally, 4,6-diamidino-2-phenylindole (DAPI) (Vector Laboratories, Burlingame, USA) was added to counterstain nuclear DNA.

3.9.8. Phalloidin labeling

To visualize the actin cytoskeleton of murine optic nerve astrocytes after different treatment, the cells were labeled with phalloidin-TRITC (Phallloidin-Tetramethylrodamine B isothiocyanate; Sigma-Aldrich, Taufkirchen, Germany) 1:1000 for 1 h at RT.

3.9.9. β-galactosidase activity staining

Before enucleation of the eyes, mice were anesthetized with CO_2 and euthanized by atlanto-occipital dislocation. In this study mice with different age (P1, P5, P10, P15; P20, P49 and 1 year) were used for the following experiments. Embryos were obtained from time mating with noon of the day of vaginal plug discovery designated as 0.5 days of gastation (E 0.5). CTGF expression was analyzed at E11 and E16.5. Eyes and embryos were fixed with 2 % glutaraldehyde in 5mM EGTA (pH 7.3) and 2 mM $MgCl_2$ dissolved in 0.1 M phosphate buffer for 30 min at RT. Followed by three washing steps with washing buffer (1 M $MgCl_2$, 1 % NaDC, 2 % Tergitol in 0.1 M Php) and stained for 24 h at 37°C in the dark with X-Gal staining solution (2 mM $MgCl_2$, 0.01 % sodium

deoxycholate, 0.02 % Nonidet-P40, 5 mM potassium ferrocyanide, 5 mM potassium ferricyanide, 1 mg/ml X-Gal dissolved in 0.1 M Php) to visualize β-galactosidase activity. Afterwards tissues were washed three times for 10 min with washing buffer, following a second washing step for three times for 10 min with 0.1 M phosphate buffer. After the incubation for 1 h with 50% isopropanol and 1 h with 70% isopropanol, the tissues were embedded in paraffin. Finally, 6 µm sections were produced on the Supercut microtom (Reichert-Jung, Kirchseeon, Germany).

3.9.10. β-galactosidase activity staining of retinal flat mounts

Animal were sacrificed at P15 and both eyes were enucleated. Eyes were incubated in 2% PFA for 1 h at RT, washed 3 times with LacZ washing buffer (1 M $MgCl_2$, 1 % NaDC, 2 % Tergitol in 0.1 M Php) for 10 min. Afterwards the whole retina was dissected and put on an object slide. The retina flat mounts were stained for 24 h at 37°C in the dark with X-Gal staining solution (2 mM $MgCl_2$, 0.01% sodium deoxycholate, 0.02 % Nonidet-P40, 5 mM potassium ferrocyanide, 5mM potassium ferricyanide, 1mg/ml X-Gal dissolved in 0.1 M Php) to visualize β-galactosidase activity. Afterwards retinae were washed three times for 10 min with washing buffer, following a second washing step for three times for 10 min with 0.1 M phosphate buffer. In a next step the tissues were mounted with Mowiol. The retinae were dried overnight before microscopy.

3.10. Preparation of Polydimethylsiloxane Cell Substrata

were purchased from Evonik Hanse GmbH, Gesthach, Germany. In the first step, the components, addition-curing basic polymer VS100 000 (vinyl-functional polydimethylsiloxane), the chain extender modifier 700 (SIH-terminated polydimethyl siloxane, difunctional structure), the reactive diluent MV2000 (mono-vinyl functional polydimethylsiloxane) and the inhibitor DVS (divinyl tetramethyl disiloxane) together with the plasticizer silicone oil (linear, non-reactive polydimethylsiloxane) AK10 (Wacker Chemie AG, Munich, Germany) were rotationally mixed for 6 min at 1000 rpm to form a basic elastomer (BE1) mixture. The mixing ratio of BE1 is shown in Table 3-38.

Mixtures	Component	Amount
Basic elastomer mixture (BE1)	VS100 000	14 g
	MV2000	2.5 g
	AK10	44 g
	Inhibitor DVS	250 µl
	Modifier 700	50 µl
10 kPa	BE1	12 g
	Cross linker AB116655	0.38 g
	Catalyst 510	40 µl
30 kPa	BE1	12 g
	Cross linker AB116655	0.38 g
	Cross linker 510	5 µl
	Catalyst 510	40 µl
	Inhibitor DVS	10 µl
60 kPa	BE1	12 g
	Cross linker AB116655	0.38 g
	Cross linker 510	20 µl
	Catalyst 510	70µl
	Inhibitor DVS	70µl

Table 3-38: Elastomer mixtures of PDMS substrata, showing the parameters of the basic elastomer mixture and the additional amounts for the different substrata.

In the next step, three different elastomers were prepared. All substrata (nominal indentation modulus E_{IT} = 10 kPa, 30 kPa, 60 kPa) based on the BE1 (12 g) were mixed with a cross linker AB116655 0.5-1% methylhydrosiloxane–dimethylsiloxane copolymer (ABCR GmbH, Karlsruhe, Germany), and a Pt-catalyst 510 (Evonik Hanse GmbH) in a defined mixture ratio. The “30 kPa” and “60 kPa” samples differ only in a small amount of additional cross linker 210 (Evonik Hanse GmbH) and a necessary additional catalyst and inhibitor ratio (Table 3-38). Depending on the batch, the parts corresponding to standard values must be slightly modified in order to precisely achieve target mechanical properties. In addition, air bubbles were removed by placing the elastomers in a vacuum chamber for 15 min. In conclusion, Petri dishes (µ-dish 35 mm high, uncoated, ibidi, Martinsried, Germany or greiner bio-one 94x16 mm PS) were coated (ibidi 0.5 g/greiner 4.5 g) with the finished, but uncured elastomer. In a further step, remaining air bubbles in the coating were removed using a vacuum chamber for 3 min. The substrata were then cured in a universal oven (Memmert UF30Plus, Memmert GmbH, Schwabach, Germany) at 80°C for 1 hour and finally cured at 65°C 24 h (with

forced air circulation). The finished coated petri dishes were then washed twice with 70% isopropanol for 5 min and again with 99.5% ethanol for 5 min under slow shaking (Microplate mixer MX-M, China). The surfaces were then rinsed in ethanol 99.5% and dried in air. The cleaned coatings were then treated in an in-house designed ultra-violet/ozone (UVO) emitter employing three 4 W (12 µW/cm^2 at 1 m distance) low pressure mercury vapor lamps. The exposure times were 10 min with a 4 cm distance between the lamps and the sample's surface in the same manner as documented (35). Directly after the UVO treatment, the surfaces were silanized with 3% aminopropyl-triethoxysilane (APTES) in autoclaved deionized water (ddH_2O) for 25 min at RT under slow shaking and washed five times in autoclaved water. In the next step, the petri dishes were treated with 0.3% glutardialdehyde (GDH) in filtered ddH_2O for 40 min at RT under slow shaking and washed again five times in autoclaved ddH_2O.

3.11. Image Analysis

The images were analyzed using ImageJ's built-in measuring feature (Wayne Rasband, formerly National Institutes of Health, Bethesda, MD, USA). The surface area of the ONH section was calculated and the amount of area emitting fluorescent signal for GFAP or CTGF within the outlines of the ONH section was determined by a standardized macro routine consisting of ImageJ's color threshold plugin and particle analyzer. The resulting values were used to calculate the percentage of area within the ONH section. These measurements were performed for each individual specimen after calibrating ImageJ with the scale bar.

3.12. Light and Fluorescence Microscopy

Histochemical, immunohistochemical and immunocytochemical stainings were analyzed using the Axio Imager Z1 microscope (Carl Zeiss, Göttingen, Germany). Immunocytochemical staining of stiffness experiments were analyzed on the Zeiss Observer Z1 (Carl Zeiss, Göttingen, Germany) and immunohistochemical staining of perfusion experiments were analyzed using the LSM 510 microscope (Carl Zeiss, Göttingen, Germany).

3.13. Statistical Analysis

Western blot and real-time RT-PCR was repeated at least three times with RNA and protein extract. Each real-time RT-PCR analysis was performed in triplicates. Data are presented as mean ± SD or SEM (quoted in each figure legend). Immunohistochemical and histological staining were performed at least three times on individual animals or cell lines. Student's t-test was used for statistical analysis of the real-time RT-PCR and Western Blot. P value of < 0.05 was considered to reflect statistical significance.

4. Results

4.1. CTGF expression in the mouse eye

Little is known about the localization and distribution of CTGF in the eye, especially during development. Since CTGF is a secreted protein, the CTGF expressing tissue and cell types cannot be identified by immunohistochemical staining. Therefore, the $CTGF^{LacZ+/-}$ mouse model, expressing β-galactosidase under the control of the CTGF promotor was used to determine the CTGF promotor activity in the relevant tissue and cell types. Histochemical and immunohistochemical studies in $CTGF^{LacZ+/-}$ mice were performed to identify the CTGF expressing tissue und cell types during development and in the adult mouse eye.

Prior to the experiments each animal was genotyped (Figure 4-1). Since homozygote CTGF knockout mice are embryonic lethal (Ivkovic et al., 2003), the genotype of the offspring is either WT or heterozygous. The $CTGF^{LacZ+/-}$ PCR results is a single 500bp DNA band for $CTGF^{LacZ+/-}$ and no band for WT animals (Figure 4-1).

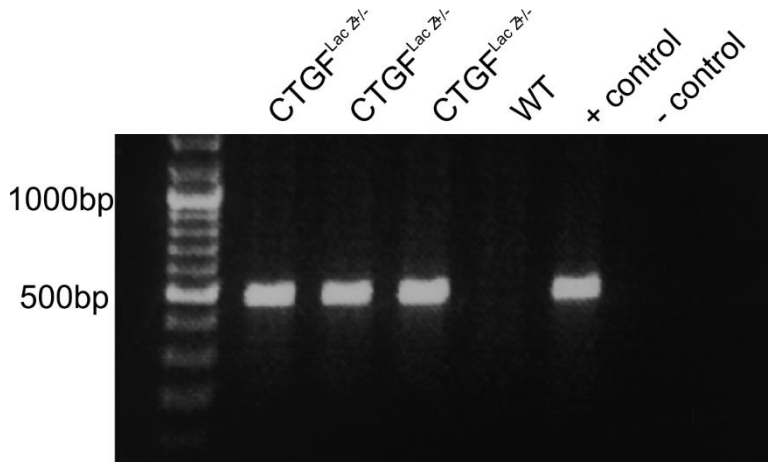

Figure 4-1: $CTGF^{LacZ+/-}$ Genotyping. A representative $CTGF^{LacZ+/-}$ PCR showing the 500bp DNA band in heterozygous $CTGF^{LacZ+/-}$ mice. WT littermates exhibited no band in the $CTGF^{LacZ+/-}$ PCR.

4.1.1. Verification of heterozygous CTGF knockout

To verify the heterozygous knockout of CTGF mRNA and protein analysis were performed on retinal tissue of CTGF$^{LacZ/+}$ and WT mice, exemplary.

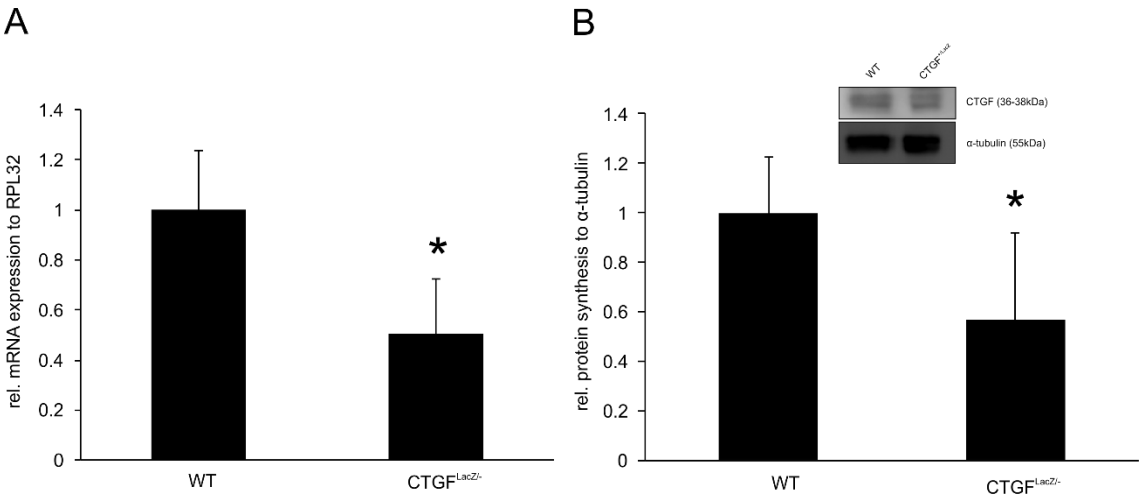

Figure 4-2: Real-time RT-PCR and Western Blot analysis of CTGF in the retina of CTGF$^{LacZ/+}$ and WT mice. (A) mRNA expression of CTGF in the retina of CTGF$^{LacZ/+}$ mice (n=4; 0.50 ± 0.12 *p= 0.02) showed a significant heterozygous knockout in comparison to WT littermates (n=3; 1 ± 0.14). The mean value of WT mice was set at 1. *RPL32* was used as housekeeping gene. (B) Densitometric analysis of CTGF protein synthesis in retinal tissue of CTGF$^{LacZ/+}$ and WT mice. CTGF protein synthesis is significantly reduced in retina of CTGF$^{LacZ/+}$ mice (n=6; 0.57± 0.35; *p=0.04) compared to WT littermates (n=6; 1 ± 0.23). A representative Western Blot is shown for CTGF$^{LacZ/+}$ and WT mice. Mean value of WT mice was set at 1. α-tubulin was used as loading control. Data represented as mean ± SD.

Real-time RT-PCR analysis showed a significantly reduced mRNA expression of CTGF in the retina of CTGF$^{LacZ/+}$ mice (n=4; 0.50 ± 0.12 *p=0.02) in comparison to WT littermates (n=3; 1 ± 0.14) (Figure 4-2 A). Furthermore, the heterozygous knockout of CTGF could be confirmed by Western Blot analysis of retinal tissue (Figure 4-2 B). CTGF protein level of CTGF$^{LacZ/+}$ (n=6; 0.57± 0.35; *p=0.04) retina tissue showed a significant reduction compared to WT control (n=6; 1 ± 0.23) (Figure 4-2 B).

4.1.2. CTGF distribution during embryonic eye development

To identify the CTGF promotor activity during the embryonic development of the mouse eye, two different timepoints were chosen for following experiments (Figure 4-3). The prenatal development of the mouse eye starts at 8 day of gestation (E8), therefore the timepoint E11 and E16.5 were analyzed for CTGF distribution in this study. At E11 the outer layer (future pigment layer of the retina) and the inner layer (future nervous layer of the retina) of the optic cup, as well as the lens vesicle are already developed (Figure 4-3 A). By staining of the β-galactosidase activity at this timepoint, an expression of CTGF can be detected in the outer and inner layer of the optic cup, as well as in the lens vesicle (Figure 4-3 A). At the second analyzed timepoint (E16.5) several structures of the eye, as cornea, lens, sclera, ON, neural and pigment layer of the retina and a small

angle cavity, including the developing TM are well defined. At this future timepoint E16.5, CTGF expression can be observed in the anterior and posterior eye segment. In the anterior eye segment, CTGF expression can be detected in the epithelium of the cornea and in the anterior chamber angle, including the TM and the ciliary body. In the posterior eye segment, CTGF expression can be observed in the sclera, the choroidea, in the hyaloid artery and in the dura mater around the ON. (Figure 4-3 B). As the lens is adhered to the corneal endothelium at this timepoint of development it cannot be distinguished if the LacZ staining is located to the endothelium of the cornea or the epithelium of the lens. (Figure 4-3 B).

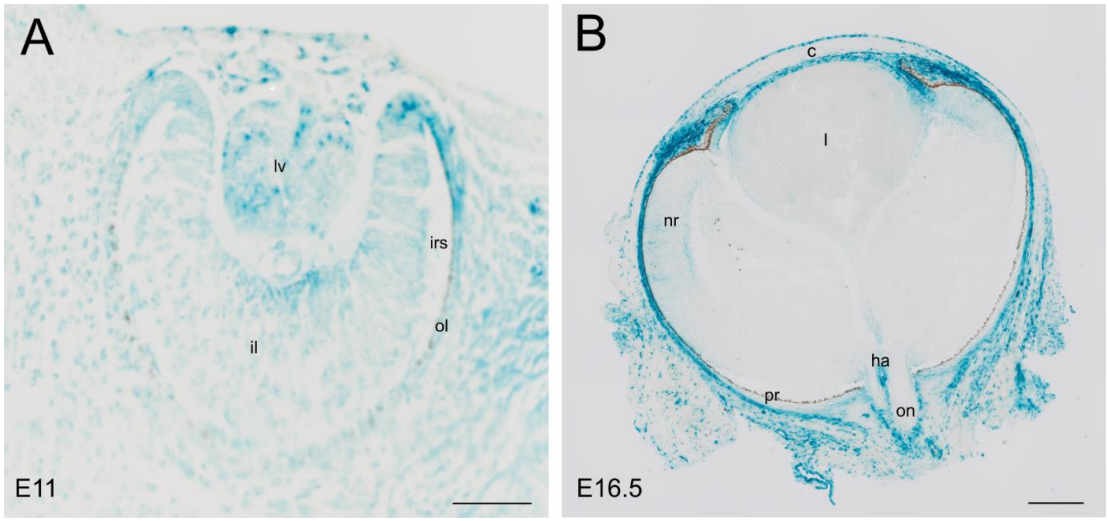

Figure 4-3: Staining of β-galactosidase activity during the embryonic development. (A) At E11, CTGF can be observed in the outer and inner layer of the optic cup and the lens vesicle. (B) At E16.5, CTGF expression can be detected in the endothelium and epithelium of the cornea, the lens epithelium, the sclera, the hyaloid artery and in the region of the developing TM. lv=lens vesicle; il = inner layer of the optic cup; ol = outer layer of the optic cup; irs = interretinal space; nr = nervous layer of the retina; pr = pigment layer of the retina; l = lens; c = cornea; ha = hyaloid artery; on = optic nerve; Scale bar: A = 50µm, B = 200µm.

4.1.3. CTGF expression during postnatal development and in the adult eye

In contrast to the human eye, several structures in the mouse eye are immature at birth and reach its maturation around postnatal day 21. For this reason, the mouse eye provides the ideal model to study developmental processes and expression pattern of proteins during eye development. Therefore, different timepoints were chosen to study the expression and distribution of CTGF in the postnatal developing mouse eye. CTGF expression was assessed on postnatal day 1, 5, 10, 15 and 20 (P1, P5, P10, P15, P20) (Figure 4-4 A-F). Additionally, adult mouse eyes were analyzed at the age of 7 weeks (Figure 4-4 G, H). The LacZ staining on WT littermates served as control and is shown for the timepoint P20 and the adult eye (Figure 4-4 F, H).

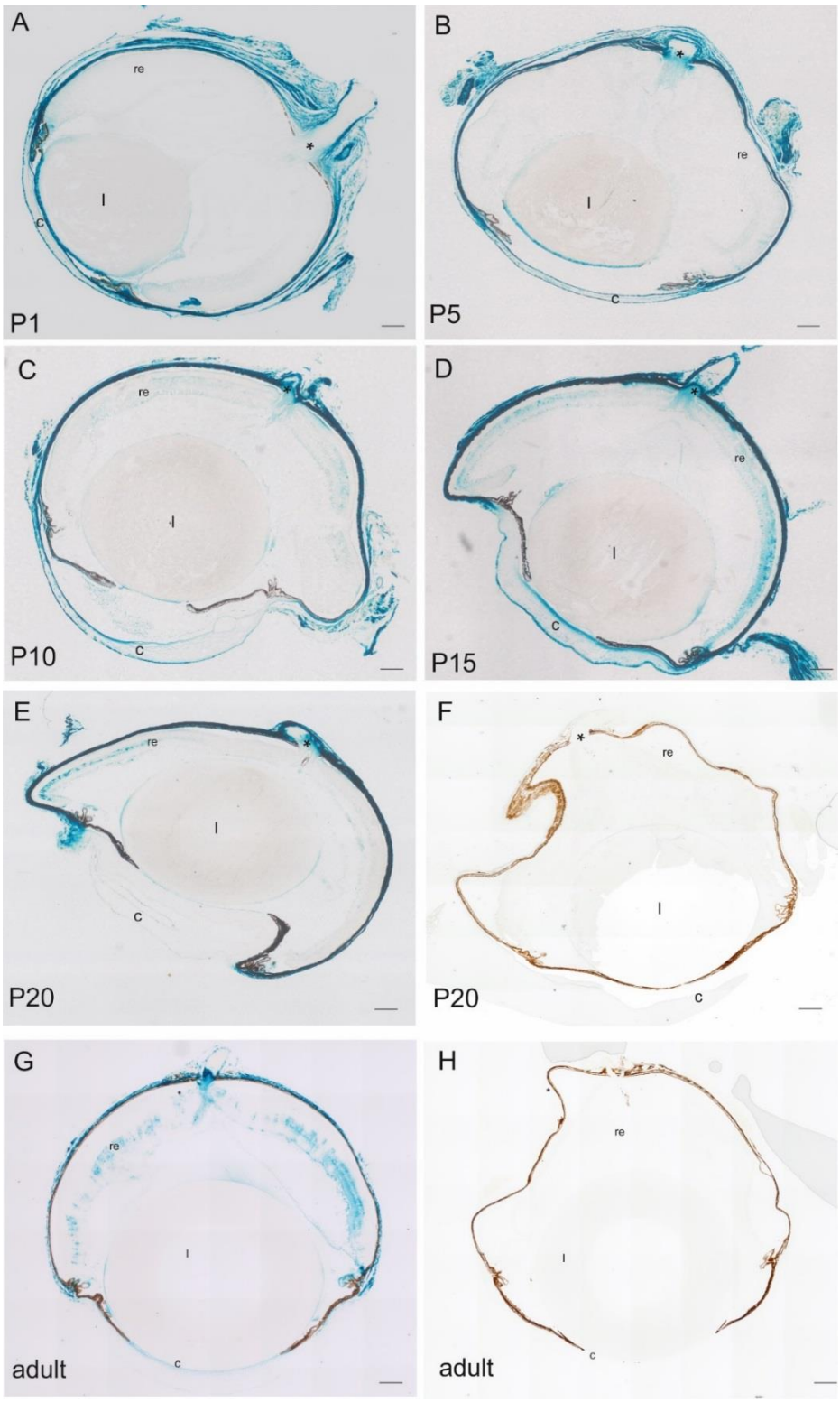

Figure 4-4: LacZ staining in sagittal sections of postnatal and adult CTGF$^{LacZ+/-}$ eyes. (A) CTGF expression at P1 was shown in the corneal endothelium and epithelium, in the sclera and in the developing TM. (B) In P5 eyes CTGF is expressed in the corneal endothelium, epithelium and stroma, the sclera, in the developing TM and additionally in the ON. (C) At P10 a CTGF expression was observed in the corneal endothelium, epithelium and stroma, in the sclera, the retina, the TM and the ON. (D) At P15, LacZ staining visualized a comparable CTGF localization to P10, except the retina where the CTGF expression is increased. The CTGF expression at P20 (E) were finally restricted to the corneal endothelium, the sclera, the TM, the retina and the ONH. (F) LacZ staining in WT eyes showed no signal. re: retina; l: lens; c: cornea; *: ONH; Scale bar: 200µm.

4.1.3.1. CTGF expression in the anterior eye segment during postnatal development and in the adult eye

In the anterior eye CTGF promotor activity is detected in the cornea, the TM and the ciliary body, with variations in the expression pattern depending on the developmental stage. The CTGF expression pattern in the cornea changes during development. At P1, a staining against β-galactosidase is detected in the corneal epithelium and stroma (Figure 4-4 A). As the lens is still adhered to the endothelium, it cannot clearly distinguish if the staining is located at the corneal endothelium or the epithelium of the lens capsule, but there is first evidence that the CTGF expression is localized to both structures (Figure 4-4 A). By P5, the lens detaches from the corneal endothelium completely, whereby a LacZ staining in the corneal endothelium and epithelium of the lens can be detected. The CTGF expression in the corneal stroma and epithelium remains constant at this developmental stage (Figure 4-4 B). At P10 and P15 no changes in the CTGF expression in the different layers of the cornea are present (Figure 4-4 C, D). The LacZ staining in the lens epithelium is reduced, but still present at P10 and P15 (Figure 4-4 C, D). By P20, a shift in the corneal CTGF expression is observed. The LacZ staining is restricted to the corneal endothelium by this developmental point (Figure 4-4 E). The restricted CTGF promotor activity in the corneal endothelium is also observed in the adult eye (Figure 4-4 G). In the lens epithelium a low expression for CTGF is detected at P20 and in the adult eye, respectively (Figure 4-4 E, G).

The LacZ staining of the anterior chamber angle indicated a high and persistent expression for CTGF in this region of the eye (Figure 4-5). The eye structures in the anterior chamber angle are derived from different origin. The formation of the iris and the ciliary body occurs at the peripheral edge of the optic cup. Therefore, the epithelial layers of iris and ciliary body have a neuroectoderm origin. In contrast, the stroma of both tissues is formed by a migration of mesenchyme cells along the epithelial layers. Additionally, the TM has a mesenchymal origin. At the embryonic timepoint E16.5, no differentiation into iris and ciliary had occurred, but lens and cornea are well defined. The anterior layer of future iris and ciliary body is heavily pigmented. At this timepoint, CTGF expression is present in the undifferentiated angle mesenchyme (Figure 4-6 B). One day after birth, the mesenchyme of developing iris and TM regions are distinguishable and the ciliary body processes have begun to form. CTGF promotor activity can be detected in mesenchyme of the developing iris, TM and in the pigmented epithelium of the ciliary body (Figure 4-5 C). By P5, the iris and the ciliary body are well formed. The CTGF expression is located to the inner surface of the pars plana of the ciliary body, the external epithelial layer of the iris and to the developing TM (Figure 4-5 D). The staining at P10 is similar to that detected at P5 (Figure 4-5 E). At P15, the CTGF promotor activity is

markedly increased with an intense staining in the TM, the inner surface of the pars plana, and both the pigmented and non-pigmented epithelium of the ciliary body (Figure 4-5 F). Interestingly, at P20 CTGF is the restricted to the inner surface of the pars plana and the non-pigmented epithelium of the ciliary body. In the TM the CTGF expression remains constant (Figure 4-5 G). Finally, in the adult eye, the CTGF is located in the TM and the non-pigmented epithelium of the ciliary body (Figure 4-5 H).

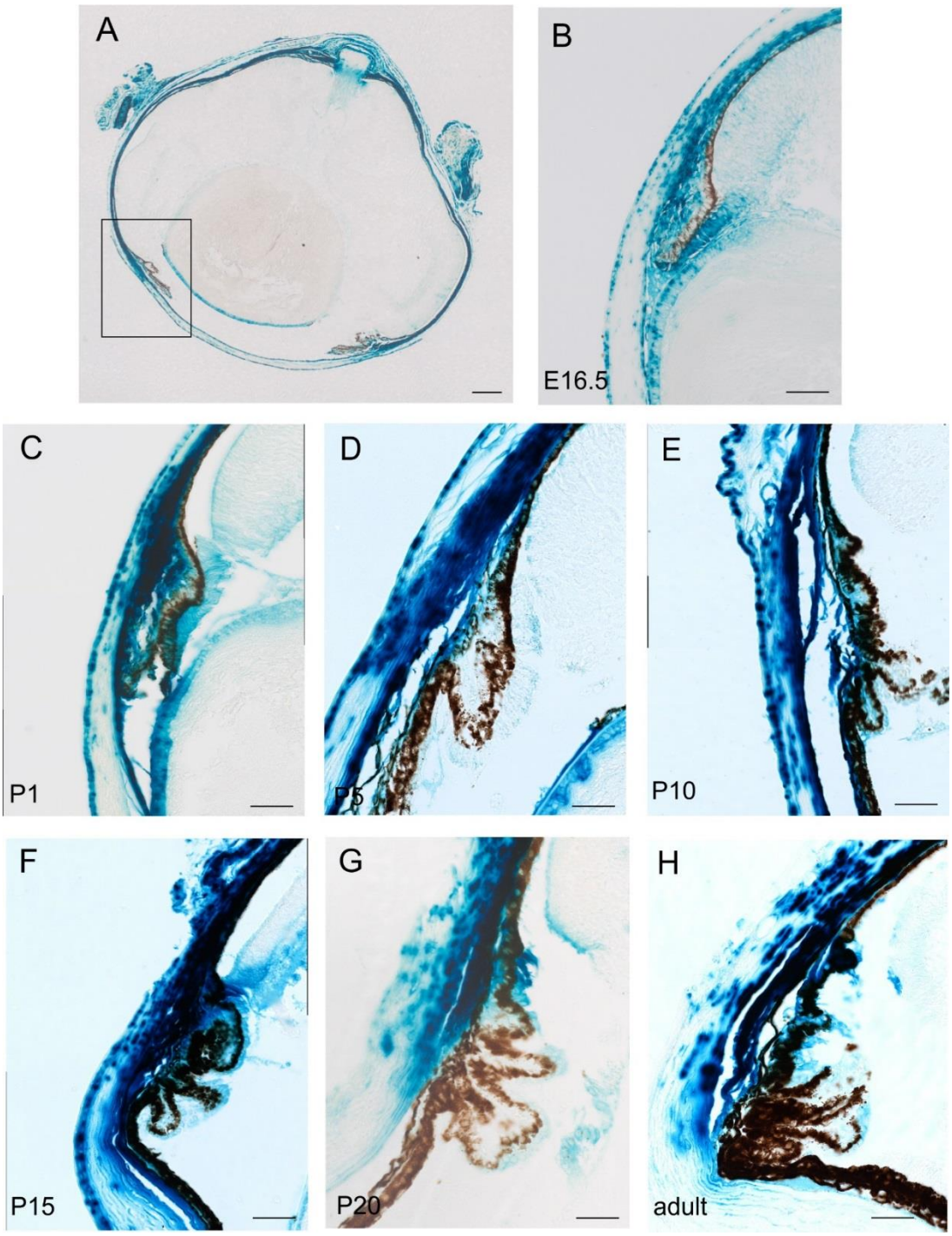

Figure 4-5: Histological LacZ staining in the anterior chamber angle during development and in the adult eye. Panel shows enlarged excerpt of the anterior chamber angle of whole eye sections shown in Figure 4-4. Region of the enlarged excerpt is marked by the rectangle in A. (B) At E16.5, CTGF expression was detected in the undifferentiated angle mesenchyme. (C) At P1, CTGF promotor activity was shown in the mesenchyme of the developing iris and TM, and in the pigmented epithelium of the ciliary body. (D) At P5, CTGF expression was located in the pars plana of the ciliary body, the external layer of the iris and the developing TM. (E) At P10, CTGF expression is similar to P5. (F) At P15, CTGF expression was detected in the pars plana, the pigmented and the non-pigmented epithelium of the ciliary body. (G) At P20, CTGF expression was detected in the pars plana and the non-pigmented epithelium of the ciliary body as well as the TM. (H) In the adult eye, the CTGF expression was restricted to the TM and non-pigmented epithelium of the ciliary body. Scale bar: 50µm.

4.1.3.2. CTGF expression in the posterior eye during development and in the adult eye

In the posterior part of the eye, CTGF promotor activity is detected in the retina, sclera, choroidea und ON with variations in the expression depending on the developmental timepoint (Figure 4-4 A-H). At P1, CTGF expression can be observed in the sclera and choroidea (Figure 4-6 A), in progress of the following developmental stages (P5, P10, P15 and P20) the expression is increased in both tissues (Figure 4-6 B-E). Additionally, CTGF promotor activity is detected in the RPE at these timepoints (Figure 4-6 B-E). In the adult eye, the expression in both choroidea and sclera is diminished and is completely absent in the RPE (Figure 4-6 F). Interestingly, in the retina CTGF expression is detected for the first time at P10 (Figure 4-4 C) and is persistent during the following developmental stages and in the mature eye (Figure 4-4 D, E, G). In detail, CTGF promotor activity visualized by LacZ staining is detected in the INL, ONL and GCL. In the ON, CTGF expression is first detected at P5 and increases during development and in the adult eye (Figure 4-4 A-G). Additionally, the dura mater around the ON revealed an intense CTGF promotor activity. The progress of the CTGF expression in the ON, ONH and dura mater is analyzed in detail in a following chapter. The LacZ staining in WT controls showed no signal either on P20 (Figure 4-4 F) nor in the adult eye (Figure 4-4 H).

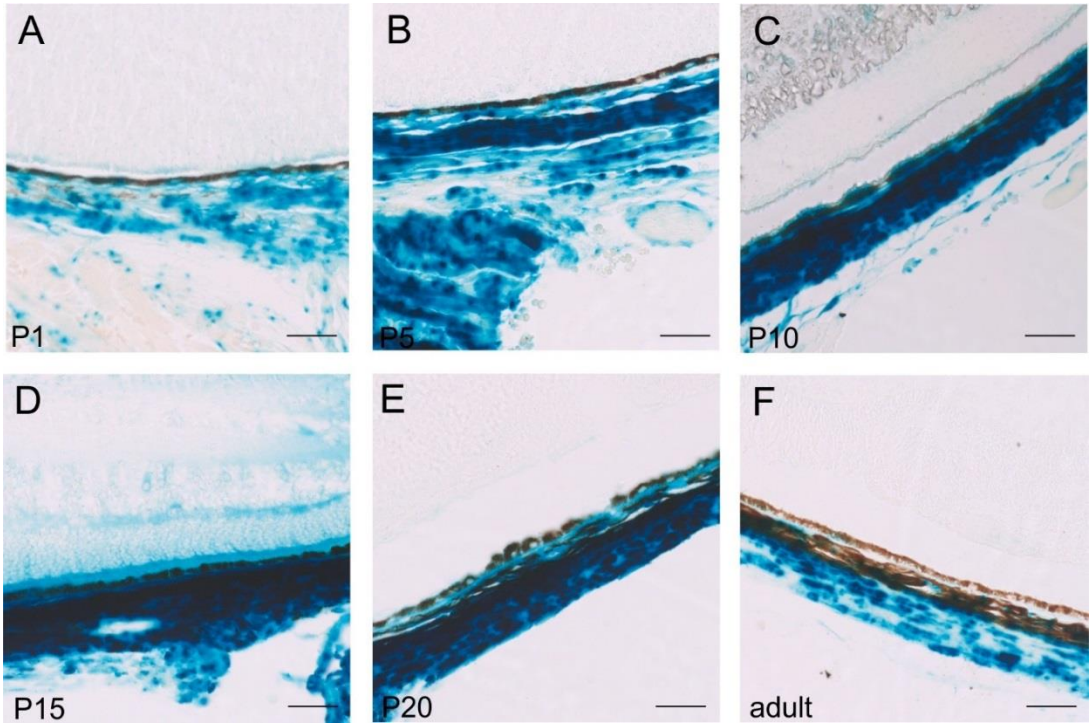

Figure 4-6: Histological LacZ staining in the choroidea and sclera during development and in the adult eye. Panel shows enlarged excerpts of the sections of the whole eyes in Figure 4-4. (A) At P1, CTGF promotor activity was detected in choroidea and sclera. (B) At P5, CTGF promotor activity was detected in the choroidea, sclera and in the RPE. (C) At P10, CTGF promotor activity was detected in the choroidea, sclera and RPE. (D) At P15, CTGF promotor activity was detected in the choroidea, sclera and RPE. (E) At P20, CTGF promotor activity was detected in the choroidea, sclera and RPE. (F) In the adult eye a CTGF promotor activity in the choroidea and sclera was detected. Scale bar: 50µm.

Overall, an intense CTGF promotor activity is detected in the ONH during the development (Figure 4-7). At E16.5, the LacZ staining shows a CTGF promotor activity in the dura mater surrounding the ON and in the hyaloid artery (Figure 4-7 B). At P1, CTGF expression is increased in the dura mater (Figure 4-7 C). At P5, a strong alteration in the distribution of the CTGF expression can be observed as there is an intense expression in the glial lamina and the PRL region of the ONH. CTGF promotor activity in the dura mater remains constant at this developmental timepoint (Figure 4-7 D). This expression pattern of CTGF is persistent at all investigated developmental stages (Figure 4-7 E-G). Only in the adult eye a reduced expression was observed in the dura mater (Figure 4-7 H).

All in all, CTGF is highly expressed in the ONH during development and in the adult eye, mainly restricted to the region of the glial lamina and the PRL region.

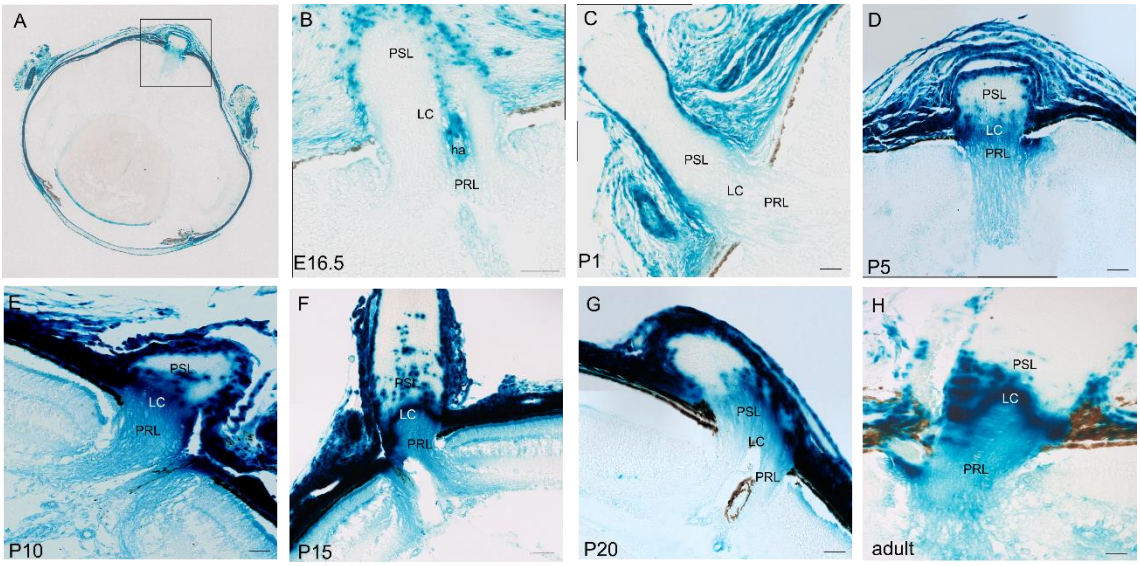

Figure 4-7: Histological LacZ staining in the ON during development and in the adult eye. Panel shows enlarged excerpt of the region of the ONH of whole eye sections shown in Figure 4-4. Region of the enlarged excerpt is marked by the rectangle in A. (B) At E16.5, CTGF expression was detected in the dura mater around the ON and in the hyaloid artery. (C) At P1, CTGF expression was still located at the dura mater. (D) At P5, an intense CTGF promotor activity was detected in the glial lamina, the PRL region and the dura mater. (E, F) At P10 and P15, CTGF promotor activity was increased in the glial lamina, the PRL and the dura mater, and it shows a slight expression in the PSL. (G) At P20, CTGF expression was extenuated in the glial lamina but increased in the dura mater. (H) In the adult eye CTGF was expressed in the glial lamina and the PRL, and with a lower extent in the dura mater. PSL: postlaminar region; LC: Lamina cribrosa region; PRL: prelaminar region; ha: hyaloid artery. Scale bar: 50µm.

Since it was difficult to localize the exact expression pattern of CTGF in the retina in the sagittal sections of the whole eye, retinal flat mounts were performed and analyzed by histological LacZ staining according to the detailed CTGF promotor activity. Based on the observed CTGF expression pattern P15 was chosen for the flat mount analysis. In retinal flat mounts, CTGF promotor activity is observed in the retinal vasculature and in cells spread over the entire retina (Figure 4-8 A). In Figure 4-8 B, the staining of the superficial plexus (asterisk) in the GCL and the cells spread over the entire retina (arrow) can be observed. Furthermore, the representation of the outer layer of the retina (Figure 4-8 C) visualized a LacZ staining in the vasculature of the deep plexus (arrowhead) and also cells spread over the entire retina (arrow).

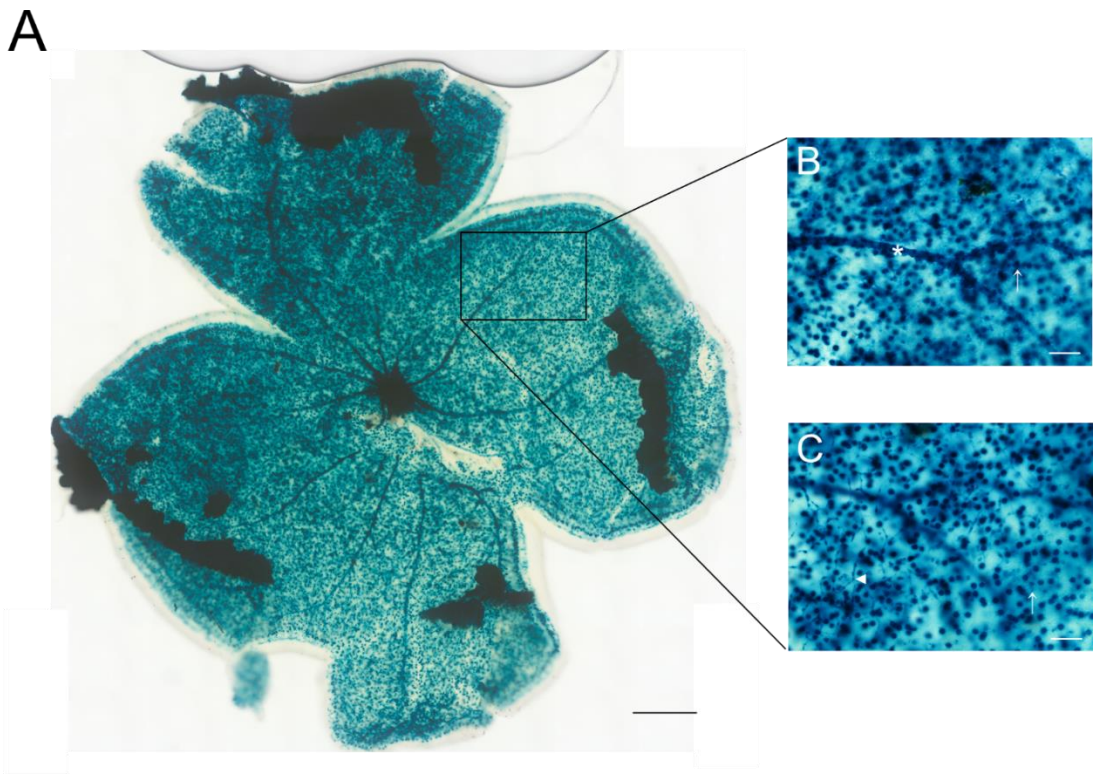

Figure 4-8: Histological LacZ staining of a retinal flat mount of P15 CTGF$^{LacZ+/-}$ mice. (A) In retinal flat mounts, the retinal vasculature and cells spread over the entire retina are detected. (B) Enlarged excerpt of the retinal flat mount showed the LacZ staining in the blood vessels of the superficial plexus (asterisk) and cells spread of the entire retina (arrow). (C) Enlarged excerpt of the retinal flat mount shoed the LacZ staining in the blood vessels of the deep plexus (arrowhead) and the cells spread of the entire retina (arrow). Scale bars: 500µm (A); 50µm (B, C).

4.1.3.3. Immunohistochemical localization of CTGF expression in the anterior eye segment

Since it is not possible to perform histological LacZ staining in combination with immunofluorescence staining, immunohistochemical staining with an antibody specific against β-galactosidase was performed to identify CTGF expressing cell types. Furthermore, the already identified CTGF expression pattern was confirmed by immunohistochemical staining against β-galactosidase. Following experiments were performed on sagittal and tangential sections of eyes at the developmental stage P15 and the adult of the CTGF$^{LacZ+/-}$ mice.

Immunohistochemical staining against β-galactosidase of sagittal section of the cornea verified the specific CTGF promotor activity depending on the developmental stage, which was already shown by histological LacZ staining in the previous experiments. At P15, CTGF expression is present in the corneal endothelium, epithelium and stroma (Figure 4-9 A). Whereas in the adult eye, CTGF promotor activity is restricted to the corneal endothelium (Figure 4-9 B).

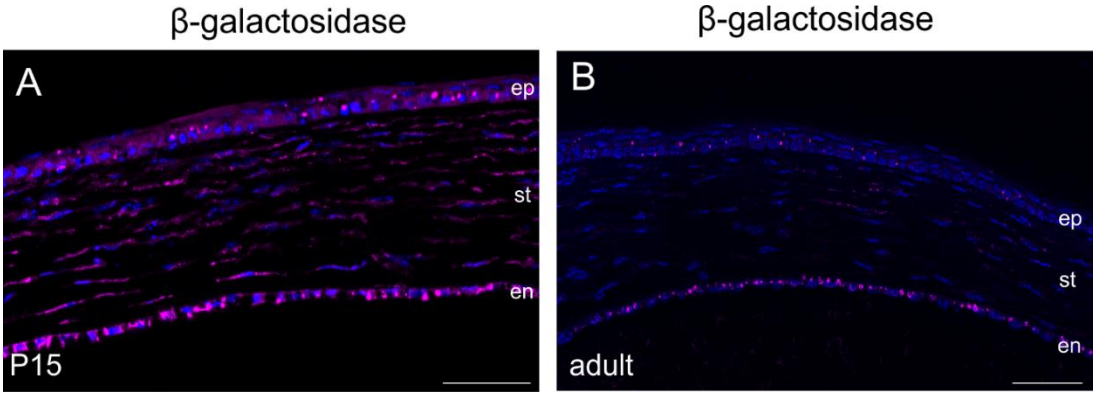

Figure 4-9: CTGF promotor activity in the cornea. (A) Immunohistochemical staining against β-galactosidase (purple) in sagittal sections of the cornea of P15 CTGF$^{LacZ+/-}$ mice. CTGF promotor activity was detected in the corneal epithelium, stroma and endothelium. (B) Immunohistochemical staining in sagittal sections of the cornea of adult CTGF$^{LacZ+/-}$ mice. CTGF promotor activity was detected in the corneal endothelium. Nuclear DNA is labeled with DAPI (blue). ep: epithelium; st: stroma; en: endothelium. Scale bar: 50µm.

Immunohistochemical staining against β-galactosidase in the anterior chamber angel could verify the previous findings in this region. CTGF shows an intense and persistent expression in the TM during development (P15) (Figure 4-10 A) and in the adult mouse eye (Figure 4-10 B). CTGF promotor activity in the ciliary body changes during the development and in the adult eye. At P15, CTGF is expressed in the ciliary stroma and the pigmented epithelium of the ciliary body (Figure 4-10 A). In the adult eye, CTGF promotor activity is detected mostly in the nonpigmented epithelium and with a low expression in the ciliary stroma (Figure 4-10 B).

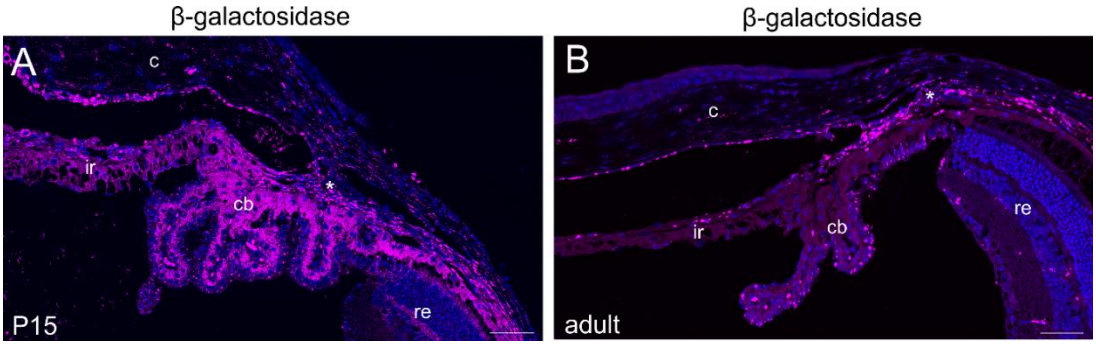

Figure 4-10: CTGF promotor activity in the anterior chamber angle. (A) Immunohistochemical staining against β-galactosidase (purple) in the anterior chamber angle of P15 CTGF$^{LacZ+/-}$ mice showed an intense CTGF expression in the TM, the ciliary body and the cornea. (A) Immunohistochemical staining against β-galactosidase in the anterior chamber angle of adult CTGF$^{LacZ+/-}$ mice showed CTGF promotor activity in the TM, the non-pigmented epithelium of the ciliary body and the corneal endothelium. c: cornea; ir: iris; cb: ciliary body; re: retina; TM is depicted by an asterisk. Nuclear DNA is labeled with DAPI (blue). Scale bar: 50µm.

To identify CTGF promotor activity in the endothelial lining of SC, sagittal sections of the anterior chamber angle of adult CTGF$^{LacZ+/-}$ mice were double stained with β-galactosidase and CD31, a specific marker for endothelial cells (Figure 4-11 A, B). The endothelial lining of SC was nicely stained by CD31 (Figure 4-11 A, B). CTGF promotor

activity was detected directly adjacent to the SC, showing the expression in the TM and to a lower extent in endothelial cells of the SC (Figure 4-11 A'', B''; arrow).

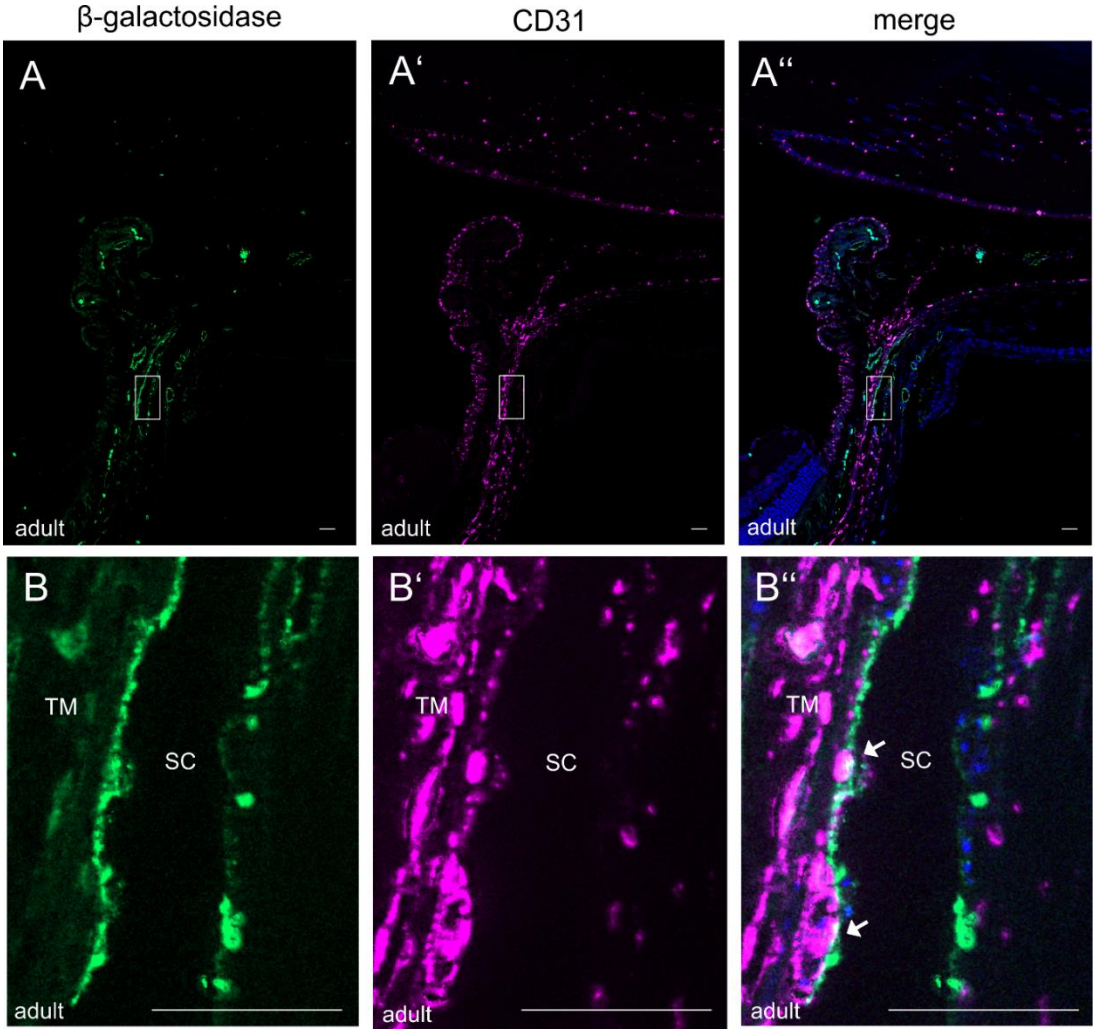

Figure 4-11: CTGF promotor activity in the endothelial lining of SC. (A) Immunohistochemical staining against β-galactosidase (purple) and CD31 (green) in the anterior chamber angle of adult $CTGF^{LacZ+/-}$ mice. (B) Enlarged excerpt showed the colocalization of CTGF promotor activity (purple) with CD31 positive endothelial cells of the SC (green). Arrow depicts the colocalization. TM: trabecular meshwork; SC: Schlemm`s canal; Nuclear DNA is labeled with DAPI (blue). Scale bar: 20µm.

4.1.3.4. CTGF expressing cell types in the developing and adult retina

The analysis of CTGF promotor activity in the retina during development and in the adult eye by histochemical LacZ staining showed an equal expression pattern at both timepoints. CTGF expression was detected in the GCL, in cells in the innermost portion of the INL, in cell processes in the ONL, in the choroidea and in the sclera.

Immunohistochemical staining against β-galactosidase in the retina during development and in adult eye confirmed the expression pattern of CTGF by histological LacZ staining. CTGF expression is detected in the GCL, the INL and in fibers extending through the entire retina, from the ILM to the OLM. Furthermore, signal for CTGF promotor activity is

detected in the choroidea and sclera. This expression pattern remains constant at both stages (Figure 4-12 A, B).

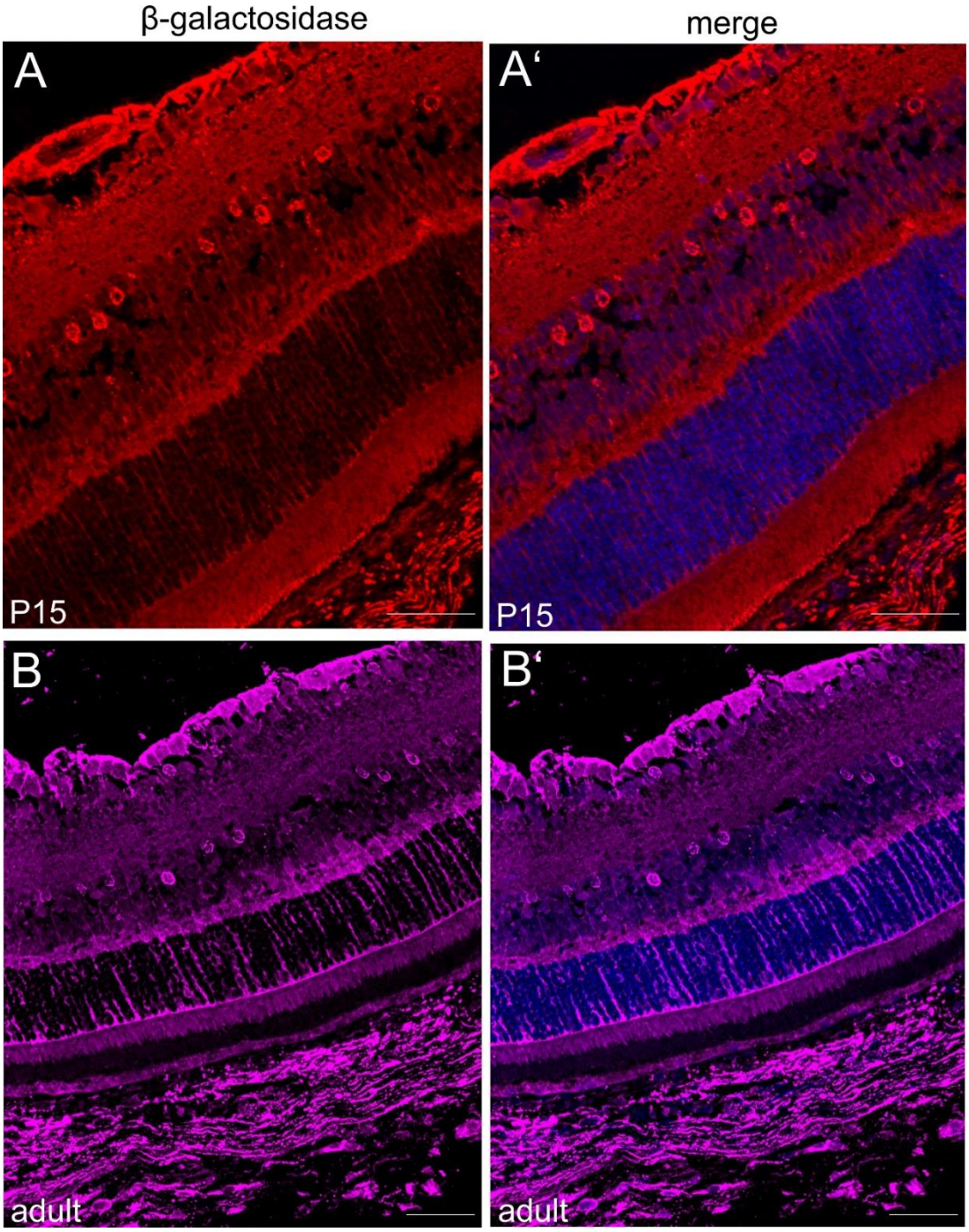

Figure 4-12: Localization of CTGF promotor activity in the retina. (A) Immunohistochemical staining against β-galactosidase (purple) in the retina of P15 CTGF$^{LacZ+/-}$ mice. CTGF promotor activity was detected in the GCL, in cells in the innermost portion of the INL, in processes extending the entire retina, the choroidea and the sclera. (B) Immunohistochemical staining against β-galactosidase (purple) in the retina of adult CTGF$^{LacZ+/-}$ mice. CTGF promotor activity was detected in the GCL, in cells in the innermost portion of the INL, in processes extending the entire retina, the choroidea and the sclera. Nuclear DNA is labeled with DAPI (blue). Scale bar: 50µm.

Retinal flat mounts at P15 were stained against β-galactosidase (Figure 4-13). The vertical view of the 3D reconstruction of z-stacks through the entire retina revealed an intense CTGF expression in the innermost layer of the retina, the GCL and in a deeper layer additionally (Figure 4-13 A). By single recording in the appropriate layer, the detailed CTGF expression in the blood vessels of the superficial plexus and the cells spreading over the entire retina (Figure 4-13 B) as well as the CTGF expressing cells in the deeper layer (Figure 4-13 C) were visualized in detail.

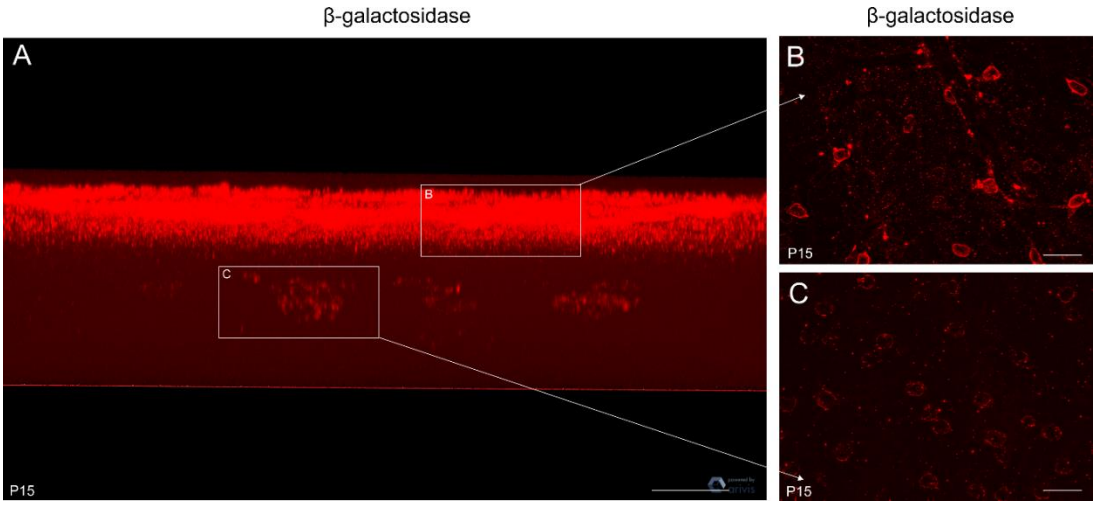

Figure 4-13: Immunohistochemical staining against β-galactosidase (red) on retinal flat mounts of P15 CTGF$^{LacZ+/-}$ mice. (A) Vertical view of 3D representation of a retinal flat mount. An intense β-galactosidase staining was detected in the most inner layer of the retina and additionally in a deeper layer of the retina. (B) Enlarged excerpt of the staining in the inner layer of the retina. β-galactosidase staining indicated an endothelial expression and was localized in an additional cell type. (C) Enlarged excerpt of the β-galactosidase staining in the deeper layer of the retina, visualized a staining of rounded cell bodies of cells spread over the entire retina. Scale bar: 20µm.

4.1.3.4.1. CTGF expression in the retinal and choroidal vasculature

As CTGF shows an intense expression in the GCL and the choroidea, it leads to the suggestion that CTGF is expressed in endothelial cells of the superficial plexus and the choroidal vasculature Therefore, FITC-Dextran perfused retinal flat mounts and immunohistochemical staining against CD31 were double stained with β-galactosidase. FITC-Dextran perfused P15 retinal flat mounts visualized the superficial plexus and the double staining with β-galactosidase showed CTGF expression in endothelial cells of the superficial plexus (Figure 4-14 A). Enlarged sections visualized the close contact of β-galactosidase positive cells to the blood vessels of the superficial plexus, indicating that endothelial cells are the source of the CTGF promotor activity in the GCL. (Figure 4-14 B, C).

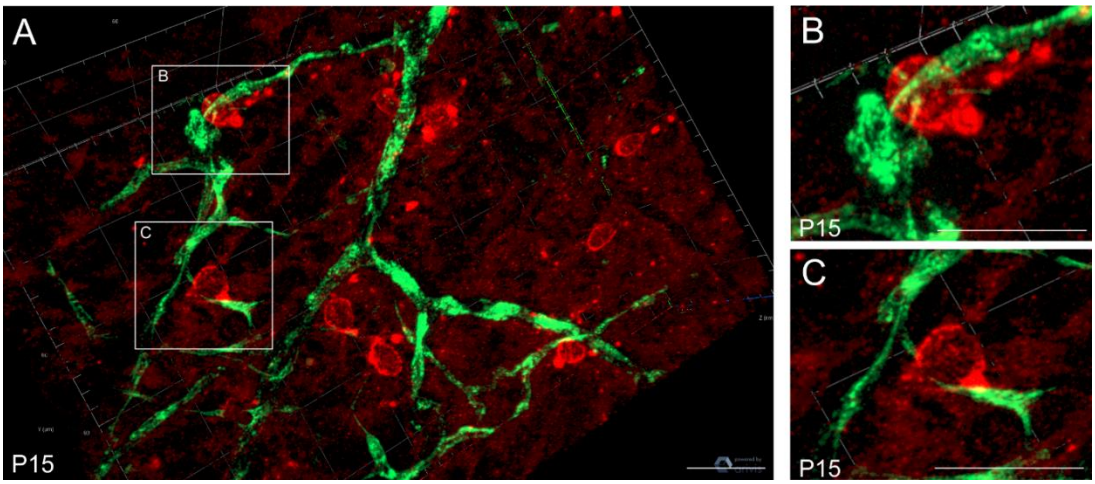

Figure 4-14: Immunohistochemical staining against β-galactosidase of FITC-Dextran perfused retinal flat mounts of CTGF$^{LacZ+/-}$ mice. (A) 3D representation of a FITC-Dextran (green) perfused retinal flat mount stained against β-galactosidase (red) indicated an endothelial localization of CTGF expression. (B, C) Enlarged excerpts demonstrated the staining of β-galactosidase in endothelial cells. Scale bar: 20µm.

Due to the thickness of retinal flat mounts, immunohistochemical staining is difficult as antibodies do not penetrate through the entire tissue Therefore, immunohistochemical staining were performed on retinal sagittal sections to identify CTGF expressing cell types. By immunohistochemical staining against CD31, the endothelial cells in the vasculature of retinal superficial plexus (Figure 4-15 A', B') and the choroidea (Figure 4-16 A', B') was visualized. In combination with β-galactosidase staining a localization of CTGF in endothelial cells of the retinal (Figure 4- 15 A'', B''; arrow) and choroidal vasculature (Figure 4-16 A'', B''; arrow) was detected.

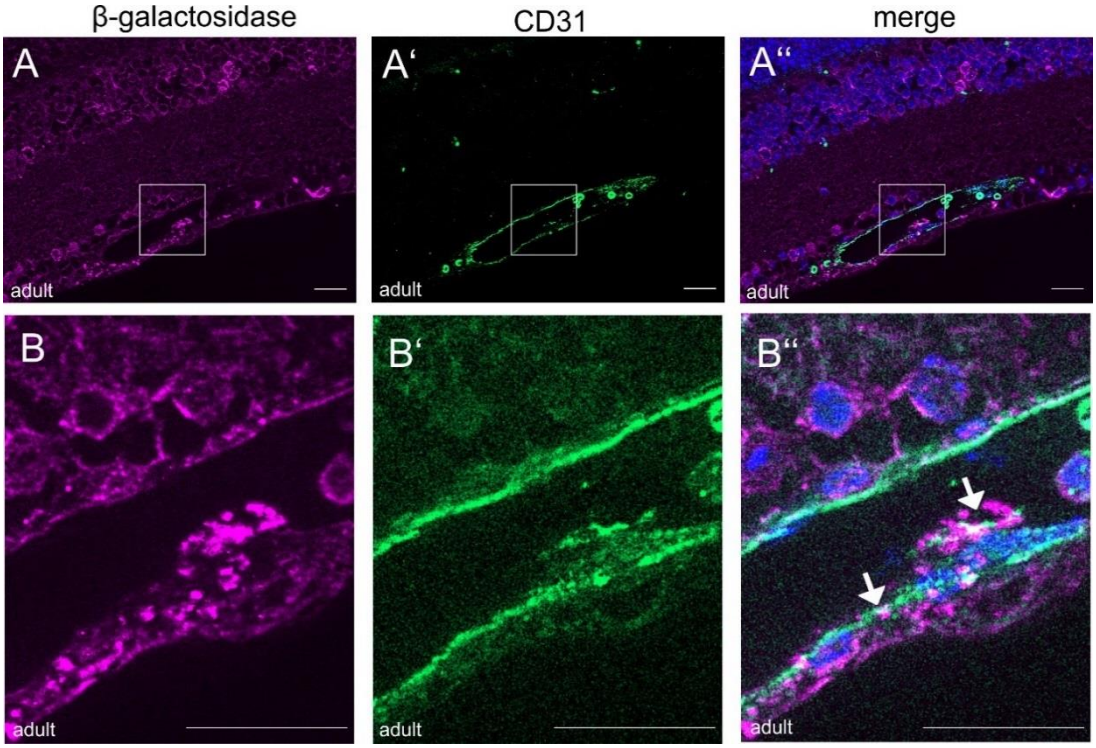

Figure 4-15: CTGF promotor activity in the adult retinal vasculature. Immunohistochemical staining against β-galactosidase (purple) and CD31 (green) of retinal sections of adult $CTGF^{LacZ+/-}$ mice. (A) CD31 (green) specifically stained the endothelial cells in the blood vessels of the superficial plexus in the GCL. Co-staining against β-galactosidase (purple) visualized a co-localization with endothelial cells. (B) Enlarged excerpt demonstrated the localization of β-galactosidase (purple) with endothelial cells, stained with CD31 (green). Arrow depicts co-localization. Nuclear DNA is labeled with DAPI (blue). Scale bar: 20µm.

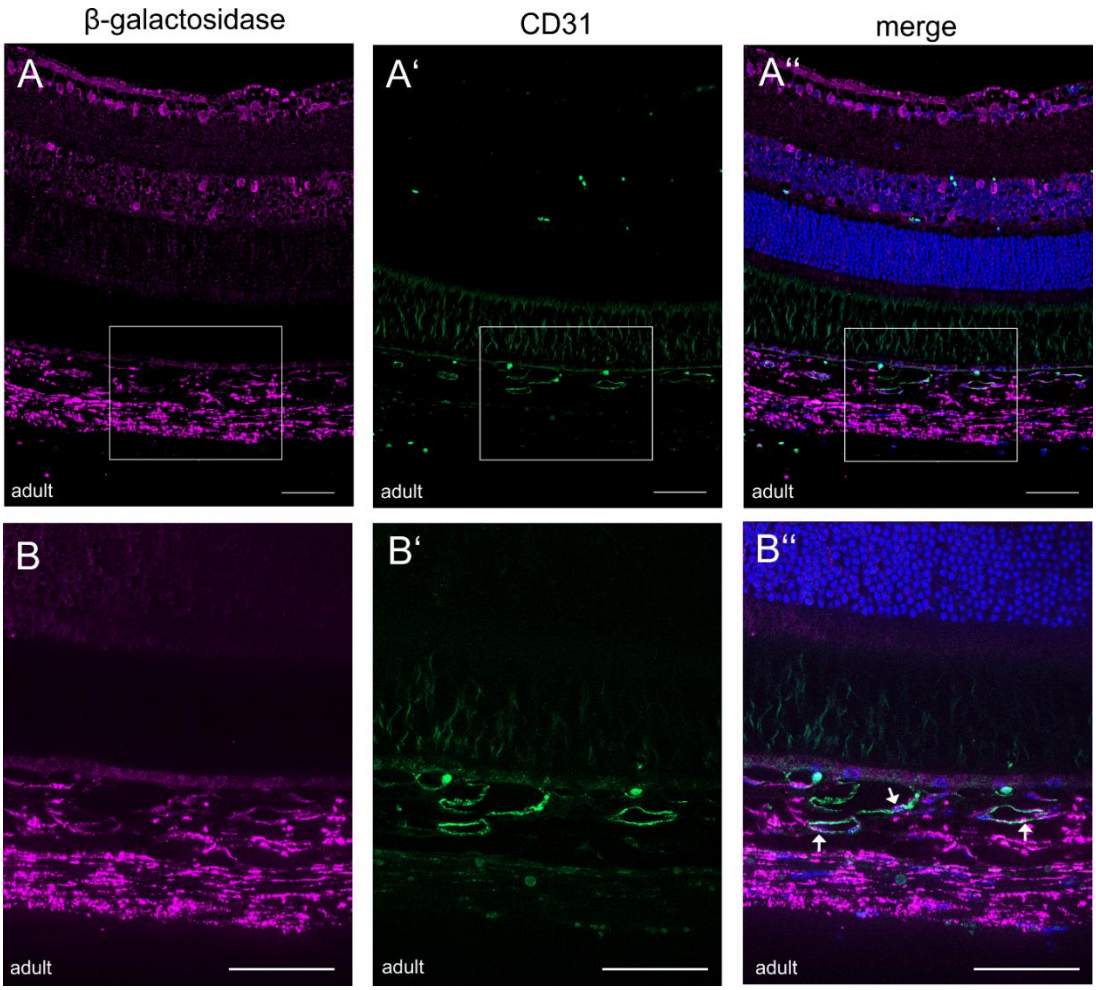

Figure 4-16: CTGF promotor activity in the choroidal vasculature. (A) Immunohistochemical staining of β-galactosidase (purple) and CD31 (green) in sagittal sections of adult CTGF$^{LacZ+/-}$ mice. Endothelial cells of the choroidal vasculature are nicely visualized by CD31 staining. β-galactosidase staining shows a CTGF expression in the retina, choroidea and sclera. (B) Enlarged excerpt of choroidal vasculature showing the localization of the CTGF promotor activity in the endothelial cells of blood vessels in the choroidea. Nuclear DNA is labeled with DAPI (blue). Scale bar: 20µm.

4.1.3.4.2. CTGF expression in retinal glial cells

Furthermore, β-galactosidase staining in the NFL and GCL leads to the suggestion that the observed CTGF expression derives from retinal astrocytes. Therefore, immunohistochemical staining against β-galactosidase in combination with GFAP, a specific marker for astrocytes were performed on sagittal retinal sections of P15 and adult CTGF$^{LacZ+/-}$ mice. GFAP immunoreactivity identified the retinal astrocytes restricted to the vitreal surface of the retina, merely located in the NFL (Figure 4-17 A’- D’). By double staining with β-galactosidase no CTGF expression was detected in retinal astrocytes either on P15 nor in the adult retina (Figure 4-17 A’’-D’’).

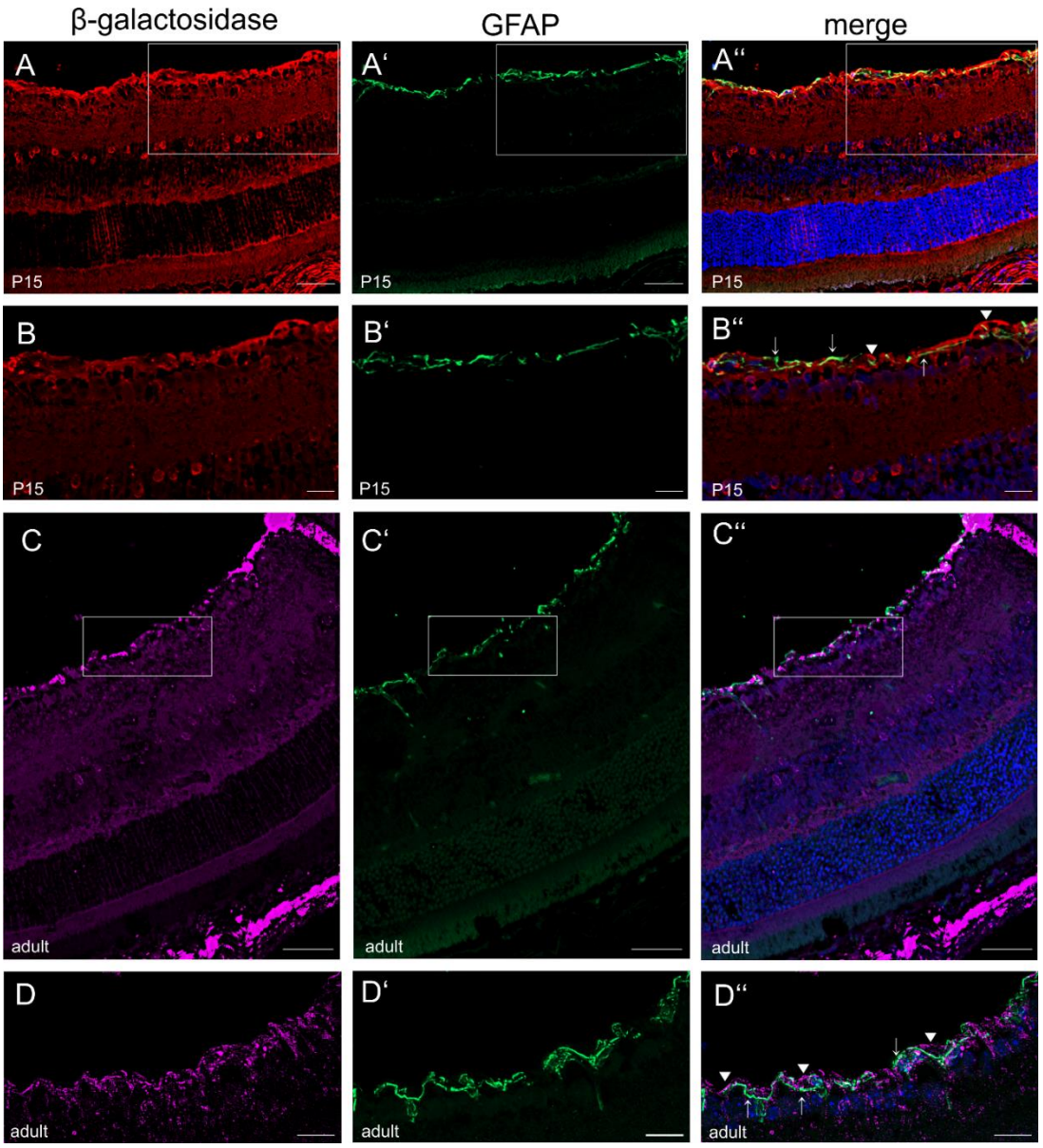

Figure 4-17: CTGF is not expressed in retinal astrocytes. (A) Immunohistochemical staining against β-galactosidase (purple) and GFAP (green) on retinal section of P15 $CTGF^{LacZ+/-}$ mice. (B) Enlarged excerpt showed no co-localization of β-galactosidase (purple) and GFAP (green). (C) Immunohistochemical staining against β-galactosidase (purple) and GFAP (green) on retinal section of adult $CTGF^{LacZ+/-}$ mice. (D) Enlarged excerpt showed no co-localization of β-galactosidase (purple) and GFAP (green). Nuclear DNA is labeled with DAPI (blue). Scale bar: A, C: 50µm; B, D: 20µm.

As it was shown that retinal astrocytes are not the source of the CTGF promotor activity in the GCL and as the expression of CTGF detected in fibers extending the entire retina, it leads to the suggestion that Müller cells are the CTGF expressing cell type. Therefore, double staining against glutamine synthetase (GS), a specific marker for Müller cells and β-galactosidase were performed (Figure 4-18 A-E). GS staining specifically visualized the Müller cell processes penetrating the whole retina, from the ILM to the OLM (Figure 4-18 A'-E'). This expression pattern of GS in Müller cells matches the immunoreactivity observed for β-galactosidase (Figure 4-18 A-E). This co-localization of GS and CTGF

promotor activity demonstrates that Müller cells are a source of CTGF promotor activity in the retina during development and in the adult eye (Figure 4-18 A''- E'').

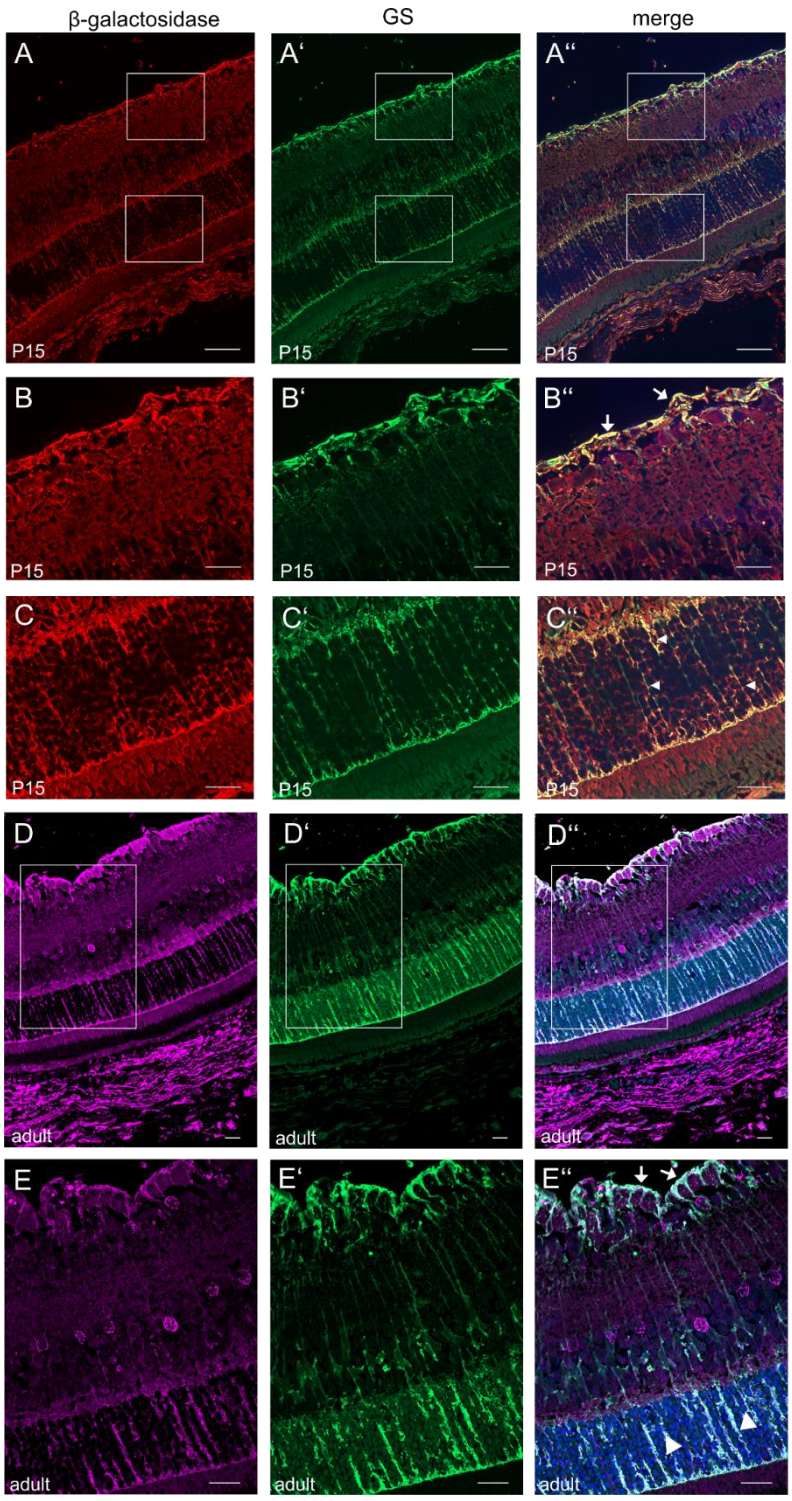

Figure 4-18: CTGF promotor activity in Müller cells of the retina. (A) Immunohistochemical staining of β-galactosidase (red) and GS (green) in retinal sagittal sections of P15 CTGF$^{LacZ+/-}$ mice. (B) Enlarged excerpt of the GCL and IPL indicated by the rectangle in A, showing CTGF expression in Müller cells, forming the ILM. (C) Enlarged excerpt of the ONL indicated by the rectangle in A, showing CTGF expression in Müller cells processes and in the OLM, formed by Müller cells. (D) Immunohistochemical staining of β-galactosidase (purple) and GS (green) in retinal sagittal sections of adult CTGF$^{LacZ+/-}$ mice. (E) Enlarged excerpt, indicated by the rectangle in D, showing CTGF expression in Müller cell processes, in the ILM and the OML. Nuclear DNA is labeled with DAPI (blue). Scale bar: 50µm (A); 20µm (B-E).

As CTGF promotor activity was detected in the GCL the possibility that microglia cells are an additional source of the CTGF expression was tested by immunohistochemical staining against the ionized calcium binding adaptor molecule 1 (IBA1), a specific marker for microglia and macrophages. It was not possible to perform double immunohistochemical staining against IBA1 and β-galactosidase as the host species of both antibodies was rabbit. Furthermore, the issue that these antibodies were the best working one, the analysis of microglia as a potential source of the CTGF promotor activity was performed on two consecutive sections of the same retina. IBA1 staining visualized the well-defined localization of microglia in the IPL and OPL as well as the GCL and the ON (Figure 4-19 B, D). To compare both staining enlarged excerpts of the same region of the retina of both sections were analyzed (Figure 4-19 C, D). No β-galactosidase staining is observed in the IPL or OPL layer, which indicates that microglia located at these retinal layers are not the CTGF expressing cells type (Figure 4-19 C, D). Since no CTGF promotor activity was observed in the IPL and OPL, it leads to the assumption that microglia are not a CTGF expressing cell type within the retina and the ON.

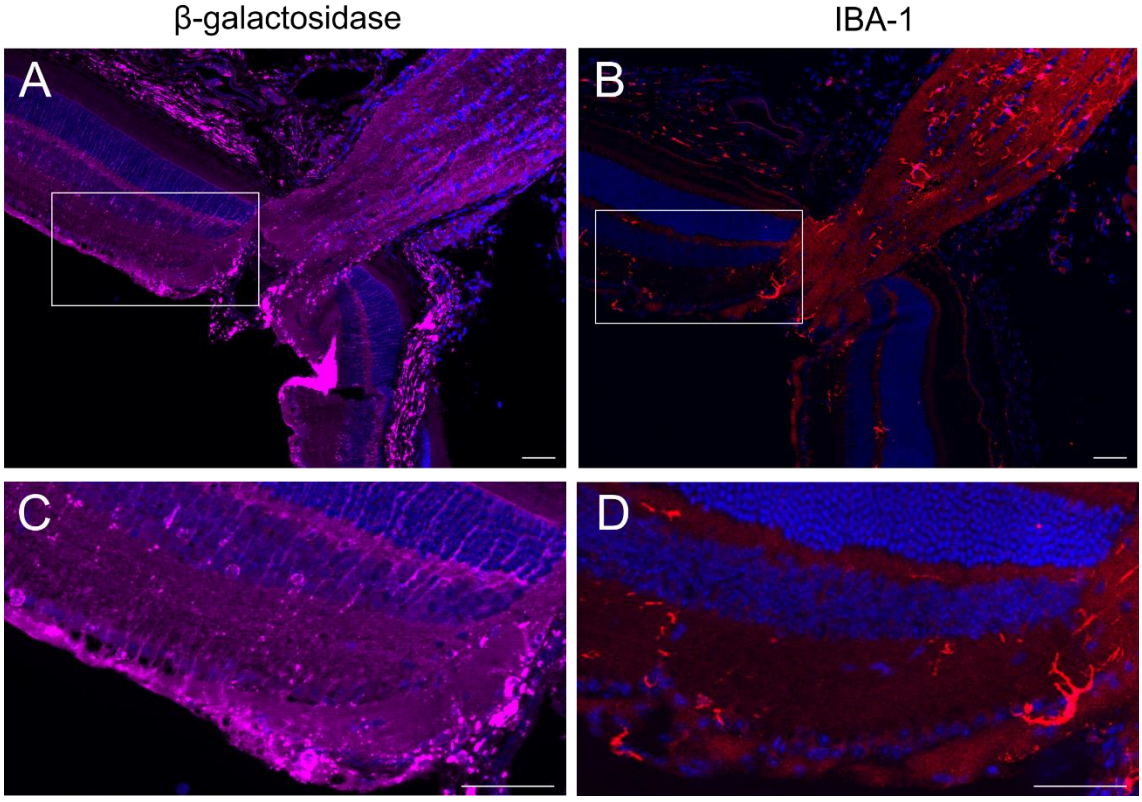

Figure 4-19: Immunohistochemical staining of retinal sections of adult CTGF$^{LacZ+/-}$ mice against β-galactosidase and IBA1. (A) β-galactosidase staining (purple) of sagittal sections of the retina and the ON. (B) IBA1 staining (red) of sagittal sections of the retina and the ON. (C) Enlarged excerpt of β-galactosidase staining (purple) showed CTGF expression in the GCL and INL. (D) Enlarged excerpt of the IBA1 staining (red) visualized microglia located at the GCL, IPL and OPL. Nuclear DNA is labeled with DAPI (blue). Scale bar: 50µm.

4.2.3.4.3. CTGF expression in retinal interneurons

Additionally, to CTGF positive Müller cells, β-galactosidase staining was detected in cells in the GCL and the innermost layer of the INL (Figure 4-20 A-D). By combination of their position within the retina, cell morphology and cell quantity, these cells have pegged as amacrine cells. Amacrine cells, a heterogeneous group of retinal interneurons, are located at the vitreal side of the INL and as displaced amacrine cells in the GCL. They can be distinguished from bipolar and horizontal cells, by their cell morphology and location within the retina. Horizontal cells are located at the outmost portion of the INL and bipolar cells are found in the INL, but not in the GCL. Additionally, by immunohistochemical staining against Syntaxin-1A, a marker for amacrine cells, it was confirmed that amacrine cells express CTGF in the adult eye (Figure 4-21 A, B).

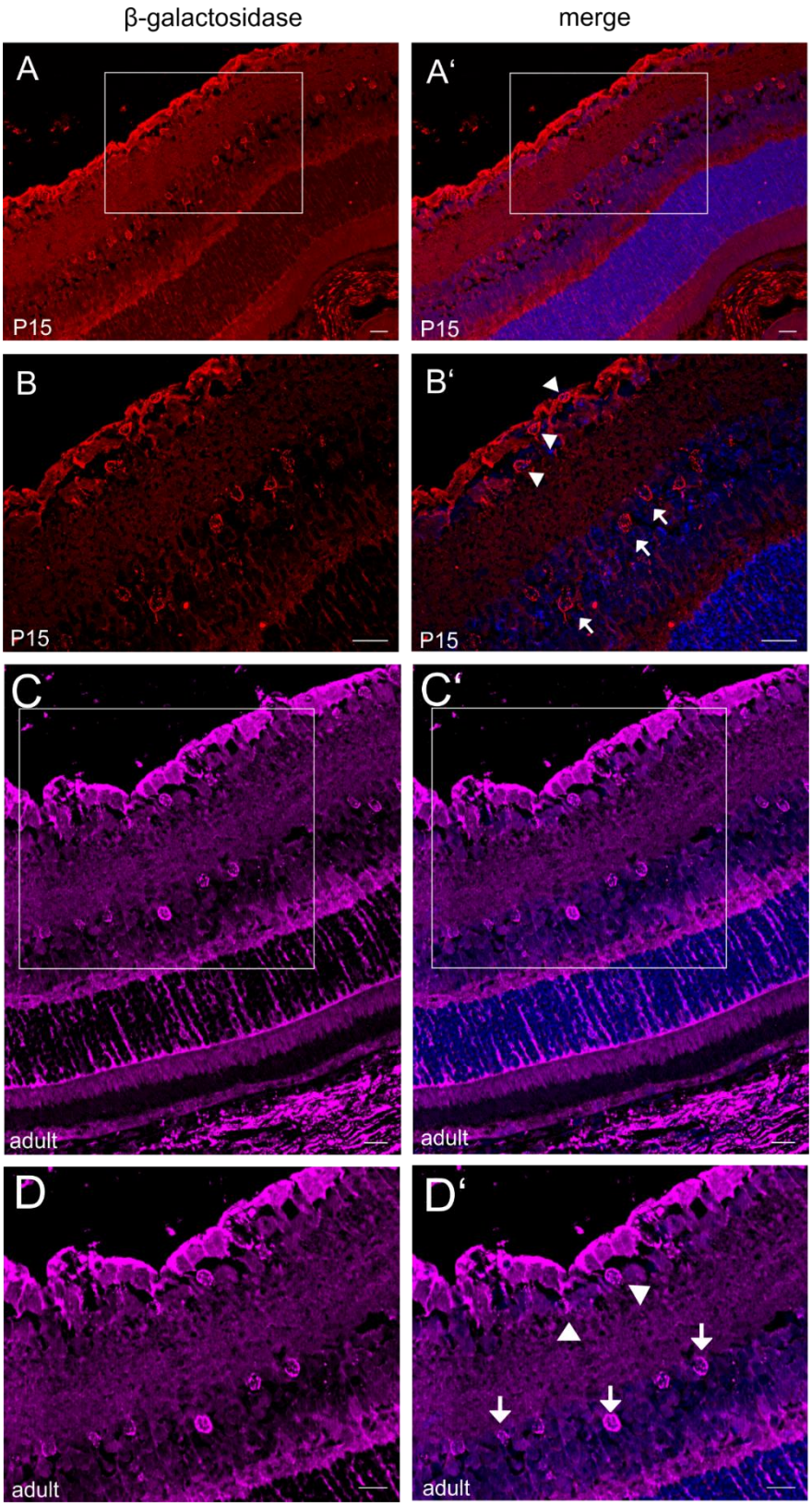

Figure 4-20: CTGF promotor activity in the INL and GCL. (A) Immunohistochemical staining against β-galactosidase (red) on retinal sections of P15 CTGF$^{LacZ+/-}$ mice. (B) Enlarged excerpts demonstrated the expression of CTGF in cells in the INL and GCL, indicating for amacrine cells as the source of the CTGF promotor activity. (C) Immunohistochemical staining against β-galactosidase (purple) on retinal sections of adult CTGF$^{LacZ+/-}$ mice. (D) Enlarged excerpts demonstrated the expression of CTGF in cells in the INL and GCL, indicating for amacrine cells as the source of the CTGF promotor activity. Nuclear DNA is labeled with DAPI (blue). Scale bar: 20µm.

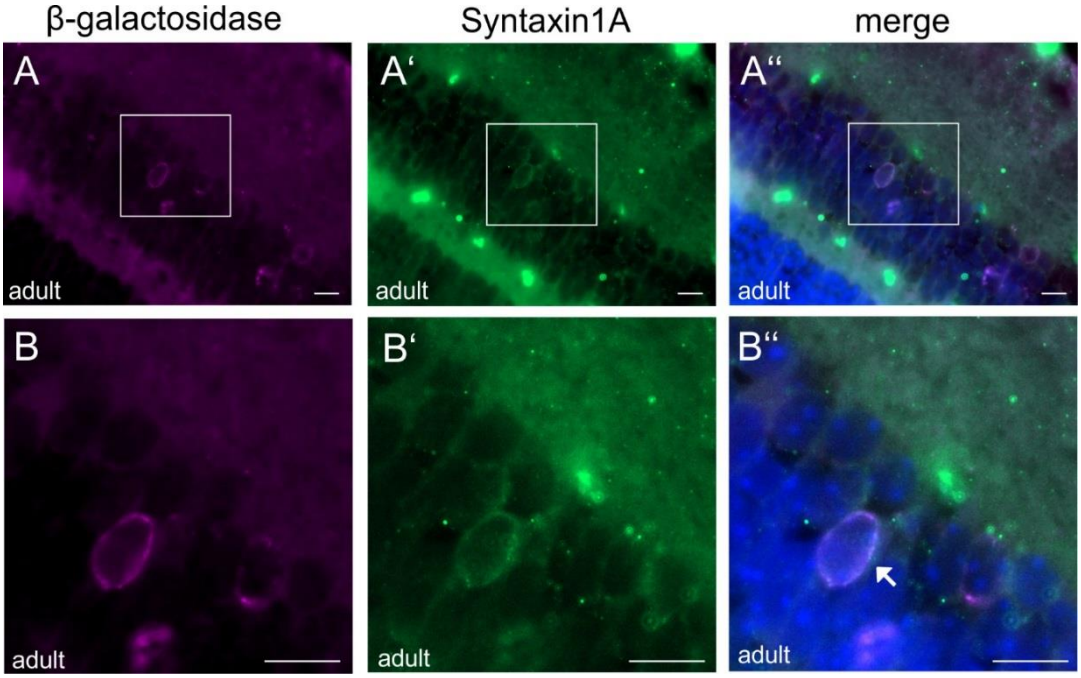

Figure 4-21: CTGF promotor activity in amacrine cells in the adult retina. (A) Immunohistochemical staining against β-galactosidase (purple) and Syntaxin-1A (green) of retinal sections of adult CTGF$^{LacZ+/-}$ mice. Syntaxin-1A staining detects specifically amacrine cells in the outermost portion of the INL. (B) Enlarged excerpt shows a Syntaxin-1A stained amacrine cell in the INL and demonstrates the CTGF promotor activity in amacrine cells by the co-localization with β-galactosidase (purple). Sytnaxin-1A and β-galactosidase co-localization is depicted by an arrow. Nuclear DNA is labeled with DAPI (blue). Scale bar: 10µm

All in all, it can be summarized that CTGF expressing cell types in the retina do not differ at P15 and in the adult eye. It was shown that Müller cells, amacrine cells and endothelial cells are the source for CTGF promotor activity in the mouse retina during development and in the adult eye.

4.1.3.5. CTGF expressing cell types in the developing and adult ON

In the ON, especially in the ONH an intense CTGF promotor activity was observed by histological LacZ staining during the development and in the mature eye. The major cell type in the ON are astrocytes, therefore immunohistochemical staining against GFAP in combination with an antibody against β-galactosidase was performed on sagittal and tangential sections of the ON. β-galactosidase expression is observed throughout the entire ON with a more intense staining in the PRL region and the glial lamina (Figure 4-22 A, C). Within the RPL region and the glial lamina, the enhanced CTGF promotor activity is mostly localized adjacent to the astrocyte nuclei (Figure 4-22 B, D) The CTGF expression pattern is equal in the developmental and adult ON. The expression intensity of P15 and adult sections cannot be compared as they the staining was not performed simultaneously.

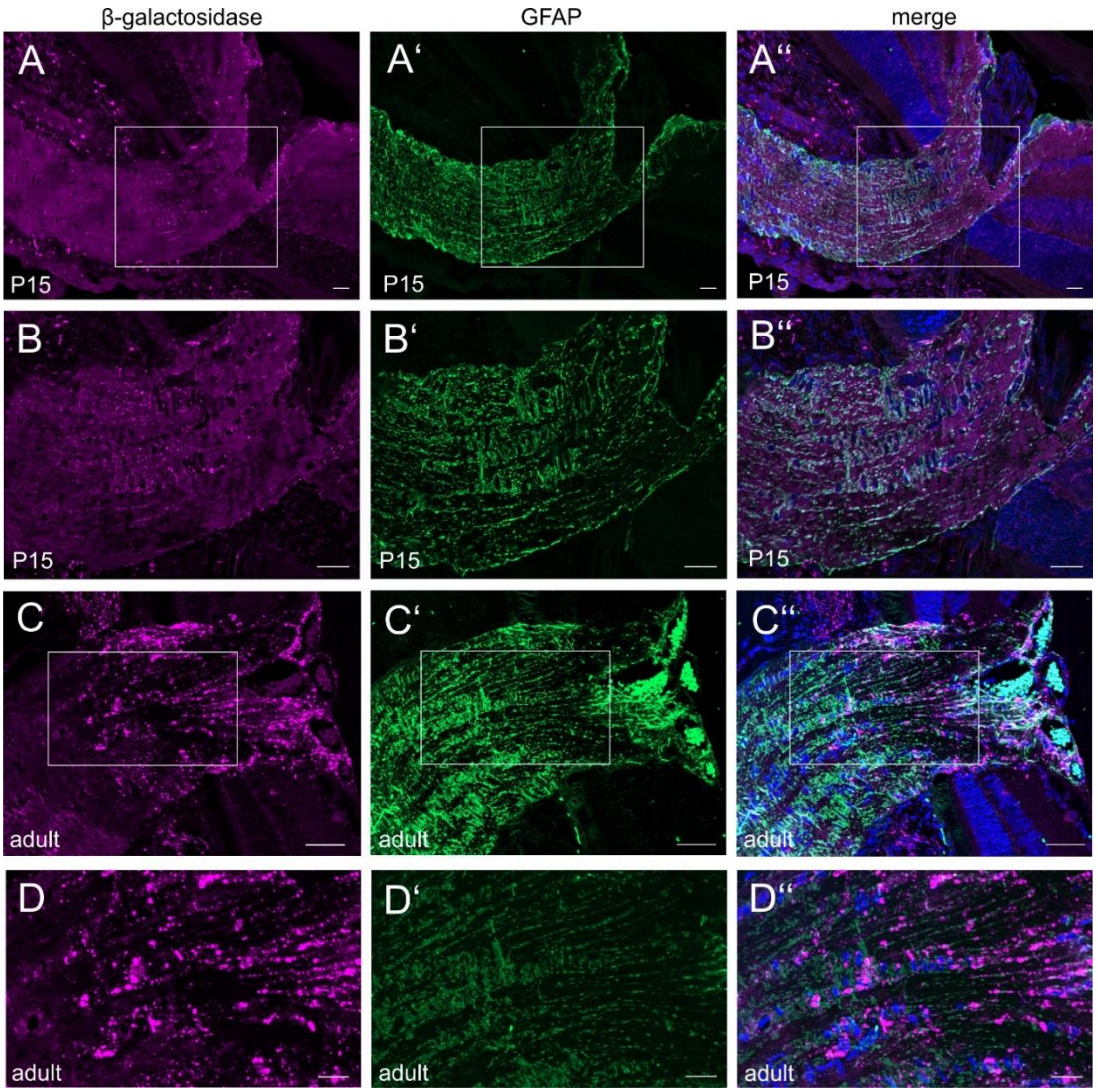

Figure 4-22: CTGF promotor activity in the ON. (A) Immunohistochemical staining against β-galactosidase (purple) and GFAP (green) on sagittal ON sections of P15 CTGF$^{LacZ+/-}$ mice. The β-galactosidase staining revealed CTGF expression in the entire ON with an enhanced expression in the glial lamina. (B) Enlarged excerpt demonstrated the co-localization of the CTGF promotor activity with ON astrocytes. (C) Immunohistochemical staining against β-galactosidase (purple) and GFAP (green) on sagittal ON sections of adult CTGF$^{LacZ+/-}$ mice. β-galactosidase staining revealed CTGF expression in the entire ON, with an enhanced expression in the glial lamina and the PRL region. (D) Enlarged excerpts demonstrated the colocalization of the CTGF promotor activity with ON astrocytes. Nuclear DNA is labeled with DAPI (blue). Scale bar: 50µm (A, B); 20 µm (B, D).

As the composition of cell types varies depending on the localization in the ON sections we analyzed variations in CTGF promotor activity in these different regions. Therefore, successive tangential sections of the same ON at different positions were produced for both P15 and adult CTGF$^{LacZ+/-}$ mice. In the schematic illustration, the ONH and the major elements are shown (Figure 4-23). The positions of the tangential sections performed in the following experiments are depicted in the schematic illustration with different letters A to C (Figure 4-23).

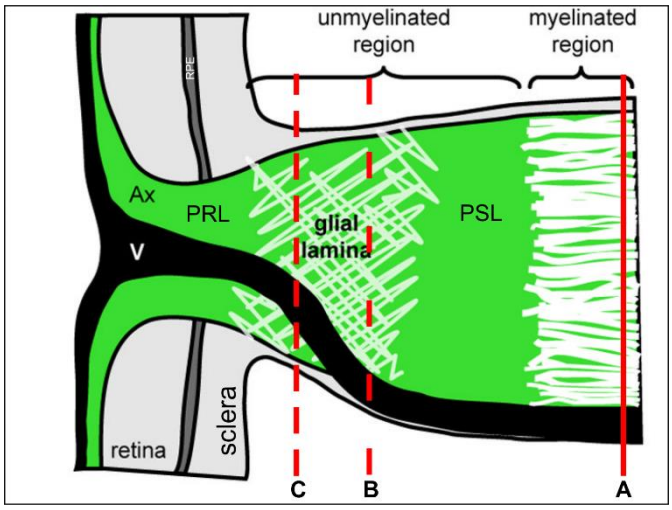

Figure 4-23: Schematic illustration of the ONH and the major elements located there. The red lines demonstrate the origin of the tangential sections performed in the following experiments. V: blood Vessel; Ax: axons; RPE: retinal pigmented epithelium; PRL: prelaminar region; PRL: postlaminar region (Adapted and modified from Sun et al., 2009; Howell et al., 2007).

The section depicted with A is located in the myelinated ON, containing mostly oligodendrocytes, myelinated axons and astrocytes with lower extent. The double staining in this region showed a slight CTGF expression colocalized with GFAP-positive astrocytes, specifically marked by GFAP (Figure 4-24 A and Figure 4-25 A). The highest expression is observed in the dura mater around the ON (Figure 4-24 A and Figure 4-25 A). In the anterior region of the ON, tangential sections in two different positions of the glial lamina were produced. The sections depicted with B was established at the posterior side of the glial lamina, indicated by the formation of astrocyte processes to glial tubes and the entering of the blood vessel (Figure 4-24 B and Figure 4-25 B). The sections depicted with C was produced in the more anterior position of the glial lamina indicated by the position of the blood vessel with in the ON sections (Figure 4-24 C and Figure 4-25 C). Immunohistochemical staining against β-galactosidase shows the highest CTGF promotor activity in the glial lamina, showed by the tangential sections B and C. The CTGF expression is colocalized with the intermediate filaments of the astrocytes. In comparison to the posterior part of the ON, an enhanced CTGF promotor activity is detected adjacent to the cell nuclei of astrocytes (Figure 4-24 B'', C'' and Figure 4-25 B'', C''). The CTGF expression pattern in the ON and the glial lamina is equal at both stages (Figure 4-24, 25).

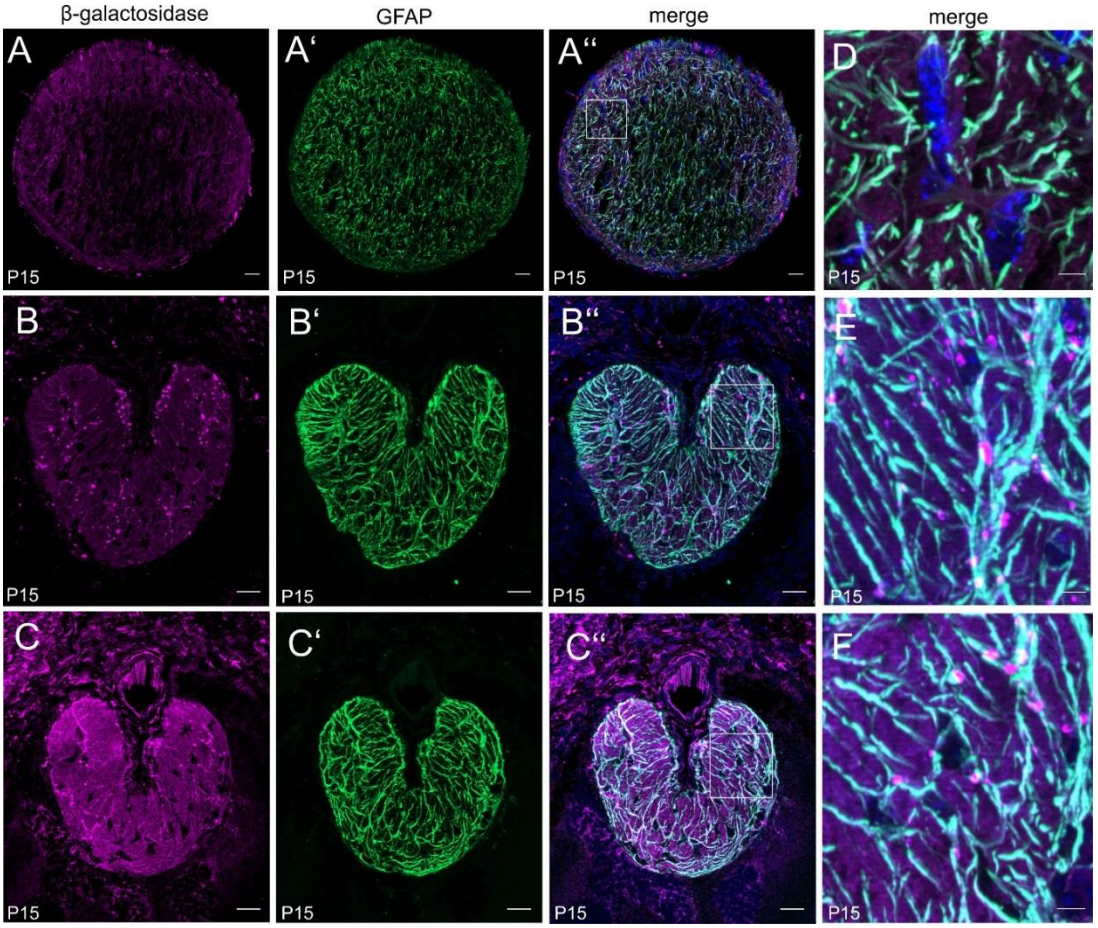

Figure 4-24: CTGF promotor activity in optic nerve astrocytes in P15 CTGF$^{LacZ+/-}$ mice. A-C show successive tangential sections from the same ON. The origin of the tangential sections was shown in the schematic illustration in Figure 4-21. Immunohistochemical staining against β-galactosidase (purple) and the astrocyte marker GFAP (green). (A) β-galactosidase staining in tangential sections of the posterior, myelinated ON revealed CTGF expression in astrocytes and the dura mater. (B, C) Immunohistochemical staining against β-galactosidase in tangential sections of the glial lamina revealed an intense CTGF expression in astrocytes, with the highest expression adjacent to the astrocyte cell nuclei. The further CTGF expression not localized in astrocytes indicated an additional cell type as the source for the expression. (D-F) Enlarged excerpts of the different tangential sections indicated by the rectangle demonstrates the CTGF expression (purple) in astrocytes (green). Nuclear DNA is labeled with DAPI (blue). Scale bar: 20µm (A-C); 5µm (D-F).

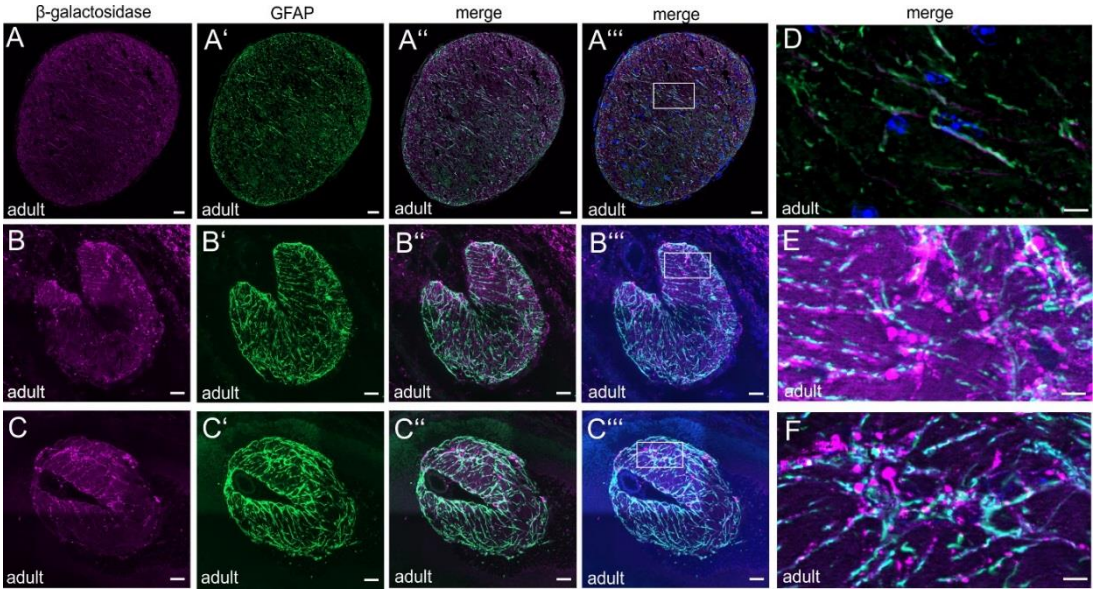

Figure 4-25: CTGF promotor activity in optic nerve astrocytes in adult CTGF$^{LacZ+/-}$ mice. A-C show successive tangential sections from the same ON. The origin of the tangential sections is shown in the schematic illustration in Figure 4-21. Immunohistochemical staining against β-galactosidase (purple) and the astrocyte marker GFAP (green). (A) β-galactosidase staining in tangential sections of the posterior, myelinated ON revealed a CTGF expression in astrocytes and the dura mater. (B, C) Immunohistochemical staining against β-galactosidase in tangential sections of the glial lamina revealed an intense CTGF expression in astrocytes, with the highest expression adjacent to the astrocyte cell nuclei. The further CTGF expression not localized in astrocytes indicates an additional cell type as the source for the expression. (D-F) Enlarged excerpts of the different tangential sections indicated by the rectangle demonstrates the CTGF expression (purple) in astrocytes (green). Nuclear DNA is labeled with DAPI (blue). Scale bar: 20µm (A-C); 5µm (D-F).

Since the observed CTGF expression was not exclusively localized in astrocytes, an additional cell type must be the source of CTGF promotor activity. Therefore, a β-galactosidase immunostaining was performed in combination with a staining against CD31 on sagittal sections of the adult ON (Figure 4-26). The double staining revealed an expression of CTGF in endothelial cells of blood vessels in the ON. CTGF promotor activity was mostly adjacent to the cell nuclei of endothelial cells (Figure 4-26 B''; arrow).

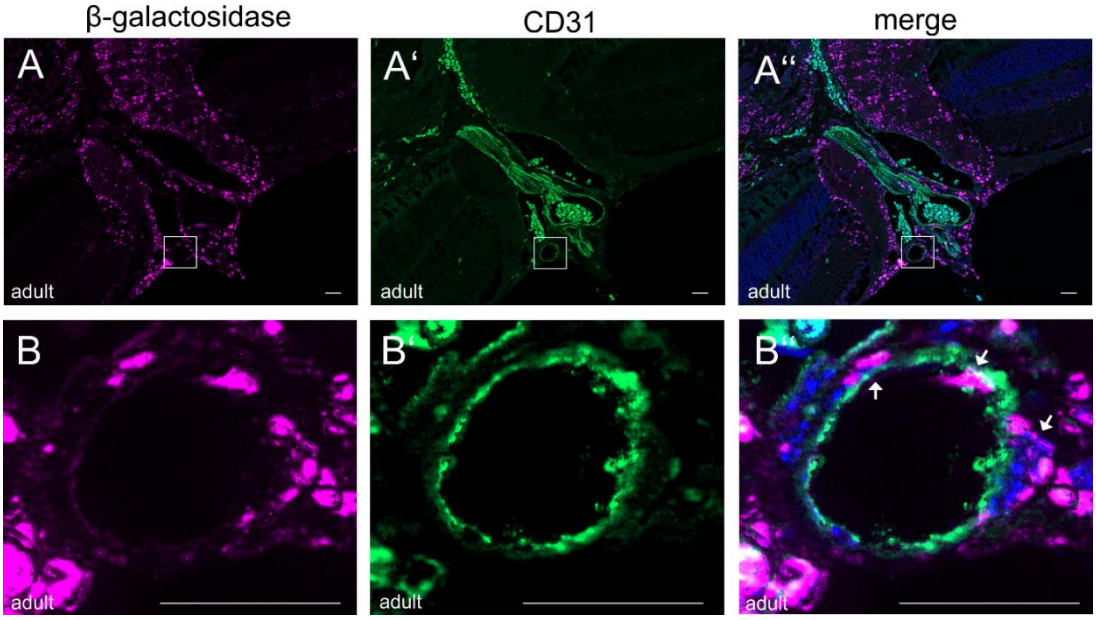

Figure 4-26: CTGF promotor activity in endothelial cells in ON blood vessels. (A) Immunohistochemical staining against β-galactosidase (purple) and CD31 (green) in ON sections of adult CTGF$^{LacZ+/-}$ mice. CTGF promotor activity is detected in endothelial cells stained with CD31 (green) of ON blood vessels, (B) Enlarged excerpt of a blood vessel in the ON. Arrow depicts CTGF promotor activity (purple) in endothelial cells (green). Nuclear DNA is labeled with DAPI (blue). Scale bar: 20µm

All in all, astrocytes and endothelial cells were identified as the source of CTGF expression in the developmental and adult ON with the highest expression in the glial lamina. Additionally, CTGF expression was detected in the dura mater around the ON. This expression is more intense during the development confirming the findings of histological LacZ staining.

Overall, it can be concluded that CTGF is expressed in various tissues in the mouse eye throughout the entire development and in the fully developed eye. A persistent expression is detected in the corneal endothelium, the TM, the SC endothelium, the ciliary body, the choroidea, the sclera, the retina, the dura mater and the ONH. Variations in the expression pattern of CTGF during development in contrast to the mature eye were investigated in the corneal stroma and epithelium and the ciliary body. Within the ONH, the dura mater and the retina a change in the expression is seen in different developmental stages. In the retina, Müller cells, amacrine cells and endothelial cells were identified as the source of the CTGF promotor activity. Furthermore, the endothelial cells of the choroidea and SC were identified as a source of CTGF expression. ONH astrocytes as well as endothelial cells were identified as the major CTGF expressing cell type.

4.2. Effect of mechanical stress and increasing substratum stiffness on astrocyte reactivity

Transgenic mice with lens-specific CTGF overexpression develop POAG characterized by higher IOP and progressive loss of axons in the ONH (Junglas et a., 2012). This glaucoma model was used to identify POAG-related changes in the glial lamina.

Prior to all following experiments animals were genotyped at the age of 3 weeks (Figure 4-27). Two different PCR were performed, both βB1 and SV40 specific for the transgenic animals. The βB1 PCR results in a 300bp product (Figure 4-27 A) and SV40 PCR results in a 360bp product (Figure 4-27 B) for transgenic animals. WT littermates show no product for both PCR.

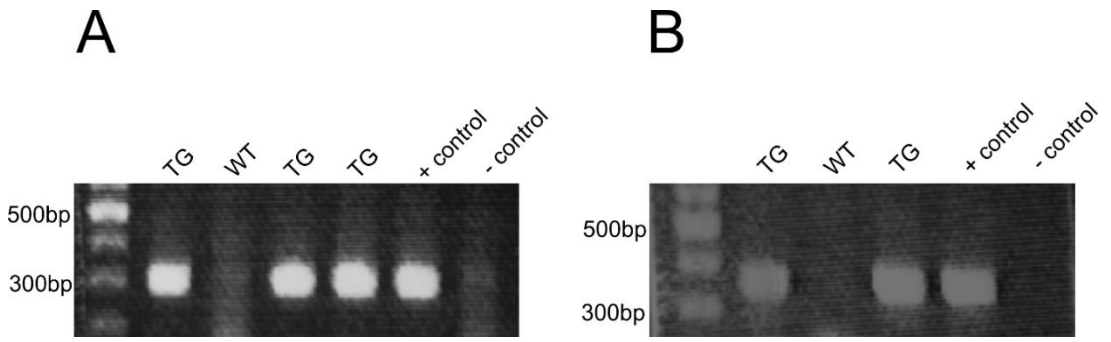

Figure 4-27: Representative βB1 (A) and SV40 (B) PCR. TG animals exhibited a DNA band in both PCR, whereas WT showed no band.

4.2.1. GFAP and CTGF alterations in the ONH of 2-month-old βB1-CTGF1 mice

To investigate POAG-related changes in the astrocytes that constitute the glial lamina of the transgenic animals, we investigated the presence of GFAP, a marker for reactive astrocytes, in tangential sections of the glial lamina of 1-month and 2-month-old βB1-CTGF mice. GFAP immunostaining in the glial lamina of the 1-month old transgenic and WT mice showed no alteration in the protein level or the morphology of the astrocytes (Figure 2-28). This finding could be confirmed by the quantification of the GFAP stained area in the glial lamina (Figure 4-30 B; WT: n=8, 69.76 ± 3.85; TG: n=4, 74.47 ± 12.39).In 2-month-old transgenic animals, the immunoreactivity for GFAP was increased and the processes of the astrocytes in the glial lamina were thickened in comparison to WT controls (Data were obtained and analyzed by Gregor R. Weber, MD thesis) Figure 4-29 C, D). As a result, the spaces between the astrocyte processes of control mice were more open than in the transgenic animals. The quantification of the GFAP stained area in the glial lamina at the ONH showed a significant increase in the TG animals compared to WT littermates (Figure 4-30 D; WT: n=10, 37.43 ± 13.12; TG: n=13, 51.99 ± 17.50; *p= 0.039). To address the question, whether the amounts of CTGF are also changed in

the glial lamina of TG animals we analyzed the immunoreactivity against CTGF. A faint staining throughout the entire ON tissue with no obvious preference for glial or neuronal tissue is observed in TG and WT littermates. Immunoreactivity against CTGF showed no changes in the glial lamina of 1-month-old TG and WT mice (Figure 4-28). Furthermore, quantification of CTGF stained area in the sections of the glial lamina could not identify any variation (Figure 4-30 A; WT: n=5, 89.60 ± 2.20; TG: n=5, 87.74 ± 3.91). 2-month-old WT animals showed the same distribution for CTGF as it was observed for the 1-month-old animals. Interestingly, the intensity of the immunoreactivity for CTGF was dramatically increased in the 2- month-old animals compared to WT animals (Gregor R. Weber, MD thesis, Figure 4-29 E, F). Measurements of CTGF stained areas in the ONH show a significant increase in the TG mice in comparison to the WT littermates (Figure 4-30 C; WT: n=3, 38.60 ± 1.51; TG: n=5, 62.21 ± 17.34; *p= 0.028).

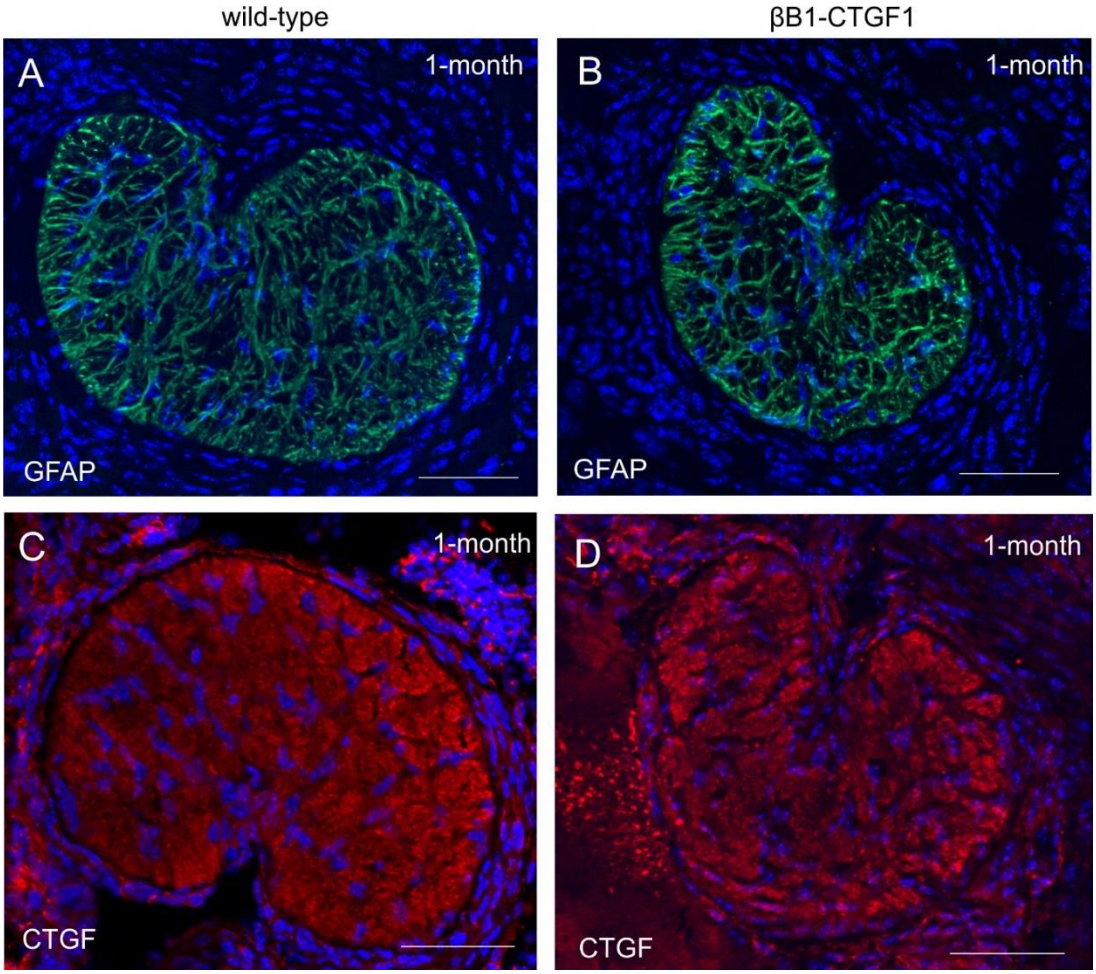

Figure 4-28: Immunostaining against GFAP and CTGF in the glial lamina of 1-month-old βB1-CTGF1 mice. (A,B) GFAP reactivity showed no alteration either in the protein synthesis nor in the astrocytes morphology in the TG mice in comparison to WT littermates. (C,D) CTGF reactivity showed no change in the TG animals compared to the WT littermates. Nuclear DNA is labeled with DAPI (blue). Scale bar: 50µm

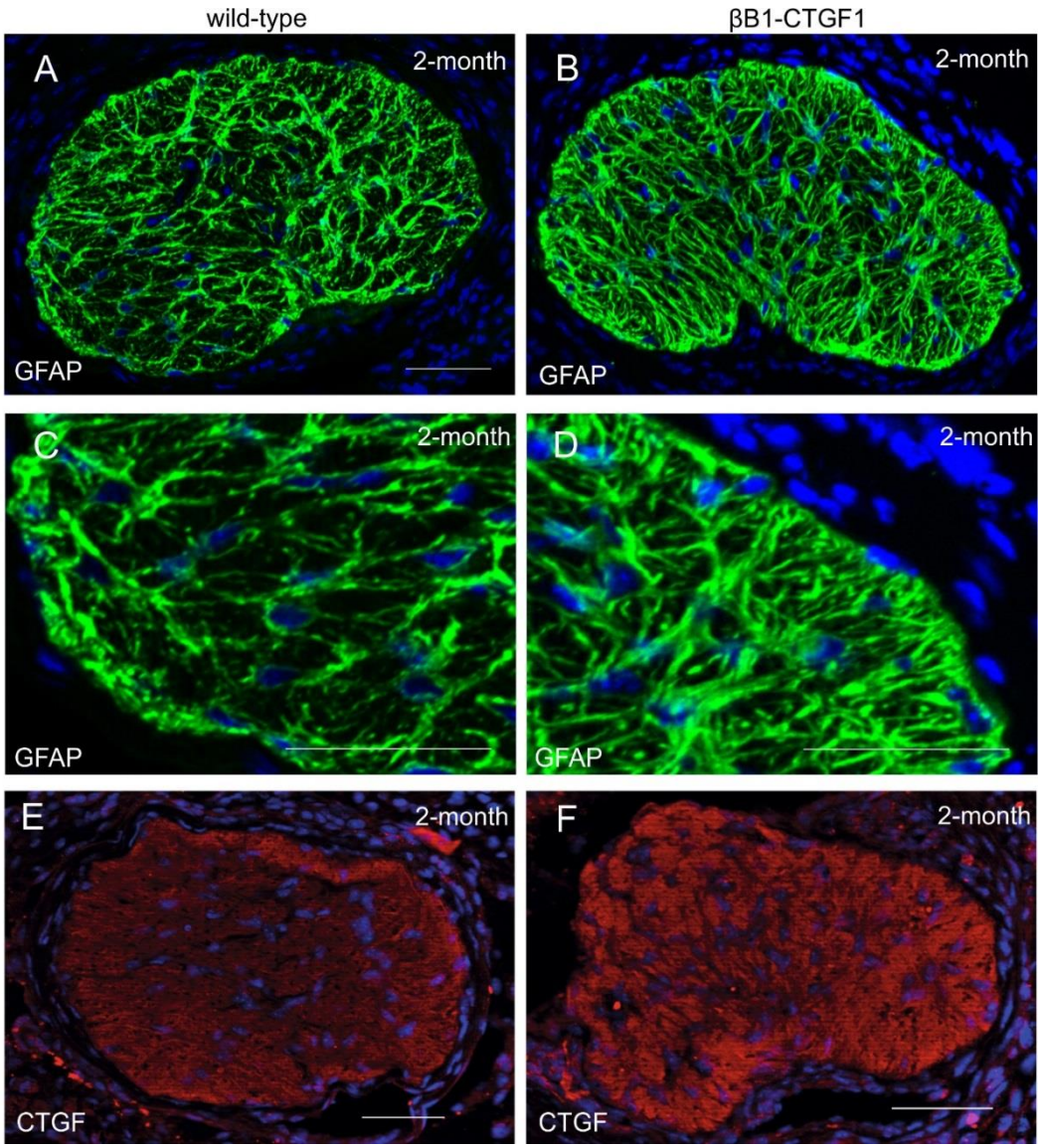

Figure 4-29: The immunoreactivity of GFAP and CTGF was altered in tangential section of 2-month-old transgenic animals. GFAP was increased and the processes of the astrocytes in the glial lamina were thickened in comparison to controls. Further in the glial lamina region of the WT animals the spaces between the astrocyte processes were more open than in TG animals. Immunohistochemical staining against CTGF showed a faint staining in WT animals, in TG animals an increased signal for CTGF was observed. Nuclear DNA is labeled with DAPI (blue). Scale bar = 50µm (Gregor R. Weber; MD thesis).

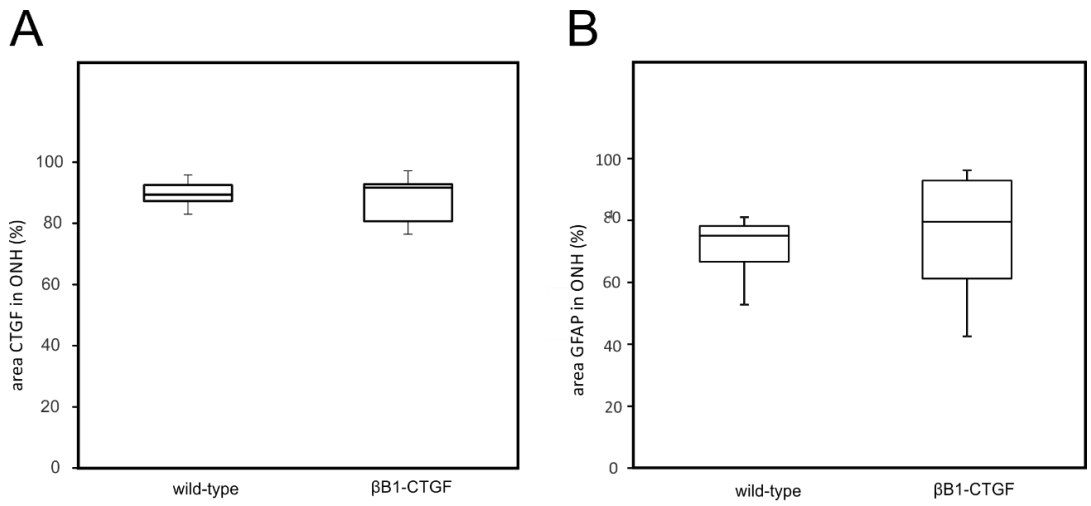

Figure 4-30: Quantification of immunohistochemistry staining of CTGF and GFAP in the glial lamina of 1-month-old WT and βB1-CTGF1 mice. The quantification showed no alternations for CTGF (A) (WT: n=5, 89.60 ± 2.20; TG: n=5, 87.74 ± 3.91) and GFAP (B) (WT: n=8, 69.76 ± 3.85; TG: n=4, 74.47 ± 12.39).

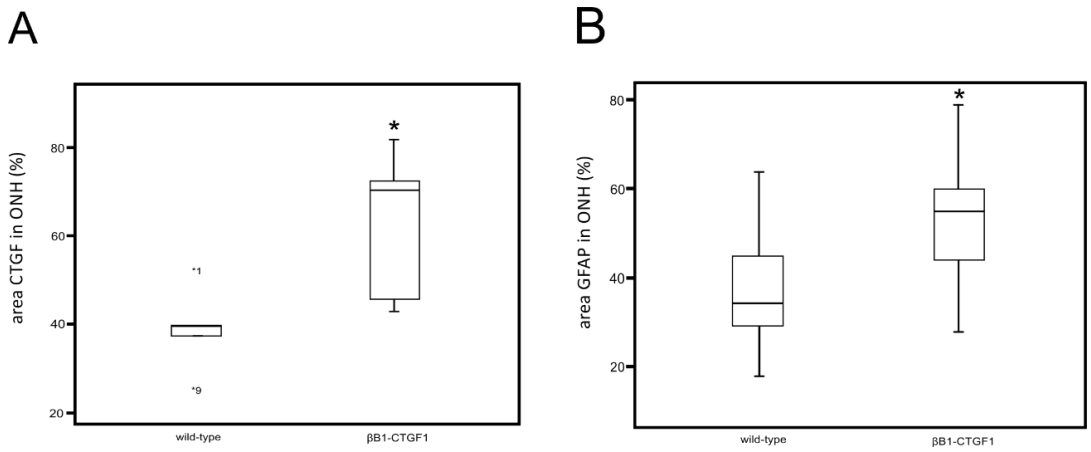

Figure 4-31: Quantification of immunohistochemistry staining of CTGF and GFAP in the glial lamina of 2-month-old WT and βB1-CTGF1 mice. The quantification showed an increase for CTGF (A) (WT: n=3, 38.60 ± 1.51; TG: n=5, 62.21 ± 17.34; *p= 0.028) and GFAP (B) (WT: n=10, 37.43 ± 13.12; TG: n=13, 51.99 ± 17.50; *p= 0.039) in TG animals compared to WT littermates. (Gregor R. Weber; thesis Dr.med.).

Real-time RT-PCR analyses were performed to determine expression levels of CTGF and GFAP in the ON and ONH of 1-month -old and 2-month-old transgenic βB1-CTGF and WT mice (Figure 4-32). Analysis for CTGF mRNA show no changes in the expression either in the ON (Figure 4-32 A; WT: n=7, 1 ± 0.10; TG: n=4, 1.21± 0.14) or in the ONH (Figure 4-32 A; WT: n=6, 1 ± 0.18; TG: n=3, 1.06 ± 0.14). Similar results were detected in the Real-time RT-PCR analysis for GFAP, in which no change for the mRNA expression in the ON (Figure 4-32 B; WT: n=7, 1 ± 0.06; TG: n=5, 1.19 ± 0.24) and the ONH (Figure 4-32 B; WT: n=6, 1 ± 0.14; TG: n=5, 1.14 ± 0.15) could be revealed.

Interestingly, real time RT-PCR experiments showed a huge increase of CTGF in the ONH of TG animals compared to WT littermates (Figure 4-32 C; WT: n=6, 1 ± 0.12; TG: n=5, 10.04 ± 1.66; **p= 0.006). Intriguingly, the mRNA analyses of the ON showed no change the CTGF expression (Figure 4-32 C; WT: n=15, 1 ± 0.69; TG: n=17, 1.07 ± 0.49). Furthermore, the examination of the GFAP mRNA level in the ON and the ONH revealed an increase in the ONH in the TG animals (Figure 4-32 D; WT: n=6, 1 ± 0.13 TG: n=5, 5.08 ± 1.62; *p= 0.04), but not in the ON (Figure 4-32 D, WT: n=15, 1 ± 0.68; TG: n=16, 0.85 ± 0.45) compared to WT control.

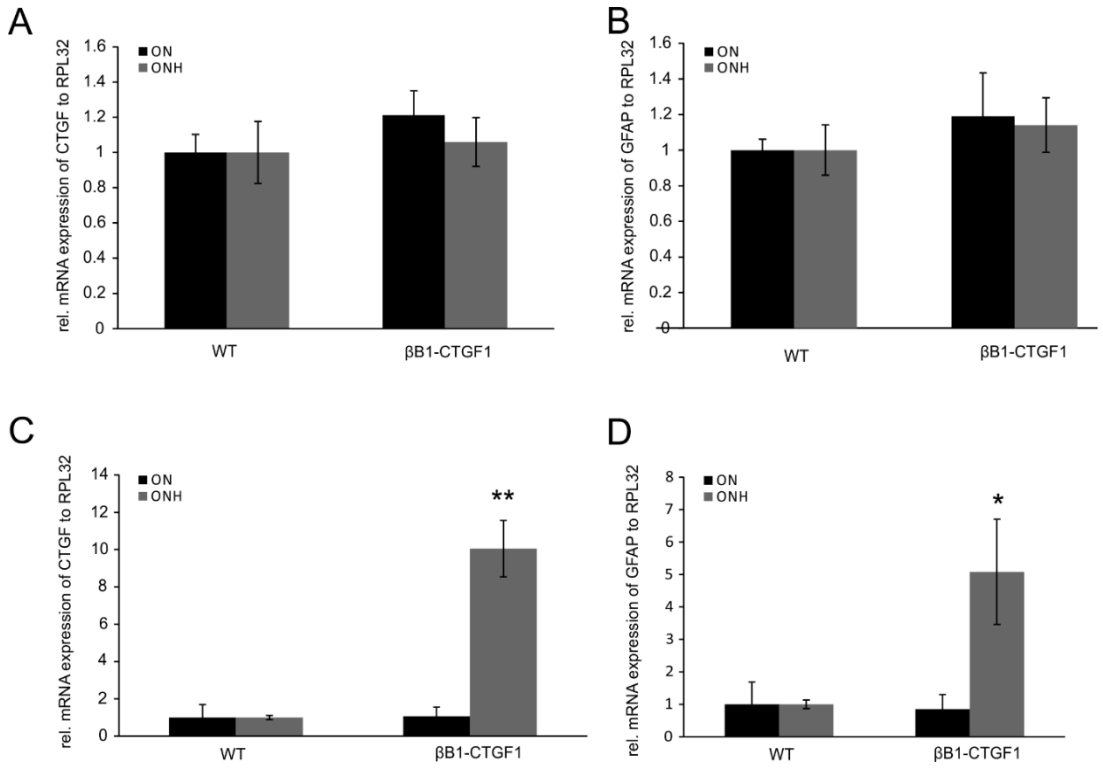

Figure 4-32: Real-time RT-PCR analysis for CTGF and GFAP in 1-month-old and 2-month-old βB1-CTGF1 and wildtype mice. (A) mRNA expression analysis showed no alternation in the ON (WT: n=7, 1 ± 0.10; TG: n=4, 1.21± 0.14) and ONH (WT: n=6, 1 ± 0.18; TG: n=3, 1.06 ± 0.14) for CTGF in the TG animals in comparison to WT littermates. (B) GFAP mRNA expression was not changed in the ON (WT: n=7, 1 ± 0.06; TG: n=5, 1.19 ± 0.24) and the ONH (WT: n=6, 1 ± 0.14; TG: n=5, 1.14 ± 0.15) of TG mice compared to WT. The mean value of WT mice was set at 1. *RPL32* was used as a housekeeping gene**.** (C) mRNA analysis of CTGF showed no change in ON (WT: n=15, 1 ± 0.69; TG: n=17, 1.07 ± 0.49), but a high significant increase in the ONH (WT: n=6, 1 ± 0.12; TG: n=5, 10.04 ± 1.66; **p= 0.006) of βB1-CTGF1 mice, compared to WT littermates. (D) GFAP mRNA expression was not changed in the ON (WT: n=15, 1 ± 0.68; TG: n=16, 0.85 ± 0.45), but was significant enhanced in the ONH (WT: n=6, 1 ± 0.13 TG: n=5, 5.08 ± 1.62; *p= 0.04) of βB1-CTGF1, in comparison to WT controls. Mean value of WT mice was set at 1. *PRL32* was used as a housekeeping gene. Data represented as mean ± SEM.

4.2.3. Establishment of murine optic nerve astrocytes

To understand what kind of effects CTGF, TGFβ2 and increasing substratum can provoke in ON astrocytes, we wanted to analyze the murine optic nerve astrocyte *in vitro*. 7 days after preparation first cells were growing out from the neuronal tissue of the ON. The neuronal tissue of the retrolaminar ON contains three different glial cell types beside axons, oligodendrocytes, astrocytes and microglial cells After another week, cells grow to confluence and the dominant cell type were astrocytes to a lesser extend oligodendrocytes and microglial cells were observed in the culture dishes, showing that with a specific supplement, astrocytes had an advantage in proliferation. After shaking the culture dishes overnight, the oligodendrocytes and microglial cells detached from the surface and were eliminated by repeated wash steps with PBS.

To prove the purity of the astrocyte culture, the cells were stained with GFAP, a specific astrocyte marker, with IBA-1, a marker for microglia, and with MBP, a marker against oligodendrocytes. Neither MBP nor IBA-1 showed any positive staining in the purified cell culture (data not shown). Only GFAP showed a positive staining in all cells, so that we had established a pure murine optic nerve astrocyte culture (Figure 4-33).

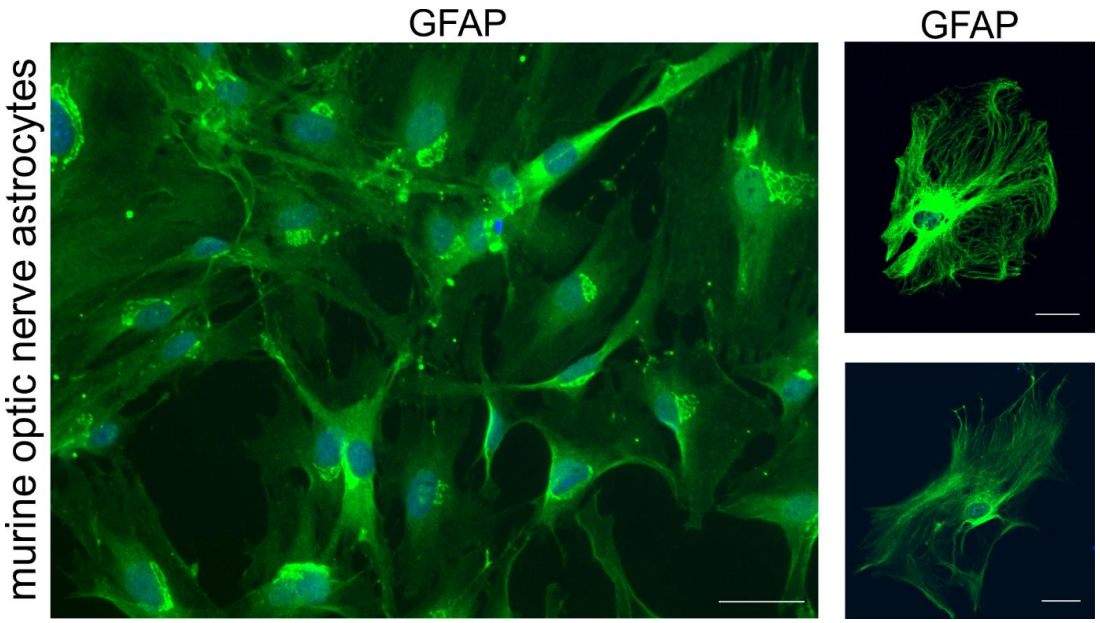

Figure 4-33: Immunocytochemical staining against GFAP in the astrocytes culture. GFAP reactivity showed a pure astrocyte cell culture. Nuclear DNA is labeled with DAPI (blue). Scale bar= 50µm.

4.2.3. Increasing substratum stiffness cause reactive changes in murine optic nerve astrocytes

To investigate the effect of increasing substratum stiffness on mouse ON astrocytes, cells were cultured on PDMS substratum with different E-moduli (10 kPa, 30 kPa, 60 kPa). To study the effect on the structure of the actin cytoskeleton, the actin stress fibers were labeled with phalloidin. We could observe an enhanced staining with increasing stiffness (Figure 4-34). Additionally, increased substratum stiffness caused an intensification in longitudinally-oriented actin stress fibers. Astrocytes grown on a substratum with a stiffness of 60 kPa contained numerous longitudinally arranged actin stress fibers (Figure 4-34), which were longer and thicker compared to those grown on substratum with 10 kPa or 30 kPa (Figure 4-34).

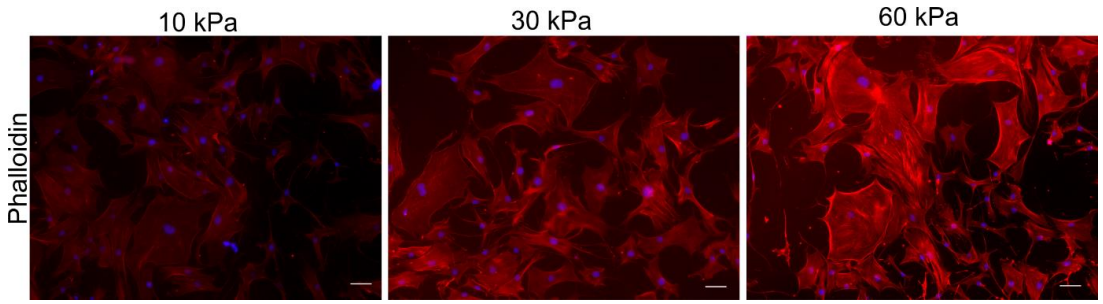

Figure 4-34: Phalloidin-labeling of murine optic nerve astrocytes cultured on increasing substratum stiffness. The visualization of the actin cytoskeleton via phalloidin labeling revealed an increase in signal with increasing substratum stiffness. Astrocytes grown on a substrate with a stiffness of 60 kPa contained numerous longitudinally arranged actin stress fibers which were longer and thicker, compared to those grown on substrate with 10 kPa or 30 kPa. Nuclear DNA is labeled with DAPI (blue). Scale bar: 50µm.

To test the effect of substratum stiffness on astrocyte reactivity, Western blot analyses for GFAP and vimentin were performed. Cells grown on substratum with a 60 kPa stiffness, showed a 3.66-fold ± 5.10-fold (*$p < 0.05$) and astrocytes grown on 30 kPa showed a 1.67-fold ± 0.51 increase (Figure 4-35 B; *$p \leq 0.02$) increased GFAP synthesis compared to those from cells grown on 10 kPa (Figure 4-35 B).). Vimentin was increased by 2.44-fold ± 1.7 for cells grown on 30kPa and by 2.58-fold ± 0.2 (Figure 4-35 C; *$p \leq 0.02$) for cells grown on 60 kPa compared to astrocytes plated on 10 kPa (Figure 4- 35 C). The results were confirmed by immunostaining with antibodies against GFAP which showed an increase in GFAP immunoreactivity in cells grown on stiffer substratum (Figure 4-35 A).

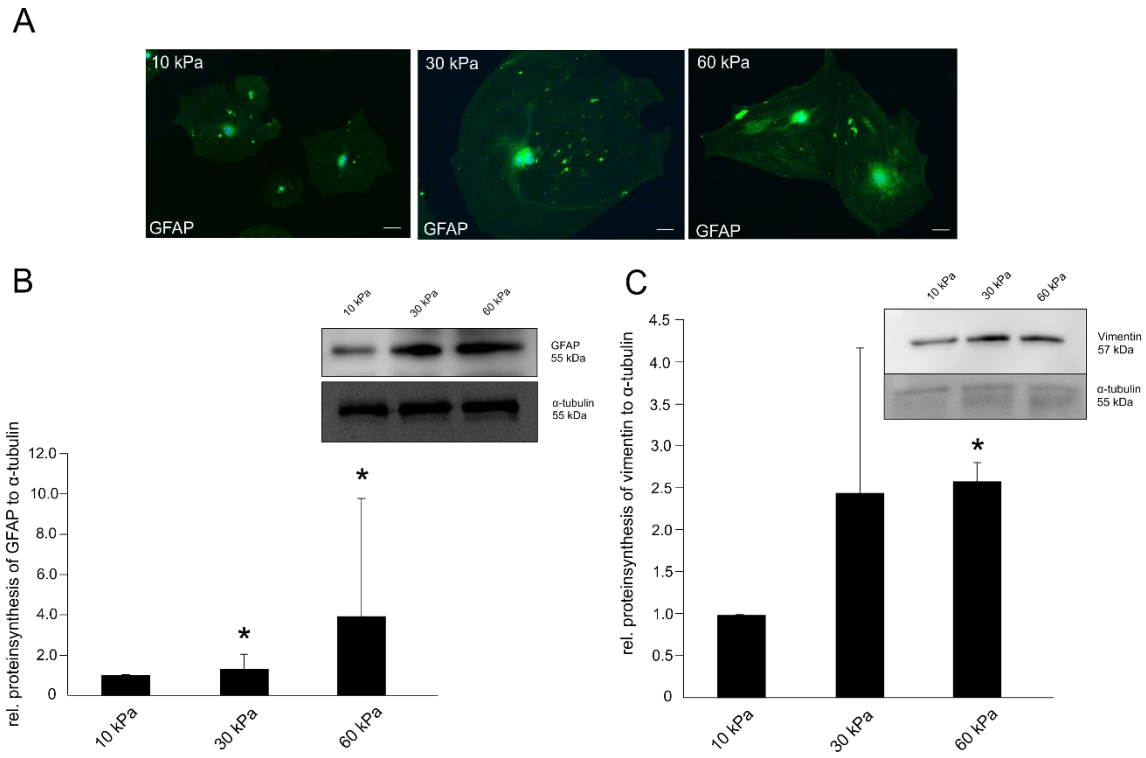

Figure 4-35: Increasing substratum stiffness lead to an increased reactivity in murine optic nerve astrocytes. (A) Immunocytochemical staining of GFAP showed an increase in immunoreactivity in astrocytes cultured on stiffer substratum compared to softer control. Nuclear DNA is labeled with DAPI (blue). Scale bar: 50µm (B) Western Blot analysis of GFAP revealed a significant increase in GFAP protein synthesis in murine optic nerve astrocytes grown on 30 or 60 kPa in comparison to the softer control (10kPa). (C) Western Blot analysis of Vimentin showed a significant increase in Vimentin protein level when the cells were cultured on 60 kPa compared to the 10 kPa control. α-tubulin was used as a loading control. The mean value of the 10kPa control was set at 1. Data represented as mean ± SD.

Next, we turned our attention to the effect of increased substratum stiffness on CTGF synthesis. Western blotting experiments of protein from astrocytes grown on a substratum with an E-modulus of 60 kPa showed an increase in the amounts of CTGF (Figure 4-36 B) (30 kPa 3.05 ± 2.05; * $p < 0.05$; 60 kPa 3.47 ±2.28; * $p < 0.05$), compared with protein from astrocytes cultured on substrata with an E-modulus with either 10 kPa or 30 kPa (Figure 4-36 B). The upregulation of CTGF in relation to increasing substratum stiffness was confirmed by immunocytochemistry (Figure 4-36 A).

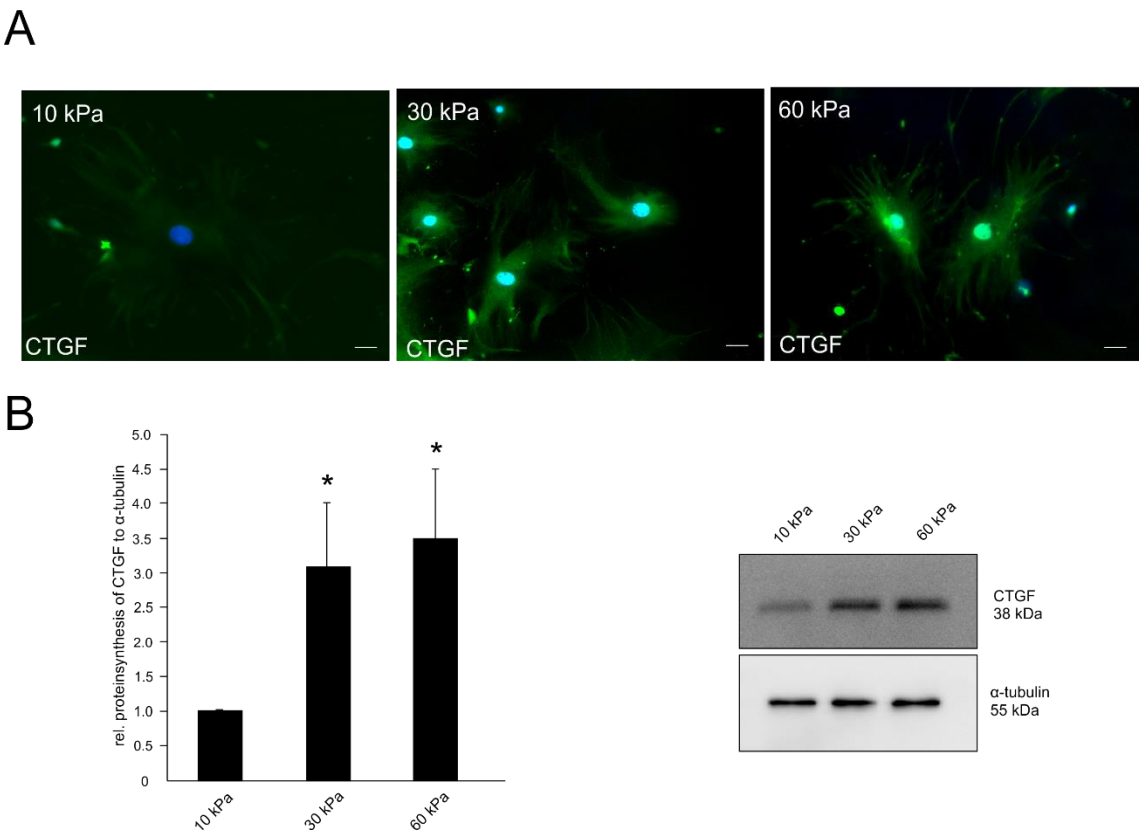

Figure 4-36: Increasing substratum stiffness causes increased CTGF level in murine optic nerve astrocytes. (A) Immunocytochemical staining of CTGF in murine optic nerve astrocytes cultured on increasing substratum stiffness showed an increased CTGF immunoreactivity in astrocytes grown on stiffer substratum, compared to those cells plated on softer substratum. Nuclear DNA is labeled with DAPI (blue). (B) Western Blot analysis of CTGF showed an increase protein synthesis in murine optic nerve astrocytes cultured on 30 kPa or 60 kPa in comparison to the 10 kPa control. α-tubulin was used as a loading control. The mean value of the 10 kPa control was set at 1. Scale bar:50µm. Data represented as mean ± SD.

Taken together, mRNA and protein level of CTGF and GFAP are increased in the ONH, but not in the ON of 2-month-old βB1-CTGF mice. Furthermore, increasing substratum stiffness lead to an increased reactivity and CTGF level in murine ON astrocytes *in vitro*.

4.2.4. Potential mechanisms of astrocyte reactivity

Since it could be observed that increasing substratum stiffness lead to astrocyte reactivity *in vitro* and astrocytes are reactivated in a murine glaucoma model *in vivo*, potential mechanism of astrocytes reactivity were investigated.

4.2.4.1. Trp-channels expression related to increasing substratum stiffness

The participation of channels of the Transient receptor potential (TRP) channel superfamily in mechanosensation and -transduction was already shown in different tissues and cell types (Dietrich et al. 2005, Earley et al. 2004, Lin & Corey 2005, Muraki et al. 2003, Numata et al. 2007a, 2007b, Welsh et al. 2002). Therefore, the expression

of different TRP channels were assessed in murine ON astrocytes and variation related to increasing substratum stiffness was investigated. TRP channel mRNA expression was studied in murine ON astrocytes growing on culture dishes with increasing substratum stiffness (10 kPa, 30 kPa, 60 kPa) (Figure 4-37). Trpc1 mRNA expression was significant decreased when astrocytes were gown on 60 kPa (Figure 4- 37; 0.60 ± 0.14; n=5; *p=0.003), compared to 10 kPa control (Figure 4-37; 1 ± 0.0; n=5). 30kPa substratum stiffness had no significant effect on Trpc1 expression (Figure 4-37; 0.75 ± 0.30; n=5). Real-time RT-PCR analysis for Trpm7 revealed a high significant decrease in murine ON astrocytes cultured on 30 kPa (Figure 4-37; 0.67 ± 0.21; n=5; **p=0.008) and on 60 kPa (Figure 4-37; 0.61 ± 0.33; n=5; *p=0.03), in comparison to control (Figure 4-37; 10kPa; 1 ± 0.0; n=4). The most prominent effect was shown for Trpv2, as astrocytes grown on 30 kPa culture dish showed a high significant decrease (Figure 4-37; 0.61 ± 0.22; n=4; **p=0.01) and seeded on 60 kPa (0.56 ± 0.13; n=4; ***p=0.0004) a highly significant reduction in Trpv2 mRNA expression, in comparison to 10kPa control (1 ± 0.0; n=4).

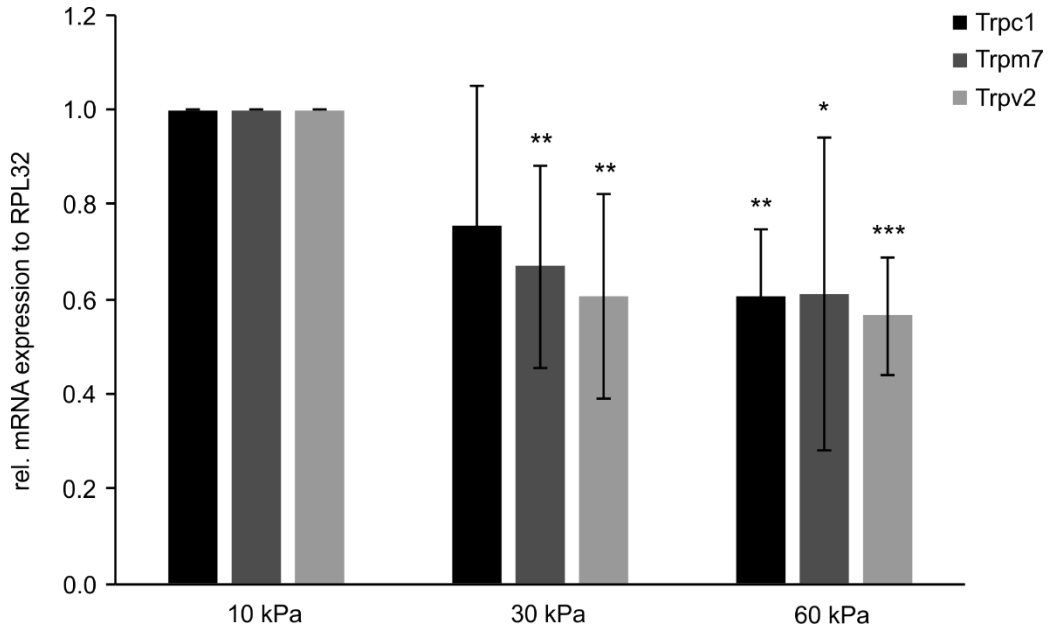

Figure 4-37: Real-time RT-PCR analysis of TRP channel expression in murine optic nerve astrocytes depending on increasing substratum stiffness. mRNA expression of Trpc1 was significantly reduced in murine ON astrocytes growing on 60 kPa, compared to 10 kPa control (10kPa: 1 ± 0.0, n=5; 30kPa: 0.75 ± 0.30, n=5; 60kPa: 0.60 ± 0.14; n=5; *p=0.003). Increasing substratum stiffness led to significant downregulation of Trpm7 in murine ON astrocytes (10kPa: 1 ± 0.0, n=4; 30kPa: 0.67 ± 0.21, n=5, **p=0.008; 60kPa: 0.61 ± 0.33, n=5, *p=0.03). Murine ON astrocytes grown on 30 or 60kPa revealed a reduced mRNA expression for Trpv2 (10kPa: 1 ± 0.0, n=4; 30kPa: 0.61 ± 0.22, n=4, **p=0.01; 60kPa: 0.56 ± 0.13; n=4; ***p=0.0004). *RPL32* was used as housekeeping gene. Mean value of 10kPa control was set at 1. Data represented as mean ± SD.

4.2.4.2. Effect of increasing substratum stiffness on Piezo channel expression

The novel ion channel family, including Piezo1 and Piezo2, showed a strong evidence to play a crucial role in response to mechanical stress (Coste et al. 2010). Therefore, it was of interest to investigate expression of these channels in response to increasing substratum stiffness. Piezo channel mRNA expression was assessed in murine ON astrocytes growing on increasing substratum stiffness. Real-time RT-PCR revealed a significant reduction of Piezo2 expression in murine ON astrocytes cultured on 60 kPa (0.37 ± 0.34; n=3; *p=0.03) compared to10 kPa control (1 ± 0.0; n=3). (30 kPa 0.79 ± 0.52; n=3; Figure 4-38). mRNA expression analysis for Piezo1 did not detect any expression changes related to increasing substratum stiffness (10 kPa: 1± 0.0, n=3; 30 kPa: 1.14 ± 0.18, n=3; 60 kPa: 1.16 ± 0.55; n=3; Figure 4-38).

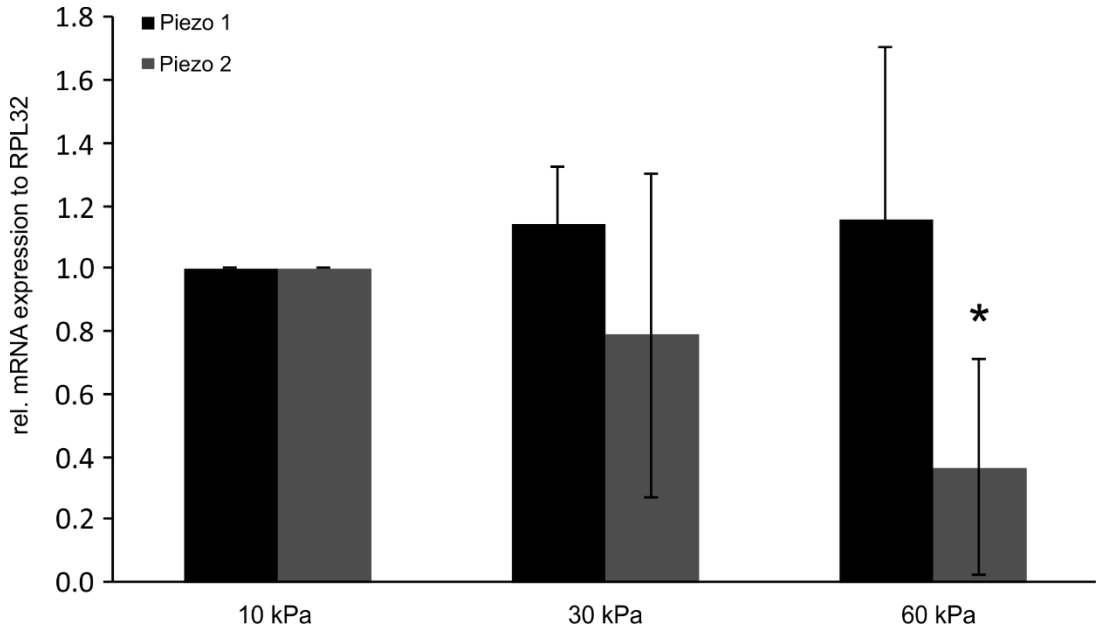

Figure 4-38: Real-time RT-PCR analysis of Piezo channel expression in murine optic nerve astrocytes depending on increasing substratum stiffness. Increasing substratum stiffness led to a significant downregulation of Piezo2 mRNA expression in murine ON astrocytes (10 kPa: 1 ± 0.0, n=3; 30 kPa: 0.79 ± 0.52, n=3; 60 kPa: 0.37 ± 0.34, n=3, *p=0.03). No differences in Piezo1 expression was observed related to increasing substratum stiffness (10 kPa:1± 0.0, n=3; 30 kPa: 1.14 ± 0.18, n=3; 60 kPa: 1.16 ± 0.55, n=3). *RPL32* was used as a housekeeping gene. Mean value of 10kPa control was set at 1. Data represented as mean ± SD.

4.2.4.3. Implication of Caveolins in astrocytes and the ONH in the pathogenesis of POAG

Since caveolae and Caveolin1, one main constitute of caveolar structure, work as mechanosensors and their maintenance is altered by external mechanical cues, it was of great interest to prove the appearance of Caveolin1 in murine optic nerve astrocytes and the implication in the pathological changes occurring the glaucomatous ON (Boyd et al. 2003, Kurzchalia et al. 1992, Park et al. 2000, Rizzo et al. 2003, Rothberg et al. 1992, Sedding et al. 2005, Sinha et al. 2011).

4.2.4.3.1. Caveolin1 expression murine ON astrocytes

For further analysis of the impact of Caveolin1 in astrocyte reactivation, the appearance of Caveolin1 in murine astrocytes was analyzed. Therefore, immunochemical staining against Caveolin1 in murine ON astrocytes were performed *in vitro* and *in vivo*. Caveolin1 was detected in murine ON astrocytes *in vitro* (Figure 4-39) und in astrocytes in the murine ON head *in vivo* (Figure 4-40, 41).

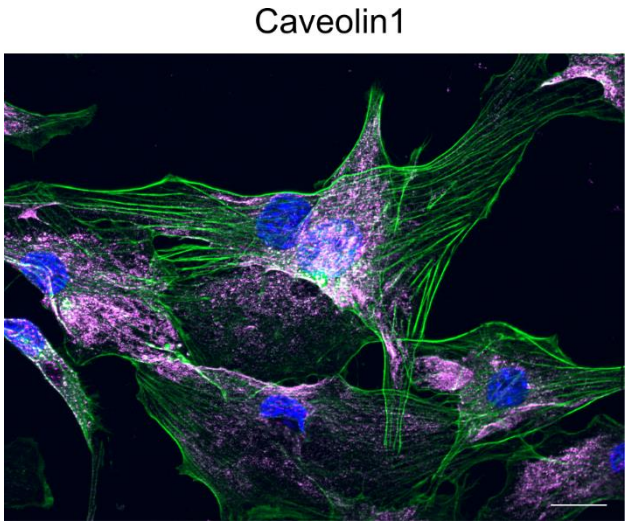

Figure 4-39: Immunocytochemical staining against Caveolin1 in murine ON astrocytes *in vitro*. Caveolin1 (purple) was expressed in murine ON astrocytes *in vitro*. Phalloidin labeling (green) visualized the astrocyte cytoskeleton. Nuclear DNA is labeled with DAPI (blue). Scale bar: 20µm.

By immunohistochemical staining, Caveolin1 is detected throughout the entire ON, and additionally in the vasculature in and adjacent to the ON. The fact that the Caveolin1 level were extremely higher in blood vessels, in contrast to ON tissue, lead to the difficulties to record the staining in the ON. In the enlarged excerpt the co-localization of Caveolin1 in ON astrocytes is shown (Figure 4-40).

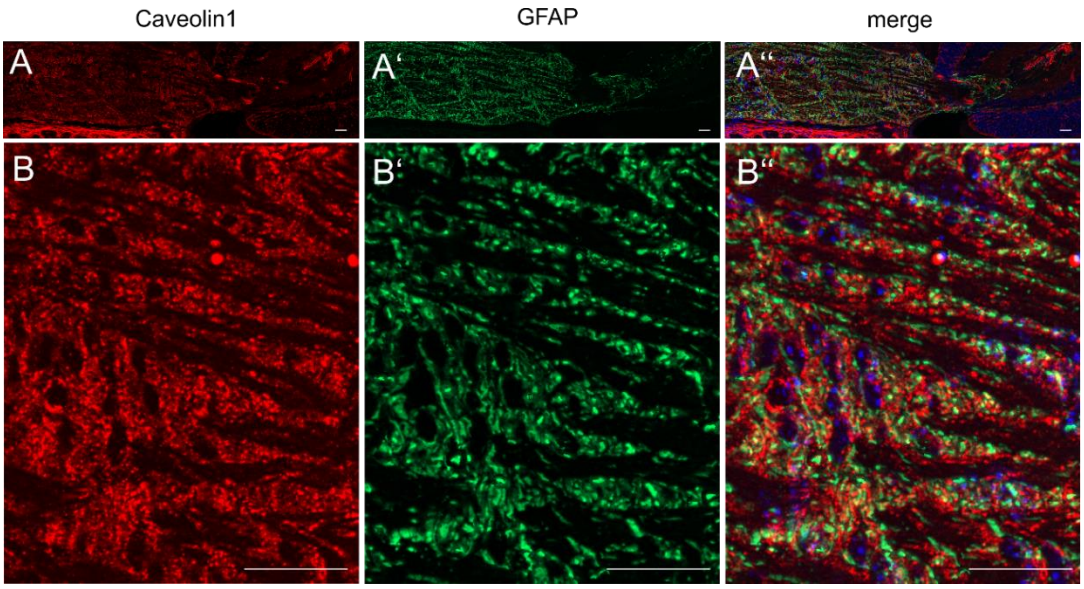

Figure 4-40: Immunohistochemical staining against Caveolin1 and GFAP in the sagittal ON of 2-month-old WT mice. (A) Immunohistochemical staining against Caveolin1 (red) and GFAP (green) were performed on sagittal section of the glial lamina of 2-month-old WT mice. (B) Enlarged excerpt showed a localization of Caveolin1 in ON astrocytes. Additionally, a staining of Caveolin1 in ON blood vessel was detected. Nuclear DNA is labeled with DAPI (blue). Scale bar: 20µm.

For a better representation of Caveolin1 localization in ON astrocytes, tangential sections of the glial lamina were double stained against Caveolin1 and GFAP. In these staining the localization of Caveolin1 could be clearly detected in GFAP positive astrocytes (Figure 4-41).

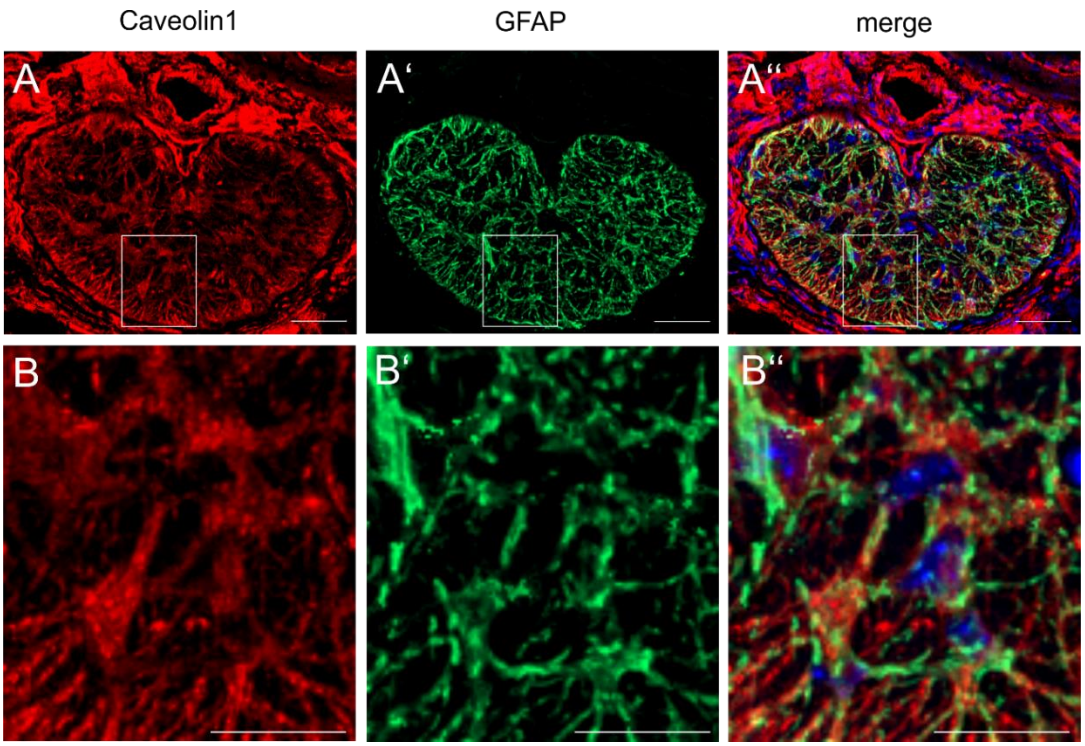

Figure 4-41: Immunohistochemical staining against Caveolin1 and GFAP in the glial lamina of 2-month-old WT mice (A) Immunohistochemical staining against Caveolin1 (red) and GFAP (green) were performed on tangential section of the glial lamina of 2-month-old WT mice. (B) Enlarged excerpt of the glial lamina showing that Caveolin1 was co-located with the astrocyte marker GFAP, indicating that Caveolin1 was expressed in murine ONH astrocytes *in vivo*. Nuclear DNA is labeled with DAPI (blue). Scale bar: 20µm.

4.2.4.3.2. Effect of increasing substratum stiffness on Caveolin1 and 2 expression

As the appearance of Caveolin1 in murine optic nerve astrocytes was shown, the effect of increasing substratum stiffness on the expression of Caveolin1 and 2 was investigated. The mRNA expression of Caveolin1 as well as Caveolin2 was assessed in murine ON astrocytes cultured on 8-10 kPa, 25-30 kPa and 50-60 kPa cell culture dishes. Real-time RT-PCR analysis showed a high significant decrease for Caveolin1 mRNA expression in murine ON astrocytes cultured on 25-30 kPa (0.61 ± 0.31; n=8; **p=0.002). In contrast, when murine ON astrocytes were grown on 50- 60 kPa the Caveolin1 mRNA is significantly increased (1.93 ± 1.08; n=8; *p=0.02), compared to the 10 kPa control (1± 0.0; n=9) (Figure 4-42). For the Caveolin2 mRNA a significant increase in murine ON astrocytes cultured on 50-60 kPa (3.51 ± 2.78; n=8; *p=0.02), in comparison to murine ON astrocytes cultured on 8-10 kPa (8- 10 kPa: 1 ± 0.0; n=9; 25-30 kPa: 1.98 ± 1.73; n=8) (Figure 4-42).

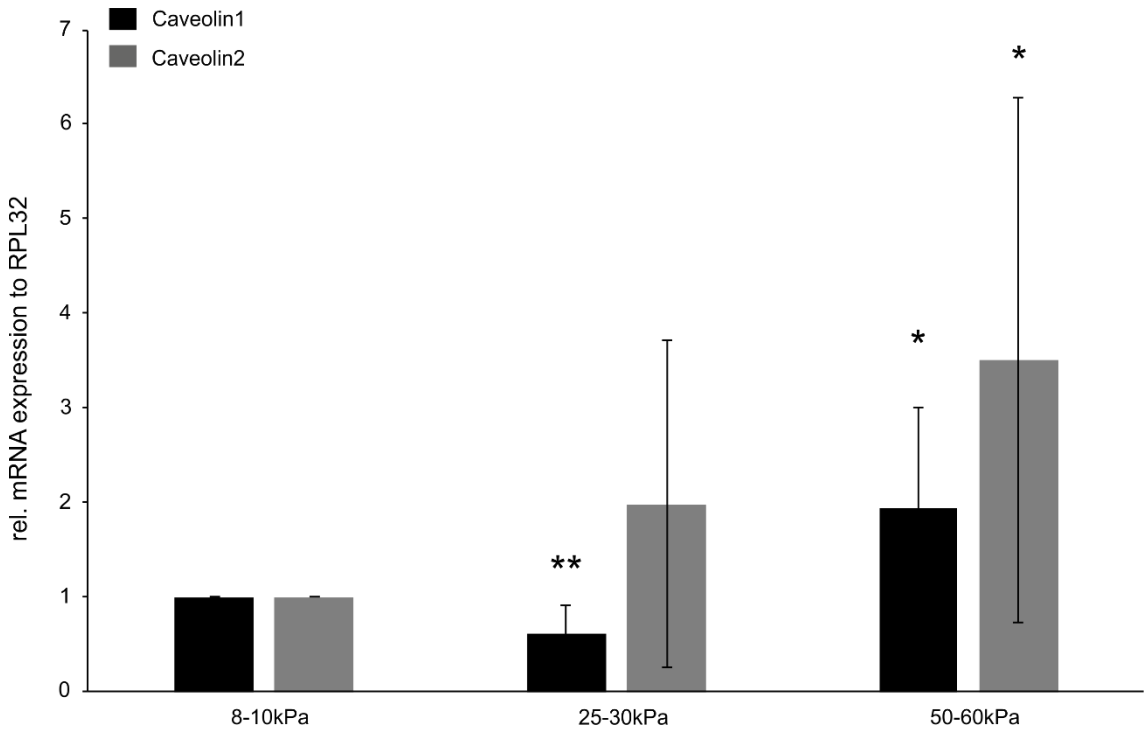

Figure 4-42: Real-time RT-PCR analysis of Caveolin1 and 2 mRNA expression related to increasing substratum stiffness. Caveolin1 mRNA was high significant reduced in murine ON astrocytes grown on 25-30 kPa (0.61 ± 0.31; n=8; **p=0.002) and significant increased on 50-60 kPa (1.93 ± 1.08; n=8; *p=0.02), compared to the 8-10 kPa control (1± 0.0; n=9). Caveolin2 mRNA was significantly increased in murine ON astrocytes grown on 50-60 kPa (3.51 ± 2.78; n=8; *p=0.02), compared to the 8-10 kPa control (8-10kPa: 1 ± 0.0; n=9; 25-30 kPa: 1.98 ± 1.73; n=8). The mean value of 8-10 kPa was set at 1. RPL32 was used as a housekeeping gene. Data represented as mean ± SD.

4.2.4.3.3. Effect of TGF-β2 and CTGF on Caveolin1 in vitro

Murine optic nerve astrocytes were treated either with 1 ng/ml TGF-β2 or 50 ng/ml CTGF, or left untreated as controls for 24 h, and Caveolin1 was assessed in Western Blot and Real-time RT-PCR analysis (Figure 4-43). Real-time RT-PCR analysis showed a significant increase in Caveolin1 mRNA expression after treatment either with 1 ng/ml TGFβ2 (1.94 ± 0.84; n=6; *p=0.02) or 50ng/ml CTGF (1.61 ± 0.60; n=6; *p=0.03), in comparison to untreated control (1±0.0; n=6) (Figure 4-43 A). Additionally, Western Blots showed enhanced levels of Caveolin1 protein after the treatment with TGF-β2 and CTGF. Relative densitometry to α-tubulin confirmed the significant increase after the treatment with TGF-β2 (1.63 ± 0.54; n=3; *p=0.03) or 50ng/ml CTGF (1.80 ±0.58; n=3; *p=0.02) compared to control (1± 0.0; n=5) (Figure 4-43 B).

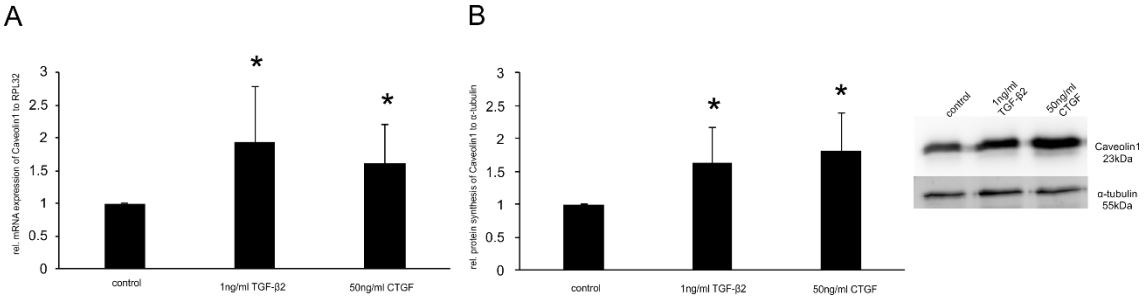

Figure 4-43: Analysis of Caveolin1 after treatment with TGFβ2 and CTGF in murine ON astrocytes. (A) Real-time RT-PCR analysis showed a significant increase of Caveolin1 mRNA expression after the treatment with 1 ng/ml TGF-β2 and 50 ng/ml CTGF for 24h (control: 1±0.0, n=6; TGF-β2:1.94 ± 0.84, n=6, *p=0.02; CTGF: 1.61 ± 0.60, n=6, *p=0.03). *RPL32* was used as a housekeeping gene. Mean value of untreated control was set a 1. (B) Western Blot analysis of Caveolin1 protein synthesis showed a significant increase in protein level after the 24h treatment with TGF-β2 (1.63 ± 0.54; n=3; *p=0.03) and CTGF (1.80 ±0.58, n=3, *p=0.02; control: 1± 0.0; n=5). Caveolin1 protein levels were normalized to α-tubulin. Mean value of untreated control was set at 1. Data represented as mean ± SD.

4.2.4.3.4. Caveolin1 in the ONH of the murine glaucoma model

POAG-related changes of Caveolin1 were assessed in 2-month-old βB1-CTGF1 mice. Real-time RT-PCR analysis could detect a high significant increase in Caveolin1 mRNA expression in the ONH of TG mice (6.64 ± 1.63; n=5; **p=0.007) compared to WT controls (1 ±0.15; n=6) (Figure 4-44 A). Additionally, it was shown that Caveolin1 expression is not altered in the ON of TG mice (1.02 ± 0.30; n=16) by contrast with WT littermates (1 ± 0.29; n=13) (Figure 4-44 A). Furthermore, a significant increase in Caveolin1 protein synthesis was shown by Western Blot analysis for TG mice (2.53 ±0.58; n=9; *p=0.05) in comparison to WT control (1± 0.09; n=9) (Figure 4-44 B).

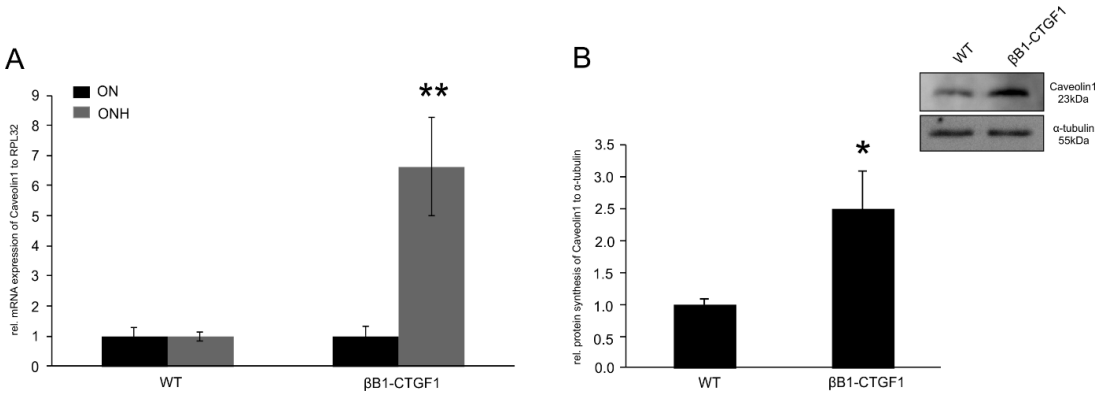

Figure 4-44: Caveolin1 levels in the ON and ONH of 2-month-old βB1-CTGF1 mice. (A) Real-time RT-PCR analysis showed a high significant increase in Caveolin1 mRNA in the ONH of TG animals (6.64 ± 1.63; n=5; **p=0.007) compared to WT littermates (1 ±0.15; n=6). No difference for Caveolin1 mRNA expression was observed in the ON of βB1-CTGF1 mice compared to WT controls (TG: 1.02 ± 0.30, n=16; WT: 1 ± 0.29; n=13). *RPL32* was used a housekeeping gene. Mean values of WT controls was set at 1. (B) Western Blot analysis showed a significant increase in Caveolin1 protein synthesis in the ON of TG animals compared to WT (TG: 2.53 ±0.58, n=9; *p=0.05; WT: 1± 0.09; n=9). Caveolin1 protein levels were normalized to α-tubulin. Mean value of WT mice were set at 1. Data represented as mean ± SEM.

All in all, the presents of proteins involved in mechanosensation, like Trpc1, Trpv2, Trpm7, Piezo1 and Piezo2, and Caveolin1 and 2 was shown in murine optic nerve astrocytes. In relation to increasing substratum stiffness, the expression of these proteins is changed, arguing for an implication in mechanosensation in murine optic nerve astrocytes. Furthermore, an increase for Caveolin1 after CTGF and TGFβ2 treatment in murine optic nerve astrocytes *in vitro* and in the ONH of 2-month-old βB1-CTGF1 mice *in vivo* was observed.

4.3. Intracameral delivery of layer-by-layer coated siRNA nanoparticles

As it was shown in this study, that CTGF is persistently expressed in the TM and the SC and its lens-specific overexpression in mice results in an elevated IOP and the progressive and significant loss of ON axons (Junglas et al., 2012), it can be suggested that CTGF is implicated in the dysregulation of AH outflow pathway. Therefore, the aim of this study was to design a tool to reduce CTGF in the cells and tissue of the outflow pathway to establish a new therapeutic strategy to reduce IOP in POAG.

Hence, nanoparticles (NP) were designed, which follow the drainage pathway of AH and reach target tissue and cells of the outflow pathway. Preparation and characterization of NP's were obtained by Michaela Guter and Miriam Breunig (Department of Pharmaceutical Technology, University of Regensburg). The core of the NP's consisted of biodegradable, FDA approved poly(D,L-lactide-co-glycolide) (PLGA) with a MW of 38-54 kDa. PLGA NP's were prepared by nanoprecipitation and then stabilized with polycationic polymer PEI with a MW of 25 kDa. PEI-NPs were then coated with negatively charged hyaluron (HA) of 13 kDa resulting in HA-NPs. As HA-NPs are coated with HA they can bind to the CD44 receptor, which is expressed in both healthy TM and SC cells (Acott et al., 2008). Therefore, a nonspecific, adhesive interaction, which can be observed for PEI can be prevented. PEI-NP's were used as control, as they nonspecifically interact with cells and tissue.

To prove the ability of CD44 as a potential target for NP delivery, expression and protein synthesis of CD44 were investigates in HTM and SC cells as well as in the outflow tissue of human glaucoma patients and in the glaucoma mouse model.

4.3.1. CD44 expression in HTM cells *in vitro*

To investigate the protein synthesis of CD44 *in vitro*, HTM cells were treated either with 1 ng/ml TGF-β2, 50 ng/ml CTGF or left untreated as control for 24h. Western Blot analysis and immunocytochemical staining against CD44 in HTM cells were performed (Figure 4-45). Treatment with TGF-β2 led to a significant increase in CD44 protein level (n=5, 2.23 ± 0.49; P=0.045) compared to the untreated control (n=6, 1.14 ± 0.14) (Figure 4-45 A). Additionally, the CTGF treatment led to a significantly enhanced CD44 protein synthesis (n=5, 3.82 ± 0.71; P=0.003; Figure 4-45 A). Immunocytochemical staining against CD44 in HTM cells treated either with 1 ng/ml TGF-β2, 50 ng/ml CTGF or left untreated as control could confirm the Western Blot results as it showed an increase in CD44 protein synthesis after both treatments (Figure 4-45 B).

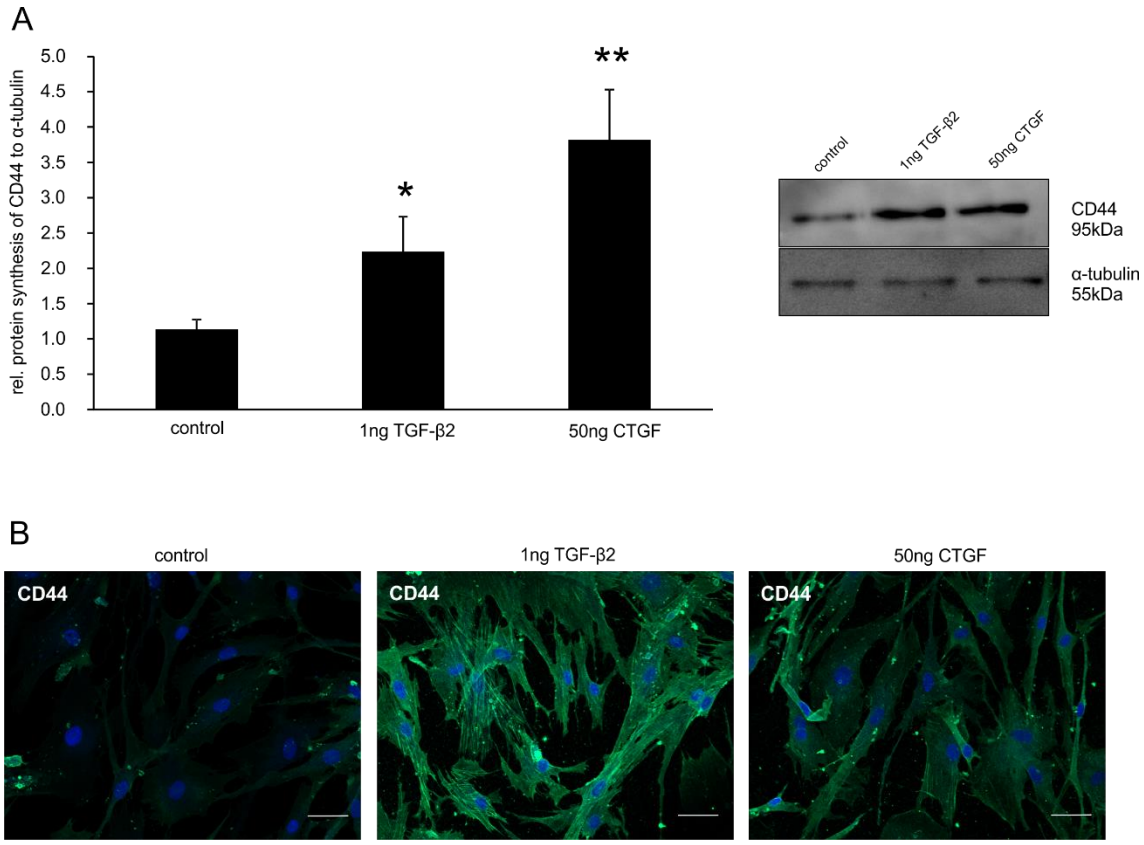

Figure 4-45: CTGF and TGF-β2 induce CD44 in HTM cells *in vitro*. (A) Western blot analysis for CD44 in proteins of HTM cells 24 hours after treatment with 1ng TGF-β2 or 50ng CTGF. The mean value obtained from untreated cells was set at 1. α-tubulin was used as loading control (n=5-6; *P= 0.045; ** P= 0.003). Data represented as mean ± SEM. (B) Immunohistochemical staining for CD44 (green) in HTM cells treated with either 1 ng TGF-β2 or 50 ng CTGF. Nuclear DNA is labeled with DAPI (blue) Scale bar: 50µm.

4.3.2. CD44 expression in βB1-CTGF1 mice in *vivo*

Transgenic mice with lens-specific CTGF overexpression (βB1-CTGF1) develop POAG characterized by higher IOP and progressive loss of axons in the ONH (Junglas et al., 2012). The increased IOP is associated with pathological changes within the outflow pathway. To analyze whether those changes are linked with alterations in CD44 expression and localization anterior eye segments of 2-month old βb1-CTGF1 and WT mice were investigated. The mRNA expression of CD44 was significantly increased in corneal-scleral rims of βB1-CTGF1 animals compared to their WT littermates (WT: 1 ± 0.06; βB1-CTGF1: 3.13 ± 0.83; p=0.04; Figure 4-46 A). The corneoscleral-rim contains the TM, SC, but also portion of the sclera, therefore we performed immunohistochemical staining to precisely analyze the localization of CD44 in the anterior eye segment. CD44 signal was localized in the iris, ciliary body, trabecular meshwork and the SC of 2-month-old WT mice, whereas no signal was observed in the sclera despite in the endothelial cells of the aqueous plexus (Figure 4- 46 B). In the βB1-CTGF1 mice, a similar distribution of CD44 was observed in the anterior chamber angle, however the signal was markedly increased in the tissues of the outflow pathway. The immunohistochemical analysis showed that CTGF induced increase of CD44 mRNA expression arises from the outflow tissues as no changes were observed in the sclera (Figure 4-46 B).

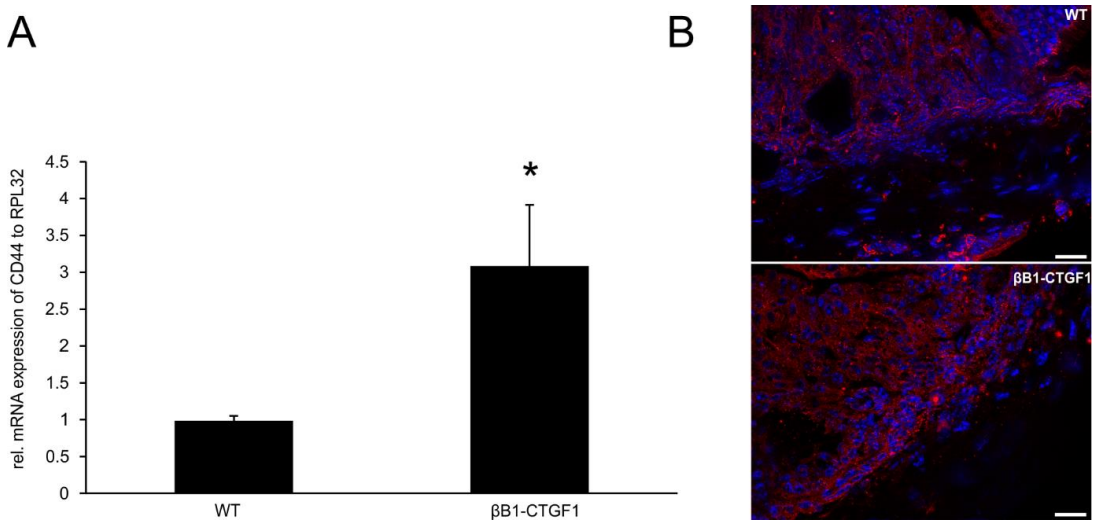

Figure 4-46: Expression and Distribution of CD44 in βB1-CTGF1 and WT mice. (A) Quantitative real-time RT-PCR analysis for mRNA of CD44 in βb1-CTGT1 and WT mice. The mean value obtained from WT mice was set at 1. *RPL32* was used as a reference gene (n=4; *P= 0.04). Data represented as mean ± SEM. (B) Immunohistochemical staining for CD44 (red) in 2-month old TG and WT mice. Nuclear DNA is labeled with DAPI (blue) Scale bar: 50µm.

4.3.3. Localization and expression of CD44 in the chamber angle of POAG patients

To evaluate CD44 expression in glaucoma versus healthy patients and to have a first impression about the sufficient targeting and binding of HA-decorated nanoparticles, CD44 levels were assessed in glaucomatous and healthy human donor eyes and in normal and glaucomatous SC cells. Expression of CD44 was studied in SC cells isolated from normal and glaucomatous human donors (Figure 4-47). Real-time RT-PCR analyzes showed a significant increase of CD44 mRNA expression in glaucomatous SC cells compared to healthy controls (normal: 1 ± 0.52, n=4; glaucomatous: 6.26 ± 3.11, n=5; *p=0.05).

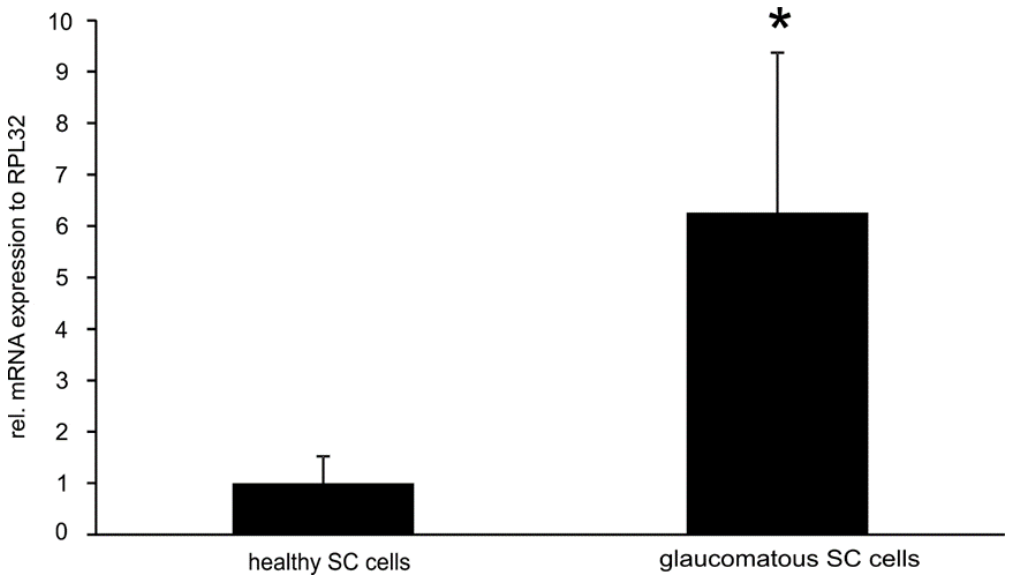

Figure 4-47: Quantitative real-time RT-PCR analysis for mRNA of CD44 in healthy and glaucomatous SC cells. CD44 mRNA expression was significantly increased in glaucomatous SC cells compared to healthy controls (healthy: 1 ± 0.52, n=4; glaucomatous: 6.26 ± 3.11, n=5; *p=0.05). Mean value of healthy controls was set at 1. *RPL32* was used as a reference gene. Data represented as mean ± SEM.

Immunohistochemical staining was performed on cryo sections of healthy and glaucomatous human donor eyes and protein level was analyzed in the iridocorneal angle. CD44 could be detected in the iris, the TM and the SC in both healthy and glaucomatous eyes. Indeed, CD44 is increased in these identified tissues in the glaucomatous human donor eyes compared to healthy control. We could detect an increased protein synthesis in the SC endothelium, the TM and the iris (Figure 4-48).

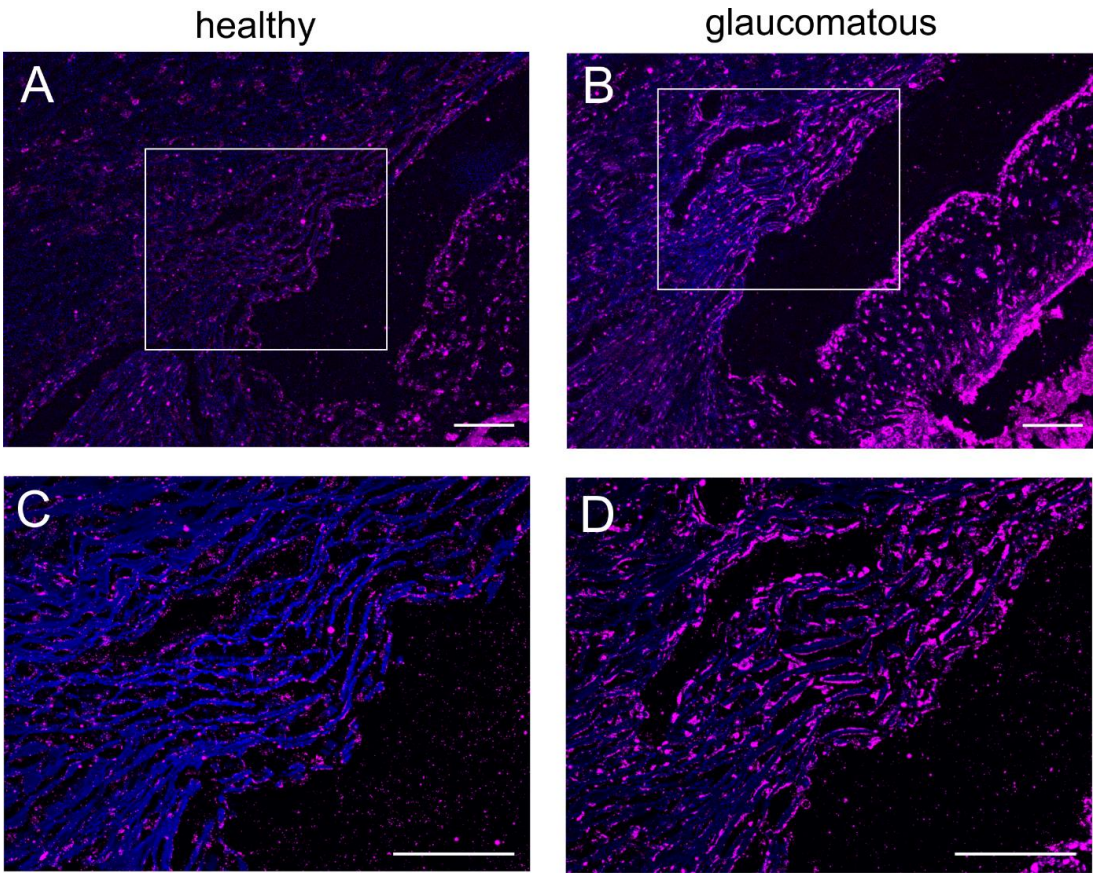

Figure 4-48: Localization and expression of CD44 in the chamber angle of POAG patients. (A, B) Immunohistochemical staining for CD44 in the chamber angle of healthy (A) and glaucomatous (B) human donor eyes. CD44 was seen adjacent to the SC, in the entire TM and in the iris. In glaucomatous donor eyes immunoreactivity was more intense in the identified tissue. (C, D) Enlarged images. Nuclear DNA is labeled with DAPI (blue). Scale bar: 100µm.

4.3.4. Perfusion of porcine eyes with nanoparticles

As it could be shown that CD44 synthesis is changed in outflow tissue of our mouse glaucoma model and in glaucomatous patients, it can be suggested that the application of nanoparticles targeting CD44 would be a promising approach. Therefore, nanoparticles coated with HA, the natural ligand, and nanoparticles coated with PEI as a control, were perfused in the anterior chamber of porcine eyes. Following perfusion, the anterior segments were dissected and the whole outflow ring was investigated. The NP-HA perfused eyes showed a consisted distribution and intensity in the entire outflow tissue, in comparison the NP-PEI perfused eyes revealed an irregular localization and a reduced abundance (Figure 4-49 A). Quantitative measurement of integrated density of NP-HA and NP-PEI perfused porcine eyes showed a significant increase in the fluorescent intensity for NP-HA perfused eyes compared to NP-PEI perfused controls (NP-PEI: n=8, 15.50 ± 1.72; NP-HA: n=9, 45.98 ± 14.21; *p =0.05) (Figure 4-49 B).

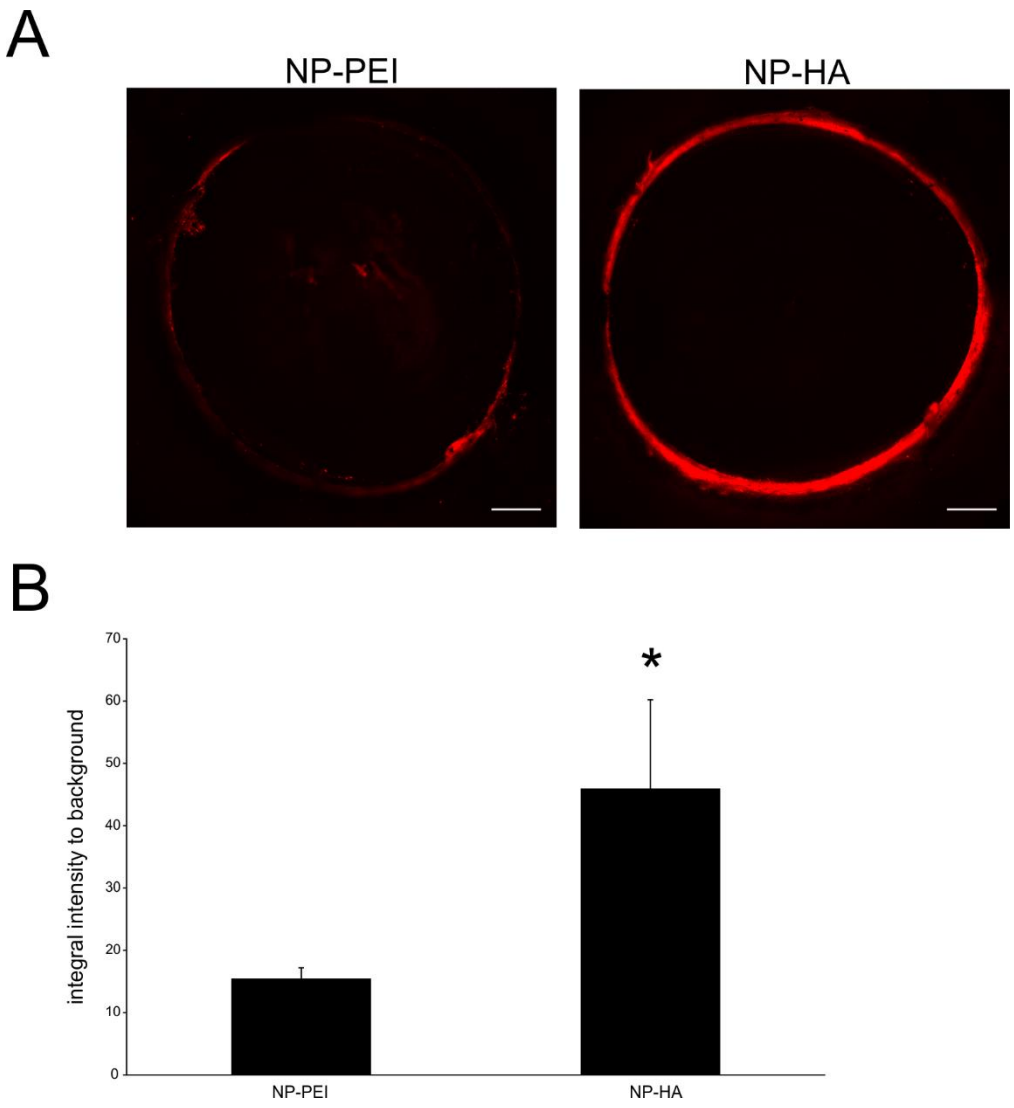

Figure 4-49: Perfusion of porcine eyes with NP-PEI and NP-HA. (A) Fluorescent imaging of porcine outflow rings after perfusion with NP-PEI (red) and NP-HA (red). Scale bar: 2000µm (B) Quantitative measurement of integrated density of NP-PEI or NP-HA perfused porcine eyes. (NP-PEI: n=8; NP-HA: n=9; *P=0.049). Data represented as mean ± SEM.

For detailed analysis of NP distribution and localization, the whole outflow ring was dissected, and sagittal sections of the outflow pathway tissue and immunohistochemical staining against CD44 and CD31 were performed. As expected, a CD44 signal was detected throughout the entire TM and the VP (venous plexus) (Figure 4-50), as it was already shown in mouse (4.3.2.) and human TM and SC (4.3.3.). HA decorated NPs were distributed in the entire TM and even reach the lumen of the VP. In contrast, PEI-NPs were accumulated at the outer region of the TM and did not enter the inner layers of TM or even the lumen of VP (Figure 4-50).

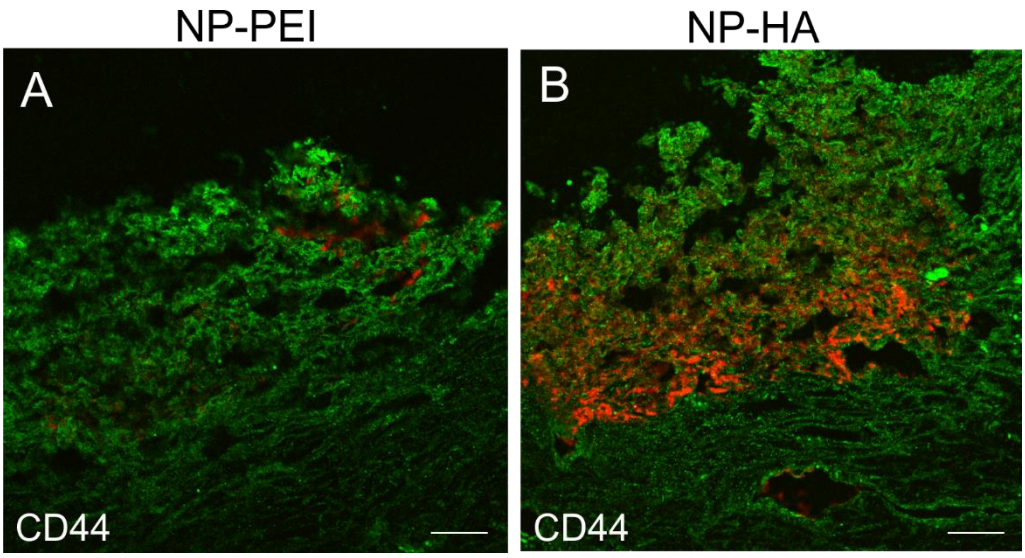

Figure 4-50: Immunohistochemical staining of NP-PEI and NP-HA perfused porcine eyes against CD44 (green). NP-PEI (red) distribution was restricted to the outer layer of the TM. NP-HA (red) entered the inner layer of the TM and the VP. CD44 (green) immunoreactivity was shown throughout the entire TM and the VP. Scale bar: 50µm

To determine the location of HA-NPs in the lumen of the VP, immunohistochemical staining against CD31 was performed to visualize the endothelial cells of VP. By CD31 the endothelial lining of VP could be nicely visualized, and the HA- coated NPs could be shown to reach the lumen of VP (Figure 4-51 B), as it was shown by the CD44 staining (Figure 4-54). In none of the performed experiments PEI-NPs were transported into the deeper layers of TM or reach the endothelial lining of the VP (Figure 4-51 A). In a higher magnification by showing a top and later view of the same sagittal sections, the HA-NPs could be detected to be taken up by the endothelial cells and enter the VP (Figure 4-51 D). Again, PEI-NPs were located at the outer layer of the TM and do not enter the deeper layers or even the VP (Figure 4-51 C).

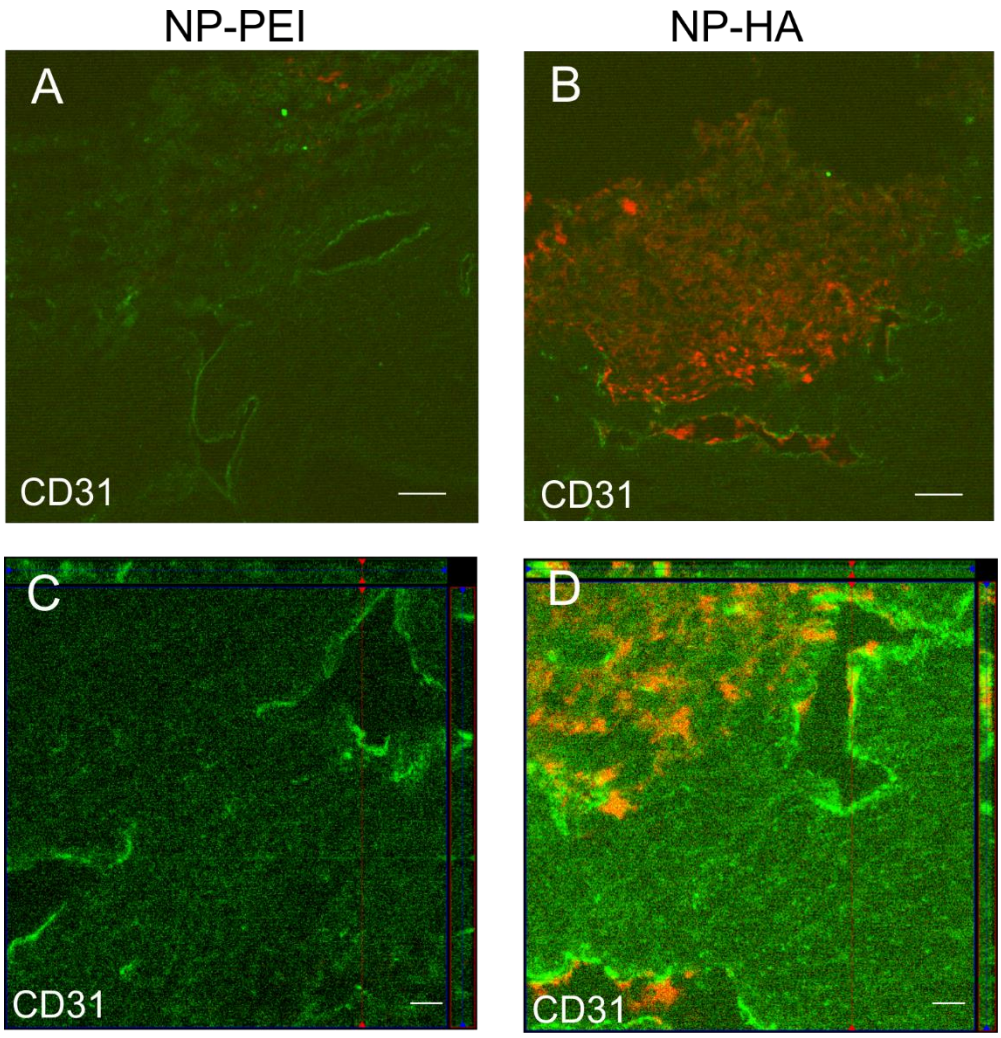

Figure 4-51: Immunohistochemical staining against CD31 of sagittal sections of NPs perfused porcine eyes. (A) NP-PEI (red) distribution was restricted to the outer layer of the TM. (B) NP-HA (red) entered the inner layer of the TM and are located in the endothelial lining of the VP. (C,D) Top and ventral view of the same sagittal sections. Scale bar: 50µm.

4.3.5. Perfusion of human eyes with nanoparticles

One eye pair of a human donor was used to investigate the distribution of NP's after perfusion. One human donor eye was perfused with PEI-coated NPs and the other one with HA-coated NPs, following by performance of sagittal sections and staining against CD44 (Figure 4-52) to evaluate NP distribution. As expected, a CD44 expression could be detected throughout the entire TM and in the SC (Figure 4-52), as it was already shown in healthy and glaucomatous donor eyes (4.3.3.). NP distribution reveal a comparable pattern as it was shown for porcine perfused eyes. PEI-coated NPs are located at the entrance and in the inner layer of the TM (Figure 4-52). In contrast, HA coated NP's are distributed in all layers of the TM (Figure 4-52), with reaching the outermost layer, the JCT, as well.

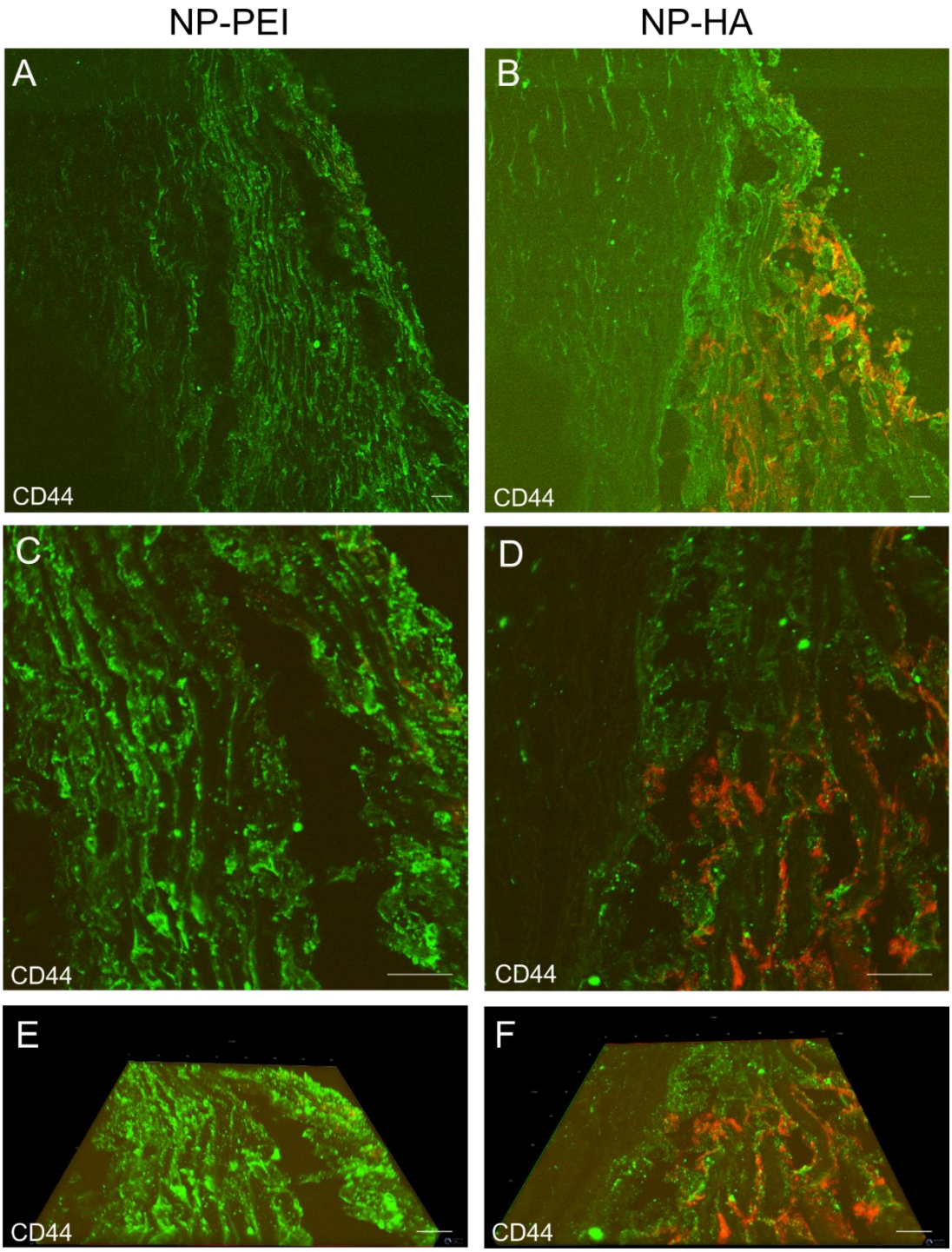

Figure 4-52: Immunohistochemical staining against CD44 (green) of sagittal sections of NP's perfused human eyes. (A) Sagittal section of NP-PEI (red) perfused human TM. (B) Sagittal section of NP-HA (red) perfused human TM. (C) Enlarged excerpt of NP-PEI perfused human TM showed the localization of the NP in the inner layer of the TM. (D) Enlarged excerpt of the NP-HA perfused human TM showed the distribution of HA coated NPs in all layers of the TM. (E,F) 3D representation of the same sections shown in C and D, shows the colocalization of NP-HA with the CD44 receptor. Scale bar: 20µm.

4.3.6. CTGF silencing by nanoparticles

For further investigations, the ability of siRNA coated NPs to reduce CTGF in HTM cells was analyzed. Therefore, HTM cells were transfected with siRNA coated nanoparticles. For further control, HTM cells were only transfected with siRNA (Figure 4- 53). Transfection of HTM cell with PEI-coated siRNA NPs showed no downregulation of CTGF (0.97 ± 0.14; n=4) in comparison to scrblsiRNA PEI-NPs (1 ± 0.00; n=4). Indeed, HTM cells transfected with HA-coated siRNA NPs revealed a highly significant downregulation of CTGF protein (0.51 ± 0.05; n=4; ***P=0.0001), compared to scrblsiRNA HA-NP control (1 ± 0.00; n=4). The internal control transfection with siRNA without NPs also lead to a highly significant downregulation of CTGF in HTM cells (0.24 ± 0.05; n=4; ***p=0.0009), in comparison to the control (1 ± 0.00; n=4) (Figure 4- 53).

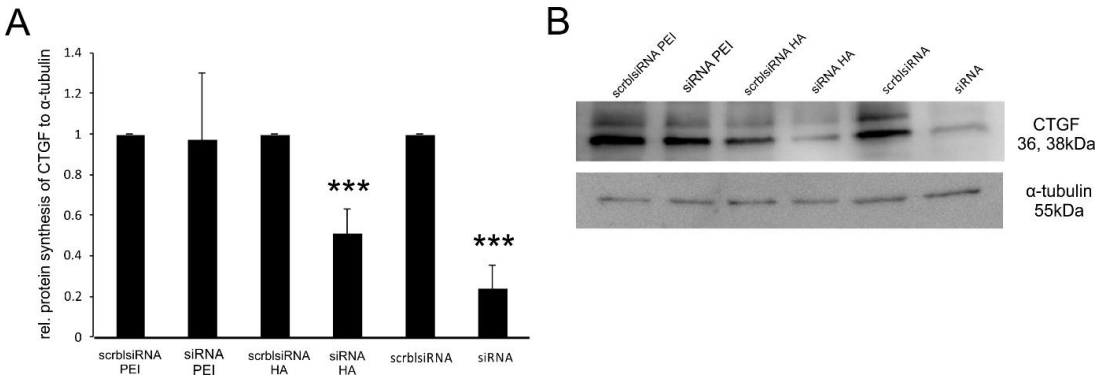

Figure 4-53: Western Blot analysis of CTGF silencing by nanoparticles in HTM cells. (A) Densitometric analysis of CTGF protein synthesis after transfection with siRNA coated NPs. (B) Representative Western blot for CTGF after transfection with siRNA coated NP`s. α-tubulin was used for normalization. The mean value of scrblsiRNA was set at 1. Data represented as mean ± SEM.

All in all, it can be stated that the target receptor CD44 for the new designed approach is expressed in both HTM and SC cells, and is upregulated in the glaucomatous outflow pathway of human donors. Furthermore, the here designed NPs are able to follow the natural outflow pathway of AH and reach the target TM cells and bind to the CD44 receptor, in both human and porcine perfused eyes. Finally, the initial experiments show the ability of siRNA coated HA-NPs to reduce CTGF expression in HTM cells.

4.4. Effect of conditional CTGF knockdown on mouse eye development

To use CTGF as a specific target for IOP reduction in the progression of POAG, the effect of a CTGF knockdown or knockout, respectively has to be proven. As it was shown in the previous analysis of this study, that CTGF is highly expressed in different ocular tissue, like TM, ONH and retina related to the pathogenesis of POAG. Therefore, the involvement of CTGF in the development of the eye has to be analyzed.

Since the homozygous knockout of CTGF is embryonic lethal and the heterozygous knockout does not result in an ocular phenotype, a conditional knockout of CTGF was generated, which allow a conditional deletion of CTGF via the Cre-loxP system to study the effect of CTGF deficiency on eye development. Mice with two Coin-Introns ($CTGF^{Coin/Coin}$) were crossed with $CTGF^{Coin/Coin}$;CAGGCre-ER mice, which are heterozygous for the Cre-recombinase. Experimental mice ($CTGF^{Coin/Coin}$;CAGGCre-ER) mice and control mice ($CTGF^{Coin/Coin}$) were treated with Tamoxifen eyedrops with a concentration of 5mg/ml three times a day from P1 to P5. For all following experiments mice were genotyped for the Cre recombinase (Figure 4-54 C) and the Coin-Intron (Figure 4-54 A) and the WT allele (Figure 4-54 B), respectively. The product of the Coin-PCR results in a 350bp PCR product for all tested animals. The Exon2 PCR, amplifying the WT allele results in a PCR product of 275bp only for the positive control, as mice homozygous for the Coin-Intron are crossed. The amplification of the CAGGCre recombinase results in a PCR product of 275bp. Mice containing the Cre recombinase were used as experimental mice ($CTGF^{Coin/Coin}$;CAGGCre-ER mice) and littermates with two non-inverted Coin-Introns are referred to as control mice.

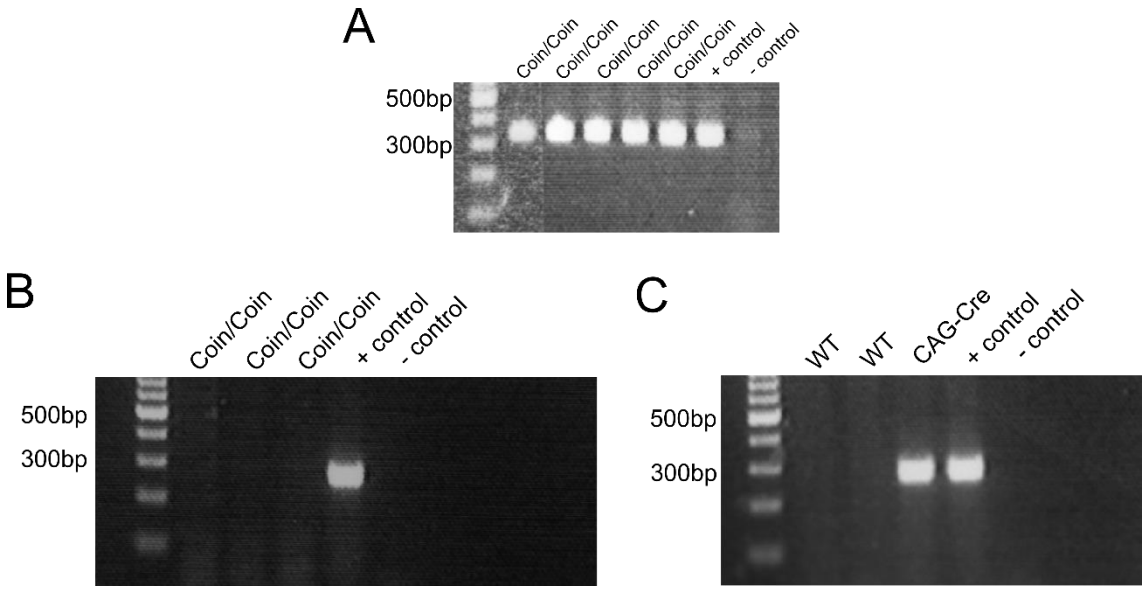

Figure 4-54: Representative CAGG-Cre, $CTGF^{Coin/Coin}$ and $CTGF^{Exon2}$ PCR. (A) $CTGF^{Coin/Coin}$ PCR product 350bp. (B) $CTGF^{Exon2}$ PCR product 270bp. (C) CAGGCre PCR product 270bp.

4.4.1. Verification of conditional CTGF knockdown

To prove efficient induction for Cre recombinase and knockdown of CTGF, Real-time RT-PCR analysis and immunohistochemical staining of retina and ON of tamoxifen treated CTGF$^{Coin/Coin}$; CAGGCre-ER and CTGF$^{Coin/Coin}$ were performed.

Real-time RT-PCR analysis of retinal tissue of P17 mice revealed a high significant knockdown of CTGF in CTGF$^{Coin/Coin}$;CAGGCre-ER mice (0.36 ± 0.05; n=8; **P=0.005) compared to control mice (1±0.13; n=7) (Figure 4-55).

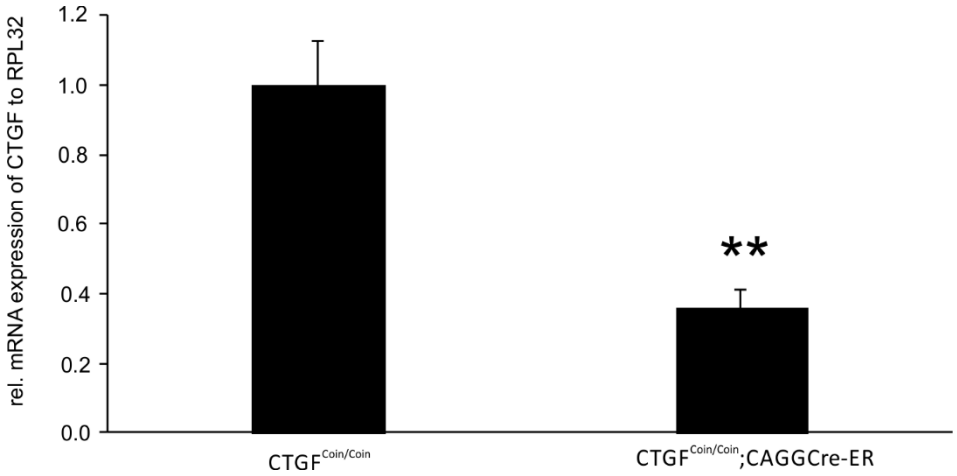

Figure 4-55: Real-time RT-PCR analysis of retinal CTGF knockdown. mRNA expression was highly significant reduced in the retina of CTGF$^{Coin/Coin}$;CAGGCre-ER (0.36 ± 0.05; n=8; **P=0.005) mice in comparison to CTGF$^{Coin/Coin}$ littermates (1±0.13; n=7). *RPL32* was used as a housekeeping gene. Mean value of CTGF$^{Coin/Coin}$ control mice was set at 1. Data represented as mean ± SD.

Additionally, the knockdown of CTGF on mRNA expression level could be confirmed on protein level. Therefore, immunohistochemical staining with a specific antibody against CTGF on retinal and ON sections of CTGF$^{Coin/Coin}$;CAGGCre-ER and CTGF$^{Coin/Coin}$ mice at P17 were performed (Figure 4-56). In comparison to the CTGF promotor expression pattern, which shows a specific expression in retinal Müller cells, amacrine cells and endothelial cells, the secreted CTGF protein is located in the entire retina, showing protein synthesis in the GCL, IPL, INL, OPL, ONL and the photoreceptor outer segments in CTGF$^{Coin/Coin}$ control mice (Figure 4-56 A). This signal is mostly reduced in the retina

of experimental mice (CTGF$^{Coin/Coin}$;CAGGCre-ER), indicating an efficient tamoxifen depending induction of the Cre recombinase, resulting in successful conditional knockdown of CTGF (Figure 4-56 B). This result is comparable with the staining observed in the ON, where CTGF protein is located in the entire ON, with no obvious preference for glial or neuronal tissue in CTGF$^{Coin/Coin}$ control mice Figure 4-56 C) and a markedly decrease in the CTGF$^{Coin/Coin}$;CAGGCre-ER mice (Figure 4-56 D).

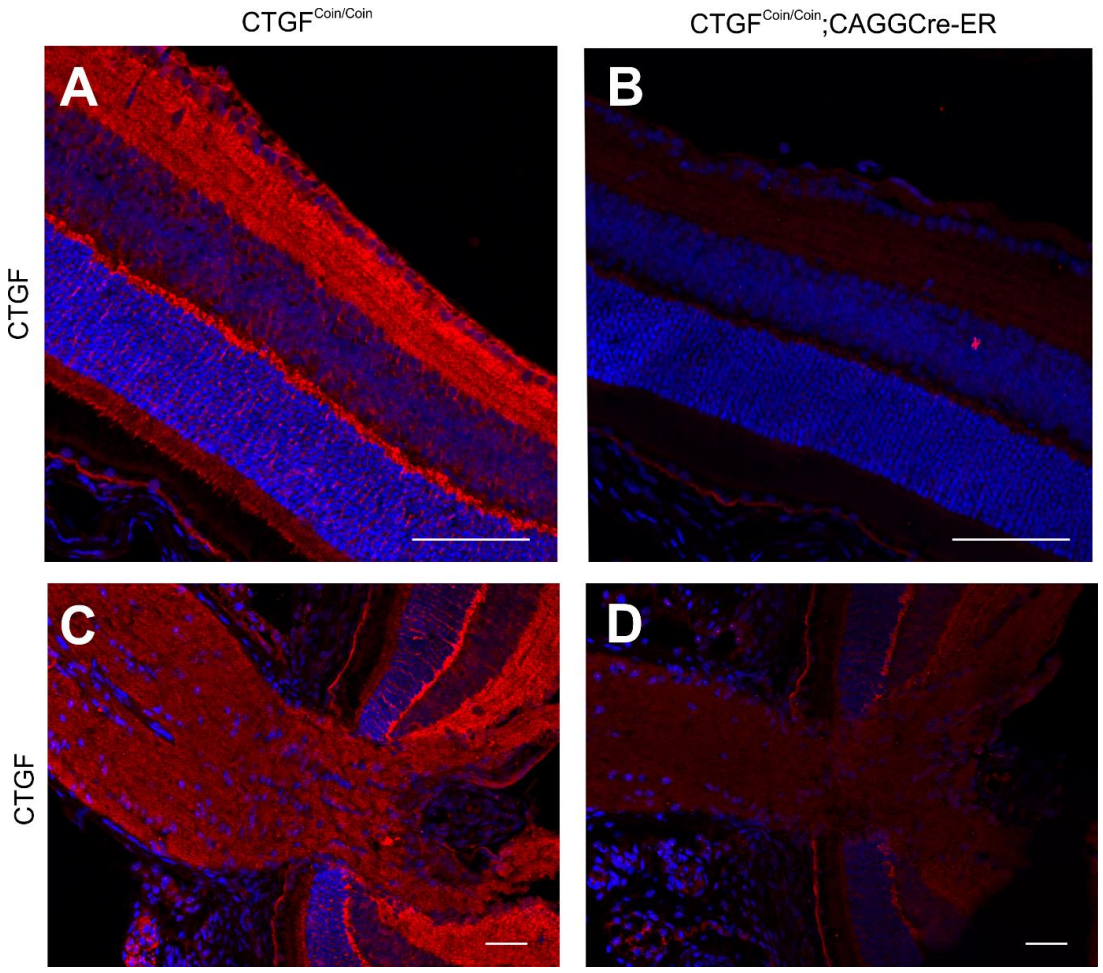

Figure 4-56: Immunohistochemical staining of CTGF on retina and ON sections of CTGF$^{Coin/Coin}$;CAGGCre-ER mice. CTGF levels were mostly reduced in the entire retina in CTGF$^{Coin/Coin}$;CAGGCre-ER mice (B) compared to CTGF$^{Coin/Coin}$ control mice (B). Additionally, the successful CTGF knockdown was shown in the ON. CTGF$^{Coin/Coin}$ control mice showed a CTGF synthesis in the whole ON (C), and a reduced CTGF signal was detected in the ON of CTGF$^{Coin/Coin}$;CAGGCre-ER mice (D). nuclear DNA is labeled with DAPI (blue). Scale bar: 50µm.

4.4.2. Morphological analysis of CTGF knockdown

Semi thin sections of CTGF$^{Coin/Coin}$ and CTGF$^{Coin/Coin}$;CAGGCre-ER mice were performed to investigate the effect of CTGF knockdown on eye morphology (Figure 4-57). Analysis of these sections revealed that the postnatal knockdown of CTGF does not result in

obvious morphological alterations in CTGF$^{Coin/Coin}$;CAGGCre-ER mice on P17 in comparison to littermate controls (Figure 4-57). Especially the eye tissue expressing high levels of CTGF during the development, like the TM, cornea, sclera and ON showed no changes in development in experimental mice (CTGF$^{Coin/Coin}$;CAGGCre-ER) (Figure 4-58). In the ON of CTGF$^{Coin/Coin}$ and CTGF$^{Coin/Coin}$;CAGGCre-ER mice no structural differences were monitored. There are no obvious signs that the conditional knockout of CTGF did lead to structural alterations in the development of the ON (Figure 4-58 A, B). Interestingly, there is evidence that the conditional knockout of CTGF did lead to a persistence or rather to a decreased regression of the hyaloid artery. The persistent hyaloid artery was not observed in every CTGF$^{Coin/Coin}$;CAGGCre-ER eye, suggesting that the decreased regression of the hyaloid artery is related to the level of the CTGF knockdown (Figure 4-58 A, B). Observing the anterior chamber angle in more detail, it was seen, that the anterior chamber angel is open in both animals and the ciliary body and the TM showed no obvious signs of differences in structure and organization, indicating that the AH outflow pathway is not influenced by the conditional knockout of CTGF (Figure 4-58 C, D). In addition, also the cornea exhibited no obvious differences in CTGF$^{Coin/Coin}$;CAGGCre-ER mice. In both animals the corneal endothelium, epithelium, stroma and Descement´s membrane, respectively are normally developed. The thickness of all layers did not differ in conditional CTGF knockdown mice in comparison to CTGF$^{Coin/Coin}$ controls (Figure 4-58 E, F).

All in all, in can be concluded that the conditional CTGF knockout did not lead to obvious structural difference in the development of different eye structures.

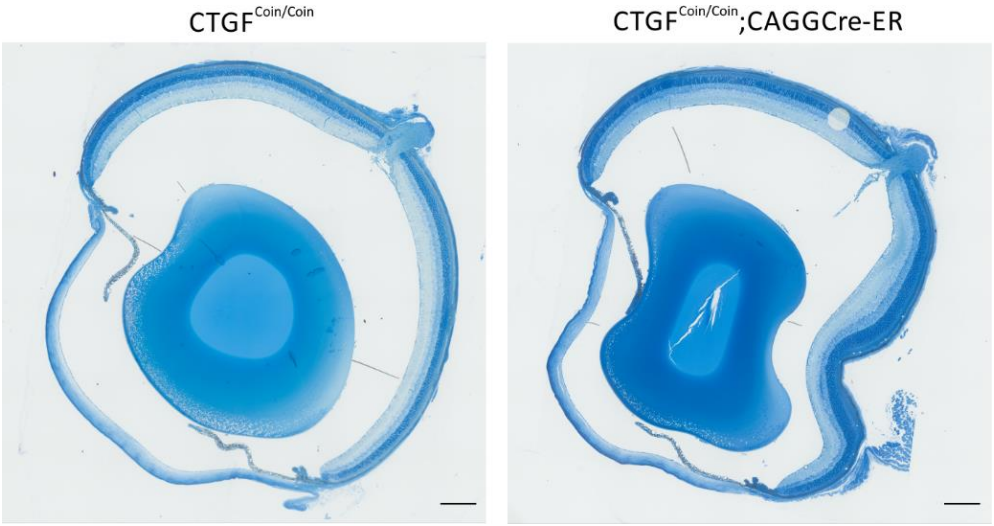

Figure 4-57: Semi-thin sections of CTGF$^{Coin/Coin}$ and CTGF$^{Coin/Coin}$;CAGGCre-ER mice. No morphological differences were observed. Scale bar: 200µm.

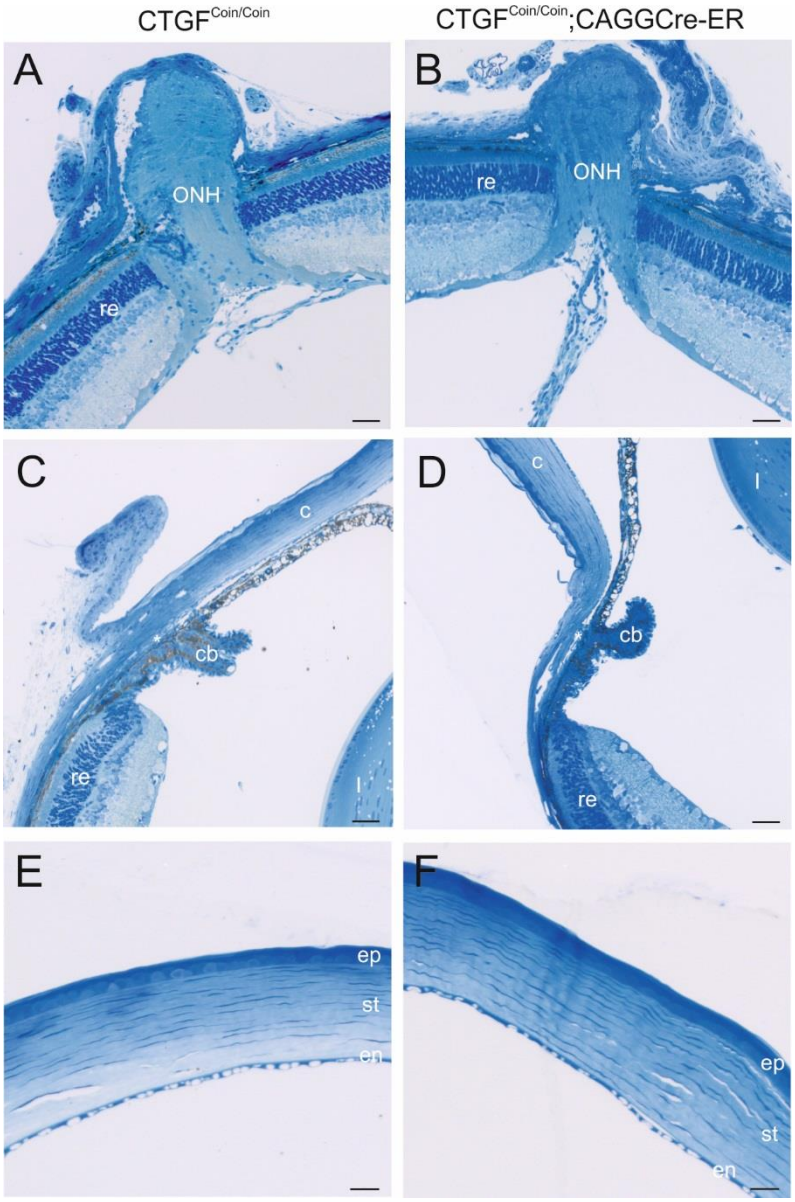

Figure 4-58: Semi-thin sections of ONH, anterior chamber angle and cornea of CTGF$^{Coin/Coin}$ and CTGF$^{Coin/Coin}$;CAGGCre-ER mice. Enlarged excerpts of semi-thin sections shown in Figure 4-57. (A) The ONH of CTGF$^{Coin/Coin}$ and CTGF$^{Coin/Coin}$;CAGGCre-ER mice showed no morphological differences. (B) The anterior chamber angle of CTGF$^{Coin/Coin}$ and CTGF$^{Coin/Coin}$;CAGGCre-ER mice showed no morphological differences. (C) The cornea of CTGF$^{Coin/Coin}$ and CTGF$^{Coin/Coin}$;CAGGCre-ER mice showed no morphological differences. Scale bar: 50µm (A-D); 20µm (E,F).

Since there is no possibility to prove the successful conditional knockdown in each individual animal, which was conducted to morphological analysis, because it is not possible to combine this experimental approach with immunohistochemical staining against CTGF, an additive approach was investigated. Therefore, it was examined a potential reduction of CTGF after the tamoxifen treatment in additional organs, for example the lung (Figure 4-59). Initial Real-time RT-PCR analysis for CTGF in lung

mRNA of CTGF$^{Coin/Coin}$ and CTGF$^{Coin/Coin}$;CAGGCre-ER mice showed a trend for a CTGF knockout to 50% in CTGF$^{Coin/Coin}$;CAGGCre-ER animals (n=2; 0.5±0,14), compared to littermate controls (n=3;1±0.33) (Figure 4-59).

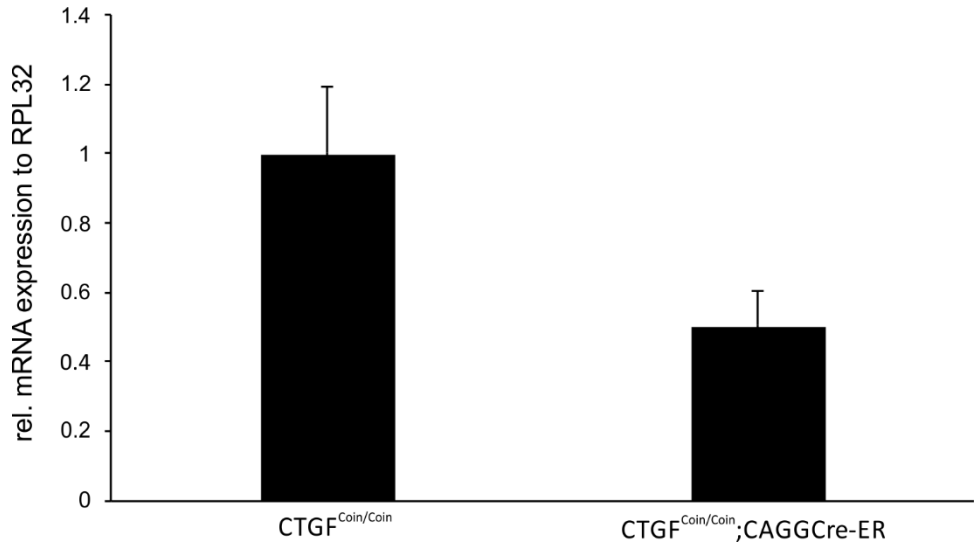

Figure 4-59: Real-time RT-PCR analysis of CTGF knockdown in the lung. mRNA expression was reduced in the lung of CTGF$^{Coin/Coin}$;CAGGCre-ER mice in comparison to CTGF$^{Coin/Coin}$ littermates. *RPL32* was used as a housekeeping gene. Mean value of CTGF$^{Coin/Coin}$ control mice was set at 1. Data represented as mean ± SD.

4.4.3. Effect of conditional CTGF knockout on astrocyte network in the retina

As studies for CTGF distribution demonstrated a high CTGF expression in the retina during development, GFAP staining on retinal flat mounts of CTGF$^{Coin/Coin}$;CAGGCre-ER and CTGF$^{Coin/Coin}$ mice were examined to analyze the development of the retinal astrocytic network. Interestingly, CTGF$^{Coin/Coin}$;CAGGCre-ER mice showed a dramatically altered astrocyte network in the retina. The connection between astrocytes and the vasculature is altered, as the blood vessels are not ensheathed with fine processes, as in CTGF$^{Coin/Coin}$ control mice which showed a normally developed astrocytic network, covering the entire retina, with astrocyte processes contacted and intertwined each other and end-feet enveloping the retinal vasculature (Figure 4-60 A, B). Instead, the astrocytes built enlarged cell somata sitting on the retinal vasculature (Figure 4-60 C, D arrow). Furthermore, alteration in the morphology of astrocyte processes can be observed, as their processes showed an increase in thickness (Figure 4-60). All in all, it can be stated that the conditional knockdown of CTGF led to thickened retinal astrocyte processes and furthermore led to the appearance that retinal blood

vessels are not ensheated with fine astrocyte processes instead, they are enlaced by the astrocyte cell bodies.

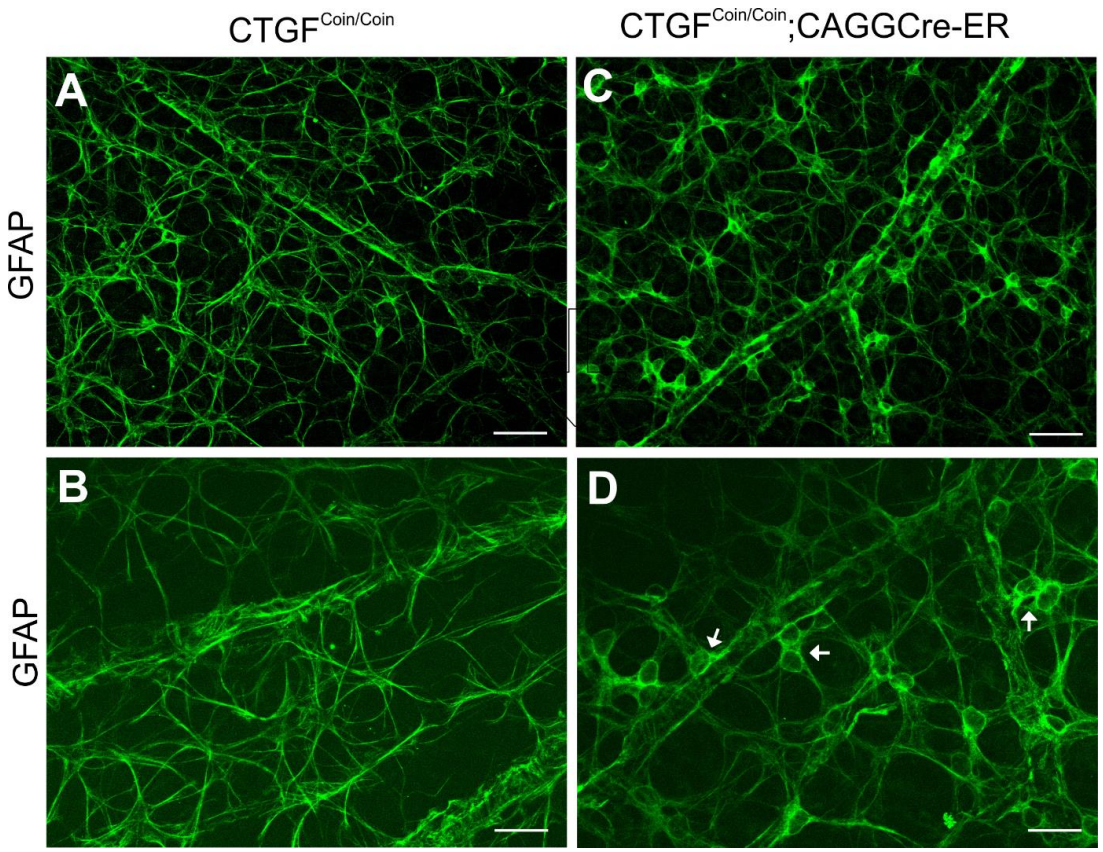

Figure 4-60: Immunohistochemical staining against GFAP of retinal flat mounts of P17 CTGF$^{Coin/Coin}$;CAGGCre-ER mice. (A,B) GFAP positive astrocyte network in CTGF$^{Coin/Coin}$ control mice. (C,D) GFAP positive astrocyte network in CTGF$^{Coin/Coin}$;CAGGCre-ER mice. Arrows depict morphologically changed retinal astrocytes. Scale bar: 50µm.

4.4.4. Effect of conditional CTGF knockdown on astrocyte structure in the ON

Since CTGF is highly expressed in astrocytes in the ON, especially in the region of the glial lamina during postnatal eye development, it was of great interest to analyze the effect of CTGF deficiency on the astrocyte development and glial lamina establishment. GFAP staining on sagittal section of CTGF$^{Coin/Coin}$;CAGGCre-ER (n=3) and CTGF$^{Coin/Coin}$ mice (n=4) were executed (Figure 4-61). The glial lamina in control mice could constituted as a region of transversely dense packed GFAP positive astrocytes (Figure 4-61 A). This special arrangement of astrocytes is missing in CTGF conditional knockdown mice. No transversely arranged astrocytes were observed, instead the astrocytes are already longitudinal orientated parallel to the long axis of the ON, which normally first occurs in the myelinated region of the ON posterior to the glial lamina (Figure 4-61 B).

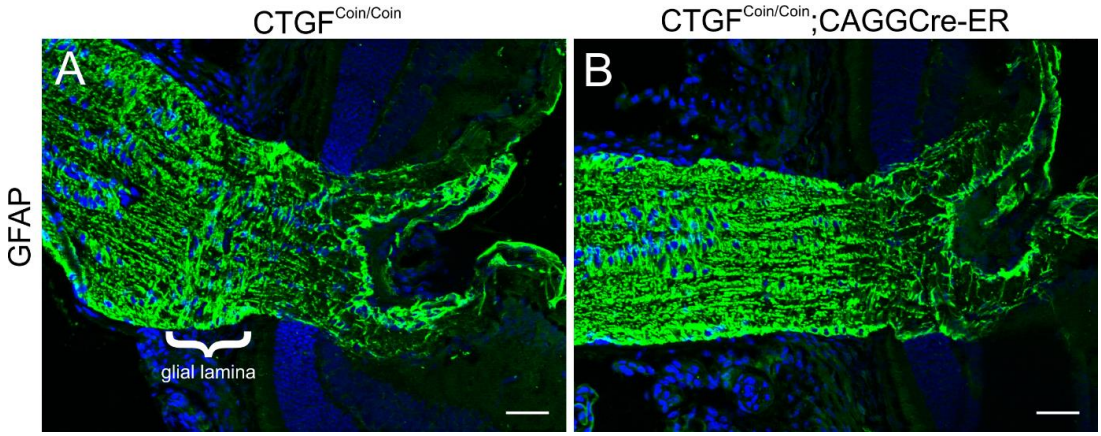

Figure 4-61: Immunohistochemical staining against GFAP (green) on sagittal ON section of CTGF$^{Coin/Coin}$ and CTGF$^{Coin/Coin}$;CAGGCre-ER mice. (A) GFAP staining in CTGF$^{Coin/Coin}$ control mice. Bracket indicates the normal presence of the glial lamina. (B) GFAP staining in CTGF knockdown mice showed no existence of the glial lamina. nuclear DNA is labeled with DAPI (blue). Scale bar: 50µm.

Based on the observation that CTGF deficiency lead to changes in formation of the glial lamina during development, immunohistochemical staining against myelin basic protein (MBP) were performed to analyze if the altered constitution of astrocyte arrangement leads to additional changes in the composition of the ON (Figure 4-62). The myelination of the ON starts typically 120-170µm behind the sclera (Sun et al., 2009). The MBP staining showed that the CTGF knockdown does not lead to variations between the unmyelinated and myelinated region of the optic nerve Figure 4- 62 A, B). The beginning of the myelination was measured in CTGF$^{Coin/Coin}$;CAGGCre-ER (n=3) and CTGF$^{Coin/Coin}$ (n=1) mice. The distance in ON of the control eye is 154 µm and ON of CTGF$^{Coin/Coin}$;CAGGCre-ER eyes showed a distance of 141 µm ± 28 µm (Figure 4-62 A, B).

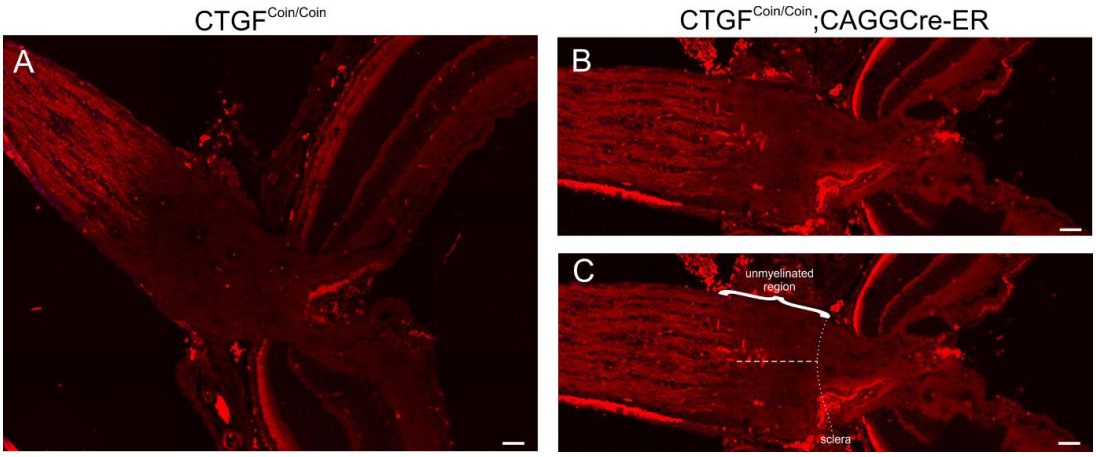

Figure 4-62: MBP staining of sagittal ON sections of CTGF$^{Coin/Coin}$ and CTGF$^{Coin/Coin}$;CAGGCre-ER mice. (A) MBP staining (red) in the CTGF$^{Coin/Coin}$ ON. (B) MBP staining in the ON of CTGF$^{Coin/Coin}$;CAGGCre-ER mice. (C) Representation of structures involved in the measurement. Dotted line represents the level of the sclera. Dashed line represents the measured distance. Unmyelinated region is depicted by brackets. Scale bar: 50µm.

All in all, initial data show that the conditional knockdown of CTGF effects the morphology of retinal astrocytes, resulting in thickened processes, increased cell bodies and an altered interaction with retinal blood vessels. Furthermore, the formation of the glial lamina constituted of ON astrocytes is altered as a result of the conditional CTGF knockout.

5. Discussion

5.1. Summary

The aim of the study was to investigate the involvement of CTGF in eye development and the pathology of POAG. The expression of CTGF during eye development and in the adult eye was investigated in the different ocular tissue, furthermore the CTGF expressing cell types were identified. The involvement of CTGF in the ONH pathology of POAG was examined by the correlation of CTGF expression changes and astrocytes reactivity in the ON and ONH after applying mechanical stress *in vivo* and by increasing substratum stiffness *in vitro*. Furthermore, siRNA coated layer-by-layer NPs were designed as a new tool to reduce CTGF in the AH outflow pathway tissue.

During eye development CTGF is expressed in various eye structures. In early embryonic development an expression in the outer and inner layer of the optic cup as well as the lens vesicle was detected. In the following embryonic and postnatal developmental stages, a CTGF expression was detected in tissues of the anterior eye segment like corneal endothelium, epithelium and stroma, in the TM and the ciliary body. In the posterior eye segment, an expression could be observed in the retina, choroidea, sclera, ONH and dura mater. During the development of the eye, an altered CTGF expression pattern could be observed in the cornea, the ciliary body, the retina, the ONH and the dura mater, whereas the expression in the TM remained constantly high. The characterization of the CTGF expressing cell types revealed that the trabecular meshwork cells, Müller cells, amacrine cells, ON astrocytes and endothelial cells of the SC and of the retinal and choroidal vasculature were the source of the CTGF signal. An important role for CTGF in the correct formation of astrocytic morphology in the retina and the ONH could be shown in CTGF conditional knockdown mice.

Besides the involvement of CTGF in developmental processes, a correlation between CTGF expression and pathological changes in the murine glaucoma model were analyzed. An increased astrocyte reactivity was associated with an enhanced CTGF synthesis in the ONH, related to the chronically elevated IOP, whereas none of those changes were observed in the adjacent parts of the ON. Interestingly, cultured murine ON astrocytes could sense changes in stiffness of the surrounding ECM, causing the same changes as in the *in vivo* glaucoma model. The analysis of mechanosensitive ion channels showed a broad spectrum of expression changes dependent on the substratum stiffness, but the most promising changes were seen in Caveolin expression. An enhanced Caveolin synthesis in ON astrocytes was detected on increasing substratum stiffness and after treatment with CTGF and TGF-β2 *in vitro* and in the ONH of the murine glaucoma model.

Based on the observation that CTGF can cause POAG-like changes, we started a cooperation with Miriam Breunig (Department of Pharmaceutical Technology, University of Regensburg) to develop a new tool to reduce CTGF in the AH outflow pathway tissues and cells. Layer-by-layer coated NPs were designed and successfully delivered by anterior chamber perfusion to the outflow pathway tissues and cells of porcine and human eyes. CD44 was identified as an ideal target for HA coated NP's, as CD44 is permanently present in cultured HTM cells, in the anterior chamber angle of the murine glaucoma model and in cells and outflow pathway tissues of human donors. The implication of CD44 in POAG could be shown by the enhanced expression in glaucomatous SC cells and the anterior chamber angle of human glaucomatous donor eyes. Finally, siRNA coated NPs could successfully reduce CTGF synthesis in HTM cells *in vitro*.

5.2. CTGF expression in ocular tissues and cell types during development and in the adult eye

To date, little is known about the function of CTGF during development and in healthy tissue, as most of the studies focus on the role under pathological conditions. CTGF is upregulated in many disorders associated with a pathological ECM increase, like scleroderma, renal and pulmonary fibrosis, inflammatory bowel disease, atherosclerosis and POAG (Cicha et al. 2005, Di Mola et al. 2004, Ito et al. 1998, Junglas et al. 2012, Sato et al. 2000, Yamamoto et al. 2005b).In processes occurring during development such as migration and differentiation, the ECM plays an essential role and provides cues for cellular metabolism (Adams & Watt 1993, Lin & Bissell 1993, Perris 1997). CTGF can function as a modulator of migration, adhesion, ECM production, cell cycle, proliferation and differentiation in various cell types (Babic et al. 1999, Bradham et al. 1991, Brigstock 2003, Frazier et al. 1996, Igarashi et al. 1993, Kireeva et al. 1997, Perbal 2001, Perbal 2004, Winter et al. 2008). Therefore, an implication of CTGF in the different processes occurring during eye development seems likely. In this study we report CTGF expression in various ocular structures during development and in the adult eye.

5.2.1. Involvement of CTGF in the development of the anterior eye segment

The morphogenesis of the anterior eye segments involves an exact interaction of various transcription factors and signaling proteins (Cvekl & Tamm 2004). In the anterior eye segment, a CTGF expression was detected in the in the ciliary body, the TM and the SC, and depending on the developmental stage in the corneal epithelium, stroma and endothelium.

During development, CTGF is expressed in all three layers of the cornea prior to eye lid opening, afterwards it is restricted with a low expression to the corneal endothelium. The fact that the expression pattern is changed after eyelid opening, which indicates the maturation of the cornea leads to the hypothesis that CTGF plays a role in the development and formation of the corneal structure. The corneal stroma constitutes of various types of collagen, like collagen type I, III, V and VI. (Birk et al. 1986, Keene et al. 1987, Marshall et al. 1991a, 1991b, Zimmermann et al. 1986). In addition, to collagen a second group of extracellular proteins, the proteoglycans, including Decorin, Lumican, Kerstocan and Mimecan are a major component of the corneal stroma. They are thought to play an essential role in maintaining position of the fibrils and controlling fibril growth (Borcherding et al. 1975, Rada et al. 1993, Scott & Orford 1981, Scott & Thomlinson 1998). Interestingly, Decorin deficient mice show no corneal phenotype. In contrast Keratocan and Lumican deficient mice reveal an impaired corneal composition (Chakravarti et al. 1998, Chakravarti et al. 2000, Danielson et al. 1997). CTGF can enable interactions with a variety of heparan sulfate containing proteoglycans via its heparin-binding domain (Chen & Lau 2010, Gao & Brigstock 2005, Leask & Abraham 2006, Vial et al. 2011). The ability of CTGF to induce collagen synthesis in corneal fibroblasts points towards the assumption that CTGF is involved in ECM formation in the cornea (Blalock et al. 2003). For the optimal transparency of the cornea it is very important that the collagen fibers are correctly orientated because a variation in collagen structure will result in opacity of the cornea. Therefore, it can be supposed that CTGF is crucial for the initial formation of the collagen fibers, a process that is completed at the timepoint of the eyelid opening, which results in a cutoff of CTGF expression to prevent a keloid matrix production. The heterogenous CTGF promotor activity in the mature cornea was already shown in CTGFp-eGFP mice (Gibson et al. 2014). The key role of the corneal endothelium is to keep the balance of corneal stroma hydration by generation of fluid outflow by ion transporters. This finding indicates a role of CTGF in the normal tissue homeostasis.

A few transcription factors and signaling molecules have been identified to play an essential role in the morphogenesis of the anterior chamber angle. In humans, a heterozygous mutation in the Pax6 gene leads to aniridia, which is associated with iris hypoplasia, corneal opacification, cataract and foveal dysplasia (Glaser et al. 1992, Jordan et al. 1992, Ton et al. 1991). In case of aniridia, 50-70% of patients develop glaucoma due to an abnormal differentiation of the TM and/or absence of SC (Nelson et al. 1984). Baulmann et al., (2002) could show a similar phenotype in heterozygous Pax6 mice, exhibiting an undifferentiated TM and the absence of SC (Baulmann et al. 2002). Similar observations were made in TGF-β2 knockout mice, where the anterior chamber

is not present and in BMP-4 heterozygous knockout mice, which develop a small or absent SC and a hypoplastic or absent TM (Chang et al. 2001, Sanford et al. 1997). The similarities between these observations point to the fact that Pax6 signaling can be controlled by members of the TGF-β superfamily. In this study, we could show that CTGF is expressed in the TM during the entire developmental process and persists in the mature TM. CTGF can arrange interactions with both BMP-4 and TGF-β2, leading to an inhibition of the BMP signaling pathway and enhancement of TGF-β signaling, suggesting a role for CTGF to keep the homeostatic balance between these different signaling molecules (Abreu et al. 2002). Furthermore, CTGF has a protective effect on HTM cell viability after different stressors (Kuespert et al. 2015), indicating a crucial role of CTGF in TM morphogenesis. An important factor in the regulation of anterior chamber development is the synthesis and remodeling of unique ECM (Cvekl & Tamm 2004). In the TM, various ECM components like different types of collagen, elastic fiber components, proteoglycans and FN are found. The exact impact of ECM on TM development, including expression, differentiation and interaction with signaling molecules is still unclear, but the ability of CTGF to interact and induce various ECM components in HTM cells suggests a possible role of CTGF in formation and maintenance of the ECM in the TM (Junglas et al. 2009). The observation that BMP7 is essential for the development of the ciliary body (Zhao et al. 2002a) and the fact that mice with an extreme overexpression of CTGF do not develop a ciliary body (unpublished data), leads furthermore to the suggestion that CTGF is necessary to keep the homeostatic balance of different growth factors.

The initial analysis of the effect of CTGF deficiency on eye development revealed no obvious morphological changes in the development of anterior eye structures. Due to the problem that parallel analysis of the CTGF knockdown and the morphological investigations can not be performed, we successfully tested the knockdown in other organs, like the lung. Additionally, compensatory pathways, including other members of the CCN protein family may restore the function of CTGF, resulting in a normal development of the anterior eye segment. It is also important to mention that this mouse model is based on an inducible conditional knockout, which results in a knockdown of CTGF. However, we can not generate a complete knockout of CTGF. Therefore, it is possible that the remaining amount of CTGF is sufficient for normal anterior eye development. For further examination we will confirm the knockdown within this experimental approach and we will analyze the phenotype, using additional techniques, like electron microscopy. This will allow for a more detailed analysis, especially of the morphological structure of the TM. Thereby we will identify the role of CTGF in anterior eye segment morphogenesis and differentiation.

5.2.2. Involvement of CTGF in the development of posterior eye structures

In the posterior eye segment CTGF is expressed in the retina, choroidea, sclera and the ONH. In the sclera CTGF is expressed throughout the entire development and is maintained in the adult eye. The sclera has a dual origin, it differentiates from neural crest cells and a small temporal portion from the mesoderm (Johnston et al. 1979). This is similar to the differentiation of cartilage and bones. The sclera is constituted of fibrillar collagens, proteoglycans, small amounts of various glycoproteins and matrix secreting fibroblasts. The expression of CTGF was already detected in cartilage, bones and teeth (Friedrichsen et al. 2003, Ivkovic et al. 2003, Safadi et al. 2003, Shimo et al. 2002). CTGF plays an essential role in skeletogenesis, as CTGF knockout mice manifest multiple skeletal dysmorphisms, due to impaired growth plate chondrogenesis, angiogenesis and bone formation (Ivkovic et al. 2003). The similarities in origin of sclera and cartilage and the important role of CTGF in skeletogenesis suggest a role of CTGF in control of the development and maintenance of the sclera. Furthermore, interaction partners of CTGF, like TGF-β2 and BMP-2 enhance ECM production and expression of cartilage-associated genes in cultured scleral cells (Hu et al. 2008, Wu et al. 2015).

5.2.2.1. Involvement of CTGF in development of the retina

In the retina, CTGF is expressed in Müller cells, endothelial cells of the retinal vasculature and amacrine cells during development in a specific time dependent expression pattern. This expression pattern is maintained in the mature retina. The distinct expression at the defined place and time suggests a role of CTGF in the retinal development. BMP signaling pathways and Notch signaling pathways are known to play a crucial role in retinal development. Müller cell differentiation is promoted by both pathways and can control various processes during retinal development (Bao & Cepko 1997, Bernardos et al. 2005, Furukawa et al. 2000, Mateos et al. 2007). Blocking of BMP signaling results in impaired retinal organization and an extenuated Müller cell differentiation (Huillard et al. 2005). CTGF has the ability to bind members of the BMP family, leading to inhibition of the signaling (Abreu et al. 2002) and is related to Notch-1 inhibition (Smerdel-Ramoya et al. 2008) and can be the target of Notch signaling (Canalis et al. 2014). As neuronal differentiation is almost complete at the time point when the expression of CTGF starts at P10 (Rapaport et al. 2004), it can be suggested that CTGF is necessary for maintenance of Müller cell and amacrine cell function and differentiation state. Amacrine cells are inhibitory interneurons, and can be classified by their neurotransmitter, GABA or glycine (MacNeil et al. 1999, MacNeil & Masland 1998). The identified CTGF expressing amacrine cells are located in the INL as well as the GCL. This distribution pattern is typical for GABAergic amacrine cells (Haverkamp & Wässle 2000). This observation suggests that GABAergic amacrine cells express CTGF and

CTGF plays a role in their normal cell function, but the exact role of CTGF has to be identified. Müller cells are important players in the inflammatory response and they are implicated in various retinal disorders. However, they provide a variety of functions to support neurons and keep the retinal homeostasis in balance, like neurotransmitter recycling and supply of neurotransmitter precursors, regulation of retinal blood flow, extracellular space volume, ion and water homeostasis and maintenance of inner blood-retina barrier in the healthy retina (Bringmann et al. 2004, Bringmann et al. 2009, Choi & Kim 2008, Metea & Newman 2006, Tout et al. 1993).

Laminins, a major component of the retinal basements membranes (BM), are important for different retinal processes, like vascular development, retinal synapse formation, formation of ILM and Bruch's membrane and guidance of RGC axons (Byström et al. 2006, Li et al. 2012, Libby et al. 1997, Morissette & Carbonetto 1995, Stenzel et al. 2011).They are mainly produced by Müller cells in the mature retina (Libby et al. 2000). Additionally, FN is located in the ILM (Vecino et al. 2015). Since CTGF could be shown to induce FN and laminin in different cell types (Fuchshofer et al. 2005, Nagai et al. 2009, Neumann et al. 2008, Zode et al. 2011), it can be speculated that one function of CTGF expressed by Müller cells is to induce ECM components in the retina by an autocrine and/or paracrine mechanism.

The expression of CTGF in endothelial cells was already shown in different species (Bradham et al. 1991, Lin et al. 1998, Wunderlich et al. 2000). In the mouse retina angiogenesis occurs within the postnatal period of development. Multiple cellular processes like proliferation, migration and cell adhesion are involved in angiogenesis. CTGF can promote and enhance endothelial cell proliferation, migration and cell adhesion (Kireeva et al. 1997, Lin et al. 1998, Shimo et al. 2002). One critical player of retinal angiogenesis is VEGF (Campochiaro et al. 2016). CTGF can build a complex with VEGF, leading to an inhibition of VEGF induced angiogenesis (He et al. 2003, Inoki et al. 2002, Jang et al. 2004, Kuiper et al. 2007, Suzuma et al. 2000). Furthermore, blocking CTGF during retinal angiogenesis results in a reduced growth of the superficial plexus (Pi et al. 2011). Due to these observations it can be suggested that CTGF plays an essential role in retinal angiogenesis. The invasion of endothelial cells from the ON into the retina, forming the superficial plexus, is guided by astrocytes migrating from the optic nerve. In turn, endothelial cells provide molecular factors, like leukemia inhibitory factor (LIF), promoting astrocyte differentiation and maturation (Bonni et al. 1997, Galli et al. 2000, Koblar et al. 1998, Mi & Barres 1999, Nakagaito et al. 1995, Richards et al. 1996, Yoshida et al. 1993). In this study we could show that a conditional CTGF knockdown leads to an altered astrocyte network in the retina. Astrocytes in CTGF deficient retinae

have enlarged cell somata, thickened processes and blood vessels are not ensheathed by fine astrocyte processes. Cells from the astrocytic lineage migrate as a mixture of astrocyte precursor cells and immature perinatal astrocytes from the ONH into the retina. The implication of CTGF in astrocyte differentiation was already shown, as CTGF can increase the number of GFAP-positive cells after treatment of neural progenitor cells (Mendes et al. 2015).

5.2.2.2. Involvement of CTGF in the development of the ONH

In the ON, the first expression of CTGF was detected at P5, following an increased expression in the glial lamina throughout development. This distinct expression pattern is maintained in the adult ON. We could identify optic nerve astrocytes as the major source of CTGF expression in mouse ON during development and in the mature eye. Abnormal differentiation of astrocytes leads to pathologies like coloboma and optic nerve dysplasia (Friedlander 2007). Additionally, ON astrocytes are essential for retinal angiogenesis (Gariano 2003). In the ON, type 1 astrocytes derive from neuroepithelial astrocyte progenitor cells in the embryonic optic stalk. In contrast, type 2 astrocytes and oligodendrocytes derive from ventricular zone neuroepithelial cells in the postnatal optic stalk (Ffrench-Constant et al. 1988, Mi et al. 2001, Mi & Barres 1999, Small et al. 1987). As CTGF is not expressed in the ON during embryogenesis, a role of CTGF in type 1 astrocyte differentiation can be excluded. As the implication of CTGF in astrocyte differentiation was already shown (Mendes et al. 2015), it can be suggested that CTGF contributes to the differentiation of type 2 astrocytes. The glial lamina of the murine ONH constitutes of transversely dense packed GFAP positive astrocytes. The characteristic property of the astrocytes within the glial lamina is established between P7 and P14 (Ding et al. 2002). This special constitution, in comparison to the random orientation in the posterior ON is thought to be due to a combination of mechanical and functional factors (Tehrani et al. 2014). The physiological IOP applies a mechanical force on the cells in the ONH, in comparison to the posterior part of the ON where the force is dramatically reduced. In cell culture it was shown that cells re-orientate their actin bundles in the direction of the force (Heidemann et al. 1999, Kaunas et al. 2005, Neidlinger-Wilke et al. 2001), CTGF is upregulated in response to mechanical stress and in cultured murine ON astrocytes CTGF can induce cytoskeletal proteins like α-actinin (Dillinger et al., in prep). In this study we could observe that in CTGF deficient mice this characteristic arrangement of astrocytes in the glial lamina is missing. Interestingly, the myelination of the optic nerve does not differ in CTGF deficient mice, although it is known

that the glial lamina functions as a barrier for oligodendrocyte migration during development.

5.3. Astrocyte reactivity in the ONH of a murine glaucoma model

In POAG, the changes in ECM observed in the LC correlate with increased reactivity of astrocytes in the ONH (Hernandez & Pena 1997, Kerr et al. 2011). These changes, including abnormal elastin deposition, increased levels and remodeling of collagen type IV and thickening of connective tissue sheathes around capillaries in the prelaminar region might occur due to a disruption of the homeostatic balance of growth factors and signaling molecules in the ONH (Fuchshofer 2011, Hernandez 1992, Hernandez et al. 1994, Pena et al. 1998, Pena et al. 2001, Tektas et al. 2010). One of these growth factors is TGFβ2, which is elevated in the AH and the ONH of glaucoma patients (Inatani et al. 2001, Min et al. 2006, Ochiai & Ochiai 2002, Ozcan et al. 2004, Pena et al. 1999, Picht et al. 2001, Tripathi et al. 1994, Trivedi et al. 2011, Yamamoto et al. 2005a, Zode et al. 2011). The increase of TGF-β2 is co-localized to reactive astrocytes in the ONH and TGF-β2 can induce the synthesis of ECM components in human ONH astrocytes. These findings lead to the assumption that reactive astrocytes are the major source of the enhanced TGF-β2 levels (Fuchshofer et al. 2005, Neumann et al. 2008, Pena et al. 2001, Zode et al. 2011). The fibrotic effect of TGF-β2 is dependent on its downstream mediator CTGF, as the silencing of CTGF inhibited the ECM increase following TGF-β2 treatment (Fuchshofer et al. 2005). Both growth factors can induce ECM expression in murine ON astrocytes (Dillinger et al., in prep). Furthermore, they can enhance migration rates and GFAP synthesis in murine ON astrocytes (Dillinger et al., in prep). These findings show the capacity of CTGF to induce a reactive phenotype in murine ON astrocytes. In this study we found an increase of CTGF in the ONH of our murine glaucoma model at the age of 2 months. At this age, the mice suffer from a significantly elevated IOP and progressive loss of axons (Junglas et al. 2012). In contrast, the analysis of the ON did not reveal any changes in the expression of CTGF. Furthermore, 1-month-old animals showed no differences in CTGF expression compared to their WT littermates. These findings lead to the assumption that long-lasting elevated IOP and the altered biomechanical properties of the peripapillary sclera can induce CTGF expression and synthesis. The possibility that the CTGF increase might be due to diffusion of transgenically overexpressed CTGF from the lens causing an autoregulatory mechanism can be excluded due to the observation that 1-month-old TG animals did not show an increase in CTGF levels in the ONH. The increased CTGF expression was associated with a reactive phenotype of ONH astrocytes, indicated by an increase in GFAP expression, thickening of astrocytes processes and reduced open spaces within the glial lamina. These changes in the astrocytic phenotype was not observed in the 1-month-old

animals. As the 1-month old animals already show an increased IOP and a loss of axons (Junglas et al. 2012), it can be argued that the gliosis reaction is not the cause for the axon loss in this mouse model. BMP signaling plays a crucial role in RGC axon development and outgrowth. BMPrIb deficient mice show an impaired axonal pathfinding and different BMPs have the ability to increase the number of outgrowing neurons in culture (Kerrison et al. 2005, Liu et al. 2004). As CTGF can inhibit BMP signaling by binding different members of the BMP family (Abreu et al. 2002), it is possible that the initial number of RGC axons is decreased in the TG animals compared to WT littermates. In a recent study it was shown that inhibition of the STAT3 pathway and thereby prevention of astrocyte gliosis reaction in an ocular hypertension model results in an increase in RGC death and visual function loss (Sun et al. 2017). It can be carefully stated that the astrocyte reactivity is beneficial for RGC axons, but involvement of STAT3 in other pathway independent from astrocyte reactivity has to be kept in mind and will be part of future investigations (Sun et al. 2017).

5.3.1. Mechanosensing of murine ON astrocytes

IOP causes changes in biomechanical properties of the peripapillary sclera, indicated by the fact that an experimentally elevated IOP leads to an increased scleral stiffness, which is similar to the observations in glaucomatous human eyes (Downs et al. 2005, Nguyen et al. 2013). Astrocytes building the glial lamina in the murine ONH, are in direct contact with the peripapillary sclera via their processes (Sun et al. 2009). Therefore, it can be assumed that ONH astrocytes are capable to directly transfer scleral wall tension to the passing ON axons (Quigley & Cone 2013). The findings of this study clearly indicate that ON astrocytes can sense changes in stiffness of their surrounding ECM and react to increasing stiffness with enhanced synthesis of GFAP, vimentin and CTGF synthesis.

Several molecules can act as regulatory candidates of mechanosensation and -transduction. Caveolin1 can act as a mechanosensor, despite its function as a main component of caveolae (Kurzchalia et al. 1992, Rothberg et al. 1992). Caveolae are small pits, 60-80 nm in diameter, representing a specialized type of microdomain in the plasma membrane (Palade 1953). Biological functions of caveolae include endocytosis, cholesterol and lipid metabolism, mechanosensation and cellular signaling (Parton & Simons 2007, van Deurs et al. 2003). Caveolin1 is synthesized in the endoplasmic reticulum (ER), forms an integral membrane protein, travels to the Golgi complex and is finally transported by exocytotic caveolar carries to the plasma membrane (Monier et al. 1995, Parton & Simons 2007, Pol et al. 2005, Tagawa et al. 2005). As the main component of caveolae, Caveolin is necessary for their induction and formation (Drab et al. 2001, Fra et al. 1995, Razani et al. 2001). Several studies could demonstrate the

implication of Caveolin1 in mechanosensing in various cell types. For instance, exposure of endothelial cells to chronic shear stress invokes the ERK pathway in a caveolae-dependent manner (Boyd et al. 2003, Park et al. 2000, Rizzo et al. 2003). In smooth-muscle cells, cyclic stretch can mediate the activation of Akt signaling, dependent on Caveolin1. Additionally, Caveolin1 is essential for cell cycle progression under cyclic stretch (Sedding et al. 2005). Caveolae provide a mechanism to extenuate an increase in membrane tension applied by acute mechanical stress by caveolae flattening (Sinha et al. 2011). Shear and cyclic stress increase the release of Nitric oxide (NO), a potent vasodilator and enhance endothelial nitric oxide synthase (eNOS) mRNA and protein (Harrison et al. 1996). eNOS hyperactivity is observed in Cav1 deficient mice and caveolae are shown to be essential for shear stress induced eNOS activation in vascular endothelium (Drab et al. 2001, Yu et al. 2006, Zhao et al. 2002b). However, the direct function of caveolae and Caveolin1 in mechanosensation and the underlying mechanisms implicated in cell response to mechanical stress occurring in astrocytes remain unknown. In addition to the function in mechanosensing, Caveolin1 has already been shown to be involved in the pathogenesis of POAG. A polymorphism in the Caveolin1/Caveolin2 gene was associated by genome wide association studies with both POAG and IOP (Chen et al. 2014, Huang et al. 2014, Hysi et al. 2014, Kim et al. 2015, Loomis et al. 2014, Ozel et al. 2014, Thorleifsson et al. 2010, van Koolwijk et al. 2012, Wiggs et al. 2011). Recently, a study investigated that Caveolin1 deficiency results in IOP elevation, reduced AH drainage and increased sensitivity of Caveolin1-deficient outflow pathway cells to rupture from acute IOP elevation (Elliott et al. 2016). This finding is in line with two other studies showing that in caveolae-deficient mice the outflow facility is reduced (Kizhatil et al. 2016, Lei et al. 2016). In contrast, a transient knockout of Caveolin1 in TM cells leads to an increase in outflow rates in anterior eye segments (Aga et al. 2014). In this study, it could be shown that both Caveolin1 and Caveolin2 expression are enhanced related to increasing substratum stiffness. This finding is in line with studies in other cell types showing the induction and implication of Caveolin1 in response to mechanical stress. Furthermore, we could show that Caveolin1 is increased in the ONH in our murine glaucoma model *in vivo* and after treatment with TGF-β2 and CTGF in murine ON astrocytes *in vitro*. Caveolin1 expression is enhanced in the ONH, but not in the ON of 2-month-old animals. Therefore, it can be assumed that changes of Caveolin1 expression in the ONH of the murine glaucoma model is a key effect to generate caveolae flattening to extenuate the increase in membrane tension. A second group of proteins known to be implicated in mechanosensation are the transient receptor potential (TRP) channels. TRP channels are non-selective cation channels permeable for Ca^{2+}, subdivided into 28 TRP channel subtypes (Nilius & Owsianik 2011). A couple

of these molecules have been implicated in mechanosensation (Arnadóttir & Chalfie 2010, Birder et al. 2002, Christensen & Corey 2007, Davis & Hill 1999). Different subtypes of TRP channels are expressed in the retina and ONH, especially in astrocytes. A direct role of TRP channels in different aspects of the pathogenesis of glaucoma was assigned (Choi et al. 2015, Gilliam & Wensel 2011, Ho et al. 2014, Križaj et al. 2014, Leonelli et al. 2009, Morgans et al. 2009, Ryskamp et al. 2011, Ryskamp et al. 2014, Sappington et al. 2009, Sappington & Calkins 2008, Shen et al. 2009, Verkhratsky et al. 2014, Ward et al. 2014, Weitlauf et al. 2014). Various subtypes of TRP channels were detected in the murine ONH, but only a few of them in mouse ON astrocytes. Choi et al., (2015) could identify an expression of Trpc1, Trpc2, Trpv2, Trpm7, Trpp1 and Trpp2. (Choi et al. 2015). Interestingly Trpc1, Trpv2, Trpm7 and Trpp2 are the most abundant isoforms within each group in the ONH. These findings are in line with our results. We could detect an expression of Trpc1, Trpv2 and Trpm7 in murine ON astrocytes *in vitro*. The expression of all detected channels was reduced by increasing substratum stiffness.

Another class of mechanosensitive cation channels are represented by the Piezo channels. Both members, Piezo1 and Piezo2, are expressed in ONH astrocytes and are a substantial constituent of distinct stretch-activated channels (Choi et al. 2015, Coste et al. 2010). Interestingly, Piezo2 is regulated in the glaucoma-prone DBA/2J mouse strain, showing an increased expression in the progression of glaucoma, in contrast a mild elevation in IOP has no influence on Piezo2 expression (Choi et al. 2015). In our study, we could show that Piezo2 expression is downregulated in response to increasing stiffness. The involvement of Piezo channels in cell morphology, adhesion and migration, is an interesting point of linking this function to morphological changes in ON astrocytes in the pathogenesis of glaucoma (McHugh et al. 2010, McHugh et al. 2012, Ranade et al. 2014, Sun et al. 2013, Volkers et al. 2015, Yang et al. 2014). However, the direct role of these mechanosensitive channel in astrocyte reactivity has to be elucidated in future investigations using specific channel blocking agents *in vitro* and knockout mouse models *in vivo*.

5.4. Intracameral delivery of layer-by-layer coated siRNA nanoparticles

Multiple, randomized clinical studies demonstrated that lowering IOP reduces the progression of POAG, which clearly reveals that IOP is a major risk factor for POAG (1998, 2000). Therefore, reducing IOP is the central point of action to prevent the progression of POAG. Current glaucoma treatments include, application of eye drops, laser procedures and surgery. The main medications involve prostaglandin analogs and beta blocker. The target of all glaucoma treatment strategies is reducing the amount of

AH produced by the ciliary body or increasing AH drainage. All these strategies have in common that they do not affect the primary cause of elevated IOP. Additionally, current glaucoma medications exhibit various disadvantages, like short duration of action, thus requiring frequent administration, systemic side effects, inadequate application by patients and usually low compliance by patients, resulting in an ineffective treatment. Application of naked siRNA frequently used as gene therapy offer drawbacks, like rapid degradation and inefficiency in crossing cellular membranes (Kanasty et al. 2013, Thakur et al. 2012). Hence, we pursued the strategy to use NP as carrier for siRNA delivery to the outflow pathway tissue of the eye to enhance stability and intracellular availability. Various types of NP were already used for drug delivery (Janagam et al. 2017).

CD44 is the principle receptor of hyaluron and is involved in its uptake and degradation (Culty et al. 1992, Entwistle et al. 1996, Sherman et al. 1996). CD44 appearance was already demonstrated in tissues of the anterior chamber, like ciliary body stroma, anterior iris, ciliary body muscle, iris root and TM (Knepper et al. 1998). In this study we could confirm these findings. We could show a CD44 expression in HTM cells and in the anterior chamber angle of mice and human donor eyes. CD44 as a POAG related target was identified, as we could observe an increased expression in glaucomatous SC cells and enhanced synthesis in the TM and SC endothelium in human donor eyes of POAG patients. In this study HA-coated NPs were successfully designed and delivered via anterior chamber perfusion in the outflow pathway tissue of human and porcine eyes. We could report that these HA-coated NPs enter the entire TM and finally reach the endothelial lining of SC, in comparison to PEI-coated NPs, which build big agglomerates, resulting in immobilization in the tissue and therefore do not enter the tissue of outflow pathway. Interestingly, we could report a cellular uptake of HA-coated NPs via CD44 receptors. These findings indicate that HA-coated NPs can pass through the TM without hindrance and overcome barriers in the TM. Finally, we could demonstrate that transfection of HTM cells with siRNA coated HA-NPs led successfully to a reduction in CTGF expression. These findings show that HA-coated NPs are the best choice, as they successfully internalized by HTM cells *in vitro* and show an intracellular uptake in perfused eyes. Furthermore, we could observe the increase in CD44 in glaucomatous tissue specific in the target region, the TM and SC. Therefore, HA coated NPs will have a high specificity to the target region in POAG.

Overall, siRNA delivery to the AH outflow pathway tissue and cells based on HA-coated NPs could have a great potential in treatment of POAG.

5.5. Outlook

In the CTGF deficient mice, the exact role of CTGF during eye development and maintenance of different eye structures has to be investigated in detail. Electron microscopy will allow for a more detailed analysis, especially of the morphological structure of the TM. Compensatory mechanisms like upregulation of other members of the CCN protein family to restore CTGF function will be investigated. The morphological alterations in the astrocyte network, observed in the conditional CTGF knockdown animals, will be investigated regarding cell specificity, using different cell type specific conditional knockout mouse model, like endothelial cell, Müller cell and astrocyte specific mouse models, currently being bred. To investigate, if morphological changes in retinal astrocytes are due to impaired differentiation, specific markers for immature astrocytes, like Pax2 will be analyzed.

Concerning a new therapeutic strategy for prevention of POAG progression by reducing CTGF, we will investigate the effect of CTGF deficiency on the maintenance of different ocular structures in adult conditional CTGF knockout mice.

As astrocyte reactivity was shown to be associated with increased CTGF synthesis *in vitro* and *in vivo*, we will investigate the impact of CTGF on astrocyte reactivity related to increasing substratum stiffness. To this end, murine ON astrocytes are already isolated from the $CTGF^{Coin/Coin}$ mice and infected with an Ad-5 virus, expressing a Cre-recombinase will be used to achieve a CTGF knockout *in vitro*. To evaluate the possibility of CTGF contributing to astrocyte reactivity in the ONH of the murine glaucoma model, the βB1-CTGF1 and $CTGF^{Coin/Coin}$;CAGGCre-ER mice were crossbred, to receive a conditional knockout of endogenous CTGF in the CTGF-overexpressing glaucoma mouse model. The mechanosensation of TRP-channels and Caveolins will be further investigated by blocking of channels and/or downregulation via siRNA. Additionally, the Ca^{2+} signaling in murine ON astrocytes cultured on increasing substratum stiffness will be analyzed. For evaluation of the implication of Caveolin1 in the pathological changes in ONH during the progression of POAG, we will analyze the glial lamina of Caveolin1 deficient mice, regarding astrocyte reactivity and CTGF level.

As NPs were successfully delivered to cells of the AH outflow pathway and siRNA coated NPs lead to a significant downregulation of CTGF synthesis in HTM cells *in vitro*, we will start to test the delivery in our glaucoma mouse model. We will analyze the distribution of NPs in the mouse eye and the knockdown of CTGF by siRNA. Thus, we will be able

to investigate the effect of CTGF downregulation in the TM and SC concerning a reduction of the IOP in the glaucoma mouse model.

6. Conclusion

In this study, we report that CTGF is expressed in various ocular tissue during development and in the adult eye. First analyses point towards the assumption that CTGF plays a role in establishment of specific astrocyte structures in the retina and ONH.

In the pathology of POAG we can state that increased CTGF levels in the ONH are associated with astrocyte reactivity related to mechanical stress *in vivo* and increasing substratum stiffness *in vitro*. Furthermore, our study shows the implication of TRP channels, Piezo channels and Caveolin1 in the mechanosensation of murine ON astrocytes.

Finally, with the layer-by-layer coated NP we develop a new tool to deliver siRNA to the target tissue in the AH outflow pathway of the eye. These NP provide a new treatment strategy to reduce IOP and thereby treat or prevent the progression of POAG.

7. References

Abreu, J. G., Ketpura, N. I., Reversade, B. & Robertis, E. M. de (2002). Connective-tissue growth factor (CTGF) modulates cell signalling by BMP and TGF-beta. *Nature cell biology* **4**, 599–604. doi:10.1038/ncb826.

Acott, T. S. & Kelley, M. J. (2008). Extracellular matrix in the trabecular meshwork. *Experimental eye research* **86**, 543–561. doi:10.1016/j.exer.2008.01.013.

Adams, J. C. & Watt, F. M. (1993). Regulation of development and differentiation by the extracellular matrix. *Development (Cambridge, England)* **117**, 1183–1198.

Adelmann HB (1929). Experimental studies on the development of the eye. I. The effect of removal of median and lateral areas of the anterior end of the urodelan neural plate on the development of the eyes. *J Exp Zool*, 249–317.

Aga, M., Bradley, J. M., Wanchu, R., Yang, Y.-f., Acott, T. S. & Keller, K. E. (2014). Differential effects of caveolin-1 and -2 knockdown on aqueous outflow and altered extracellular matrix turnover in caveolin-silenced trabecular meshwork cells. *Investigative ophthalmology & visual science* **55**, 5497–5509. doi:10.1167/iovs.14-14519.

Arnadóttir, J. & Chalfie, M. (2010). Eukaryotic mechanosensitive channels. *Annual review of biophysics* **39**, 111–137. doi:10.1146/annurev.biophys.37.032807.125836.

Ashery-Padan, R. & Gruss, P. (2001). Pax6 lights-up the way for eye development. *Current opinion in cell biology* **13**, 706–714.

Babic, A. M., Chen, C. C. & Lau, L. F. (1999). Fisp12/mouse connective tissue growth factor mediates endothelial cell adhesion and migration through integrin alphavbeta3, promotes endothelial cell survival, and induces angiogenesis in vivo. *Molecular and cellular biology* **19**, 2958–2966.

Bao, Z. Z. & Cepko, C. L. (1997). The expression and function of Notch pathway genes in the developing rat eye. *The Journal of neuroscience the official journal of the Society for Neuroscience* **17**, 1425–1434.

Baulmann, D. C., Ohlmann, A., Flügel-Koch, C., Goswami, S., Cvekl, A. & Tamm, E. R. (2002). Pax6 heterozygous eyes show defects in chamber angle differentiation that are associated with a wide spectrum of other anterior eye segment abnormalities. *Mechanisms of development* **118**, 3–17.

Bellezza, A. J., Hart, R. T. & Burgoyne, C. F. (2000). The optic nerve head as a biomechanical structure: Initial finite element modeling. *Investigative ophthalmology & visual science* **41**, 2991–3000.

Bernardos, R. L., Lentz, S. I., Wolfe, M. S. & Raymond, P. A. (2005). Notch-Delta signaling is required for spatial patterning and Müller glia differentiation in the

zebrafish retina. *Developmental biology* **278**, 381–395. doi:10.1016/j.ydbio.2004.11.018.

Birder, L. A., Nakamura, Y., Kiss, S., Nealen, M. L., Barrick, S., Kanai, A. J., Wang, E., Ruiz, G., Groat, W. C. de, Apodaca, G., Watkins, S. & Caterina, M. J. (2002). Altered urinary bladder function in mice lacking the vanilloid receptor TRPV1. *Nature neuroscience* **5**, 856–860. doi:10.1038/nn902.

Birk, D. E., Fitch, J. M. & Linsenmayer, T. F. (1986). Organization of collagen types I and V in the embryonic chicken cornea. *Investigative ophthalmology & visual science* **27**, 1470–1477.

Blalock, T. D., Duncan, M. R., Varela, J. C., Goldstein, M. H., Tuli, S. S., Grotendorst, G. R. & Schultz, G. S. (2003). Connective tissue growth factor expression and action in human corneal fibroblast cultures and rat corneas after photorefractive keratectomy. *Investigative ophthalmology & visual science* **44**, 1879–1887.

Boland, M. V. & Quigley, H. A. (2007). Risk factors and open-angle glaucoma: Classification and application. *Journal of glaucoma* **16**, 406–418. doi:10.1097/IJG.0b013e31806540a1.

Bonni, A., Sun, Y., Nadal-Vicens, M., Bhatt, A., Frank, D. A., Rozovsky, I., Stahl, N., Yancopoulos, G. D. & Greenberg, M. E. (1997). Regulation of gliogenesis in the central nervous system by the JAK-STAT signaling pathway. *Science (New York, N.Y.)* **278**, 477–483.

Borcherding, M. S., Blacik, L. J., Sittig, R. A., Bizzell, J. W., Breen, M. & Weinstein, H. G. (1975). Proteoglycans and collagen fibre organization in human corneoscleral tissue. *Experimental eye research* **21**, 59–70.

Bork, P. (1993). The modular architecture of a new family of growth regulators related to connective tissue growth factor. *FEBS letters* **327**, 125–130.

Bornstein, P. (2001). Thrombospondins as matricellular modulators of cell function. *The Journal of clinical investigation* **107**, 929–934. doi:10.1172/JCI12749.

Boyd, N. L., Park, H., Yi, H., Boo, Y. C., Sorescu, G. P., Sykes, M. & Jo, H. (2003). Chronic shear induces caveolae formation and alters ERK and Akt responses in endothelial cells. *American journal of physiology. Heart and circulatory physiology* **285**, H1113-22. doi:10.1152/ajpheart.00302.2003.

Braakman, S. T., Read, A. T., Chan, D. W.-H., Ethier, C. R. & Overby, D. R. (2015). Colocalization of outflow segmentation and pores along the inner wall of Schlemm's canal. *Experimental eye research* **130**, 87–96. doi:10.1016/j.exer.2014.11.008.

Bradham, D. M., Igarashi, A., Potter, R. L. & Grotendorst, G. R. (1991). Connective tissue growth factor: A cysteine-rich mitogen secreted by human vascular endothelial cells

is related to the SRC-induced immediate early gene product CEF-10. *The Journal of cell biology* **114**, 1285–1294.

Brigstock, D. R. (2003). The CCN family: A new stimulus package. *The Journal of endocrinology* **178**, 169–175.

Bringmann, A., Pannicke, T., Biedermann, B., Francke, M., Iandiev, I., Grosche, J., Wiedemann, P., Albrecht, J. & Reichenbach, A. (2009). Role of retinal glial cells in neurotransmitter uptake and metabolism. *Neurochemistry international* **54**, 143–160. doi:10.1016/j.neuint.2008.10.014.

Bringmann, A., Reichenbach, A. & Wiedemann, P. (2004). Pathomechanisms of cystoid macular edema. *Ophthalmic research* **36**, 241–249. doi:10.1159/000081203.

Browne, J. G., Ho, S. L., Kane, R., Oliver, N., Clark, A. F., O'Brien, C. J. & Crean, J. K. (2011). Connective tissue growth factor is increased in pseudoexfoliation glaucoma. *Investigative ophthalmology & visual science* **52**, 3660–3666. doi:10.1167/iovs.10-5209.

Byström, B., Virtanen, I., Rousselle, P., Gullberg, D. & Pedrosa-Domellöf, F. (2006). Distribution of laminins in the developing human eye. *Investigative ophthalmology & visual science* **47**, 777–785. doi:10.1167/iovs.05-0367.

Campochiaro, P. A., Aiello, L. P. & Rosenfeld, P. J. (2016). Anti-Vascular Endothelial Growth Factor Agents in the Treatment of Retinal Disease: From Bench to Bedside. *Ophthalmology* **123**, S78-S88. doi:10.1016/j.ophtha.2016.04.056.

Canalis, E., Zanotti, S., Beamer, W. G., Economides, A. N. & Smerdel-Ramoya, A. (2010). Connective tissue growth factor is required for skeletal development and postnatal skeletal homeostasis in male mice. *Endocrinology* **151**, 3490–3501. doi:10.1210/en.2010-0145.

Canalis, E., Zanotti, S. & Smerdel-Ramoya, A. (2014). Connective tissue growth factor is a target of notch signaling in cells of the osteoblastic lineage. *Bone* **64**, 273–280. doi:10.1016/j.bone.2014.04.028.

Chakravarti, S., Magnuson, T., Lass, J. H., Jepsen, K. J., LaMantia, C. & Carroll, H. (1998). Lumican regulates collagen fibril assembly: Skin fragility and corneal opacity in the absence of lumican. *The Journal of cell biology* **141**, 1277–1286.

Chakravarti, S., Petroll, W. M., Hassell, J. R., Jester, J. V., Lass, J. H., Paul, J. & Birk, D. E. (2000). Corneal opacity in lumican-null mice: Defects in collagen fibril structure and packing in the posterior stroma. *Investigative ophthalmology & visual science* **41**, 3365–3373.

Chang, B., Smith, R. S., Peters, M., Savinova, O. V., Hawes, N. L., Zabaleta, A., Nusinowitz, S., Martin, J. E., Davisson, M. L., Cepko, C. L., Hogan, B. L. & John, S.

W. (2001). Haploinsufficient Bmp4 ocular phenotypes include anterior segment dysgenesis with elevated intraocular pressure. *BMC genetics* **2**, 18.

Chen, C.-C. & Lau, L. F. (2010). Deadly liaisons: Fatal attraction between CCN matricellular proteins and the tumor necrosis factor family of cytokines. *Journal of cell communication and signaling* **4**, 63–69. doi:10.1007/s12079-009-0080-4.

Chen, F., Klein, A. P., Klein, B. E. K., Lee, K. E., Truitt, B., Klein, R., Iyengar, S. K. & Duggal, P. (2014). Exome array analysis identifies CAV1/CAV2 as a susceptibility locus for intraocular pressure. *Investigative ophthalmology & visual science* **56**, 544–551. doi:10.1167/iovs.14-15204.

Choi, H. J., Sun, D. & Jakobs, T. C. (2015). Astrocytes in the optic nerve head express putative mechanosensitive channels. *Molecular vision* **21**, 749–766.

Choi, Y. K. & Kim, K.-W. (2008). Blood-neural barrier: Its diversity and coordinated cell-to-cell communication. *BMB reports* **41**, 345–352.

Chomczynski, P. & Sacchi, N. (1987). Single-step method of RNA isolation by acid guanidinium thiocyanate-phenol-chloroform extraction. *Analytical biochemistry* **162**, 156–159. doi:10.1006/abio.1987.9999.

Chow, R. L. & Lang, R. A. (2001). Early eye development in vertebrates. *Annual review of cell and developmental biology* **17**, 255–296. doi:10.1146/annurev.cellbio.17.1.255.

Christensen, A. P. & Corey, D. P. (2007). TRP channels in mechanosensation: Direct or indirect activation? *Nature reviews. Neuroscience* **8**, 510–521. doi:10.1038/nrn2149.

Cicha, I., Yilmaz, A., Klein, M., Raithel, D., Brigstock, D. R., Daniel, W. G., Goppelt-Struebe, M. & Garlichs, C. D. (2005). Connective tissue growth factor is overexpressed in complicated atherosclerotic plaques and induces mononuclear cell chemotaxis in vitro. *Arteriosclerosis, thrombosis, and vascular biology* **25**, 1008–1013. doi:10.1161/01.ATV.0000162173.27682.7b.

Collinson, J. M., Quinn, J. C., Buchanan, M. A., Kaufman, M. H., Wedden, S. E., West, J. D. & Hill, R. E. (2001). Primary defects in the lens underlie complex anterior segment abnormalities of the Pax6 heterozygous eye. *Proceedings of the National Academy of Sciences of the United States of America* **98**, 9688–9693. doi:10.1073/pnas.161144098.

(1998). Comparison of glaucomatous progression between untreated patients with normal-tension glaucoma and patients with therapeutically reduced intraocular pressures. Collaborative Normal-Tension Glaucoma Study Group. *American journal of ophthalmology* **126**, 487–497.

Congdon, N. G., Broman, A. T., Bandeen-Roche, K., Grover, D. & Quigley, H. A. (2006). Central corneal thickness and corneal hysteresis associated with glaucoma damage. *American journal of ophthalmology* **141**, 868–875. doi:10.1016/j.ajo.2005.12.007.

Coste, B., Mathur, J., Schmidt, M., Earley, T. J., Ranade, S., Petrus, M. J., Dubin, A. E. & Patapoutian, A. (2010). Piezo1 and Piezo2 are essential components of distinct mechanically activated cation channels. *Science (New York, N.Y.)* **330**, 55–60. doi:10.1126/science.1193270.

Coudrillier, B., Boote, C., Quigley, H. A. & Nguyen, T. D. (2013). Scleral anisotropy and its effects on the mechanical response of the optic nerve head. *Biomechanics and modeling in mechanobiology* **12**, 941–963. doi:10.1007/s10237-012-0455-y.

Coudrillier, B., Tian, J., Alexander, S., Myers, K. M., Quigley, H. A. & Nguyen, T. D. (2012). Biomechanics of the human posterior sclera: Age- and glaucoma-related changes measured using inflation testing. *Investigative ophthalmology & visual science* **53**, 1714–1728. doi:10.1167/iovs.11-8009.

Crawford, L. A., Guney, M. A., Oh, Y. A., Deyoung, R. A., Valenzuela, D. M., Murphy, A. J., Yancopoulos, G. D., Lyons, K. M., Brigstock, D. R., Economides, A. & Gannon, M. (2009). Connective tissue growth factor (CTGF) inactivation leads to defects in islet cell lineage allocation and beta-cell proliferation during embryogenesis. *Molecular endocrinology (Baltimore, Md.)* **23**, 324–336. doi:10.1210/me.2008-0045.

Crawley, L., Zamir, S. M., Cordeiro, M. F. & Guo, L. (2012). Clinical options for the reduction of elevated intraocular pressure. *Ophthalmology and eye diseases* **4**, 43–64. doi:10.4137/OED.S4909.

Culty, M., Nguyen, H. A. & Underhill, C. B. (1992). The hyaluronan receptor (CD44) participates in the uptake and degradation of hyaluronan. *The Journal of cell biology* **116**, 1055–1062.

Cvekl, A. & Duncan, M. K. (2007). Genetic and epigenetic mechanisms of gene regulation during lens development. *Progress in retinal and eye research* **26**, 555–597. doi:10.1016/j.preteyeres.2007.07.002.

Cvekl, A. & Tamm, E. R. (2004). Anterior eye development and ocular mesenchyme: New insights from mouse models and human diseases. *BioEssays news and reviews in molecular, cellular and developmental biology* **26**, 374–386. doi:10.1002/bies.20009.

Danielson, K. G., Baribault, H., Holmes, D. F., Graham, H., Kadler, K. E. & Iozzo, R. V. (1997). Targeted disruption of decorin leads to abnormal collagen fibril morphology and skin fragility. *The Journal of cell biology* **136**, 729–743.

Davis, M. J. & Hill, M. A. (1999). Signaling mechanisms underlying the vascular myogenic response. *Physiological reviews* **79**, 387–423. doi:10.1152/physrev.1999.79.2.387.

Di Mola, F. F., Di Sebastiano, P., Gardini, A., Innocenti, P., Zimmermann, A., Büchler, M. W. & Friess, H. (2004). Differential expression of connective tissue growth factor in inflammatory bowel disease. *Digestion* **69**, 245–253. doi:10.1159/000079845.

Dietrich, A., Mederos Y Schnitzler, M., Gollasch, M., Gross, V., Storch, U., Dubrovska, G., Obst, M., Yildirim, E., Salanova, B., Kalwa, H., Essin, K., Pinkenburg, O., Luft, F. C., Gudermann, T. & Birnbaumer, L. (2005). Increased vascular smooth muscle contractility in TRPC6-/- mice. *Molecular and cellular biology* **25**, 6980–6989. doi:10.1128/MCB.25.16.6980-6989.2005.

Dillinger, A.E.; Mayer M.; Schneider M.; Weber G.R.; Goeppner C.; Tamm E.R.; Shamonin M.; Monkman G.J.; Fuchshofer R. (in prep.). Increased extracellular matrix stiffness changes the biological properties of murine optic nerve astrocytes towards a glaucomatous phenotype.

Ding, L., Yamada, K., Takayama, C. & Inoue, Y. (2002). Development of astrocytes in the lamina cribrosa sclerae of the mouse optic nerve, with special reference to myelin formation. *Okajimas folia anatomica Japonica* **79**, 143–157.

Dockrell, M. E. C., Phanish, M. K. & Hendry, B. M. (2009). Tgf-beta auto-induction and connective tissue growth factor expression in human renal tubule epithelial cells requires N-ras. *Nephron. Experimental nephrology* **112**, e71-9. doi:10.1159/000221834.

Downs, J. C., Roberts, M. D. & Burgoyne, C. F. (2008). Mechanical environment of the optic nerve head in glaucoma. *Optometry and vision science official publication of the American Academy of Optometry* **85**, 425–435. doi:10.1097/OPX.0b013e31817841cb.

Downs, J. C., Suh, J.-K. F., Thomas, K. A., Bellezza, A. J., Hart, R. T. & Burgoyne, C. F. (2005). Viscoelastic material properties of the peripapillary sclera in normal and early-glaucoma monkey eyes. *Investigative ophthalmology & visual science* **46**, 540–546. doi:10.1167/iovs.04-0114.

Drab, M., Verkade, P., Elger, M., Kasper, M., Lohn, M., Lauterbach, B., Menne, J., Lindschau, C., Mende, F., Luft, F. C., Schedl, A., Haller, H. & Kurzchalia, T. V. (2001). Loss of caveolae, vascular dysfunction, and pulmonary defects in caveolin-1 gene-disrupted mice. *Science (New York, N.Y.)* **293**, 2449–2452. doi:10.1126/science.1062688.

Dudley, A. T., Lyons, K. M. & Robertson, E. J. (1995). A requirement for bone morphogenetic protein-7 during development of the mammalian kidney and eye. *Genes & development* **9**, 2795–2807.

Earley, S., Waldron, B. J. & Brayden, J. E. (2004). Critical role for transient receptor potential channel TRPM4 in myogenic constriction of cerebral arteries. *Circulation research* **95**, 922–929. doi:10.1161/01.RES.0000147311.54833.03.

Elliott, M. H., Ashpole, N. E., Gu, X., Herrnberger, L., McClellan, M. E., Griffith, G. L., Reagan, A. M., Boyce, T. M., Tanito, M., Tamm, E. R. & Stamer, W. D. (2016). Caveolin-1 modulates intraocular pressure: Implications for caveolae mechanoprotection in glaucoma. *Scientific reports* **6**, 37127. doi:10.1038/srep37127.

Entwistle, J., Hall, C. L. & Turley, E. A. (1996). HA receptors: Regulators of signalling to the cytoskeleton. *Journal of cellular biochemistry* **61**, 569–577. doi:10.1002/(SICI)1097-4644(19960616)61:4<569:AID-JCB10>3.0.CO;2-B.

Fahmy IA. Role of Aqueous Humor Matrix Metalloproteinase-2 and Its Inhibitor and Connective Tissue Growth Factor in the Pathogenesis of Primary Open Angle Glaucoma and pseudoexfoliative glaucoma. *Rawal Med J.* **2008**, 179–183.

Ferrara, N., Carver-Moore, K., Chen, H., Dowd, M., Lu, L., O'Shea, K. S., Powell-Braxton, L., Hillan, K. J. & Moore, M. W. (1996). Heterozygous embryonic lethality induced by targeted inactivation of the VEGF gene. *Nature* **380**, 439–442. doi:10.1038/380439a0.

Ffrench-Constant, C., Miller, R. H., Burne, J. F. & Raff, M. C. (1988). Evidence that migratory oligodendrocyte-type-2 astrocyte (O-2A) progenitor cells are kept out of the rat retina by a barrier at the eye-end of the optic nerve. *Journal of neurocytology* **17**, 13–25.

Fra, A. M., Williamson, E., Simons, K. & Parton, R. G. (1995). De novo formation of caveolae in lymphocytes by expression of VIP21-caveolin. *Proceedings of the National Academy of Sciences of the United States of America* **92**, 8655–8659.

Frazier, K., Williams, S., Kothapalli, D., Klapper, H. & Grotendorst, G. R. (1996). Stimulation of fibroblast cell growth, matrix production, and granulation tissue formation by connective tissue growth factor. *The Journal of investigative dermatology* **107**, 404–411.

Friedlander, M. (2007). Fibrosis and diseases of the eye. *The Journal of clinical investigation* **117**, 576–586. doi:10.1172/JCI31030.

Friedrichsen, S., Heuer, H., Christ, S., Winckler, M., Brauer, D., Bauer, K. & Raivich, G. (2003). CTGF expression during mouse embryonic development. *Cell and tissue research* **312**, 175–188. doi:10.1007/s00441-003-0712-6.

Fuchshofer, R. (2011). The pathogenic role of transforming growth factor-β2 in glaucomatous damage to the optic nerve head. *Experimental eye research* **93**, 165–169. doi:10.1016/j.exer.2010.07.014.

Fuchshofer, R., Birke, M., Welge-Lussen, U., Kook, D. & Lütjen-Drecoll, E. (2005). Transforming growth factor-beta 2 modulated extracellular matrix component expression in cultured human optic nerve head astrocytes. *Investigative ophthalmology & visual science* **46**, 568–578. doi:10.1167/iovs.04-0649.

Fuchshofer, R., Welge-Lussen, U. & Lütjen-Drecoll, E. (2003). The effect of TGF-beta2 on human trabecular meshwork extracellular proteolytic system. *Experimental eye research* **77**, 757–765.

Fuchshofer, R., Welge-Lüssen, U., Lütjen-Drecoll, E. & Birke, M. (2006). Biochemical and morphological analysis of basement membrane component expression in corneoscleral and cribriform human trabecular meshwork cells. *Investigative ophthalmology & visual science* **47**, 794–801. doi:10.1167/iovs.05-0292.

Fujita, Y., Imagawa, T. & Uehara, M. (2000). Comparative study of the lamina cribrosa and the pial septa in the vertebrate optic nerve and their relationship to the myelinated axons. *Tissue & cell* **32**, 293–301. doi:10.1054/tice.2000.0115.

Fukuchi, T., Sawaguchi, S., Hara, H., Shirakashi, M. & Iwata, K. (1992). Extracellular matrix changes of the optic nerve lamina cribrosa in monkey eyes with experimentally chronic glaucoma. *Graefe's archive for clinical and experimental ophthalmology = Albrecht von Graefes Archiv fur klinische und experimentelle Ophthalmologie* **230**, 421–427.

Fukuchi, T., Sawaguchi, S., Yue, B. Y., Iwata, K., Hara, H. & Kaiya, T. (1994). Sulfated proteoglycans in the lamina cribrosa of normal monkey eyes and monkey eyes with laser-induced glaucoma. *Experimental eye research* **58**, 231–243.

Furukawa, T., Mukherjee, S., Bao, Z. Z., Morrow, E. M. & Cepko, C. L. (2000). rax, Hes1, and notch1 promote the formation of Müller glia by postnatal retinal progenitor cells. *Neuron* **26**, 383–394.

Furuta, Y. & Hogan, B. L. (1998). BMP4 is essential for lens induction in the mouse embryo. *Genes & development* **12**, 3764–3775.

Galli, R., Pagano, S. F., Gritti, A. & Vescovi, A. L. (2000). Regulation of neuronal differentiation in human CNS stem cell progeny by leukemia inhibitory factor. *Developmental neuroscience* **22**, 86–95. doi:10.1159/000017430.

Gao, R. & Brigstock, D. R. (2005). Connective tissue growth factor (CCN2) in rat pancreatic stellate cell function: Integrin alpha5beta1 as a novel CCN2 receptor. *Gastroenterology* **129**, 1019–1030. doi:10.1053/j.gastro.2005.06.067.

Gariano, R. F. (2003). Cellular mechanisms in retinal vascular development. *Progress in retinal and eye research* **22**, 295–306.

Gehring, W. J. & Ikeo, K. (1999). Pax 6: Mastering eye morphogenesis and eye evolution. *Trends in genetics TIG* **15**, 371–377.

Gelman, S., Cone, F. E., Pease, M. E., Nguyen, T. D., Myers, K. & Quigley, H. A. (2010). The presence and distribution of elastin in the posterior and retrobulbar regions of the mouse eye. *Experimental eye research* **90**, 210–215. doi:10.1016/j.exer.2009.10.007.

Gibson, D. J., Pi, L., Sriram, S., Mao, C., Petersen, B. E., Scott, E. W., Leask, A. & Schultz, G. S. (2014). Conditional knockout of CTGF affects corneal wound healing. *Investigative ophthalmology & visual science* **55**, 2062–2070. doi:10.1167/iovs.13-12735.

Gilliam, J. C. & Wensel, T. G. (2011). TRP channel gene expression in the mouse retina. *Vision research* **51**, 2440–2452. doi:10.1016/j.visres.2011.10.009.

Girard, M. J. A., Downs, J. C., Bottlang, M., Burgoyne, C. F. & Suh, J.-K. F. (2009a). Peripapillary and posterior scleral mechanics--part II: Experimental and inverse finite element characterization. *Journal of biomechanical engineering* **131**, 51012. doi:10.1115/1.3113683.

Girard, M. J. A., Downs, J. C., Burgoyne, C. F. & Suh, J.-K. F. (2009b). Peripapillary and posterior scleral mechanics--part I: Development of an anisotropic hyperelastic constitutive model. *Journal of biomechanical engineering* **131**, 51011. doi:10.1115/1.3113682.

Glaser, T., Walton, D. S. & Maas, R. L. (1992). Genomic structure, evolutionary conservation and aniridia mutations in the human PAX6 gene. *Nature genetics* **2**, 232–239. doi:10.1038/ng1192-232.

Gong, H., Freddo, T. F. & Johnson, M. (1992). Age-related changes of sulfated proteoglycans in the normal human trabecular meshwork. *Experimental eye research* **55**, 691–709.

Gong, H., Ye, W., Freddo, T. F. & Hernandez, M. R. (1997). Hyaluronic acid in the normal and glaucomatous optic nerve. *Experimental eye research* **64**, 587–595.

Gordon, M. O., Beiser, J. A., Brandt, J. D., Heuer, D. K., Higginbotham, E. J., Johnson, C. A., Keltner, J. L., Miller, J. P., Parrish, R. K., Wilson, M. R. & Kass, M. A. (2002). The Ocular Hypertension Treatment Study: Baseline factors that predict the onset of primary open-angle glaucoma. *Archives of ophthalmology (Chicago, Ill. 1960)* **120**, 714-20; discussion 829-30.

Gramage, E., Li, J. & Hitchcock, P. (2014). The expression and function of midkine in the vertebrate retina. *British journal of pharmacology* **171**, 913–923. doi:10.1111/bph.12495.

Grierson, I. & Lee, W. R. (1974). Changes in the monkey outflow apparatus at graded levels of intraocular pressure: A qualitative analysis by light microscopy and scanning electron microscopy. *Experimental eye research* **19**, 21–33.

Grierson, I. & Lee, W. R. (1978). Pressure effects on flow channels in the lining endothelium of Schlemm's canal. A quantitative study by transmission electron microscopy. *Acta ophthalmologica* **56**, 935–952.

Grierson, I., Lee, W. R., Moseley, H. & Abraham, S. (1979). The trabecular wall of Schlemm's canal: A study of the effects of pilocarpine by scanning electron microscopy. *The British journal of ophthalmology* **63**, 9–16.

Grotendorst, G. R., Okochi, H. & Hayashi, N. (1996). A novel transforming growth factor beta response element controls the expression of the connective tissue growth factor gene. *Cell growth & differentiation the molecular biology journal of the American Association for Cancer Research* **7**, 469–480.

GYLLENSTEN, L. J. & HELLSTROM, B. E. (1954). Experimental approach to the pathogenesis of retrolental fibroplasia. I. Changes of the eye induced by exposure of newborn mice to concentrated oxygen. *Acta paediatrica. Supplementum* **43**, 131–148.

Hann, C. R., Springett, M. J., Wang, X. & Johnson, D. H. (2001). Ultrastructural localization of collagen IV, fibronectin, and laminin in the trabecular meshwork of normal and glaucomatous eyes. *Ophthalmic research* **33**, 314–324. doi:10.1159/000055687.

Harrison, D. G., Sayegh, H., Ohara, Y., Inoue, N. & Venema, R. C. (1996). Regulation of expression of the endothelial cell nitric oxide synthase. *Clinical and experimental pharmacology & physiology* **23**, 251–255.

Haverkamp, S. & Wässle, H. (2000). Immunocytochemical analysis of the mouse retina. *The Journal of comparative neurology* **424**, 1–23.

Haydon, P. G. (2001). GLIA: Listening and talking to the synapse. *Nature reviews. Neuroscience* **2**, 185–193. doi:10.1038/35058528.

Hayreh, S. S. (1978). Ischemic optic neuropathy. *International ophthalmology* **1**, 9–18.

Hayreh, S. S. (2011). *Ischemic Optic Neuropathies*.

He, S., Jin, M. L., Worpel, V. & Hinton, D. R. (2003). A role for connective tissue growth factor in the pathogenesis of choroidal neovascularization. *Archives of ophthalmology (Chicago, Ill. 1960)* **121**, 1283–1288. doi:10.1001/archopht.121.9.1283.

Heidemann, S. R., Kaech, S., Buxbaum, R. E. & Matus, A. (1999). Direct observations of the mechanical behaviors of the cytoskeleton in living fibroblasts. *The Journal of cell biology* **145**, 109–122.

Hernandez, M. R. (1992). Ultrastructural immunocytochemical analysis of elastin in the human lamina cribrosa. Changes in elastic fibers in primary open-angle glaucoma. *Investigative ophthalmology & visual science* **33**, 2891–2903.

Hernandez, M. R. (2000). The optic nerve head in glaucoma: Role of astrocytes in tissue remodeling. *Progress in retinal and eye research* **19**, 297–321.

Hernandez, M. R., Agapova, O. A., Yang, P., Salvador-Silva, M., Ricard, C. S. & Aoi, S. (2002). Differential gene expression in astrocytes from human normal and glaucomatous optic nerve head analyzed by cDNA microarray. *Glia* **38**, 45–64.

Hernandez, M. R., Andrzejewska, W. M. & Neufeld, A. H. (1990). Changes in the extracellular matrix of the human optic nerve head in primary open-angle glaucoma. *American journal of ophthalmology* **109**, 180–188.

Hernandez, M. R., Igoe, F. & Neufeld, A. H. (1988). Cell culture of the human lamina cribrosa. *Investigative ophthalmology & visual science* **29**, 78–89.

Hernandez, M. R., Luo, X. X., Igoe, F. & Neufeld, A. H. (1987). Extracellular matrix of the human lamina cribrosa. *American journal of ophthalmology* **104**, 567–576.

Hernandez, M. R., Miao, H. & Lukas, T. (2008). Astrocytes in glaucomatous optic neuropathy. *Progress in brain research* **173**, 353–373. doi:10.1016/S0079-6123(08)01125-4.

Hernandez, M. R. & Pena, J. D. (1997). The optic nerve head in glaucomatous optic neuropathy. *Archives of ophthalmology (Chicago, Ill. 1960)* **115**, 389–395.

Hernandez, M. R., Wang, N., Hanley, N. M. & Neufeld, A. H. (1991). Localization of collagen types I and IV mRNAs in human optic nerve head by in situ hybridization. *Investigative ophthalmology & visual science* **32**, 2169–2177.

Hernandez, M. R., Yang, J. & Ye, H. (1994). Activation of elastin mRNA expression in human optic nerve heads with primary open-angle glaucoma. *Journal of glaucoma* **3**, 214–225.

Heusinger-Ribeiro, J., Eberlein, M., Wahab, N. A. & Goppelt-Struebe, M. (2001). Expression of connective tissue growth factor in human renal fibroblasts: Regulatory roles of RhoA and cAMP. *Journal of the American Society of Nephrology JASN* **12**, 1853–1861.

Ho, K. W., Lambert, W. S. & Calkins, D. J. (2014). Activation of the TRPV1 cation channel contributes to stress-induced astrocyte migration. *Glia* **62**, 1435–1451. doi:10.1002/glia.22691.

Hommer, A., Fuchsjäger-Mayrl, G., Resch, H., Vass, C., Garhofer, G. & Schmetterer, L. (2008). Estimation of ocular rigidity based on measurement of pulse amplitude using pneumotonometry and fundus pulse using laser interferometry in glaucoma. *Investigative ophthalmology & visual science* **49**, 4046–4050. doi:10.1167/iovs.07-1342.

Howell, G. R., Libby, R. T., Jakobs, T. C., Smith, R. S., Phalan, F. C., Barter, J. W., Barbay, J. M., Marchant, J. K., Mahesh, N., Porciatti, V., Whitmore, A. V., Masland, R. H. & John, S. W. M. (2007). Axons of retinal ganglion cells are insulted in the optic nerve early in DBA/2J glaucoma. *The Journal of cell biology* **179**, 1523–1537. doi:10.1083/jcb.200706181.

Hu, J., Cui, D., Yang, X., Wang, S., Hu, S., Li, C. & Zeng, J. (2008). Bone morphogenetic protein-2: A potential regulator in scleral remodeling. *Molecular vision* **14**, 2373–2380.

Huang, W., Wang, W., Zhou, M. & Zhang, X. (2014). Association of single-nucleotide polymorphism rs4236601 near caveolin 1 and 2 with primary open-angle glaucoma: A meta-analysis. *Clinical & experimental ophthalmology* **42**, 515–521. doi:10.1111/ceo.12201.

Huillard, E., Laugier, D. & Marx, M. (2005). Defects in chicken neuroretina misexpressing the BMP antagonist Drm/Gremlin. *Developmental biology* **283**, 335–344. doi:10.1016/j.ydbio.2005.04.027.

Hysi, P. G., Cheng, C.-Y., Springelkamp, H., Macgregor, S., Bailey, J. N. C., Wojciechowski, R., Vitart, V., Nag, A., Hewitt, A. W., Höhn, R., Venturini, C., Mirshahi, A., Ramdas, W. D., Thorleifsson, G., Vithana, E., Khor, C.-C., Stefansson, A. B., Liao, J., Haines, J. L., Amin, N., Wang, Y. X., Wild, P. S., Ozel, A. B., Li, J. Z., Fleck, B. W., Zeller, T., Staffieri, S. E., Teo, Y.-Y., Cuellar-Partida, G., Luo, X., Allingham, R. R., Richards, J. E., Senft, A., Karssen, L. C., Zheng, Y., Bellenguez, C., Xu, L., Iglesias, A. I., Wilson, J. F., Kang, J. H., van Leeuwen, E. M., Jonsson, V., Thorsteinsdottir, U., Despriet, D. D. G., Ennis, S., Moroi, S. E., Martin, N. G., Jansonius, N. M., Yazar, S., Tai, E.-S., Amouyel, P., Kirwan, J., van Koolwijk, L. M. E., Hauser, M. A., Jonasson, F., Leo, P., Loomis, S. J., Fogarty, R., Rivadeneira, F., Kearns, L., Lackner, K. J., Jong, P. T. V. M. de, Simpson, C. L., Pennell, C. E., Oostra, B. A., Uitterlinden, A. G., Saw, S.-M., Lotery, A. J., Bailey-Wilson, J. E., Hofman, A., Vingerling, J. R., Maubaret, C., Pfeiffer, N., Wolfs, R. C. W., Lemij, H. G., Young, T. L., Pasquale, L. R., Delcourt, C., Spector, T. D., Klaver, C. C. W., Small, K. S., Burdon, K. P., Stefansson, K., Wong, T.-Y., Viswanathan, A., Mackey, D. A., Craig, J. E., Wiggs, J. L., van Duijn, C. M., Hammond, C. J. & Aung, T. (2014). Genome-wide analysis of multi-ancestry cohorts identifies new loci influencing intraocular

pressure and susceptibility to glaucoma. *Nature genetics* **46**, 1126–1130. doi:10.1038/ng.3087.

Iadecola, C. & Nedergaard, M. (2007). Glial regulation of the cerebral microvasculature. *Nature neuroscience* **10**, 1369–1376. doi:10.1038/nn2003.

Igarashi, A., Okochi, H., Bradham, D. M. & Grotendorst, G. R. (1993). Regulation of connective tissue growth factor gene expression in human skin fibroblasts and during wound repair. *Molecular biology of the cell* **4**, 637–645.

Inatani, M., Tanihara, H., Katsuta, H., Honjo, M., Kido, N. & Honda, Y. (2001). Transforming growth factor-beta 2 levels in aqueous humor of glaucomatous eyes. *Graefe's archive for clinical and experimental ophthalmology = Albrecht von Graefes Archiv fur klinische und experimentelle Ophthalmologie* **239**, 109–113.

Inoki, I., Shiomi, T., Hashimoto, G., Enomoto, H., Nakamura, H., Makino, K.-i., Ikeda, E., Takata, S., Kobayashi, K.-i. & Okada, Y. (2002). Connective tissue growth factor binds vascular endothelial growth factor (VEGF) and inhibits VEGF-induced angiogenesis. *FASEB journal official publication of the Federation of American Societies for Experimental Biology* **16**, 219–221. doi:10.1096/fj.01-0332fje.

Ito, Y., Aten, J., Bende, R. J., Oemar, B. S., Rabelink, T. J., Weening, J. J. & Goldschmeding, R. (1998). Expression of connective tissue growth factor in human renal fibrosis. *Kidney international* **53**, 853–861. doi:10.1111/j.1523-1755.1998.00820.x.

Ivkovic, S., Yoon, B. S., Popoff, S. N., Safadi, F. F., Libuda, D. E., Stephenson, R. C., Daluiski, A. & Lyons, K. M. (2003). Connective tissue growth factor coordinates chondrogenesis and angiogenesis during skeletal development. *Development (Cambridge, England)* **130**, 2779–2791.

Janagam, D. R., Wu, L. & Lowe, T. L. (2017). Nanoparticles for drug delivery to the anterior segment of the eye. *Advanced drug delivery reviews* **122**, 31–64. doi:10.1016/j.addr.2017.04.001.

Jang, H.-S., Kim, H.-J., Kim, J.-M., Lee, Y.-S., Kim, K. L., Kim, J.-A., Lee, J.-Y., Suh, W., Choi, J.-H., Jeon, E.-S., Byun, J. & Kim, D.-K. (2004). A novel ex vivo angiogenesis assay based on electroporation-mediated delivery of naked plasmid DNA to skeletal muscle. *Molecular therapy the journal of the American Society of Gene Therapy* **9**, 464–474. doi:10.1016/j.ymthe.2003.12.002.

Jena, N., Martín-Seisdedos, C., McCue, P. & Croce, C. M. (1997). BMP7 null mutation in mice: Developmental defects in skeleton, kidney, and eye. *Experimental cell research* **230**, 28–37.

Jiang, B., Bezhadian, M. A. & Caldwell, R. B. (1995). Astrocytes modulate retinal vasculogenesis: Effects on endothelial cell differentiation. *Glia* **15**, 1–10. doi:10.1002/glia.440150102.

Johnson, C. A., Keltner, J. L., Cello, K. E., Edwards, M., Kass, M. A., Gordon, M. O., Budenz, D. L., Gaasterland, D. E. & Werner, E. (2002). Baseline visual field characteristics in the ocular hypertension treatment study. *Ophthalmology* **109**, 432–437.

Johnson, M. (2006). 'What controls aqueous humour outflow resistance?'. *Experimental eye research* **82**, 545–557. doi:10.1016/j.exer.2005.10.011.

Johnston, M. C., Noden, D. M., Hazelton, R. D., Coulombre, J. L. & Coulombre, A. J. (1979). Origins of avian ocular and periocular tissues. *Experimental eye research* **29**, 27–43.

Jordan, T., Hanson, I., Zaletayev, D., Hodgson, S., Prosser, J., Seawright, A., Hastie, N. & van Heyningen, V. (1992). The human PAX6 gene is mutated in two patients with aniridia. *Nature genetics* **1**, 328–332. doi:10.1038/ng0892-328.

Junglas, B., Kuespert, S., Seleem, A. A., Struller, T., Ullmann, S., Bösl, M., Bosserhoff, A., Köstler, J., Wagner, R., Tamm, E. R. & Fuchshofer, R. (2012). Connective tissue growth factor causes glaucoma by modifying the actin cytoskeleton of the trabecular meshwork. *The American journal of pathology* **180**, 2386–2403. doi:10.1016/j.ajpath.2012.02.030.

Junglas, B., Yu, A. H. L., Welge-Lüssen, U., Tamm, E. R. & Fuchshofer, R. (2009). Connective tissue growth factor induces extracellular matrix deposition in human trabecular meshwork cells. *Experimental eye research* **88**, 1065–1075. doi:10.1016/j.exer.2009.01.008.

Kanasty, R., Dorkin, J. R., Vegas, A. & Anderson, D. (2013). Delivery materials for siRNA therapeutics. *Nature materials* **12**, 967–977. doi:10.1038/nmat3765.

Kass, M. A., Heuer, D. K., Higginbotham, E. J., Johnson, C. A., Keltner, J. L., Miller, J. P., Parrish, R. K., Wilson, M. R. & Gordon, M. O. (2002). The Ocular Hypertension Treatment Study: A randomized trial determines that topical ocular hypotensive medication delays or prevents the onset of primary open-angle glaucoma. *Archives of ophthalmology (Chicago, Ill. 1960)* **120**, 701-13; discussion 829-30.

Kaunas, R., Nguyen, P., Usami, S. & Chien, S. (2005). Cooperative effects of Rho and mechanical stretch on stress fiber organization. *Proceedings of the National Academy of Sciences of the United States of America* **102**, 15895–15900. doi:10.1073/pnas.0506041102.

Keene, D. R., Sakai, L. Y., Bächinger, H. P. & Burgeson, R. E. (1987). Type III collagen can be present on banded collagen fibrils regardless of fibril diameter. *The Journal of cell biology* **105**, 2393–2402.

Kerr, N. M., Johnson, C. S., Green, C. R. & Danesh-Meyer, H. V. (2011). Gap junction protein connexin43 (GJA1) in the human glaucomatous optic nerve head and retina. *Journal of clinical neuroscience official journal of the Neurosurgical Society of Australasia* **18**, 102–108. doi:10.1016/j.jocn.2010.06.002.

Kerrison, J. B., Lewis, R. N., Otteson, D. C. & Zack, D. J. (2005). Bone morphogenetic proteins promote neurite outgrowth in retinal ganglion cells. *Molecular vision* **11**, 208–215.

Kim, S., Kim, K., Heo, D. W., Kim, J.-S., Park, C. K., Kim, C.-s. & Kang, C. (2015). Expression-associated polymorphisms of CAV1-CAV2 affect intraocular pressure and high-tension glaucoma risk. *Molecular vision* **21**, 548–554.

Kimball, E. C., Nguyen, C., Steinhart, M. R., Nguyen, T. D., Pease, M. E., Oglesby, E. N., Oveson, B. C. & Quigley, H. A. (2014). Experimental scleral cross-linking increases glaucoma damage in a mouse model. *Experimental eye research* **128**, 129–140. doi:10.1016/j.exer.2014.08.016.

Kireeva, M. L., Latinkić, B. V., Kolesnikova, T. V., Chen, C. C., Yang, G. P., Abler, A. S. & Lau, L. F. (1997). Cyr61 and Fisp12 are both ECM-associated signaling molecules: Activities, metabolism, and localization during development. *Experimental cell research* **233**, 63–77. doi:10.1006/excr.1997.3548.

Kirwan, R. P., Leonard, M. O., Murphy, M., Clark, A. F. & O'Brien, C. J. (2005). Transforming growth factor-beta-regulated gene transcription and protein expression in human GFAP-negative lamina cribrosa cells. *Glia* **52**, 309–324. doi:10.1002/glia.20247.

Kirwan, R. P., Wordinger, R. J., Clark, A. F. & O'Brien, C. J. (2009). Differential global and extra-cellular matrix focused gene expression patterns between normal and glaucomatous human lamina cribrosa cells. *Molecular vision* **15**, 76–88.

Kizhatil, K., Chlebowski, A., Tolman, N. G., Freeburg, N. F., Ryan, M. M., Shaw, N. N., Kokini, A. D. M., Marchant, J. K. & John, S. W. M. (2016). An In Vitro Perfusion System to Enhance Outflow Studies in Mouse Eyes. *Investigative ophthalmology & visual science* **57**, 5207–5215. doi:10.1167/iovs.16-19481.

Knepper, P. A., Goossens, W. & Mayanil, C. S. (1998). CD44H localization in primary open-angle glaucoma. *Investigative ophthalmology & visual science* **39**, 673–680.

Koblar, S. A., Turnley, A. M., Classon, B. J., Reid, K. L., Ware, C. B., Cheema, S. S., Murphy, M. & Bartlett, P. F. (1998). Neural precursor differentiation into astrocytes

requires signaling through the leukemia inhibitory factor receptor. *Proceedings of the National Academy of Sciences of the United States of America* **95**, 3178–3181.

Križaj, D., Ryskamp, D. A., Tian, N., Tezel, G., Mitchell, C. H., Slepak, V. Z. & Shestopalov, V. I. (2014). From mechanosensitivity to inflammatory responses: New players in the pathology of glaucoma. *Current eye research* **39**, 105–119. doi:10.3109/02713683.2013.836541.

Kuespert, S., Junglas, B., Braunger, B. M., Tamm, E. R. & Fuchshofer, R. (2015). The regulation of connective tissue growth factor expression influences the viability of human trabecular meshwork cells. *Journal of cellular and molecular medicine* **19**, 1010–1020. doi:10.1111/jcmm.12492.

Kuiper, E. J., Hughes, J. M., van Geest, R. J., Vogels, I. M. C., Goldschmeding, R., van Noorden, C. J. F., Schlingemann, R. O. & Klaassen, I. (2007). Effect of VEGF-A on expression of profibrotic growth factor and extracellular matrix genes in the retina. *Investigative ophthalmology & visual science* **48**, 4267–4276. doi:10.1167/iovs.06-0804.

Kurzchalia, T. V., Dupree, P., Parton, R. G., Kellner, R., Virta, H., Lehnert, M. & Simons, K. (1992). VIP21, a 21-kD membrane protein is an integral component of trans-Golgi-network-derived transport vesicles. *The Journal of cell biology* **118**, 1003–1014.

Laemmli, U. K. (1970). Cleavage of structural proteins during the assembly of the head of bacteriophage T4. *Nature* **227**, 680–685.

Lau, L. F. & Lam, S. C. (1999). The CCN family of angiogenic regulators: The integrin connection. *Experimental cell research* **248**, 44–57. doi:10.1006/excr.1999.4456.

Leask, A. & Abraham, D. J. (2006). All in the CCN family: Essential matricellular signaling modulators emerge from the bunker. *Journal of cell science* **119**, 4803–4810. doi:10.1242/jcs.03270.

Lei, Y., Song, M., Wu, J., Xing, C. & Sun, X. (2016). eNOS Activity in CAV1 Knockout Mouse Eyes. *Investigative ophthalmology & visual science* **57**, 2805–2813. doi:10.1167/iovs.15-18841.

Leonelli, M., Martins, D. O., Kihara, A. H. & Britto, L. R. G. (2009). Ontogenetic expression of the vanilloid receptors TRPV1 and TRPV2 in the rat retina. *International journal of developmental neuroscience the official journal of the International Society for Developmental Neuroscience* **27**, 709–718. doi:10.1016/j.ijdevneu.2009.07.003.

Leske, M. C., Heijl, A., Hussein, M., Bengtsson, B., Hyman, L. & Komaroff, E. (2003). Factors for glaucoma progression and the effect of treatment: The early manifest glaucoma trial. *Archives of ophthalmology (Chicago, Ill. 1960)* **121**, 48–56.

Li, H., Tierney, C., Wen, L., Wu, J. Y. & Rao, Y. (1997). A single morphogenetic field gives rise to two retina primordia under the influence of the prechordal plate. *Development (Cambridge, England)* **124**, 603–615.

Li, Y. N., Radner, S., French, M. M., Pinzón-Duarte, G., Daly, G. H., Burgeson, R. E., Koch, M. & Brunken, W. J. (2012). The γ3 chain of laminin is widely but differentially expressed in murine basement membranes: Expression and functional studies. *Matrix biology journal of the International Society for Matrix Biology* **31**, 120–134. doi:10.1016/j.matbio.2011.12.002.

Libby, R. T., Champliaud, M. F., Claudepierre, T., Xu, Y., Gibbons, E. P., Koch, M., Burgeson, R. E., Hunter, D. D. & Brunken, W. J. (2000). Laminin expression in adult and developing retinae: Evidence of two novel CNS laminins. *The Journal of neuroscience the official journal of the Society for Neuroscience* **20**, 6517–6528.

Libby, R. T., Xu, Y., Selfors, L. M., Brunken, W. J. & Hunter, D. D. (1997). Identification of the cellular source of laminin beta2 in adult and developing vertebrate retinae. *The Journal of comparative neurology* **389**, 655–667.

Lichter, P. R., Musch, D. C., Gillespie, B. W., Guire, K. E., Janz, N. K., Wren, P. A. & Mills, R. P. (2001). Interim clinical outcomes in the Collaborative Initial Glaucoma Treatment Study comparing initial treatment randomized to medications or surgery. *Ophthalmology* **108**, 1943–1953.

Lin, C. Q. & Bissell, M. J. (1993). Multi-faceted regulation of cell differentiation by extracellular matrix. *FASEB journal official publication of the Federation of American Societies for Experimental Biology* **7**, 737–743.

Lin, J., Liliensiek, B., Kanitz, M., Schimanski, U., Böhrer, H., Waldherr, R., Martin, E., Kauffmann, G., Ziegler, R. & Nawroth, P. P. (1998). Molecular cloning of genes differentially regulated by TNF-alpha in bovine aortic endothelial cells, fibroblasts and smooth muscle cells. *Cardiovascular research* **38**, 802–813.

Lin, S.-Y. & Corey, D. P. (2005). TRP channels in mechanosensation. *Current opinion in neurobiology* **15**, 350–357. doi:10.1016/j.conb.2005.05.012.

Ling, T. L., Mitrofanis, J. & Stone, J. (1989). Origin of retinal astrocytes in the rat: Evidence of migration from the optic nerve. *The Journal of comparative neurology* **286**, 345–352. doi:10.1002/cne.902860305.

Liu, B. & Neufeld, A. H. (2000). Expression of nitric oxide synthase-2 (NOS-2) in reactive astrocytes of the human glaucomatous optic nerve head. *Glia* **30**, 178–186.

Liu, S.-Y., Zhang, Z.-Y., Song, Y.-C., Qiu, K.-J., Zhang, K.-C., An, N., Zhou, Z., Cai, W.-Q. & Yang, H. (2004). SVZa neural stem cells differentiate into distinct lineages in response to BMP4. *Experimental neurology* **190**, 109–121. doi:10.1016/j.expneurol.2004.07.015.

Loomis, S. J., Kang, J. H., Weinreb, R. N., Yaspan, B. L., Cooke Bailey, J. N., Gaasterland, D., Gaasterland, T., Lee, R. K., Lichter, P. R., Budenz, D. L., Liu, Y., Realini, T., Friedman, D. S., McCarty, C. A., Moroi, S. E., Olson, L., Schuman, J. S., Singh, K., Vollrath, D., Wollstein, G., Zack, D. J., Brilliant, M., Sit, A. J., Christen, W. G., Fingert, J., Kraft, P., Zhang, K., Allingham, R. R., Pericak-Vance, M. A., Richards, J. E., Hauser, M. A., Haines, J. L., Pasquale, L. R. & Wiggs, J. L. (2014). Association of CAV1/CAV2 genomic variants with primary open-angle glaucoma overall and by gender and pattern of visual field loss. *Ophthalmology* **121**, 508–516. doi:10.1016/j.ophtha.2013.09.012.

Luo, G., Hofmann, C., Bronckers, A. L., Sohocki, M., Bradley, A. & Karsenty, G. (1995). BMP-7 is an inducer of nephrogenesis, and is also required for eye development and skeletal patterning. *Genes & development* **9**, 2808–2820.

Lupo, G., Liu, Y., Qiu, R., Chandraratna, R. A. S., Barsacchi, G., He, R.-Q. & Harris, W. A. (2005). Dorsoventral patterning of the Xenopus eye: A collaboration of Retinoid, Hedgehog and FGF receptor signaling. *Development (Cambridge, England)* **132**, 1737–1748. doi:10.1242/dev.01726.

Lütjen-Drecoll, E. (1999). Functional morphology of the trabecular meshwork in primate eyes. *Progress in retinal and eye research* **18**, 91–119.

Lütjen-Drecoll, E., Futa, R. & Rohen, J. W. (1981). Ultrahistochemical studies on tangential sections of the trabecular meshwork in normal and glaucomatous eyes. *Investigative ophthalmology & visual science* **21**, 563–573.

Lütjen-Drecoll, E., Rittig, M., Rauterberg, J., Jander, R. & Mollenhauer, J. (1989). Immunomicroscopical study of type VI collagen in the trabecular meshwork of normal and glaucomatous eyes. *Experimental eye research* **48**, 139–147.

Lütjen-Drecoll, E., Schenholm, M., Tamm, E. & Tengblad, A. (1990). Visualization of hyaluronic acid in the anterior segment of rabbit and monkey eyes. *Experimental eye research* **51**, 55–63.

Lutjen-Drecoll E, R. J. W. (1994). Anatomy of aqueous humor formation and drainage. *In: Podos SM, Yanoff M, editors. Textbook of Ophthalmology. Mosby; London*, pp. 1.1–1.16.

Lutjen-Drecoll E, R. J. W. (2001). Functional Morphology of the Trabecular Meshwork. *In: Tasman W, Jaeger EA, editors. Duane's Foundations of Clinical Ophthalmology. J.B. Lippincott Company; Philadelphia*, pp. 1–30.

Lye-Barthel, M., Sun, D. & Jakobs, T. C. (2013). Morphology of astrocytes in a glaucomatous optic nerve. *Investigative ophthalmology & visual science* **54**, 909–917. doi:10.1167/iovs.12-10109.

MacNeil, M. A., Heussy, J. K., Dacheux, R. F., Raviola, E. & Masland, R. H. (1999). The shapes and numbers of amacrine cells: Matching of photofilled with Golgi-stained cells in the rabbit retina and comparison with other mammalian species. *The Journal of comparative neurology* **413**, 305–326.

MacNeil, M. A. & Masland, R. H. (1998). Extreme diversity among amacrine cells: Implications for function. *Neuron* **20**, 971–982.

Magistretti, P. J. (2006). Neuron-glia metabolic coupling and plasticity. *The Journal of experimental biology* **209**, 2304–2311. doi:10.1242/jeb.02208.

Makarenkova, H. P., Ito, M., Govindarajan, V., Faber, S. C., Sun, L., McMahon, G., Overbeek, P. A. & Lang, R. A. (2000). FGF10 is an inducer and Pax6 a competence factor for lacrimal gland development. *Development (Cambridge, England)* **127**, 2563–2572.

Marquardt, T., Ashery-Padan, R., Andrejewski, N., Scardigli, R., Guillemot, F. & Gruss, P. (2001). Pax6 is required for the multipotent state of retinal progenitor cells. *Cell* **105**, 43–55.

Marquardt, T. & Gruss, P. (2002). Generating neuronal diversity in the retina: One for nearly all. *Trends in neurosciences* **25**, 32–38.

Marshall, G. E., Konstas, A. G. & Lee, W. R. (1991a). Immunogold fine structural localization of extracellular matrix components in aged human cornea. I. Types I-IV collagen and laminin. *Graefe's archive for clinical and experimental ophthalmology = Albrecht von Graefes Archiv fur klinische und experimentelle Ophthalmologie* **229**, 157–163.

Marshall, G. E., Konstas, A. G. & Lee, W. R. (1991b). Immunogold fine structural localization of extracellular matrix components in aged human cornea. II. Collagen types V and VI. *Graefe's archive for clinical and experimental ophthalmology = Albrecht von Graefes Archiv fur klinische und experimentelle Ophthalmologie* **229**, 164–171.

Martinez-Morales, J.-R., Del Bene, F., Nica, G., Hammerschmidt, M., Bovolenta, P. & Wittbrodt, J. (2005). Differentiation of the vertebrate retina is coordinated by an FGF signaling center. *Developmental cell* **8**, 565–574. doi:10.1016/j.devcel.2005.01.022.

Mateos, S., Amarir, S., Laugier, D., Marx, M. & Calothy, G. (2007). Stable expression of intracellular Notch suppresses v-Src-induced transformation in avian neural cells. *Oncogene* **26**, 3338–3351. doi:10.1038/sj.onc.1210124.

May, C. A. & Lütjen-Drecoll, E. (2002). Morphology of the murine optic nerve. *Investigative ophthalmology & visual science* **43**, 2206–2212.

McHugh, B. J., Buttery, R., Lad, Y., Banks, S., Haslett, C. & Sethi, T. (2010). Integrin activation by Fam38A uses a novel mechanism of R-Ras targeting to the endoplasmic reticulum. *Journal of cell science* **123**, 51–61. doi:10.1242/jcs.056424.

McHugh, B. J., Murdoch, A., Haslett, C. & Sethi, T. (2012). Loss of the integrin-activating transmembrane protein Fam38A (Piezo1) promotes a switch to a reduced integrin-dependent mode of cell migration. *PloS one* **7**, e40346. doi:10.1371/journal.pone.0040346.

McMenamin, P. G. & Steptoe, R. J. (1991). Normal anatomy of the aqueous humour outflow system in the domestic pig eye. *Journal of anatomy* **178**, 65–77.

Mendes, F. A., Coelho Aguiar, J. M., Kahn, S. A., Reis, A. H., Dubois, L. G., Romão, L. F., Ferreira, L. S. S., Chneiweiss, H., Moura Neto, V. & Abreu, J. G. (2015). Connective-Tissue Growth Factor (CTGF/CCN2) Induces Astrogenesis and Fibronectin Expression of Embryonic Neural Cells In Vitro. *PloS one* **10**, e0133689. doi:10.1371/journal.pone.0133689.

Metea, M. R. & Newman, E. A. (2006). Glial cells dilate and constrict blood vessels: A mechanism of neurovascular coupling. *The Journal of neuroscience the official journal of the Society for Neuroscience* **26**, 2862–2870. doi:10.1523/JNEUROSCI.4048-05.2006.

Mi, H. & Barres, B. A. (1999). Purification and characterization of astrocyte precursor cells in the developing rat optic nerve. *The Journal of neuroscience the official journal of the Society for Neuroscience* **19**, 1049–1061.

Mi, H., Haeberle, H. & Barres, B. A. (2001). Induction of astrocyte differentiation by endothelial cells. *The Journal of neuroscience the official journal of the Society for Neuroscience* **21**, 1538–1547.

Min, S. H., Lee, T.-I., Chung, Y. S. & Kim, H. K. (2006). Transforming growth factor-beta levels in human aqueous humor of glaucomatous, diabetic and uveitic eyes. *Korean journal of ophthalmology KJO* **20**, 162–165. doi:10.3341/kjo.2006.20.3.162.

Monier, S., Parton, R. G., Vogel, F., Behlke, J., Henske, A. & Kurzchalia, T. V. (1995). VIP21-caveolin, a membrane protein constituent of the caveolar coat, oligomerizes in vivo and in vitro. *Molecular biology of the cell* **6**, 911–927.

Morcos, Y. & Chan-Ling, T. (2000). Concentration of astrocytic filaments at the retinal optic nerve junction is coincident with the absence of intra-retinal myelination: Comparative and developmental evidence. *Journal of neurocytology* **29**, 665–678.

Morgans, C. W., Zhang, J., Jeffrey, B. G., Nelson, S. M., Burke, N. S., Duvoisin, R. M. & Brown, R. L. (2009). TRPM1 is required for the depolarizing light response in retinal ON-bipolar cells. *Proceedings of the National Academy of Sciences of the United States of America* **106**, 19174–19178. doi:10.1073/pnas.0908711106.

Morissette, N. & Carbonetto, S. (1995). Laminin alpha 2 chain (M chain) is found within the pathway of avian and murine retinal projections. *The Journal of neuroscience the official journal of the Society for Neuroscience* **15**, 8067–8082.

Morrison, J. C., Dorman-Pease, M. E., Dunkelberger, G. R. & Quigley, H. A. (1990). Optic nerve head extracellular matrix in primary optic atrophy and experimental glaucoma. *Archives of ophthalmology (Chicago, Ill. 1960)* **108**, 1020–1024.

Morrison, J. C., Jerdan, J. A., Dorman, M. E. & Quigley, H. A. (1989). Structural proteins of the neonatal and adult lamina cribrosa. *Archives of ophthalmology (Chicago, Ill. 1960)* **107**, 1220–1224.

Moussad, E. E. & Brigstock, D. R. (2000). Connective tissue growth factor: What's in a name? *Molecular genetics and metabolism* **71**, 276–292. doi:10.1006/mgme.2000.3059.

Muraki, K., Iwata, Y., Katanosaka, Y., Ito, T., Ohya, S., Shigekawa, M. & Imaizumi, Y. (2003). TRPV2 is a component of osmotically sensitive cation channels in murine aortic myocytes. *Circulation research* **93**, 829–838. doi:10.1161/01.RES.0000097263.10220.0C.

Nagai, N., Klimava, A., Lee, W.-H., Izumi-Nagai, K. & Handa, J. T. (2009). CTGF is increased in basal deposits and regulates matrix production through the ERK (p42/p44mapk) MAPK and the p38 MAPK signaling pathways. *Investigative ophthalmology & visual science* **50**, 1903–1910. doi:10.1167/iovs.08-2383.

Nakagaito, Y., Yoshida, T., Satoh, M. & Takeuchi, M. (1995). Effects of leukemia inhibitory factor on the differentiation of astrocyte progenitor cells from embryonic mouse cerebral hemispheres. *Brain research. Developmental brain research* **87**, 220–223.

Nedergaard, M., Ransom, B. & Goldman, S. A. (2003). New roles for astrocytes: Redefining the functional architecture of the brain. *Trends in neurosciences* **26**, 523–530. doi:10.1016/j.tins.2003.08.008.

Neidlinger-Wilke, C., Grood, E. S., Wang, J.-C., Brand, R. A. & Claes, L. (2001). Cell alignment is induced by cyclic changes in cell length: Studies of cells grown in cyclically stretched substrates. *Journal of orthopaedic research official publication of the Orthopaedic Research Society* **19**, 286–293. doi:10.1016/S0736-0266(00)00029-2.

Nelson, L. B., Spaeth, G. L., Nowinski, T. S., Margo, C. E. & Jackson, L. (1984). Aniridia. A review. *Survey of ophthalmology* **28**, 621–642.

Neufeld, A. H., Hernandez, M. R. & Gonzalez, M. (1997). Nitric oxide synthase in the human glaucomatous optic nerve head. *Archives of ophthalmology (Chicago, Ill. 1960)* **115**, 497–503.

Neumann, C., Yu, A., Welge-Lüssen, U., Lütjen-Drecoll, E. & Birke, M. (2008). The effect of TGF-beta2 on elastin, type VI collagen, and components of the proteolytic degradation system in human optic nerve astrocytes. *Investigative ophthalmology & visual science* **49**, 1464–1472. doi:10.1167/iovs.07-1053.

Newman, E. A. (2003). New roles for astrocytes: Regulation of synaptic transmission. *Trends in neurosciences* **26**, 536–542. doi:10.1016/S0166-2236(03)00237-6.

Nguyen, C., Cone, F. E., Nguyen, T. D., Coudrillier, B., Pease, M. E., Steinhart, M. R., Oglesby, E. N., Jefferys, J. L. & Quigley, H. A. (2013). Studies of scleral biomechanical behavior related to susceptibility for retinal ganglion cell loss in experimental mouse glaucoma. *Investigative ophthalmology & visual science* **54**, 1767–1780. doi:10.1167/iovs.12-10952.

Nilius, B. & Owsianik, G. (2011). The transient receptor potential family of ion channels. *Genome biology* **12**, 218. doi:10.1186/gb-2011-12-3-218.

Norman, R. E., Flanagan, J. G., Sigal, I. A., Rausch, S. M. K., Tertinegg, I. & Ethier, C. R. (2011). Finite element modeling of the human sclera: Influence on optic nerve head biomechanics and connections with glaucoma. *Experimental eye research* **93**, 4–12. doi:10.1016/j.exer.2010.09.014.

Numata, T., Shimizu, T. & Okada, Y. (2007a). Direct mechano-stress sensitivity of TRPM7 channel. *Cellular physiology and biochemistry international journal of experimental cellular physiology, biochemistry, and pharmacology* **19**, 1–8. doi:10.1159/000099187.

Numata, T., Shimizu, T. & Okada, Y. (2007b). TRPM7 is a stretch- and swelling-activated cation channel involved in volume regulation in human epithelial cells. *American journal of physiology. Cell physiology* **292**, C460-7. doi:10.1152/ajpcell.00367.2006.

Ochiai, Y. & Ochiai, H. (2002). Higher concentration of transforming growth factor-beta in aqueous humor of glaucomatous eyes and diabetic eyes. *Japanese journal of ophthalmology* **46**, 249–253.

Overby, D. R., Zhou, E. H., Vargas-Pinto, R., Pedrigi, R. M., Fuchshofer, R., Braakman, S. T., Gupta, R., Perkumas, K. M., Sherwood, J. M., Vahabikashi, A., Dang, Q., Kim, J. H., Ethier, C. R., Stamer, W. D., Fredberg, J. J. & Johnson, M. (2014). Altered mechanobiology of Schlemm's canal endothelial cells in glaucoma. *Proceedings of the National Academy of Sciences of the United States of America* **111**, 13876–13881. doi:10.1073/pnas.1410602111.

Oyama, T., Abe, H. & Ushiki, T. (2006). The connective tissue and glial framework in the optic nerve head of the normal human eye: Light and scanning electron microscopic studies. *Archives of histology and cytology* **69**, 341–356.

Ozcan, A. A., Ozdemir, N. & Canataroglu, A. (2004). The aqueous levels of TGF-beta2 in patients with glaucoma. *International ophthalmology* **25**, 19–22.

Ozel, A. B., Moroi, S. E., Reed, D. M., Nika, M., Schmidt, C. M., Akbari, S., Scott, K., Rozsa, F., Pawar, H., Musch, D. C., Lichter, P. R., Gaasterland, D., Branham, K., Gilbert, J., Garnai, S. J., Chen, W., Othman, M., Heckenlively, J., Swaroop, A., Abecasis, G., Friedman, D. S., Zack, D., Ashley-Koch, A., Ulmer, M., Kang, J. H., Liu, Y., Yaspan, B. L., Haines, J., Allingham, R. R., Hauser, M. A., Pasquale, L., Wiggs, J., Richards, J. E. & Li, J. Z. (2014). Genome-wide association study and meta-analysis of intraocular pressure. *Human genetics* **133**, 41–57. doi:10.1007/s00439-013-1349-5.

Palade, G. E. (1953). Fine structure of blood capillaries. *J.Appl.Phys.*, 1424.

Park, H., Go, Y. M., Darji, R., Choi, J. W., Lisanti, M. P., Maland, M. C. & Jo, H. (2000). Caveolin-1 regulates shear stress-dependent activation of extracellular signal-regulated kinase. *American journal of physiology. Heart and circulatory physiology* **278**, H1285-93. doi:10.1152/ajpheart.2000.278.4.H1285.

Parton, R. G. & Simons, K. (2007). The multiple faces of caveolae. *Nature reviews. Molecular cell biology* **8**, 185–194. doi:10.1038/nrm2122.

Pease, M. E., McKinnon, S. J., Quigley, H. A., Kerrigan-Baumrind, L. A. & Zack, D. J. (2000). Obstructed axonal transport of BDNF and its receptor TrkB in experimental glaucoma. *Investigative ophthalmology & visual science* **41**, 764–774.

Pei, Y. F. & Rhodin, J. A. (1970). The prenatal development of the mouse eye. *The Anatomical record* **168**, 105–125. doi:10.1002/ar.1091680109.

Pena, J. D., Agapova, O., Gabelt, B. T., Levin, L. A., Lucarelli, M. J., Kaufman, P. L. & Hernandez, M. R. (2001). Increased elastin expression in astrocytes of the lamina cribrosa in response to elevated intraocular pressure. *Investigative ophthalmology & visual science* **42**, 2303–2314.

Pena, J. D., Netland, P. A., Vidal, I., Dorr, D. A., Rasky, A. & Hernandez, M. R. (1998). Elastosis of the lamina cribrosa in glaucomatous optic neuropathy. *Experimental eye research* **67**, 517–524. doi:10.1006/exer.1998.0539.

Pena, J. D., Roy, S. & Hernandez, M. R. (1996). Tropoelastin gene expression in optic nerve heads of normal and glaucomatous subjects. *Matrix biology journal of the International Society for Matrix Biology* **15**, 323–330.

Pena, J. D., Varela, H. J., Ricard, C. S. & Hernandez, M. R. (1999). Enhanced tenascin expression associated with reactive astrocytes in human optic nerve heads with primary open angle glaucoma. *Experimental eye research* **68**, 29–40. doi:10.1006/exer.1998.0577.

Perbal, B. (2001). The CCN family of genes: A brief history. *Molecular pathology MP* **54**, 103–104.

Perbal, B. (2004). CCN proteins: Multifunctional signalling regulators. *Lancet (London, England)* **363**, 62–64. doi:10.1016/S0140-6736(03)15172-0.

Perris, R. (1997). The extracellular matrix in neural crest-cell migration. *Trends in neurosciences* **20**, 23–31. doi:10.1016/S0166-2236(96)10063-1.

Pi, L., Xia, H., Liu, J., Shenoy, A. K., Hauswirth, W. W. & Scott, E. W. (2011). Role of connective tissue growth factor in the retinal vasculature during development and ischemia. *Investigative ophthalmology & visual science* **52**, 8701–8710. doi:10.1167/iovs.11-7870.

Picht, G., Welge-Luessen, U., Grehn, F. & Lütjen-Drecoll, E. (2001). Transforming growth factor beta 2 levels in the aqueous humor in different types of glaucoma and the relation to filtering bleb development. *Graefe's archive for clinical and experimental ophthalmology = Albrecht von Graefes Archiv fur klinische und experimentelle Ophthalmologie* **239**, 199–207.

Pijanka, J. K., Coudrillier, B., Ziegler, K., Sorensen, T., Meek, K. M., Nguyen, T. D., Quigley, H. A. & Boote, C. (2012). Quantitative mapping of collagen fiber orientation in non-glaucoma and glaucoma posterior human sclerae. *Investigative ophthalmology & visual science* **53**, 5258–5270. doi:10.1167/iovs.12-9705.

Pol, A., Martin, S., Fernández, M. A., Ingelmo-Torres, M., Ferguson, C., Enrich, C. & Parton, R. G. (2005). Cholesterol and fatty acids regulate dynamic caveolin trafficking through the Golgi complex and between the cell surface and lipid bodies. *Molecular biology of the cell* **16**, 2091–2105. doi:10.1091/mbc.E04-08-0737.

Quigley, H. A. (1983). Experimental glaucoma damage mechanism. *Archives of ophthalmology (Chicago, Ill. 1960)* **101**, 1301–1302.

Quigley, H. A. (1996). Number of people with glaucoma worldwide. *The British journal of ophthalmology* **80**, 389–393.

Quigley, H. A. (2011). Glaucoma. *Lancet (London, England)* **377**, 1367–1377. doi:10.1016/S0140-6736(10)61423-7.

Quigley, H. A. & Cone, F. E. (2013). Development of diagnostic and treatment strategies for glaucoma through understanding and modification of scleral and lamina cribrosa connective tissue. *Cell and tissue research* **353**, 231–244. doi:10.1007/s00441-013-1603-0.

Quigley, H. A., Dorman-Pease, M. E. & Brown, A. E. (1991). Quantitative study of collagen and elastin of the optic nerve head and sclera in human and experimental monkey glaucoma. *Current eye research* **10**, 877–888.

Quigley, H. A., Katz, J., Derick, R. J., Gilbert, D. & Sommer, A. (1992). An evaluation of optic disc and nerve fiber layer examinations in monitoring progression of early glaucoma damage. *Ophthalmology* **99**, 19–28.

Quigley, H. A., McKinnon, S. J., Zack, D. J., Pease, M. E., Kerrigan-Baumrind, L. A., Kerrigan, D. F. & Mitchell, R. S. (2000). Retrograde axonal transport of BDNF in retinal ganglion cells is blocked by acute IOP elevation in rats. *Investigative ophthalmology & visual science* **41**, 3460–3466.

Rada, J. A., Cornuet, P. K. & Hassell, J. R. (1993). Regulation of corneal collagen fibrillogenesis in vitro by corneal proteoglycan (lumican and decorin) core proteins. *Experimental eye research* **56**, 635–648. doi:10.1006/exer.1993.1081.

Rada, J. A. S., Shelton, S. & Norton, T. T. (2006). The sclera and myopia. *Experimental eye research* **82**, 185–200. doi:10.1016/j.exer.2005.08.009.

Raghunathan, V. K., Morgan, J. T., Dreier, B., Reilly, C. M., Thomasy, S. M., Wood, J. A., Ly, I., Tuyen, B. C., Hughbanks, M., Murphy, C. J. & Russell, P. (2013). Role of substratum stiffness in modulating genes associated with extracellular matrix and mechanotransducers YAP and TAZ. *Investigative ophthalmology & visual science* **54**, 378–386. doi:10.1167/iovs.12-11007.

Ranade, S. S., Qiu, Z., Woo, S.-H., Hur, S. S., Murthy, S. E., Cahalan, S. M., Xu, J., Mathur, J., Bandell, M., Coste, B., Li, Y.-S. J., Chien, S. & Patapoutian, A. (2014). Piezo1, a mechanically activated ion channel, is required for vascular development in mice. *Proceedings of the National Academy of Sciences of the United States of America* **111**, 10347–10352. doi:10.1073/pnas.1409233111.

Rapaport, D. H., Wong, L. L., Wood, E. D., Yasumura, D. & LaVail, M. M. (2004). Timing and topography of cell genesis in the rat retina. *The Journal of comparative neurology* **474**, 304–324. doi:10.1002/cne.20134.

Razani, B., Engelman, J. A., Wang, X. B., Schubert, W., Zhang, X. L., Marks, C. B., Macaluso, F., Russell, R. G., Li, M., Pestell, R. G., Di Vizio, D., Hou, H., Kneitz, B., Lagaud, G., Christ, G. J., Edelmann, W. & Lisanti, M. P. (2001). Caveolin-1 null mice are viable but show evidence of hyperproliferative and vascular abnormalities. *The Journal of biological chemistry* **276**, 38121–38138. doi:10.1074/jbc.M105408200.

Richards, L. J., Kilpatrick, T. J., Dutton, R., Tan, S. S., Gearing, D. P., Bartlett, P. F. & Murphy, M. (1996). Leukaemia inhibitory factor or related factors promote the differentiation of neuronal and astrocytic precursors within the developing murine spinal cord. *The European journal of neuroscience* **8**, 291–299.

Rizzo, V., Morton, C., DePaola, N., Schnitzer, J. E. & Davies, P. F. (2003). Recruitment of endothelial caveolae into mechanotransduction pathways by flow conditioning in

vitro. *American journal of physiology. Heart and circulatory physiology* **285**, H1720-9. doi:10.1152/ajpheart.00344.2002.

Rogers, R. S., Dharsee, M., Ackloo, S., Sivak, J. M. & Flanagan, J. G. (2012). Proteomics analyses of human optic nerve head astrocytes following biomechanical strain. *Molecular & cellular proteomics MCP* **11**, M111.012302. doi:10.1074/mcp.M111.012302.

Rossi, D. J., Brady, J. D. & Mohr, C. (2007). Astrocyte metabolism and signaling during brain ischemia. *Nature neuroscience* **10**, 1377–1386. doi:10.1038/nn2004.

Rothberg, K. G., Heuser, J. E., Donzell, W. C., Ying, Y. S., Glenney, J. R. & Anderson, R. G. (1992). Caveolin, a protein component of caveolae membrane coats. *Cell* **68**, 673–682.

Ryskamp, D. A., Redmon, S., Jo, A. O. & Križaj, D. (2014). TRPV1 and Endocannabinoids: Emerging Molecular Signals that Modulate Mammalian Vision. *Cells* **3**, 914–938. doi:10.3390/cells3030914.

Ryskamp, D. A., Witkovsky, P., Barabas, P., Huang, W., Koehler, C., Akimov, N. P., Lee, S. H., Chauhan, S., Xing, W., Rentería, R. C., Liedtke, W. & Krizaj, D. (2011). The polymodal ion channel transient receptor potential vanilloid 4 modulates calcium flux, spiking rate, and apoptosis of mouse retinal ganglion cells. *The Journal of neuroscience the official journal of the Society for Neuroscience* **31**, 7089–7101. doi:10.1523/JNEUROSCI.0359-11.2011.

Safadi, F. F., Xu, J., Smock, S. L., Kanaan, R. A., Selim, A.-H., Odgren, P. R., Marks, S. C., Owen, T. A. & Popoff, S. N. (2003). Expression of connective tissue growth factor in bone: Its role in osteoblast proliferation and differentiation in vitro and bone formation in vivo. *Journal of cellular physiology* **196**, 51–62. doi:10.1002/jcp.10319.

Saika, S., Liu, C. Y., Azhar, M., Sanford, L. P., Doetschman, T., Gendron, R. L., Kao, C. W. & Kao, W. W. (2001). TGFbeta2 in corneal morphogenesis during mouse embryonic development. *Developmental biology* **240**, 419–432. doi:10.1006/dbio.2001.0480.

Sambrook J. **1989** "Molecular Cloning: A Laboratory Manual".

Sanford, L. P., Ormsby, I., Gittenberger-de Groot, A. C., Sariola, H., Friedman, R., Boivin, G. P., Cardell, E. L. & Doetschman, T. (1997). TGFbeta2 knockout mice have multiple developmental defects that are non-overlapping with other TGFbeta knockout phenotypes. *Development (Cambridge, England)* **124**, 2659–2670.

Sappington, R. M. & Calkins, D. J. (2008). Contribution of TRPV1 to microglia-derived IL-6 and NFkappaB translocation with elevated hydrostatic pressure. *Investigative ophthalmology & visual science* **49**, 3004–3017. doi:10.1167/iovs.07-1355.

Sappington, R. M., Sidorova, T., Long, D. J. & Calkins, D. J. (2009). TRPV1: Contribution to retinal ganglion cell apoptosis and increased intracellular Ca2+ with exposure to hydrostatic pressure. *Investigative ophthalmology & visual science* **50**, 717–728. doi:10.1167/iovs.08-2321.

Sasagawa, S., Takabatake, T., Takabatake, Y., Muramatsu, T. & Takeshima, K. (2002). Axes establishment during eye morphogenesis in Xenopus by coordinate and antagonistic actions of BMP4, Shh, and RA. *Genesis (New York, N.Y. 2000)* **33**, 86–96. doi:10.1002/gene.10095.

Sato, S., Nagaoka, T., Hasegawa, M., Tamatani, T., Nakanishi, T., Takigawa, M. & Takehara, K. (2000). Serum levels of connective tissue growth factor are elevated in patients with systemic sclerosis: Association with extent of skin sclerosis and severity of pulmonary fibrosis. *The Journal of rheumatology* **27**, 149–154.

Scott, J. E. & Orford, C. R. (1981). Dermatan sulphate-rich proteoglycan associates with rat tail-tendon collagen at the d band in the gap region. *The Biochemical journal* **197**, 213–216.

Scott, J. E. & Thomlinson, A. M. (1998). The structure of interfibrillar proteoglycan bridges (shape modules') in extracellular matrix of fibrous connective tissues and their stability in various chemical environments. *Journal of anatomy* **192 (Pt 3)**, 391–405.

Sedding, D. G., Hermsen, J., Seay, U., Eickelberg, O., Kummer, W., Schwencke, C., Strasser, R. H., Tillmanns, H. & Braun-Dullaeus, R. C. (2005). Caveolin-1 facilitates mechanosensitive protein kinase B (Akt) signaling in vitro and in vivo. *Circulation research* **96**, 635–642. doi:10.1161/01.RES.0000160610.61306.0f.

Shen, Y., Heimel, J. A., Kamermans, M., Peachey, N. S., Gregg, R. G. & Nawy, S. (2009). A transient receptor potential-like channel mediates synaptic transmission in rod bipolar cells. *The Journal of neuroscience the official journal of the Society for Neuroscience* **29**, 6088–6093. doi:10.1523/JNEUROSCI.0132-09.2009.

Sherman, L., Sleeman, J., Dall, P., Hekele, A., Moll, J., Ponta, H. & Herrlich, P. (1996). The CD44 proteins in embryonic development and in cancer. *Current topics in microbiology and immunology* **213 (Pt 1)**, 249–269.

Shimo, T., Wu, C., Billings, P. C., Piddington, R., Rosenbloom, J., Pacifici, M. & Koyama, E. (2002). Expression, gene regulation, and roles of Fisp12/CTGF in developing tooth germs. *Developmental dynamics an official publication of the American Association of Anatomists* **224**, 267–278. doi:10.1002/dvdy.10109.

Shubham, K. & Mishra, R. (2012). Pax6 interacts with SPARC and TGF-β in murine eyes. *Molecular vision* **18**, 951–956.

Sigal, I. A., Flanagan, J. G., Tertinegg, I. & Ethier, C. R. (2005). Reconstruction of human optic nerve heads for finite element modeling. *Technology and health care official journal of the European Society for Engineering and Medicine* **13**, 313–329.

Sigal, I. A., Yang, H., Roberts, M. D., Grimm, J. L., Burgoyne, C. F., Demirel, S. & Downs, J. C. (2011). IOP-induced lamina cribrosa deformation and scleral canal expansion: Independent or related? *Investigative ophthalmology & visual science* **52**, 9023–9032. doi:10.1167/iovs.11-8183.

Sigal IA, Roberts MD, Girard MJA, Burgoyne CF & Downs JC (2009). Biomechanical changes of the optic disc. Ocular disease: mechanisms and management.

Sinha, B., Köster, D., Ruez, R., Gonnord, P., Bastiani, M., Abankwa, D., Stan, R. V., Butler-Browne, G., Vedie, B., Johannes, L., Morone, N., Parton, R. G., Raposo, G., Sens, P., Lamaze, C. & Nassoy, P. (2011). Cells respond to mechanical stress by rapid disassembly of caveolae. *Cell* **144**, 402–413. doi:10.1016/j.cell.2010.12.031.

Small, R. K., Riddle, P. & Noble, M. (1987). Evidence for migration of oligodendrocyte--type-2 astrocyte progenitor cells into the developing rat optic nerve. *Nature* **328**, 155–157. doi:10.1038/328155a0.

Smerdel-Ramoya, A., Zanotti, S., Deregowski, V. & Canalis, E. (2008). Connective tissue growth factor enhances osteoblastogenesis in vitro. *The Journal of biological chemistry* **283**, 22690–22699. doi:10.1074/jbc.M710140200.

Smith, R. S., Zabaleta, A., Savinova, O. V. & John, S. W. (2001). The mouse anterior chamber angle and trabecular meshwork develop without cell death. *BMC developmental biology* **1**, 3.

Spemann H.H. (1901). Über Korrelationen in der Entwicklung des Auges. *Verh Anat Ges*, 61–79.

Stamer, D. W., Roberts, B. C., Epstein, D. L. & Allingham, R. R. (2000). Isolation of primary open-angle glaucomatous trabecular meshwork cells from whole eye tissue. *Current eye research* **20**, 347–350.

Stamer, W. D., Seftor, R. E., Williams, S. K., Samaha, H. A. & Snyder, R. W. (1995). Isolation and culture of human trabecular meshwork cells by extracellular matrix digestion. *Current eye research* **14**, 611–617.

Stenzel, D., Franco, C. A., Estrach, S., Mettouchi, A., Sauvaget, D., Rosewell, I., Schertel, A., Armer, H., Domogatskaya, A., Rodin, S., Tryggvason, K., Collinson, L., Sorokin, L. & Gerhardt, H. (2011). Endothelial basement membrane limits tip cell formation by inducing Dll4/Notch signalling in vivo. *EMBO reports* **12**, 1135–1143. doi:10.1038/embor.2011.194.

Stone, J. & Dreher, Z. (1987). Relationship between astrocytes, ganglion cells and vasculature of the retina. *The Journal of comparative neurology* **255**, 35–49. doi:10.1002/cne.902550104.

Sun, D. & Jakobs, T. C. (2012). Structural remodeling of astrocytes in the injured CNS. *The Neuroscientist a review journal bringing neurobiology, neurology and psychiatry* **18**, 567–588. doi:10.1177/1073858411423441.

Sun, D., Lye-Barthel, M., Masland, R. H. & Jakobs, T. C. (2009). The morphology and spatial arrangement of astrocytes in the optic nerve head of the mouse. *The Journal of comparative neurology* **516**, 1–19. doi:10.1002/cne.22058.

Sun, D., Lye-Barthel, M., Masland, R. H. & Jakobs, T. C. (2010). Structural remodeling of fibrous astrocytes after axonal injury. *The Journal of neuroscience the official journal of the Society for Neuroscience* **30**, 14008–14019. doi:10.1523/JNEUROSCI.3605-10.2010.

Sun, D., Moore, S. & Jakobs, T. C. (2017). Optic nerve astrocyte reactivity protects function in experimental glaucoma and other nerve injuries. *The Journal of experimental medicine* **214**, 1411–1430. doi:10.1084/jem.20160412.

Sun, D., Qu, J. & Jakobs, T. C. (2013). Reversible reactivity by optic nerve astrocytes. *Glia* **61**, 1218–1235. doi:10.1002/glia.22507.

Suzuma, K., Naruse, K., Suzuma, I., Takahara, N., Ueki, K., Aiello, L. P. & King, G. L. (2000). Vascular endothelial growth factor induces expression of connective tissue growth factor via KDR, Flt1, and phosphatidylinositol 3-kinase-akt-dependent pathways in retinal vascular cells. *The Journal of biological chemistry* **275**, 40725–40731. doi:10.1074/jbc.M006509200.

Tagawa, A., Mezzacasa, A., Hayer, A., Longatti, A., Pelkmans, L. & Helenius, A. (2005). Assembly and trafficking of caveolar domains in the cell: Caveolae as stable, cargo-triggered, vesicular transporters. *The Journal of cell biology* **170**, 769–779. doi:10.1083/jcb.200506103.

Takano, T., Tian, G.-F., Peng, W., Lou, N., Libionka, W., Han, X. & Nedergaard, M. (2006). Astrocyte-mediated control of cerebral blood flow. *Nature neuroscience* **9**, 260–267. doi:10.1038/nn1623.

Tamm, E. R. (2009). The trabecular meshwork outflow pathways: Structural and functional aspects. *Experimental eye research* **88**, 648–655. doi:10.1016/j.exer.2009.02.007.

Tamm, E. R., Siegner, A., Baur, A. & Lütjen-Drecoll, E. (1996). Transforming growth factor-beta 1 induces alpha-smooth muscle-actin expression in cultured human and monkey trabecular meshwork. *Experimental eye research* **62**, 389–397. doi:10.1006/exer.1996.0044.

Tawara, A., Varner, H. H. & Hollyfield, J. G. (1989). Distribution and characterization of sulfated proteoglycans in the human trabecular tissue. *Investigative ophthalmology & visual science* **30**, 2215–2231.

Tehrani, S., Johnson, E. C., Cepurna, W. O. & Morrison, J. C. (2014). Astrocyte processes label for filamentous actin and reorient early within the optic nerve head in a rat glaucoma model. *Investigative ophthalmology & visual science* **55**, 6945–6952. doi:10.1167/iovs.14-14969.

Tektas, O.-Y. & Lütjen-Drecoll, E. (2009). Structural changes of the trabecular meshwork in different kinds of glaucoma. *Experimental eye research* **88**, 769–775. doi:10.1016/j.exer.2008.11.025.

Tektas, O.-Y., Lütjen-Drecoll, E. & Scholz, M. (2010). Qualitative and quantitative morphologic changes in the vasculature and extracellular matrix of the prelaminar optic nerve head in eyes with POAG. *Investigative ophthalmology & visual science* **51**, 5083–5091. doi:10.1167/iovs.09-5101.

Thakur, A., Fitzpatrick, S., Zaman, A., Kugathasan, K., Muirhead, B., Hortelano, G. & Sheardown, H. (2012). Strategies for ocular siRNA delivery: Potential and limitations of non-viral nanocarriers. *Journal of biological engineering* **6**, 7. doi:10.1186/1754-1611-6-7.

Tham, Y.-C., Li, X., Wong, T. Y., Quigley, H. A., Aung, T. & Cheng, C.-Y. (2014). Global prevalence of glaucoma and projections of glaucoma burden through 2040: A systematic review and meta-analysis. *Ophthalmology* **121**, 2081–2090. doi:10.1016/j.ophtha.2014.05.013.

(2000). The Advanced Glaucoma Intervention Study (AGIS): 7. The relationship between control of intraocular pressure and visual field deterioration.The AGIS Investigators. *American journal of ophthalmology* **130**, 429–440.

Thorleifsson, G., Walters, G. B., Hewitt, A. W., Masson, G., Helgason, A., DeWan, A., Sigurdsson, A., Jonasdottir, A., Gudjonsson, S. A., Magnusson, K. P., Stefansson, H., Lam, D. S. C., Tam, P. O. S., Gudmundsdottir, G. J., Southgate, L., Burdon, K. P., Gottfredsdottir, M. S., Aldred, M. A., Mitchell, P., St Clair, D., Collier, D. A., Tang, N., Sveinsson, O., Macgregor, S., Martin, N. G., Cree, A. J., Gibson, J., Macleod, A., Jacob, A., Ennis, S., Young, T. L., Chan, J. C. N., Karwatowski, W. S. S., Hammond, C. J., Thordarson, K., Zhang, M., Wadelius, C., Lotery, A. J., Trembath, R. C., Pang, C. P., Hoh, J., Craig, J. E., Kong, A., Mackey, D. A., Jonasson, F., Thorsteinsdottir, U. & Stefansson, K. (2010). Common variants near CAV1 and CAV2 are associated with primary open-angle glaucoma. *Nature genetics* **42**, 906–909. doi:10.1038/ng.661.

Tian, B., Geiger, B., Epstein, D. L. & Kaufman, P. L. (2000). Cytoskeletal involvement in the regulation of aqueous humor outflow. *Investigative ophthalmology & visual science* **41**, 619–623.

Ton, C. C., Hirvonen, H., Miwa, H., Weil, M. M., Monaghan, P., Jordan, T., van Heyningen, V., Hastie, N. D., Meijers-Heijboer, H. & Drechsler, M. (1991). Positional cloning and characterization of a paired box- and homeobox-containing gene from the aniridia region. *Cell* **67**, 1059–1074.

Tout, S., Chan-Ling, T., Holländer, H. & Stone, J. (1993). The role of Müller cells in the formation of the blood-retinal barrier. *Neuroscience* **55**, 291–301.

Tripathi, R. C., Li, J., Chan, W. F. & Tripathi, B. J. (1994). Aqueous humor in glaucomatous eyes contains an increased level of TGF-beta 2. *Experimental eye research* **59**, 723–727.

Trivedi, R. H., Nutaitis, M., Vroman, D. & Crosson, C. E. (2011). Influence of race and age on aqueous humor levels of transforming growth factor-beta 2 in glaucomatous and nonglaucomatous eyes. *Journal of ocular pharmacology and therapeutics the official journal of the Association for Ocular Pharmacology and Therapeutics* **27**, 477–480. doi:10.1089/jop.2010.0100.

Tsacopoulos, M. & Magistretti, P. J. (1996). Metabolic coupling between glia and neurons. *The Journal of neuroscience the official journal of the Society for Neuroscience* **16**, 877–885.

Ueda, J., Wentz-Hunter, K. & Yue, B. Y. J. T. (2002). Distribution of myocilin and extracellular matrix components in the juxtacanalicular tissue of human eyes. *Investigative ophthalmology & visual science* **43**, 1068–1076.

Ullian, E. M., Sapperstein, S. K., Christopherson, K. S. & Barres, B. A. (2001). Control of synapse number by glia. *Science (New York, N.Y.)* **291**, 657–661. doi:10.1126/science.291.5504.657.

van Deurs, B., Roepstorff, K., Hommelgaard, A. M. & Sandvig, K. (2003). Caveolae: Anchored, multifunctional platforms in the lipid ocean. *Trends in cell biology* **13**, 92–100.

van Koolwijk, L. M. E., Ramdas, W. D., Ikram, M. K., Jansonius, N. M., Pasutto, F., Hysi, P. G., Macgregor, S., Janssen, S. F., Hewitt, A. W., Viswanathan, A. C., Brink, J. B. ten, Hosseini, S. M., Amin, N., Despriet, D. D. G., Willemse-Assink, J. J. M., Kramer, R., Rivadeneira, F., Struchalin, M., Aulchenko, Y. S., Weisschuh, N., Zenkel, M., Mardin, C. Y., Gramer, E., Welge-Lüssen, U., Montgomery, G. W., Carbonaro, F., Young, T. L., Bellenguez, C., McGuffin, P., Foster, P. J., Topouzis, F., Mitchell, P., Wang, J. J., Wong, T. Y., Czudowska, M. A., Hofman, A., Uitterlinden, A. G., Wolfs, R. C. W., Jong, P. T. V. M. de, Oostra, B. A., Paterson, A. D., Mackey, D. A., Bergen,

A. A. B., Reis, A., Hammond, C. J., Vingerling, J. R., Lemij, H. G., Klaver, C. C. W. & van Duijn, C. M. (2012). Common genetic determinants of intraocular pressure and primary open-angle glaucoma. *PLoS genetics* **8**, e1002611. doi:10.1371/journal.pgen.1002611.

van Raay, T. J. & Vetter, M. L. (2004). Wnt/frizzled signaling during vertebrate retinal development. *Developmental neuroscience* **26**, 352–358. doi:10.1159/000082277.

Varela, H. J. & Hernandez, M. R. (1997). Astrocyte responses in human optic nerve head with primary open-angle glaucoma. *Journal of glaucoma* **6**, 303–313.

Vecino, E., Heller, J. P., Veiga-Crespo, P., Martin, K. R. & Fawcett, J. W. (2015). Influence of extracellular matrix components on the expression of integrins and regeneration of adult retinal ganglion cells. *PloS one* **10**, e0125250. doi:10.1371/journal.pone.0125250.

Verkhratsky, A., Reyes, R. C. & Parpura, V. (2014). TRP channels coordinate ion signalling in astroglia. *Reviews of physiology, biochemistry and pharmacology* **166**, 1–22. doi:10.1007/112_2013_15.

Vial, C., Gutiérrez, J., Santander, C., Cabrera, D. & Brandan, E. (2011). Decorin interacts with connective tissue growth factor (CTGF)/CCN2 by LRR12 inhibiting its biological activity. *The Journal of biological chemistry* **286**, 24242–24252. doi:10.1074/jbc.M110.189365.

Volkers, L., Mechioukhi, Y. & Coste, B. (2015). Piezo channels: From structure to function. *Pflugers Archiv European journal of physiology* **467**, 95–99. doi:10.1007/s00424-014-1578-z.

Ward, N. J., Ho, K. W., Lambert, W. S., Weitlauf, C. & Calkins, D. J. (2014). Absence of transient receptor potential vanilloid-1 accelerates stress-induced axonopathy in the optic projection. *The Journal of neuroscience the official journal of the Society for Neuroscience* **34**, 3161–3170. doi:10.1523/JNEUROSCI.4089-13.2014.

Wawersik, S., Purcell, P., Rauchman, M., Dudley, A. T., Robertson, E. J. & Maas, R. (1999). BMP7 acts in murine lens placode development. *Developmental biology* **207**, 176–188. doi:10.1006/dbio.1998.9153.

Weitlauf, C., Ward, N. J., Lambert, W. S., Sidorova, T. N., Ho, K. W., Sappington, R. M. & Calkins, D. J. (2014). Short-term increases in transient receptor potential vanilloid-1 mediate stress-induced enhancement of neuronal excitation. *The Journal of neuroscience the official journal of the Society for Neuroscience* **34**, 15369–15381. doi:10.1523/JNEUROSCI.3424-14.2014.

Welsh, D. G., Morielli, A. D., Nelson, M. T. & Brayden, J. E. (2002). Transient receptor potential channels regulate myogenic tone of resistance arteries. *Circulation research* **90**, 248–250.

Wiederholt, M., Thieme, H. & Stumpff, F. (2000). The regulation of trabecular meshwork and ciliary muscle contractility. *Progress in retinal and eye research* **19**, 271–295.

Wiggs, J. L., Kang, J. H., Yaspan, B. L., Mirel, D. B., Laurie, C., Crenshaw, A., Brodeur, W., Gogarten, S., Olson, L. M., Abdrabou, W., DelBono, E., Loomis, S., Haines, J. L. & Pasquale, L. R. (2011). Common variants near CAV1 and CAV2 are associated with primary open-angle glaucoma in Caucasians from the USA. *Human molecular genetics* **20**, 4707–4713. doi:10.1093/hmg/ddr382.

Willermain, F., Libert, S., Motulsky, E., Salik, D., Caspers, L., Perret, J. & Delporte, C. (2014). Origins and consequences of hyperosmolar stress in retinal pigmented epithelial cells. *Frontiers in physiology* **5**, 199. doi:10.3389/fphys.2014.00199.

Wilson, S. W. & Houart, C. (2004). Early steps in the development of the forebrain. *Developmental cell* **6**, 167–181.

Winter, P. de, Leoni, P. & Abraham, D. (2008). Connective tissue growth factor: Structure-function relationships of a mosaic, multifunctional protein. *Growth factors (Chur, Switzerland)* **26**, 80–91. doi:10.1080/08977190802025602.

Wu, P.-C., Tsai, C.-L., Gordon, G. M., Jeong, S., Itakura, T., Patel, N., Shi, S. & Fini, M. E. (2015). Chondrogenesis in scleral stem/progenitor cells and its association with form-deprived myopia in mice. *Molecular vision* **21**, 138–147.

Wunderlich, K., Senn, B. C., Todesco, L., Flammer, J. & Meyer, P. (2000). Regulation of connective tissue growth factor gene expression in retinal vascular endothelial cells by angiogenic growth factors. *Graefe's archive for clinical and experimental ophthalmology = Albrecht von Graefes Archiv fur klinische und experimentelle Ophthalmologie* **238**, 910–915.

Yamamoto, N., Itonaga, K., Marunouchi, T. & Majima, K. (2005a). Concentration of transforming growth factor beta2 in aqueous humor. *Ophthalmic research* **37**, 29–33. doi:10.1159/000083019.

Yamamoto, T., Sawada, Y., Katayama, I. & Nishioka, K. (2005b). Nodular scleroderma: Increased expression of connective tissue growth factor. *Dermatology (Basel, Switzerland)* **211**, 218–223. doi:10.1159/000087015.

Yan, X., Tezel, G., Wax, M. B. & Edward, D. P. (2000). Matrix metalloproteinases and tumor necrosis factor alpha in glaucomatous optic nerve head. *Archives of ophthalmology (Chicago, Ill. 1960)* **118**, 666–673.

Yang, X.-N., Lu, Y.-P., Liu, J.-J., Huang, J.-K., Liu, Y.-P., Xiao, C.-X., Jazag, A., Ren, J.-L. & Guleng, B. (2014). Piezo1 is as a novel trefoil factor family 1 binding protein that promotes gastric cancer cell mobility in vitro. *Digestive diseases and sciences* **59**, 1428–1435. doi:10.1007/s10620-014-3044-3.

Ye, H., Yang, J. & Hernandez, M. R. (1994). Localization of collagen type III mRNA in normal human optic nerve heads. *Experimental eye research* **58**, 53–63. doi:10.1006/exer.1994.1194.

Yoshida, T., Satoh, M., Nakagaito, Y., Kuno, H. & Takeuchi, M. (1993). Cytokines affecting survival and differentiation of an astrocyte progenitor cell line. *Brain research. Developmental brain research* **76**, 147–150.

Yu, J., Bergaya, S., Murata, T., Alp, I. F., Bauer, M. P., Lin, M. I., Drab, M., Kurzchalia, T. V., Stan, R. V. & Sessa, W. C. (2006). Direct evidence for the role of caveolin-1 and caveolae in mechanotransduction and remodeling of blood vessels. *The Journal of clinical investigation* **116**, 1284–1291. doi:10.1172/JCI27100.

Zaghloul, N. A., Yan, B. & Moody, S. A. (2005). Step-wise specification of retinal stem cells during normal embryogenesis. *Biology of the cell* **97**, 321–337. doi:10.1042/BC20040521.

Zhao, S., Chen, Q., Hung, F.-C. & Overbeek, P. A. (2002a). BMP signaling is required for development of the ciliary body. *Development (Cambridge, England)* **129**, 4435–4442.

Zhao, Y.-Y., Liu, Y., Stan, R.-V., Fan, L., Gu, Y., Dalton, N., Chu, P.-H., Peterson, K., Ross, J. & Chien, K. R. (2002b). Defects in caveolin-1 cause dilated cardiomyopathy and pulmonary hypertension in knockout mice. *Proceedings of the National Academy of Sciences of the United States of America* **99**, 11375–11380. doi:10.1073/pnas.172360799.

Zimmermann, D. R., Trüeb, B., Winterhalter, K. H., Witmer, R. & Fischer, R. W. (1986). Type VI collagen is a major component of the human cornea. *FEBS letters* **197**, 55–58.

Zode, G. S., Sethi, A., Brun-Zinkernagel, A.-M., Chang, I.-F., Clark, A. F. & Wordinger, R. J. (2011). Transforming growth factor-β2 increases extracellular matrix proteins in optic nerve head cells via activation of the Smad signaling pathway. *Molecular vision* **17**, 1745–1758.

8. Supplement

8.1. List of Abbreviations

ng/µg/g	Nanogram/microgram/gram
µl/ml	Microliter/milliliter
µm/nm/mm	Micrometer/nanometer/millimeter
AGS	Astrocyte Growth Supplement
AH	Aqueous humor
AP	Alkaline phosphatase
APS	Ammonium persulfate
Ax	Axon
BM	Basement membrane
BMP	Bone morphogenic protein
BSA	Bovine serum albumin
c	Cornea
Cav1	Caveolin1
cb	Ciliary body
CCN	**C**onnective Tissue Growth Factor, **C**ystein rich protein, **N**ephroblastoma overexpressed gene
CD31	Cluster of differentiation 31
CD44	Cluster of differentiation 44
CT	C-terminal module
CTGF	Connective tissue growth factor
CWFG	Cold water fish gelatin
Cyr61	Cystein rich protein 61
DAPI	4',6-diamidino-2-phenylindole
DCN	Decorin
DMEM	Dulbecco's Modified Eagle's medium
DMSO	Dimethyl sulfoxide
DNA	Deoxyribonucleic acid
DTT	Dithiothreitol
E	Embryonic day
ECM	Extracellular matrix
eNOS	Endothelial nitric oxide synthase
ER	Endoplasmatic reticulum
FCS	Fetal calf serum
FITC	Fluorescein isothiocyanate
FGF	Fibroblast growth factor
FN	Fibronectin
GFAP	Glial fibrillary acidic protein
GS	Glutamine synthetase
h	Hour
ha	Hyaloid artery
HA	Hyaluron
HTM	Human trabecular meshwork
HRP	Horseradish peroxidase
IGBP	Insulin-like growth factor-binding protein
IGF	Insulin-like growth factor
il	Inner layer of the optic cup
ILM	Inner limiting membrane
INL	Inner nuclear layer
IOP	Intraocular pressure

IPL	Inner plexiform layer
irs	Interretinal space
JCT	Juxtacanalicular tissue
kPa	Kilopascal
l	Lens
LC	Lamina cribrosa
lv	Lens vesicle
mA	Milliampere
MBP	Myelin basic protein
min	Minute
MGB	Minor groove binder
MP	Milk Powder
MMP2	Matrix metalloproteinase-2
n	number
NFQ	Non-fluorescent quencher
NO	Nitric oxide
NOV	Nephroblastoma overexpressed gene
NP	Nanoparticles
nr	Neuronal layer of the retina
ol	Outer layer of the optic cup
OLM	Outer limiting membrane
ON	Optic nerve
ONH	Optic nerve head
ONL	Outer nuclear layer
OPL	Outer plexiform layer
os	Optic stalk
ov	Optic vesicle
P	Postnatal day
PBS	Phosphate-buffered saline
PCR	Polymerase chain reaction
PDMS	Polydimethylsiloxane
PEI	Polycationic polymer
PFA	Paraformaldehyde
Php	Phosphate buffer
PLGA	Poly(D,L-lactide-co-glycolide)
POAG	Primary open angle glaucoma
pr	Pigmented layer of the retina
PRL	Prelaminar region
PSL	Postlaminar region
RA	Retinoic acid
RNA	Ribonucleic acid
RT	Reverse transcriptase
RT	Room temperature
re	Retina
RPE	Retinal pigmented epithelium
SEM	Standard error of the mean
SC	Schlemm’s canal
scrblsiRNA	Scramble small interfering RNA
SD	Standard deviation
SDS	Sodium dodecyl sulfate
se	Surface ectoderm
sec	Seconds
Shh	Sonic hedgehog
siRNA	Small interfering RNA

SV-40	Simian-Virus 40
TBE	Tris-borate-EDTA
TBS	Tris-buffered saline
TGFβ2	Transforming growth factor β2
TEMED	Tetramethylethylenediamine
TG	Transgenic
TIMP-1	Tissue inhibitors of metalloproteinases-1
TM	Trabecular meshwork
TRP	Transient receptor potential
Trpc1	Transient receptor potential channel c1
Trpm7	Transient receptor potential channel v2
Trpv2	Transient receptor potential channel m7
TSP1	Thrombospondin 1
UNG	Uracil-N glycosylase
V	Volt
VEGF	Vascular endothelial growth factor
VP	Venous plexus
VWC	von Willebrand type c domain
WISP1	WNT1-inducible-signaling pathway protein 1
WISP2	WNT1-inducible-signaling pathway protein 2
WISP3	WNT1-inducible-signaling pathway protein 3
WT	Wildtype

8.2. Congress contributions

- ARVO 2015, Denver, USA; active participation with poster; Title of poster: Reactive changes in optic nerve astrocytes are mediated by TGFβ2, CTGF and increasing substratum stiffness

- 31. Arbeitstagung der Anatomischen Gesellschaft 2015, Würzburg, Germany; active participation with poster; Title of poster: Reactive changes in optic nerve astrocytes are mediated by TGFβ2, CTGF and increasing substratum stiffness

- 32. Arbeitstagung der Anatomischen Gesellschaft 2017, Würzburg, Germany; active participation with talk; Title of talk: Reactive changes in murine optic nerve astrocytes are mediated by growth factors and increasing substratum stiffness

8.3. Declaration/Erklärung

Hiermit erkläre ich, dass ich die vorliegende Dissertation selbstständig und ohne unerlaubte Hilfsmittel angefertigt habe.

Regensburg, den

Andrea Dillinger

9. Acknowledgment

Mein Dank gilt Prof. Dr. Ernst Tamm für die Möglichkeit meine Arbeit an seinem Lehrstuhl durchzuführen. Des Weiteren bedanke ich mich für die Übernahme des Vorsitzes meines Promotionskolloquiums.

Ich danke PD Dr. Miriam Breunig für die Übernahme des Zweitgutachtens meiner Arbeit. Des Weiteren danke ich Prof. Dr. Charlotte Wagner und Prof. Dr. Veronika Egger für die Übernahme des Amts des Dritt- und des Ersatzprüfers meines Promotionskolloquiums. Danke möchte ich auch PD Dr. Andreas Ohlmann für die Übernahme des Mentorats meiner Dissertation und den Beitrag und die guten Ideen zu meinen Projekten.

Besonders bedanken möchte ich mich bei Prof. Dr. Rudolf Fuchshofer für die hervorragende Betreuung in den letzten Jahren und für die Übernahme des Erstgutachtens meiner Arbeit. Ich habe unheimlich viel von dir gelernt und die Zusammenarbeit mit dir hat mir immer großen Spaß gemacht. Danke für die tollen, unterhaltsamen und interessanten letzten Jahre.

An dieser Stelle möchte ich allen meinen Kooperationspartner für die tolle Zusammenarbeit in den letzten Jahren danken. Dr. Michael Elliott für die tollen Wochen die ich in seinem Labor verbringen durfte und seinen Beitrag zum Caveolin Projekt. Meinen Kooperationspartner von der OTH Regensburg danke ich für die Zusammenarbeit und Prof. Dr. Mikhail Chamonine für die Übernahme des Mentorats meiner Dissertation. Mein herzlicher Dank gilt Miriam Breunig, Michaela Guter und Renate Liebl für die erstklassige Zusammenarbeit im Nanopartikel Projekt.

Mein besonderer Dank gilt Franziska Scherl, Anita Grundl, Gregor Weber und Anja Schlecht. Vielen Dank für all die gemeinsamen Stunden in den letzten Jahren sowohl im Labor als auch außerhalb. Ihr wart mir jederzeit eine sehr große Hilfe und Stütze. Danke für eure tolle Unterstützung. Hier möchte ich vor allem Gregor Weber danken der mit seiner Doktorarbeit maßgeblich zu einem Teil meiner Projekte beigetragen hat. Ganz besonders hervorheben möchte ich dabei Franziska Scherl. Danke, die für die tolle Zusammenarbeit und deine unglaubliche Unterstützung vor allem in den letzten Monaten.

Besonders hervor heben möchte ich Sabrina Schmitt. Du bist für mich in den letzten Jahren ein sehr wichtiger Teil meines Lebens geworden. Vielen Dank für die unvergesslichen Stunden im Labor, aber vor allem außerhalb. Danke, dass du dir immer

meine Sorgen und Problemchen angehört hast und auch immer einen guten Rat wusstest.

Mein Dank gilt auch allen weiteren Kollegen und Kolleginnen des Lehrstuhls. Vor allem möchte ich mich bei Margit Schimmel, Angelika Pach und Silvia Babl für ihre tatkräftige Unterstützung bedanken. Hier möchte ich Elke Stauber besonders hervorheben. Danke, dass du mir immer mit Rat und Tat zur Seite standst und mich jederzeit so toll unterstützt hast.

Aus tiefem Herzen möchte ich allen danken, die mich in den Jahren meines Studiums und meiner Doktorarbeit begleitet haben und immer ein offenes Ohr für mich hatten. Aber natürlich vor allem meiner Familie, die mich in all der Zeit während meines Studiums und meiner Doktorarbeit so unglaublich unterstützt hat. Danke, für euer Verständnis wenn ich mit dem Kopf nicht zu Hause sondern in der Arbeit war. Ich bin euch unendlich dankbar. Ihr seid die Besten.